THE UNIVERSITY OF QUEENSLAND

AUSTRALIA

Unravelling the sensory control of behaviour in honeybees using virtual reality paradigms

Gavin Jonathan Taylor

BEng (Hons)

A thesis submitted for the degree of Doctor of Philosophy at The University of Queensland in 2014

Queensland Brain Institute

Abstract

Insects use sensory information to control their behaviour when performing complex tasks. For example, an insect can navigate using visual cues, allowing it to move from its current location to a goal. As the insect moves towards that goal, it must also perform other tasks such as stabilising its course against disturbances, avoiding obstacles, and minimising its energy expenditure. These tasks also make use of visual cues, and the information from other senses, such as mechanoreception. At any point during its journey towards its goal, an insect may well use information from multiple senses to perform multiple tasks. Further, the insect can also adapt its control, based on sensory feedback, to optimize its performance. Despite their relatively small brain sizes, insects present a complex model of how an organism can use sensory information to control behaviour.

Many experimental paradigms seeking to unravel how insects control their behaviour have used virtual reality to display sensory stimuli to a tethered insect, but have often used a reductionist approach. For instance, an experiment may expose insects to stimulation in only a single sensory modality. Alternatively, experiments may be conducted in open-loop, where an insect cannot influence the sensory experience it receives. Both of these paradigms have allowed researchers to study the relationships between the sensory information an insect receives and the behavioural choices it makes. However, studies have also found that multi-sensory integration, and also closed-loop interaction with a stimulus, can affect how insects process information at both the neural and behavioural levels. This thesis aims to develop models, based on experimental data, of how insects use multi-sensory information to control their behaviour.

To address those points, honeybees are used as a model organism in experiments conducted using tethered virtual reality techniques, to allow for controlled and quantitative tests of their behaviour. With regards to multi-sensory information processing, the methods used by *flying* bees to integrate two measures of flight speed, visual motion and air speed, are examined by measuring the influence of these stimuli on the honeybee's streamlining response. The streamlining response results from an interaction between the two stimuli, and a relatively simple non-linear model could predict the bee's behaviour.

A detailed study of how *walking* honeybees control a fixation stimulus in closed-loop is also conducted. This study uses a recently developed measurement technology, FicTrac, to measure the walking bee's behaviour when interacting with closed-loop visual stimulus. Surprisingly, bees behave differently when the closed-loop feedback loop uses FicTrac, as compared to when less accurate measurements from other sensors (with systematic biases) are used. When the biased sensors are used, the bee's change in behaviour allowed them to improve their fixation, indicating insects can learn to adapt and take advantage of the peculiarities in measurements from some sensors; an important consideration for future research in the field.

To analyse the control scheme underlying honeybees' ability to fixate, analysis techniques are developed to model the control system in manner comparable to previous open-loop studies. These techniques show that bees also adapt their control scheme depending on the coupling ratio (the gain) between their actions and the fixation stimulus. Honeybees adapt the relationship between their turning rate and the observed position and velocity of the fixation stimulus depending on the gain. Simulations indicate that the adaptations the honeybees made increase the stability of the fixation stimulus during closed-loop control at high gains. Surprisingly, bees also modulated their walking speed in response to the position of the fixation stimulus, even though this did not influence the stimulus. The bees' walking speed modulation allows them to efficiently move towards the stimulus, even if they could not control it stably at high gains.

This thesis contributes to a broader understanding of how sensory control is used to guide insect behaviour. The models of insect behaviour that are developed, particularly where derived from closed-loop experiments, provide a better understand control schemes linking complex sensory information to behaviour. Knowledge of such control schemes is important in discovering how they are realized by neural mechanisms, and can also inform the design of robotic systems using biologically inspired control methods.

Declaration by author

This thesis is composed of my original work, and contains no material previously published or written by another person except where due reference has been made in the text. I have clearly stated the contribution by others to jointly-authored works that I have included in my thesis.

I have clearly stated the contribution of others to my thesis as a whole, including statistical assistance, survey design, data analysis, significant technical procedures, professional editorial advice, and any other original research work used or reported in my thesis. The content of my thesis is the result of work I have carried out since the commencement of my research higher degree candidature and does not include a substantial part of work that has been submitted to qualify for the award of any other degree or diploma in any university or other tertiary institution. I have clearly stated which parts of my thesis, if any, have been submitted to qualify for another award.

I acknowledge that an electronic copy of my thesis must be lodged with the University Library and, subject to the General Award Rules of The University of Queensland, immediately made available for research and study in accordance with the *Copyright Act 1968*.

I acknowledge that copyright of all material contained in my thesis resides with the copyright holder(s) of that material. Where appropriate I have obtained copyright permission from the copyright holder to reproduce material in this thesis.

Publications during candidature

Moore, R. J. D, **Taylor, G. J.**, Paulk, A.C ., Pearson, T. W. J., van Swinderen, B. & Srinivasan, M. V. (2014). FicTrac: a visual method for tracking spherical motion and generating fictive animal paths. *Journal of Neuroscience Methods*. 225(1), 106-119

Paulk, A. C., Stacey, J. A., Pearson, T., **Taylor, G. J.**, Moore, R. J. D., Srinivasan, M. V. & van Swinderen, B. (2014). Selective attention in the honeybee optic lobes precedes behavioral choices. *Proceedings of the National Academy of Sciences of the U.S.A.*

Taylor, G. J., Luu, T., Ball, D. & Srinivasan, M. V. (2013). Vision and airflow combine to streamline flying honeybees. *Scientific Reports*. 3

Publications included in this thesis

Taylor, G.J., Luu, T., Ball, D. & Srinivasan, M. V. (2013). Vision and airflow combine to streamline flying honeybees. *Scientific Reports*. 3

This publication is included in the thesis as Chapter 2 and Appendix A. *Contributions*: **GJT**, design (60%), experiments (95%), analysis (90%), modelling (95%), and writing (80%); TL, design (10%), experiments (5%), and analysis (5%); DB, design (10%), writing (5%), and other assistance; MVS, design (20%), analysis (5%), modelling (5%), and writing (15%).

Contributions by others to the thesis

The thesis contains four results chapters that are each formatted as multi-author research articles. The first of these articles (Chapter 2) has been published, and the authors and their contributions are detailed in the preceding section. Chapters 3, 4 and 5 represent work that has been prepared for submission in the future. A preamble at the start of each results chapter briefly details the journal the material has been prepared for (or published in) and the significance of the work. Additionally, M. V. Srinivasan provided critical comments on the General Introduction and Discussion, Chapters 1 and 6 respectively.

The authors for Chapter 3 (and Appendix B) are, **Taylor, G. J.**, Paulk, A. C., Pearson, T. W. L., Moore, R. J. D., Stacey, J. A., Ball, D., van Swinderen, B. & Srinivasan, M. V. *Contributions*: **GJT**, design (30%), analysis (75%), and writing (65%); ACP, design (30%), experiments (20%), analysis (10%), and writing (20%); TWLP, design (20%), and experiments (75%); RJDM, analysis (5%), and other assistance; JAS, design (5%), and experiments (5%); DB, design (5%), and other assistance; BvS, design (5%), and writing (5%); MVS, design (5%), analysis (10%), and writing (10%).

The authors for Chapter 4 (and Appendix C) are, **Taylor, G. J.**, Paulk, A. C., Pearson, T. W. L., van Swinderen, B. & Srinivasan, M. V. *Contributions*: **GJT**, design (60%), analysis (90%), modelling (90%), and writing (80%); ACP, design (20%), experiments (20%), analysis (5%), modelling (5%), and writing (10%); TWLP, design (10%), and experiments (80%); BvS, design (5%); MVS, design (5%), analysis (5%), modelling (5%), and writing (10%).

The authors for Chapter 5 (and Appendix D) are **Taylor, G. J.**, Paulk, A. C., Pearson, T. W. L., van Swinderen, B. & Srinivasan, M. V. *Contributions*: **GJT**, design (60%), analysis (90%), modelling (90%), and writing (80%); ACP, design (20%), experiments (20%), analysis (5%), modelling (10%) and writing (10%); TWLP, design (10%), and experiments (80%); BvS, design (5%); MVS, design (5%), analysis (5%) modelling (5%), and writing (10%).

Statement of parts of the thesis submitted to qualify for the award of another degree

None

Acknowledgements

First and foremost I would like to thank my advisors – Dr. Tien Luu, Dr. David Ball and Prof. Mandyam Srinivasan. All three have my utmost gratitude, Tien for helping me think like a biologist, David for reminding me of good engineering practice, Srini for always advocating an enthusiastic approach to both, and all for providing excellent advice and encouragement along the way.

At the Queensland Brain Institute, I was part of the Srinivasan group and also regularly worked with the Claudianos, Reinhard and van Swinderen groups; the people in these groups, and more generally, all the students and staff at QBI made it a pleasure to come in to work every day. Specifically, I am grateful for the technical support provided by Daniel Bland, Dean Soccol, and Saul Thurrowgood, and also to Richard Moore, Angelique Paulk, Thomas Pearson, Jacqueline Stacey, and Bruno van Swinderen for their involvement in a fruitful collaborative project. During my candidature I was involved with the QBI Students and Postdocs Association and also the ACEVS Young Visionaries, and would like to thank the convenors of both for hosting many informative and social ECR events.

I appreciate all of my friends in Brisbane, and in particular my housemates over the years for helping me to unwind, and I also cannot thank Flávia Freitas enough, as she was a constant source of motivation and kind words during the final stages of my PhD. Finally, I am grateful to my parents Wendy and Stephen Taylor for supporting me throughout my studies and encouraging me all along.

My primary scholarship funding was provided by a University of Queensland Research Scholarship, with 'top-up' scholarships provided by both the Queensland Brain Institute and the ARC Centre of Excellence in Vision Science at different stages of my candidature. I am grateful for travel funds that were provided by the Queensland Brain Institute, the ARC Centre of Excellence in Vision Science and the UQ Graduate School. In addition, my research was also partly supported by grants from the ARC Special Research Initiative on Thinking Systems (TS0669699), the ARC Centre of Excellence in Vision Science (CE0561903), the US Asian Office of Aerospace R&D (Award No. FA4869-07-1-0010), and a Queensland Smart State Premier's Fellowship (M. V. Srinivasan).

Keywords

Apis mellifera, vision, air speed perception, adaptive control, multi-sensory, systems identification, insect flight, insect walking, streamlining, fixation

Australian and New Zealand Standard Research Classifications (ANZSRC)

ANZSRC code: 060801, Animal Behaviour, 60%

ANZSRC code: 110906, Sensory Systems, 30%

ANZSRC code: 060603, Animal Physiology - Systems, 20%

Fields of Research (FoR) Classification

ANZSRC code: 0608, Zoology, 60%

ANZSRC code: 1109, Neurosciences, 30%

ANZSRC code: 0606, Physiology, 20%

To Daniel Taylor,

for always enjoying things in your own way.

Table of Contents

List of Figures

List of Tables

List of Abbreviations and Symbols

AbP	Abdomen pitch
AS	Air speed
CCW	Counter-clockwise
CM	Computer mice
CW	Clockwise
DAQ	Data acquisition unit
df	Statistical degrees of freedom
E	Expected value
F	Test statistic from ANOVA and variants
fps	Frames per second
G	Gain
GKR	Gaussian kernel regression
OF	Optic flow
$M(\psi)$	Motion-dependent response
$M_{CW}(\psi)$	Motion-dependent response to CW motion
$M_{CCW}(\psi)$	Motion-dependent response to CCW motion
$M_{D}(\psi)$	Directionally dependent motion response
$M^{Sh.}(\psi)$	Shape of the motion dependent response (RMS scale equals 1)
$P^{*}_{Par.}$	Body mass specific parasitic power
$P^{*}_{Tot.}$	Body mass specific total power
$P(\psi)$	Position-dependent response
p	Probability value
P	Path
$P^{Sc.}$	Scale of a position dependent response
P^{Y}	Total distance moved in the y direction over an experiment
PWM	Pulse width modulated
R	Response
Sat.	Saturating function
S.E.M	Standard error of the mean
SNR	Signal to noise ratio
SS	Sum of squares
t	Test statistic from Student's *t*-test and variants
W	Walking speed vector magnitude, or test statistic from Shapiro-Wilk test, or Wilcoxon signed rank test and variants (depending on context)
W^{L}	Longitudinal walking speed
W^{T}	Transverse walking speed
z	Test statistic from Rayleigh's test of uniformity
β	Walking speed vector direction
ε	Deviation from sphericity (in relation to Mauchly's test of sphericity)
θ	Angular offset due to latency
v	Angular velocity of a stimulus
χ^2	Test statistic from Mauchly's test of sphericity, or Freidman's test (depending on context)
ψ	Azimuthal angular position of a stimulus
ω	Turning rate

Function notation	
x_t	Denotes the current value of the variable x
x_{t-1}	Denotes the prior value of the variable x
$\tilde{Y}$	Denotes Y is a function with zero mean
$Y\uparrow$	Denotes the function Y is offset such that its minimum value is zero
Y^A	Denotes Y is an anti-symmetric function
Y^M	Denotes Y is an mirror-symmetric function
Y^{RMS}	Denotes the RMS value of the function Y

Abbreviations and symbols are also defined when initially used in the main text. Several additional abbreviations and symbols are used in a limited context, and the meanings for those are also defined when initially used.

Chapter 1 General introduction

Many insects lead active lives and, whether walking or flying, they frequently perform challenging manoeuvres. As they move through their environment, insects utilise various sources of sensory information to control crucial behaviours, such as moment-to-moment stabilisation of their flight, avoiding obstacles and more challenging tasks such as navigation. The processing and use of information for sensorimotor control by insects for these purposes appears robust, and may also have adaptive aspects. This thesis investigates sensorimotor control in both flying and walking honeybees at the behavioural level. The use of multisensory information for the control of body posture is described (Chapter 2), as well as the adaptive and robust behaviours employed when using visual information to control their orientation with respect to an object (Chapters 3, 4 and 5).

This chapter provides a brief introduction on how insects use information for sensorimotor control, and the methods used to characterise these behaviours. Although all experimental work included in this thesis was conducted using honeybees as a model organism, the background material in this chapter is intentionally broad, covering a variety of walking and flying insect species. Additional, more specific, background information is included in the 'Introduction' sections of each of the results chapters. It is also pertinent to note that this thesis refers to insect behaviour and sensorimotor processing primarily in the context of locomotion.

1.1 Sensory control of behaviour

An insect's sensorimotor control is largely defined by its ecological needs, as it will differentially employ behaviours and sensory mechanisms depending on its needs for survival and reproduction. For example, most insects forage for food, avoid predators and other hazards, and find conspecifics for reproduction by moving around the habitat they occupy. Although there is a diverse range of insects living in different environments in the world, common motor routines and sensory mechanisms are present across many taxa. By combining sensory mechanisms and motor routines with robust multi-sensory integration and adaptive control mechanisms, insects are able to fill many ecological niches (Price, 1997).

1.1.1 Sensory mechanisms

Sensory organs allow an insect to perceive visual, mechanoreceptive, and chemoreceptive classes of stimuli (Christensen, 2005). When properly transduced and processed, sensory information can identify the source of a stimulus and determine its orientation, intensity, distance, and motion, although the specific information is highly dependent on the sensory modality that the stimulus represents (Campan, 1997; Jander, 1975). The behaviours of many insects are influenced by external cues, thus, perception of external stimuli is critically important to allow an insect to control its locomotion with respect to the environment. The locations of the various classes of sensory organs on a bee are noted in Figure 1-1.

Arguably, vision provides the richest source of information for animals moving in a complex environment. Light sensed by the compound eyes or the ocelli allows an insect to measure its orientation, position and motion with respect to the world as a whole, and also with respect to specific, visually identifiable objects (Borst, Haag, & Reiff, 2010; Land & Nilsson, 2002; Wehner, 1981).

Mechanoreception involves the perception of forces, which are sensed by a broad category of receptors located over an insect's cuticle that measure both externally and internally generated forces (Keil, 1997). Two specific organs of interest relating to mechanoreception are the halteres and antennae. The halteres are mechanosensory organs specific to Diptera, which the insects use to measure angular velocity using Coriolis forces (Fraenkel & Pringle, 1938; Hengstenberg, Sandeman, & Hengstenberg, 1986). The antennae also transduce information on angular velocity through Coriolis forces (Hinterwirth & Daniel, 2010; Sane, Dieudonne, Willis, & Daniel, 2007), and detect the speed (Gewecke, 1974) and the direction of air flow (Heinzel & Gewecke, 1979; Heinzel & Böhm, 1989). Further, the antennae can detect acoustic vibrations that can identify the source of a sound and its direction (Robert & Göpfert, 2002), tactile cues that identify nearby objects and their distance and direction (Camhi & Johnson, 1999; Erber, Kierzek, Sander, & Grandy, 1998; Okada & Toh, 2006), and information on electric fields (Greggers et al., 2013; Newland et al., 2008). The above list is not exhaustive; mechanosensory transduction is often duplicated by other organs, as in the case of other air flow receptors (Kanzaki, Arbas, & Hildebrand, 1991; Neese, 1965; Weis-Fogh, 1949), acoustic receptors (Hoy & Robert, 1996), and tactile receptors (Goyret, 2010; Kress & Egelhaaf, 2012; Schütz & Dürr, 2011). Other variables are also sensed, such as loading of the wings (Frye,

2001; Gettrup, 1966) and legs and measurement of body posture through proprioception (Schmitz, 1993; Zill, Schmitz, & Büschges, 2004).

Finally, chemoreception allows an insect to perceive odours and tastes (Dahanukar, Hallem, & Carlson, 2005). An insect's gustatory apparatus can taste proximal food items, primarily using the proboscis and tarsae (Mitchell, Itagaki, & Rivet, 1999). Olfactory cues are primarily detected by the antennae, which can identify chemicals (Galizia & Rössler, 2010) and distinguish gradients to determine the sources direction (Duistermars, Chow, & Frye, 2009; Willis, Ford, & Avondet, 2013). Although the specific design and efficacy of sensory systems varies between insect species, nearly all have some capacity to detect visual, mechanosensory and chemosensory stimuli in the environment.

If the measurement transduced directly by an animal's sensory organs (or at least with minimal neuronal computation) are directly useful for sensorimotor control, then that sense can be described as a matched filter for the required information from the environment (Wehner, 1987). For example, in flies, the axes of measurement of a subset of interneurons that visually detects angular velocity (Krapp, 2000; Taylor & Krapp, 2007), and the equivalent mechanoreceptive measurement from the halteres (Nalbach, 1994), closely correspond to the measurement axes required to stabilise flight (Faruque & Humbert, 2010; Krapp, Taylor, & Humbert, 2012). Matched filtering is a useful concept when considering how information is sensed from the environment, as the capabilities of any insect's sensory system are expected to closely match the information that is required for its sensorimotor control.

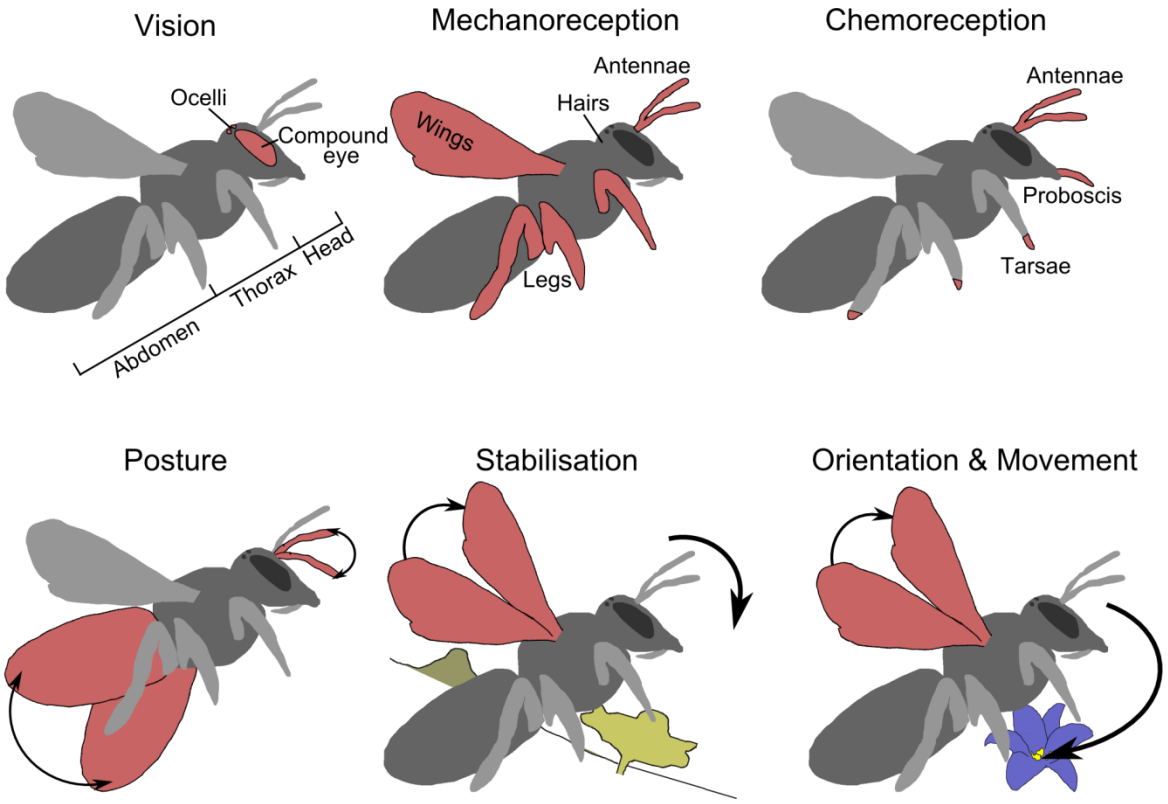

Figure 1-1: Sensory perception and sensorimotor control. Top row, stimulus classes perceived by insects and the respective sensory organs necessary for perception. Bottom row, sensory motor behaviours exhibited by insects that are related to locomotion, which can be altered by sensory information. Both are described further in Sections 1.1.1 and 1.1.2.

1.1.2 Locomotory behaviours

Insects control their locomotion over a wide range of spatial and temporal scales, from adjusting their attitude within milliseconds of a disturbance (Sandeman & Markl, 1980) to migrating between continents over months (Srygley & Dudley, 2008). Locomotory behaviours can be broadly classified into four groups: controlling the posture of body parts, stabilisation of position and attitude, orientating towards external cues, and controlling locomotory speed through the environment. The behavioural classes are broadly represented in Figure 1-1.

An insect body is highly articulated and active movements of all body parts relative to the thorax are common during both flight and walking. The wings or legs are moved to generate propulsive forces during flight or walking respectively. Postural adjustments can be made to improve sensory perception during movement. One example is the antennal positioning reaction, which readjusts the position of the antennae such that they maintain the angle of optimal sensitivity for the measurement of changes in air speed at all flight speeds, despite being deflected by varying amounts due to drag at different speeds (Gewecke, 1974; Heran,

1959). Alternatively, the passive properties of the body may also be adjusted. For instance, the abdomen can be moved laterally, which acts as a rudder in flight by re-directing air flow produce a yaw torque (Camhi, 1970b; Pollack & Plourde, 1982; Zanker, 1988a), or moved vertically to reduce drag (Camhi, 1970a; Luu, Cheung, Ball, & Srinivasan, 2011) and to adjust the attitude of the insect in flight (Dyhr, Morgansen, Daniel, & Cowan, 2013). Further, the legs are not merely stowed in flight, but actively adjusted for stability (Combes & Dudley, 2009) and steering (Arbas, 1986; Gotz, Hengstenberg, & Biesinger, 1979). Although not all of an insect's body structure is primarily designed to contribute to all modes of locomotion, many components contribute in some way.

Several reflexes act to stabilise aspects of an insect's attitude and position, to counteract disturbances arising from external influences (Vance, Faruque, & Humbert, 2013) or mitigate against the inherent instability of many flying insects (Sun, Wang, & Xiong, 2007; Sun & Xiong, 2005). Unexpected rotations about the yaw, pitch, or roll axes are detected by vision or mechanoreception, and will trigger a compensatory turning response (Blondeau & Heisenberg, 1982; Rowell, 1988; Sherman & Dickinson, 2003). Attitude can also be kept level and stable by maintaining a consistent angle between the insect and prominent features in the environment, such as the horizon (Stange & Howard, 1979; Taylor, 1981). Likewise, position can be stabilised by compensating for unexpected translational velocity with compensatory changes in altitude and lateral position (Straw, Lee, & Dickinson, 2010; Tanaka & Kawachi, 2006), by maintaining a fixed location relative to prominent features in the environment (Cowan, Lee, & Full, 2006; Sprayberry & Daniel, 2007; Straw et al., 2010), or by keeping an equal distance to surrounding objects (Kirchner & Srinivasan, 1989; Portelli, Ruffier, Roubieu, & Franceschini, 2011; Srinivasan, Lehrer, Kirchner, & Zhang, 1991). Stabilisation reflexes can be used to hold a set attitude and position when hovering (Collett & Land, 1975; Kelber & Zeil, 1990), or to stabilise a subset of attitude and position components during directed movement, such as when orientating and flying towards an object (Land & Collett, 1974; Wehrhahn, Poggio, & Bülthoff, 1982). In the latter case, where an insect is making a voluntary action, stabilisation reflexes would interfere with the movement if they remained active. Various methods for preventing stabilisation reflexes have been suggested, such as suppressing or otherwise preventing the usual action of the reflex (Egelhaaf, 1987; Srinivasan & Bernard, 1977; Trischler, Kern, & Egelhaaf, 2010), changing the set point of stabilising reflexes to match the predicted stimulus resulting from the action (Chan, Prete, & Dickinson, 1998), or

subtracting a prediction of the expected sensory feedback resulting from the voluntary action to negate the actual sensory input for the reflex (Payne, Hedwig, & Webb, 2010).

Turning responses allow an insect to orientate towards, away from, or relative to cues representing global features of the environment or local objects. Global cues indicate a direction an insect can orient towards, and are stable over a wide spatial and temporal range. They do not always represent a specific object towards which insect moves (such as, visual: Collett, 1996; celestial: Dacke, Byrne, Scholtz, & Warrant, 2004; magnetic: Etheredge, Perez, Taylor, & Jander, 1999; polarisation: Evangelista, Kraft, Dacke, Labhart, & Srinivasan, 2014; wind: Heinzel & Böhm, 1989), but are important when navigating between distant locations (Collett, 2009; Srinivasan, 2011). Alternatively, the insect may be able to directly perceive an object that provides the orientation cue, based on its unique visual (Bahl, Ammer, Schilling, & Borst, 2013; Zhang, Si, & Pahl, 2012), acoustic (Hedwig & Poulet, 2005) or tactile (Okada & Toh, 2006) properties, or because of its movement (Bülthoff, 1981; Lehrer & Srinivasan, 1992; Reiser & Dickinson, 2013). Odours also provide orientation cues, either as trails or in plumes, but may be unreliable due to influences from wind. Hence, plumes do not necessarily allow an insect following them to move to their source directly (Cardé & Willis, 2008; Vickers, 2000). Regardless of the underlying sensory mechanism, orientation cues often cause a turning response from tethered insects that varies sinusoidally with the cue's azimuthal position, with the maximum turning response occurring when stimuli are positioned perpendicular to the insect's preferred orientation (wind: Böhm, Heinzel, Scharstein, & Wendler, 1991a; acoustic: Böhm, Schildberger, & Huber, 1991b; polarisation: Mappes & Homberg, 2004; visual: Reichardt & Poggio, 1976; motion: Reiser & Dickinson, 2013). Orientation cues are important regardless of whether they are local or global, as theoretical predictions show that an external orientation reference is required to maintain movement in a straight line (Cheung, Zhang, Stricker, & Srinivasan, 2007).

As insects move through the world, most vary their longitudinal, or forwards, speed. When walking, proprioceptive variables such as stride frequency are regulated and can control walking speed (Zollikofer, 1994). External factors may have minor (Götz & Wenking, 1973; Schone, 1996) or no influence (Zanker & Collett, 1985). However, external factors strongly influence flight speed, which is regulated either solely depending on visual perception of ground speed (Baird, Srinivasan, Zhang, & Cowling, 2005; David, 1979; Fry, Rohrseitz, Straw, & Dickinson, 2009; Srinivasan, Zhang, Lehrer, & Collett, 1996), or by maintaining a consistent

air speed (Gewecke, 1974; Niehaus, 1981). When approaching a specific object, both walking and flying insects are also observed to regulate their speed based on the distance to their target (Boeddeker, Kern, & Egelhaaf, 2003; Collett & Land, 1975; Cook, 1979; Wehrhahn et al., 1982). Although it is not as important for navigation as controlling orientation, controlling speed relative to an object is critical if an insect is to land on an object (Baird, Boeddeker, Ibbotson, & Srinivasan, 2013; Srinivasan, Zhang, Chahl, Barth, & Venkatesh, 2000; van Breugel & Dickinson, 2012), or to follow it at a fixed distance (Cook, 1979; Land, 1993; van Praagh, Ribi, Wehrhahn, & Wittmann, 1980).

Although walking and flying are distinctly different modes of locomotion, with the latter involving an extra spatial dimension, commonalities exist for the responses to stimuli in both modes (Kanzaki, 1998). For instance, gaze stabilisation based on visual motion is seen in many insects when walking and in flight (Boeddeker & Hemmi, 2010; Hengstenberg, 1993; Kral, 2003). A cricket's response when orientating towards acoustic targets is also similar between both modes (Böhm et al., 1991b; Hedwig & Poulet, 2004; Pollack & Plourde, 1982). Similar behaviours between walking and flying (i.e. when height changes are negligible) may share a variety of common aspects of sensory processing and behavioural control.

The behaviours discussed here are by no-means an exhaustive list of those observed in insects. However, the general principles involve maintaining an appropriate posture, stabilisation against disturbances, and controlling speed and orientation with respect to external cues all constitute core components of an insect's sensorimotor control (Dickinson, 2013).

1.1.3 Multi-sensory control

Similar quantities are encoded by multiple sensory modalities, and a single object may provide information to multiple senses. Anatomical projections from many sensory organs converge in the peripheral and central nervous systems of insects (Homberg, 2005; Rowell & Reichert, 1986; Strausfeld & Seyan, 1985), and present possibilities for sensorimotor control using the perception of multi-sensory stimuli. Multi-sensory information is combined in linear and non-linear methods at the behavioural level, and context dependency is also frequently observed; these topics will be described in the remainder of the section.

Context dependency, also called gating, occurs when two or more sensory cues modulate a motor action. Often the measurement from a sense functions in an on/off type manner, whilst a second sense controls the magnitude of the response. For example, context dependency occurs in a set of muscles controlling compensatory head movements in flies, such that the direction of visual movement controls the response strength, and afferent signals from the halteres or antennae indicating flight function in an on/off role (Haag, Wertz, & Borst, 2010; Huston & Krapp, 2009). Similarly, neurons in *Drosophila* have been found that only respond to translational optic flow when the insect is actively flying (Weir, Schnell, & Dickinson, 2014), and the response of circuits sensitive to visual rotation are similarly increased during active locomotion (Chiappe, Seelig, Reiser, & Jayaraman, 2010; Maimon, Straw, & Dickinson, 2010). However, whether afferent feedback is required for the context modulation was not determined in these studies. Context dependency ensures that the appropriate motor outputs are activated given an insect's state of locomotion.

At the behavioural level, many multi-sensory inputs result in a linear, or weighted linear, summation of the responses to each individual stimulus, particularly when the stimuli represent similar quantities. The turning response from the visual optomotor reflex is combined linearly with that expected from mechanoreceptors in *Drosophila* (Sherman & Dickinson, 2004) and *Manduca* (Hinterwirth & Daniel, 2010), where both modalities measure a value of angular velocity. A direct benefit of combining senses in this manner is the different temporal tuning between visual and mechanosensory information. In *Drosophila*, mechanoreceptors are tuned to detect rotations up ten times faster (Hengstenberg et al., 1986; Sherman & Dickinson, 2003) than the visual system, which is itself capable of detecting rotations up to 100 $^{o}.s^{-1}$ (Hengstenberg, 1984), and also typically have latency of only several milliseconds (Collett & Land, 1975; Sandeman & Markl, 1980), whereas latency in behaviours mediated by the compound eyes may be an order of magnitude greater (Warzecha & Egelhaaf, 2000). Likewise, information on angular rotations encoded by two different visual systems, the ocelli and the compound eyes, is linearly combined to control turning responses (Haag, Wertz, & Borst, 2007; Parsons, Krapp, & Laughlin, 2006), again benefiting from one sensor, the ocelli, responding rapidly compared to the compound eyes. Responses to azimuthally positioned acoustic and visual cues are also linearly summed (Böhm et al., 1991b), and allow an insect to continue towards the visual direction a sound is emitted from, even if the acoustic signal stops (von Helversen & Wendler, 2000). In instances where variables represent different quantities, summation is also observed, such as for *Drosophila's* wingbeat modulation in response to

visual and olfactory cues (Frye & Dickinson, 2004), which prime it to fly towards an odour source. In these examples, summation of the response to both modalities appears sufficient to increase the efficacy of behavioural responses.

In some cases, non-linear interactions are found to occur beyond that provided by context dependency. In fact, the mechanism used by the halteres to provide context dependency for gaze stabilisation allows the fast phasic responses from the halteres to 'clock' slower tonic responses from the compound eyes, resulting in a rapid motor response combining both variables (Huston & Krapp, 2009). In other cases a multiplicative, rather than linear combination has been found, such as where an attractive odour acts to scale up *Drosophila's* stabilising response to rotational visual motion (Chow & Frye, 2008; Wasserman, Lu, Aptekar, & Frye, 2012), but scales down their aversive response to visual expansion (Chow & Frye, 2008). Error checking can also form an inherent part of multi-sensory interactions. In locusts, the signals from the compound eyes, ocelli, and wind sensitive hairs indicating rotational disturbances are integrated in descending neurons, which respond with progressively increasing strength as the signals become consistent across all three modalities as compared with when they conflict (Rowell & Reichert, 1986). This potentially prevents an unreliable measurement in any one sense from triggering compensatory turning unless there is agreement in the measurements from all modalities. It is known that vertebrates can combine multiple sources of information, weighted depending on each senses reliability, in order to improve the measurement accuracy of the system (Baddeley, Ingram, & Miall, 2003; Körding & Wolpert, 2006; Oie, Kiemel, & Jeka, 2002). This is analogous to the technique of Kalman filtering that is used in engineering applications to statistically optimise the combination of multiple sources of sensory information (Haykin, 2001). Some cases of changing behaviour based on sensory reliability are also observed in insects; ants are observed to adjust their navigation strategy based on uncertainties in path integration (Merkle, Knaden, & Wehner, 2006; Wolf & Wehner, 2005), and nocturnal insects can use neural spatial and temporal summation of visual information to improve vision in low light (Theobald, Greiner, Wcislo, & Warrant, 2006; Warrant, 1999). Regardless of whether information is re-weighted based on sensor reliability, non-linear integration undoubtedly provides greater flexibility in multi-sensory integration, particularly when the measured quantities represent different physical values.

Multi-sensory integration encodes both similar and different sources of information, and appears to make insect sensorimotor control more robust than measurements from a single

modality. Given that multi-sensory information contributes to higher level tasks such as navigation and learning (Menzel & Giurfa, 2001; Reinhard, Srinivasan, Guez, & Zhang, 2004; Steck, Hansson, & Knaden, 2011), it is likely that further instances of multisensory integration for sensorimotor control will be discovered.

1.1.4 Adaptive control

Insect behaviour is often described as being highly robust to varying conditions. Insects walk capably despite leg damage (Götz & Wenking, 1973; Wittlinger, Wehner, & Wolf, 2007), and on slippery or springy surfaces (Epstein & Graham, 1983; Spence, Revzen, Seipel, Mullens, & Full, 2010). Similarly, insect flight is not drastically impaired by severe wing damage (Dukas & Dukas, 2011; Haas & Cartar, 2008) or flight in low density air (Altshuler, Dickson, Vance, Roberts, & Dickinson, 2005; Dillon & Dudley, 2014; Dudley, 1995). The intrinsic properties of sensory processing can make receptors inherently robust to disturbances (Borst, Flanagin, & Sompolinsky, 2005; Brinkworth & O'Carroll, 2009). Furthermore, integration of information from multiple sensory modalities contributes to robust behaviours. In addition to their robust control, there is growing evidence to suggest that insects adapt their sensorimotor control to improve their performance given the task at hand (Hesselberg & Lehmann, 2009; Webb, 2004; Wolf & Heisenberg, 1990).

The behaviour of flies when controlling the position of a narrow vertical bar, a behaviour known as fixation (Reichardt & Poggio, 1976), illustrates adaptive control. When tethered, but not shown any visual stimulus, flies will produce random fluctuations of yaw torque (Heisenberg & Wolf, 1979; Maye, Hsieh, Sugihara, & Brembs, 2007; Poggio & Reichardt, 1973). However, as soon the fixation stimulus is shown, the flies will control their yaw torque as a function of the position and motion of the stimulus. If the measured yaw torque is made to control the position of the stimulus in real time, the fly positions the fixation stimulus in its frontal visual field (Heisenberg & Wolf, 1984; Reichardt & Poggio, 1976). Other investigations showed that tethered *Drosophila* adapted to use both their flight thrust (Wolf & Heisenberg, 1991) and leg movements (Wolf, Voss, Hein, & Heisenberg, 1992) to control the position of the fixation stimulus. Both types of motor commands are rather unnatural ways of controlling yaw, but the flies learn each task within seconds. *Drosophila* can also adapt to control the stimulus when the polarity between their yaw torque and the stimulus motion is inverted from that normal free flight (i.e. when the fly turns clockwise the stimulus also turns clockwise,

rather than counter-clockwise as expected), although adapting to this coupling can take tens of minutes (Heisenberg & Wolf, 1984). Yet the previously mentioned coupling changes were drastic, and a fly is more likely to require the ability to fine-tune its sensorimotor commands to the task at hand. Experiments have also been conducted to examine the fly's ability to adapt to changes in the coupling, or gain, between its yaw torque and the movement of the fixation stimulus. The results have shown that flies indeed adapt to these changes and modify their motor commands within 200 ms of the coupling change (Wolf & Heisenberg, 1990). Further, a recent study has shown that *Drosophila* raised in a vial that prohibits flight have lower responses to open-loop fixation stimuli than their normally raised counterparts (Hesselberg & Lehmann, 2009). However, after the flight deprived flies are allowed to control the stimulus in closed-loop experiments the differences disappear, providing further support that flies can learn to fine-tune sensorimotor commands for fixation, in a surprisingly similar manner to vertebrates (Wolpert, Ghahramani, & Jordan, 1995).

In the fixation experiments described, trial and error allowed an insect to improve its motor commands to achieve some desired state of a stimulus. One proposed method for generating adaptive motor commands is by correlating the changes in motor output with changes in the velocity of the stimulus to be controlled (Wolf & Heisenberg, 1990; Wolf & Heisenberg, 1991). Whether a given motor command affects the stimulus, and the coupling coefficient, can then be determined from the correlation. The above description of sensorimotor adaptation is based on fixation experiments with *Drosophila*, although similar adaptive behaviours were also found in locusts (Möhl, 1988; Möhl, 1989). Rather than correlating motor output with the sensory state of the stimulus, another mechanism that would enable adaptive control is to have a predictive, or forward model, of how actions will influence the resulting sensory perception of the environment (Sperry, 1950; von Holst & Mittelstaedt, 1950). By comparing the forward model to the actual sensory perception resulting from a given action, incorrect predictions could then form the basis for sensorimotor adaptations (Miall & Wolpert, 1996; Wolpert & Kawato, 1998). Experimental evidence supports the existence of a forward model in vertebrates (Kawato, 1999). In insects the use of a forward model to negate stabilising reflexes during voluntary motion has support (Payne et al., 2010; Webb & Reeve, 2003), and may also be used for predictive gaze stabilisation during voluntary actions (Schwyn et al., 2011; Viollet & Zeil, 2013). The explicit use of a forward model for motor adaption in insects has yet to be established (Webb, 2004), although the correlative method mentioned at the start of this

paragraph is analogous to a simple forward model to identify which of an insect's motor outputs influence its sensory perception (Wolf & Heisenberg, 1990; Wolf & Heisenberg, 1991).

As with multi-sensory integration, adaptive control contributes to robust insect behaviours. In addition, adaptive control allows an insect to rapidly adopt new methods of responding to stimuli in the environment, potentially reducing the requirements for evolving matched filtering in its sensory system.

1.2 Unpacking sensory control

Fully understanding how an insect's sensorimotor control system works requires detailed knowledge of the anatomy and physiology of the sensory, nervous and motor systems, as well as the sensory environment through which it moves (Chiel & Beer, 1997; Dickinson et al., 2000). Classically, an input-output approach seeks to characterise insect behaviour as a 'black box' system by describing the relationship between sensory inputs and motor outputs, without taking into account the underlying mechanisms. Virtual-reality paradigms and input-output models are both useful approaches for quantifying and describing behaviours. Although input-output characterisation does not describe the physiological mechanisms underlying behaviour directly, it frequently provides insightful information concerning general control principles, and may inform subsequent, more targeted, investigations of the underlying biological mechanisms.

1.2.1 Input-output modelling

Based on the results of behavioural experiments, input-output models can be developed that predict some aspects of an animal's response to stimuli. Such models, using systems identification techniques (Ljung, 1999; Nise, 2008; Westwick & Kearney, 2003) or based on first principles, do not necessarily incorporate the properties of the neurons and networks underlying behaviours. Rather, a phenomenological description links the state of the environment to some behavioural output, abstracting the underlying sensory, processing and motor mechanisms. Despite this abstraction, an input-output model can be used to make experimentally testable predictions of biological function, leading to its refinement or abandonment. A model of beetle motion vision, the correlation type motion detector

(Hassenstein & Reichardt, 1956), exemplifies this approach, as its initial formulation can explain many aspects of invertebrate visual motion detection (Borst et al., 2010).

Regardless of whether the underlying mechanisms are determined, input-output models can also be informative when designing artificial control systems, particularly for robotic agents that attempt to perform tasks in a similar environment as insects (Srinivasan, Thurrowgood, & Soccol, 2010; Webb, Harrison, & Willis, 2004). Indeed, as the underlying mechanisms built into an *in silico* realisation of a model will not duplicate those observed in the *in vivo* realisation, extracting the simplest model description of the observed behaviour is advantageous. For example, landing honeybees implement a simple strategy that maintains a constant rate of optic flow in their ventral eye region during descent, resulting in deceleration to a gentle touch down (Baird et al., 2013; Srinivasan et al., 2000). This visually guided strategy has been used to successfully control landing on a variety of robotic platforms, such as; a precision gantry (Chahl, Srinivasan, & Zhang, 2004), a rotorcraft (Ruffier & Franceschini, 2005) and an ultra-light fixed wing plane (Zufferey & Floreano, 2006). In the case of landing, the identified model has proven useful for control of robots with different sensory and motor mechanisms, acting at different physical scales, to the insect themselves.

1.2.2 Virtual-reality paradigms

Experiments with freely moving insects examine their behaviour under the most realistic conditions possible, as each sense obtains the appropriate feedback from the environment, and motor commands influence the insect's position and orientation as expected. Disturbing the insect's movement or manipulating aspects of the sensory environment can provide information on how it controls its behaviour, but disturbances are usually rapidly corrected for, and it is difficult to directly manipulate the coupling between an animal's actions and their perceived effect. An alternative is virtual-reality, where a tethered insect is placed in a simulated environment. Both experiments with freely moving insects and those in virtual-reality can provide information for top-down modelling. However, virtual-reality allows for experiments that separate the contributions from different senses and manipulation of the usual coupling in the action-perception loop (Roth, Sponberg, & Cowan, 2014; Taylor et al., 2008).

Two common types of experiments that are performed to characterise control systems in virtual-reality are open-loop and closed-loop experiments. In open-loop, an insect's reactions

are recorded, but these reactions do not alter the stimuli that are presented. In a closed-loop protocol, real time measurements are made of the tethered insect's motor actions, which are used to vary the stimuli that the insect experiences. Open-loop paradigms can be used to expose insects to stimuli far away from their stable control parameters, testing their responses to situations that rarely occur in flight (Reiser & Dickinson, 2013). However, open-loop stimulation is not likely to fully replicate the sensory experience of self-controlled flight (Taylor et al., 2008). Whilst fly neurons involved in visual processing appear to encode visual motion in a similar manner in both open- and closed-loop experiments (Ejaz, Krapp, & Tanaka, 2013), neurons in the central brain region of honeybee's appear to respond differently during closed-loop behaviour when compared to replays of identical stimulus movements in open-loop (Paulk et al., 2014). Differences are also observed at the behavioural level, for instance, *Drosophila* have a reduced reaction to stimuli displayed in open-loop compared to their reaction in closed-loop (Heisenberg & Wolf, 1988; Wolf & Heisenberg, 1990). Although the observed responses are likely to be qualitatively similar between open- and closed-loop, especially for reflexive actions, the magnitude and dynamics of responses may vary. Ideally closed-loop experiments allow a situation that closely replicates the sensory experience of free movement, despite the insect remaining fixed in place, and allow for controlled tests of how the insect responds to changes in certain aspects of the environment, or manipulations of the coupling in the normal action-perception loop (Roth et al., 2014). Closed-loop experiments can also show emergent behaviours arising from the feedback loop containing the nervous system, body and environment (Chiel & Beer, 1997).

Both open- and closed-loop experiments in tethered virtual reality provide unique opportunities to characterise insect control systems that are not easily accessible in freely moving animals. However, perhaps the most important benefit is that electrophysiological or cellular activity imaging techniques can be used to record the neural activity from actively behaving insects, especially as recent experiments have shown that active locomotion modulates many aspects of neural processing (Maimon, 2011).

1.3 Scientific aims and outline

Scientists over the past decades have sought to determine the principles by which insects use sensory information from the environment to control their behaviour by conducting behavioural experiments, and by investigating the underlying neural mechanisms. Robust

behavioural control has been observed in freely moving insects, and also when insects are exposed only to changes in a single sensory modality using virtual-reality paradigms. However, relatively few experiments have explicitly tested multi-sensory integration and how adaptations influence an insect's sensorimotor control, although these factors undoubtedly occur during natural movement. I investigate multi-sensory integration and sensorimotor adaption using honeybees (*Apis mellifera*) as a model organism. The honeybee has previously provided a useful model to study visually guided sensorimotor control during free flight (Srinivasan, 2011), and also higher order associative learning (Menzel & Giurfa, 2001; Zhang et al., 2012). My studies have further found honeybees use sensory information for robust multisensory and adaptive sensorimotor control, and these provide insight for control mechanisms that could be utilised on small scale robotic platforms. I describe my findings in four results chapters as follows:

Chapter 2 describes how flying honeybees respond to open-loop combinations of optic flow and air speed by streamlining their abdomen in flight, and further, how this response is affected by disabling the air speed sensing organ in the antenna. A model is developed to explain the response as a non-linear combination of the two stimuli. The energetic benefits of streamlining are compared across several insect species.

In *Chapter 3*, walking honeybees are tested with a visual fixation task in closed-loop, where they use their turning rate to control the azimuthal position of a bright green vertical bar. The bee's ability to adapt to an imposed coupling between the measurement of their walking speed and their turning rate is tested. A similar coupling occurs in optical motion sensors, which are often used in virtual-reality experiments, and tests are made as to whether bees make behavioural adaptions with these sensors.

Chapter 4 further considers how walking honeybees adapt their behaviour in a closed-loop visual fixation task, examining the case where a linear multiplier coupling their turning rate to stimulus movement is systematically varied. A novel analysis method is developed to extract non-linear control functions from temporally correlated closed-loop data, which is used to describe the honeybee's response to the position and motion of the fixation stimulus. Simulations are used to test how the behavioural adaptations made by honeybees would influence their control of the fixation stimulus.

Chapter 5 describes the modulation of longitudinal (forwards) and transverse (sideways) components of walking speed measured from honeybees performing the closed-loop fixation task in Chapter 4. Both components of walking speed are modelled as temporally correlated, non-linear functions of the position of the fixation stimulus and the bee's turning rate. The effect of walking speed on fixation success and its effect on movement towards the stimulus position is considered. Simulations are used to determine which aspects of a honeybee's walking speed modulation are most effective for making progress towards a visual target.

Following University of Queensland guidelines, each chapter is formatted as appropriate for publication in a peer reviewed journal, as detailed in the preamble in each chapter. Thus, the chapters each contain an 'Introduction', 'Methods' and 'Discussion' section in addition to the results presented therein. To conclude the main body of this thesis, *Chapter 6* is a broader discussion of the implications of the combined findings of my research.

Chapter 2 Vision and air flow combine to streamline flying honeybees

2.1 Preamble

This chapter describes the honeybee's streamlining in response to open-loop combinations of both optic flow and air speed when in tethered flight. Multi-sensory control based on optic flow and air speed has received minimal research attention compared to control based on the integration of other senses, and this Chapter suggests a quantitative model for combining the two sensory measurements that can explain the observed streamlining responses from honeybees. Preliminary results of this study were presented at the Australian Neuroscience Society Annual Meeting (2012) and the International Congress of Neuroethology (2012). The contents of this Chapter (and Appendix A) are based on a peer reviewed publication (with the same title) in the journal 'Scientific Reports' authored by G. J. Taylor (the candidate), T. Luu, D. Ball, and M. V. Srinivasan. The contributions of each author are detailed in the preliminary pages of the thesis. After publication in Scientific Reports, this work received significant media attention, which led to five local and national radio interviews, as well as national and international coverage in online articles by more than two dozen media agencies (notably The Brisbane Times, The Guardian and The Sydney Morning Herald). This publication was also awarded the annual Queensland Brain Institute student publication prize in 2013.

2.2 Abstract

Insects face the challenge of integrating multi-sensory information to control their flight. There is evidence that insects combine visual information to sense optic flow and mechanosensory cues to sense air flow. Here we study a 'streamlining' response in honeybees, whereby insects raise their abdomen to reduce drag. We find that this response, which was recently reported to be mediated by optic flow, is also strongly modulated by the presence of air flow simulating a head wind. The Johnston's organs in the antennae were found to play a role in the measurement of the air speed that is used to control the streamlining response. The response to a combination of visual motion and wind is complex and can be explained by a model that incorporates a non-linear combination of the two stimuli. The use of visual and mechanosensory cues increases the strength of the streamlining response when the stimuli are present concurrently. We propose

this multisensory integration will make the response more robust to transient disturbances in either modality.

2.3 Introduction

An insect in flight has available to it at least two sources of information about the speed of its flight through the environment. One source is the visual perception of the world's motion, derived from the pattern of image movement (optic flow) as sensed by the visual system. The second source is the movement of air over the body. Individually, these cues can be unreliable for inferring the insect's own motion in the environment, because variations in the topography of the environment, movement of objects in the world, or a gust of wind can create erroneous or conflicting sensory cues.

Many insects use visual information to control their flight. An example is the optomotor response, which allows a flying insect to correct unwanted rotations about its body axes by generating turning responses that compensate for the rotational optic flow that it senses (Götz, 1964). Other aspects of flight are also visually controlled: for example, honeybees (Baird et al., 2005) and *Drosophila* (David, 1982) have been shown to use visual cues to regulate their flight speed, to avoid dangerously close objects (honeybee: Srinivasan, Zhang, & Chandrashekara, 1993; Drosophila: Tammero & Dickinson, 2002), to orchestrate safe landings (Srinivasan et al., 2000) and to centre their flight through a narrow passage (Kirchner & Srinivasan, 1989). Honeybees have also recently been shown to use the rate of visual motion to control their abdominal posture (Luu et al., 2011). The faster the visual motion that is experienced by the bees, the greater the elevation of the abdomen. This behaviour, termed the 'streamlining response', should minimise the aerodynamic drag experienced by the insect by reducing the cross-sectional area of its body that is exposed to the wind (Nachtigall & Hanauer-Thieser, 1992). However, it is not yet known whether this streamlining response is mediated purely by optic flow, or by additional cues such as the air flow that are experienced during flight.

Vision is not the only sense that some insects use to stabilise their flight. The hindwings of Diptera have evolved into specialised club shaped masses, called halteres, which oscillate in time with the wingbeat (Pringle, 1948). These structures provide flies with a gyroscopic sense for the detection of unintended rotations, complementing their visually evoked optomotor

response (Sherman & Dickinson, 2004). The antennae of *Manduca* were also recently shown to sense gyroscopic forces in a similar way to dipteran halteres (Sane et al., 2007).

Many experiments have shown that visual and mechanosensory cues would stabilize insect's flight *against* external disturbances caused by air movements in the environment. For example, if a gust of wind blows an insect off course, the resulting optomotor response should help correct the unintended deviation from the flight path (Reichardt, 1969). Honeybees flying down a corridor were found to be able to regulate their ground speed in the presence of strong head wind (Barron & Srinivasan, 2006). This compensation was accomplished by holding constant the perceived optic flow (Barron & Srinivasan, 2006).

However, despite some reflexes that seemingly counteract the unintended disturbances caused by air movements on an insect's flight plan, air speed is also actively sensed and used to control other aspects of flight. Many insects, including honeybees (Heran, 1959), have also been shown to sense air speed and to use this to control the amplitude of their wingbeat, which may act to regulate their flight speed (Taylor & Krapp, 2007). Other insects sense air movements to detect changes in flight direction. For example, locusts (Camhi, 1970b; Rowell & Reichert, 1986), *Drosophila* (Budick, Reiser, & Dickinson, 2007), and carrion beetles (Heinzel & Böhm, 1989) respond to air flow by changing the direction of their path in a compensatory fashion.

It appears that insects are able to make use of air flow as well as visual cues to control various aspects of their flight. To investigate the effects of air flow on the control of the honeybee's streamlining response we exposed tethered bees to combinations of optic flow and air flow in a flight arena, and observed the reactions of the abdomen. We also examined whether the antennae contribute to the measurement of air speed, and developed a quantitative model that describes how this is accomplished.

2.4 Methods

2.4.1 Experimental animals

Adult honeybee foragers (*Apis mellifera*) were used in all experiments. All insects were collected from a single hive maintained by the Queensland Brain Institute at The University of

Queensland, Brisbane, Australia. Only foragers were collected, and were identified as those carrying pollen on their hind legs when returning to the hive.

2.4.2 Tethering

Honeybees were cold anaesthetized in a refrigerator for 20 to 30 minutes, after which they were removed individually for tethering. Animals spent no more than one hour under anaesthesia. While the insect was anaesthetised, the base of an L-shaped metal rod was attached to the head and the thorax by a globule of dental adhesive (shade modification, SDI), which was cured using high intensity blue light (radii plus, SDI). Whilst this globule occluded the ocelli, this is unlikely to have affected the bee's behaviour as the ocelli have a low spatial resolution (Goodman, 2003) that would be unlikely to detect the movement of the grating used in this assay. Adhesion to the tether was facilitated by gently shaving the hair on the notum using a scalpel.

Antennal manipulations were performed after tethering whilst the bee was still anaesthetised. In the case of amputation, the antennae were cut close to the base using a pair of surgical scissors (Figure 2-3D). Waxing of the antenna was performed using dental wax applied with a hand cauteriser (Change-A-Tip Deluxe Cautery Kit, Bovie Medical Corporation). The antenna was positioned such that the two segments, the flagellum and the scape were approximately at right angles (their normal orientation), and the hot wax was touched lightly to the joint. The wax wicked into the pedicle joint, and also across the flagellum; the success of immobilization was tested by gently attempting to bend the antenna with a pair of forceps (Figure 2-3C and E). The integrity of the waxing was tested both before and at the conclusion of the experiments, and honeybees were rarely found to have removed the wax (those that had were not included in the analysis). Honeybees undergoing this preparation still exhibited the proboscis extension reflex, a gustatory response to sugar water touched to their antenna, suggesting that the antennal nerve was still intact. In experiments with manipulated antennae, bees were generally more reluctant to fly, and those with waxed Johnston's organs often tried to groom the wax off.

Tethered honeybees were housed in a Styrofoam box placed on a heater, which maintained the temperature at 28 to 30 ^{o}C. A beaker of water, placed inside the box, provided an environment with the appropriate humidity. Insects typically recovered from anaesthesia after several

minutes in the humid box, and were then fed with several drops of 1 mol.L^{-1} sucrose solution, and had were given least 30 minutes to recover before their first flight.

2.4.3 Visual stimulus display and generation

Images were displayed on four 22" monitors (2209WAf, Dell) arranged in a diamond shaped arena, which provided a near panoramic virtual environment. The tethered insect was positioned in the centre of the arena by attaching the tether to a clip, which was held in the arena by an articulated arm (MA61003, Noga), with the bee's head facing a corner of the arena. The LCD monitors were driven by a computer (Intel i7 CPU (4 cores at 2.67 GHz), 2.5 GB RAM, Windows XP SP 3), with two dual headed NVIDIA GeForce GTX 260 video cards. The monitors were configured to use 1680x1050 pixel resolution at a 60 Hz update rate. The dimensions of the monitor screens were 475x300 mm, and the diamond arrangement covered approximately 61^o of the tethered honeybee's vertical visual field at the closest points and 45^o at the corners (both full angles). The black plastic frames of the monitors prevented full 360^o coverage of the insect's azimuthal visual field, leaving four gaps, each approximately 3^o wide, in the front, the rear, and the two sides.

As shown in Figure 2-1, the computer monitors provide panoramic visual stimulation in the horizontal plane, with non-stimulated areas in the dorsal and ventral view fields. Whilst not entirely true to the world an insect would observe in natural flight, the apparatus was designed to replicate the stimulus used in Luu et al. (2011) as closely as possible (the monitors are 2" smaller), to enable a direct comparison of the role of air speed in modulating the visually mediated streamlining response discovered in that study. The response to visual motion alone (at 0 m.s^{-1}, Figure 2-2A) saturates at approximately 10 ^{o}.s^{-1} lower than that observed in the previous study, but is otherwise qualitatively similar. This suggests that the smaller monitors, and areas of the monitor occluded by the fan for air flow generation (described in the following section), may have slightly reduced the strength of the visual input in stimulating the response. The visually evoked component of the streamlining response has previously been found to be the result of a non-linear spatial summation of optic flow seen across all angles of elevation (Luu et al., 2011) (within ±23^o of the insects transverse plane), and so including stimulus in the dorsal and ventral view fields may not have any substantial effect, as the response is already close to saturation.

A custom written C++ program was used to generate the visual display. This display was similar to that used by Luu et al. (2011), where motion was simulated along an apparently infinitely long tunnel of user-selectable width, displaying red and white sinusoidal gratings on the inside walls, with a spatial frequency of 0.014 cycles.degree^{-1}. At the maximum optic flow used (600 ^{o}.s^{-1}) the 60 Hz update rate resulted in images 'stepping' at 0.14 cycles.frame^{-1}. For a honeybee flying along a virtual tunnel, the maximum image velocity as experienced by the eyes occurs in the lateral viewing direction, i.e. in a viewing direction at 90^{o} to the direction of flight. The values of optic flow shown in the graphs correspond to the values pertaining to this viewing direction.

2.4.4 Air flow generation

Air flow, or simulated wind, was generated by two fans (TurboFan 12VDC 40x28MM 20000RPM, NMB Technologies Corp.) connected in series, which blew wind through a square shaped wind tunnel that incorporated a honeycombed cross section to reduce the turbulence of the flow. The end of the tunnel was approximately 140 mm in front of the insect, and subtended 22^{o} (full angle, vertically and horizontally) of the honeybee's frontal field of view. Whilst this is a sizable portion of the insect's visual field, we do not believe that its presence would have affected the visually-driven component of the streamlining response, as the frontal visual field has been shown to have minimal influence on insect's streamlining response (Luu et al., 2011), and also flight speed regulation (Baird, Kornfeldt, & Dacke, 2010).

The speed of the fan was controlled by a pulse width modulated (PWM) signal, and an anemometer measured the air speed. The PWM signal was generated by a USB data acquisition (DAQ) module (U3-HV, Labjack) which was controlled in real time by a program running on the PC. The DAQ module also acquired data from the anemometer positioned behind the insect (EE-65VB, E+E Elektronik Ges.m.b.H). The PWM signal versus air speed relationship was calibrated by placing the anemometer at the insect's usual flight position and measuring the air speed. The PWM required for a desired air speed was then found by interpolating between the calibration points. Turbulence, measured as the standard deviation of the air speed over a time interval of thirty seconds, increased in absolute value as the air speed increased, whilst the ratio of the standard deviation to the mean air velocity remained at approximately 5% for air speeds up to 5 m.s^{-1}. The airspeed was held constant during any given experimental trial (during which the optic flow was varied systematically).

Initial experiments showed that honeybees exhibited a hysteresis-like effect when exposed to different air speeds. Further investigations revealed that the order of presentation of air speed was significantly affected the honeybees response, whereas there was no variation dependent on the order optic flow was presented (Section A.1). To avoid this confound, individual bees were only stimulated with a single constant air speed during their test in the arena (excluding the transient ramps up and down at the start and end of the test protocol). For any given trial, the air speed was assigned randomly; hence measurements of data at different air speeds are independent.

2.4.5 Data acquisition and image analysis

A camera (FireFly, Point Grey) filmed the side view of the bee (perpendicular to the simulated direction of flight, at 30 fps) against a piece of white paper (80x80 mm, placed at the opposite corner of the stimulus arena from the camera). Video frames were recorded with a time stamp linked to the stimulus. The orientation of the honeybee's abdomen was measured in real time for each frame using a custom written C++ program written in-house. The program tracked the axis of the insect's abdomen, and found its angle relative to the user-defined orientation of the thorax. This was defined as the 'abdomen angle' or 'response'. Examples of abdomen tracking are shown in Figure 2-1D and E. The response was defined to be positive or negative, according to whether the abdomen was elevated or depressed relative to the axis of the thorax. The abdominal angles reported throughout this study are of the honeybee's steady-state response to each of the six stimulus speeds. The steady-state response was calculated as the mean abdominal angle measured during the last 5 s of each 10 s epoch of stimulus speed. Typically, the abdominal response reached a steady state within 1–3 s following the presentation of each new stimulus speed.

2.4.6 Statistical analysis

All statistical analyses were performed using IBM SPSS Statistics V20. Main effects were tested using ANOVA. Prior to conducting ANOVA, we conducted tests of normality, homoscedasticity and sphericity. The vast majority of data was normally distributed, but failed tests of homoscedasticity and sphericity. Sphericity was corrected using the Greenhouse-Geisser correction, and we discuss the effect of heteroscedasticity on our analysis in Section A.4, as well as providing full details of all statistical tests. Flight data from bees were included

for analysis only if the bees flew continuously through the entire optic flow ramp. Four to six trials were conducted per bee to reduce inter-animal variability, and data points from multiple flights of an individual bee were averaged.

2.4.7 Flight protocol

For each flight trial, a tethered honeybee was removed from the humid box and placed in the centre of the arena and allowed to hold a small piece of waxed paper. As soon as the visual stimulus and air flow commenced, the paper was removed from the honeybee's grasp and the tarsal reflex initiated flight. At the end of each flight the bee was returned to the humid box and offered several drops of 1 mol.L^{-1} sucrose solution. Animals were rested for at least 20 minutes between consecutive trials. We used a stimulus protocol that simulated flight at a progressively increasing flight speed, namely, 100, 200, 300, 400, 500, and 600 $^{o}.s^{-1}$. Each epoch of stimulus speed was 10 s in duration, thus each trial lasted 60 s. Air flow was started prior to the start of visual motion, and was maintained at a constant level through each trial.

2.5 Results

The effect of combined air speed and optic flow stimulation on the orientation of the honeybee's abdomen was investigated by placing tethered honeybees in a flight arena (Figure 2-1A, B and C), based on the design of Luu et al. (2011), who found that honeybees did not exhibit a streamlining response when no visual motion was displayed (0 $^{o}.s^{-1}$ optic flow). Our initial observations confirmed that, regardless of air speed, bees would not fly reliably nor hold a stable abdomen position when no visual motion was shown in the front-to-back direction. (Occasionally, the abdomen would be raised at the onset of flight, but would then drop to a non-streamlined position, after which flight would cease). Because of this, we did not include the speed of 0 $^{o}.s^{-1}$ in our optic flow test protocol.

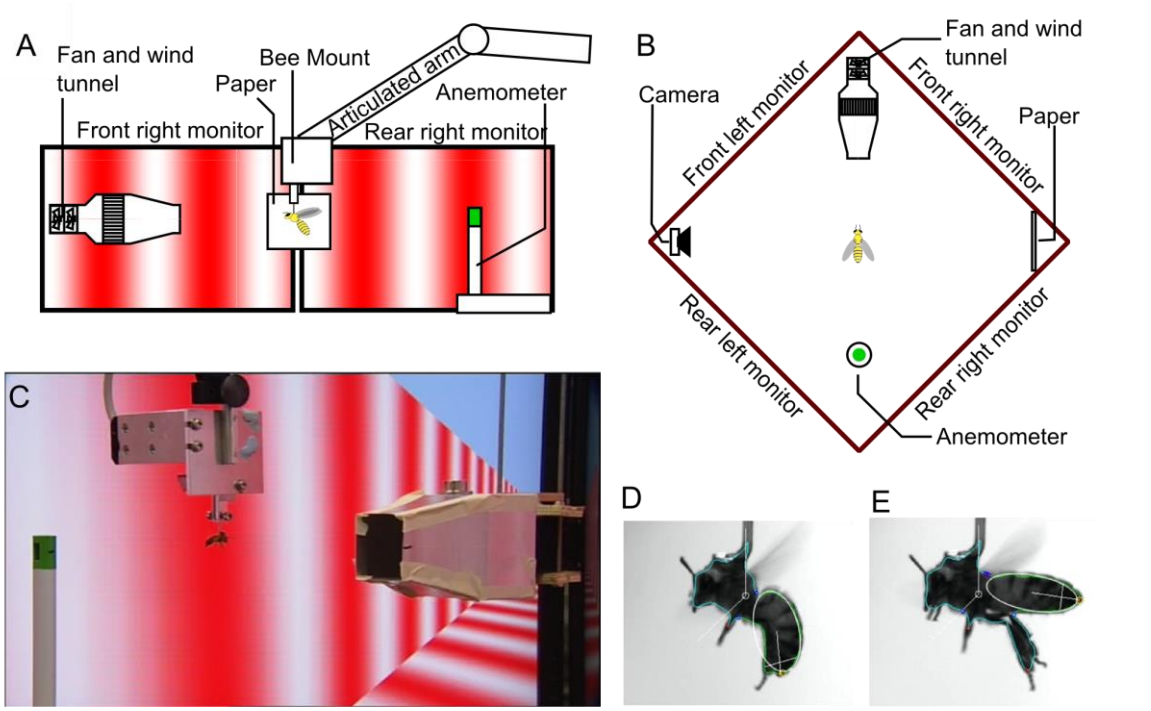

Figure 2-1: Overview of the tethered flight arena. **A**, schematic side view of flight arena, from the camera's perspective. **B**, schematic top view of flight arena (schematic bees are not to scale). **C**, photo of a tethered honeybee in flight taken from the position of the rear right monitor. **D**, image of honeybee with a lowered abdomen. **E**, image of honeybee with a raised abdomen. D and E are representative of video images used for analysis. The white ellipses depict the results of automatic image-based segmentation of the insect's abdomen and determination of its orientation, as described in Section 2.4.5.

2.5.1 Abdominal response to a combination of air speed and optic flow stimuli

In a first set of experiments, we investigated the strength of the streamlining response that was evoked by various combinations of headwind and optic flow. These experiments revealed that, in addition to visual motion, air flow plays an important role in driving the honeybee's streamlining response. Tethered honeybees flying in the arena display their characteristic streamlining response to optic flow, as described in Luu et al. (2011). We find, however, that this visually induced response is modulated by wind. Specifically, the range of the visually evoked response decreases as the air speed is increased (Figure 2-2A). The reason for this is that when the insect is stimulated with air flow, the abdomen is generally raised further, having the overall effect of making the animal more streamlined (Figure 2-2D). The variation of the response with air speed for any fixed velocity of the visual stimulus (Figure 2-2D) indicates that the abdomen angle does not increase monotonically with air speed – it shows both a local minimum and a maximum before plateauing. Air speed appears to account for a greater range

of the response than optic flow: at low optic flow (100 $^{o}.s^{-1}$), the abdomen pitch varies over a range of ~45^{o} in response to variation of air speed (Figure 2-2A - black arrow). In contrast, in the 'no wind' condition the abdomen pitch changes only over a range of ~25^{o} in response to the variation of optic flow (Figure 2-2D - black arrow).

Statistical analysis of the data in Figure 2-2A and D using ANOVA (Section A.4.1) showed a significant effect of optic flow ($F_{1.6,147.3}$=141.39, ***p*<0.001**), as well as air speed ($F_{8,95}$=6.35, ***p*<0.001**), and an interaction between the two variables ($F_{12.4,147.3}$=4.89, ***p*<0.001**) on abdominal pitch. Figure 2-2A shows that as the air speed increases, the dependence of the response on optic flow decreases (explaining the interaction effect observed), however, regardless of optic flow level, the response shows a strong dependence on air speed (Figure 2-2D). Beyond 400 $^{o}.s^{-1}$, *post-hoc* tests show that there is no significant difference in abdomen position, confirming that the response has indeed saturated (this saturation level varies between 300 and 500 $^{o}.s^{-1}$ for the antennal manipulation cases described in the following section, but is qualitatively similar across all antenna conditions, (Sections A.4.1 to A.4.3). Air speeds were divided into four different groups by *post-hoc* tests. First, the global response minimum occurs in the 'no wind' condition. This is followed by a local maximum at 0.5 $m.s^{-1}$ (the response of this depends heavily on the optic flow interaction), which is succeeded by a local minimum centred at 1.5 $m.s^{-1}$, before the response plateaus beyond 2.5 $m.s^{-1}$.

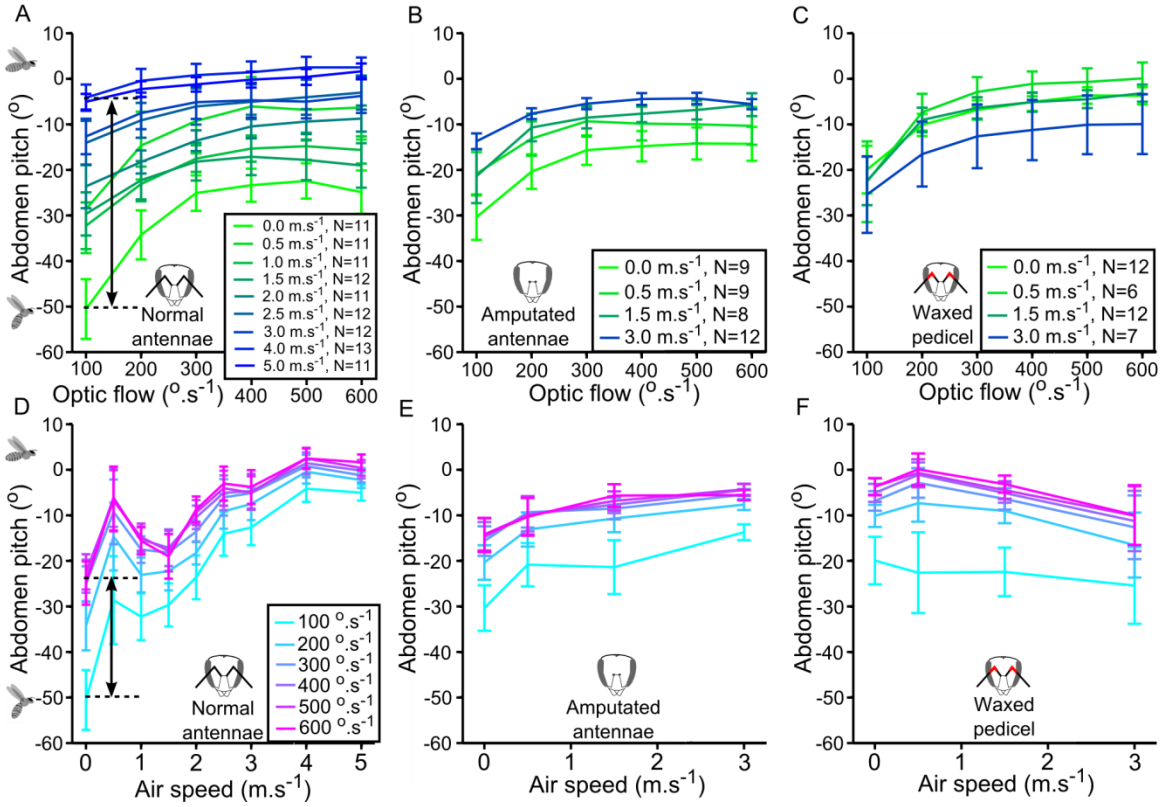

Figure 2-2: The abdomen pitch in honeybees depends on optic flow and air speed. Plotted as a function of optic flow with air speed as a parameter (A, B and C), and as a function of air speed with optic flow as a parameter (D, E and F). Note that honeybees would not fly reliably at 0 $^{o}.s^{-1}$ optic flow; hence this data point is omitted. **A** and **D** represent data from intact bees. **B** and **E** represent data from bees with amputated antennae. **C** and **G** represent data from bees with waxed pedicels. The legends in A, B and C show the sample size of bees tested at each airspeed, for a particular antenna condition. The legend in D is used for E and F. Error bars show ± S.E.M.

2.5.2 Manipulation of the antennae

The antennae, and specifically the Johnston's organs (the mechanosensors that detect movement of the flagellum; Goodman, 2003) located in the antenna's pedicle joint (Figure 2-3F), have previously been reported to provide honeybees (Heran, 1959) and other insects (Taylor & Krapp, 2007) with a measurement of air flow in flight. To examine whether these receptors provide a bee with information to regulate its flight posture, we performed two manipulation experiments, firstly, amputation of the antenna (Figure 2-2B and E), and, secondly, immobilization of the antennal pedicle with wax (Figure 2-2C and F). The abdominal responses of manipulated insects, exposed to three different air speeds: 0.5, 1.5 and 3 $m.s^{-1}$, as well as to the 'no wind' condition, were measured for comparison with the intact controls. This reduced set of air speeds were selected as the points of interest from the responses of the un-manipulated honeybees to air flow, as they represented the global minimum (0

$m.s^{-1}$), the local minima (1.5 $m.s^{-1}$), the local maximum (0.5 $m.s^{-1}$), and a point well into the saturated region of the response curve (3 $m.s^{-1}$). We hypothesized that if the antennae were responsible for the measurement of air speed, then there would be a difference between the responses of the treated animals and the untreated controls, especially at these points of interest in the original curve.

Neither the amputation of the antenna, nor waxing the pedicle appeared to affect the basic characteristics of the honeybee's response to optic flow – the response continued to increase monotonically (Figure 2-2B and C). Unexpectedly, however, at low to intermediate air speeds (0, 0.5 and 1.5 $m.s^{-1}$) the response versus optic flow profiles of the manipulated honeybees were generally *higher* than those of the controls. Furthermore the local minimum that is clearly present at an air speed of 1.5 $m.s^{-1}$ in the responses of the control animals (Figure 2-3A) was no longer evident in the manipulated animals. ANOVA tests (Sections A.4.2 and A.4.3) to examine the influence of air speed on abdomen pitch showed no significant effect in the case of the waxed pedicels ($F_{3,33}$=0.72, p=0.546), and a weak effect in the case of the amputated antennae ($F_{3,34}$=3.11, $\boldsymbol{p}$**=0.039**). Thus, the change in abdomen position in response to wind is removed or reduced in the manipulated bees. In both types of manipulation, the effect of optic flow remained similar to non-manipulated bees, whilst the interaction between air speed and optic flow was removed. This indicates that antennal manipulation removes or reduces wind-induced variation of the response.

When comparing normal honeybees with the groups of bees that had been subjected to the two kinds of antennal manipulation, we found a significant effect of antennal manipulation at 0 and 1.5 $m.s^{-1}$ air speed, but not at 0.5 and 3 $m.s^{-1}$ air speed (Figure 2-3E). *Post-hoc* testing showed that both antennal manipulation conditions were significantly different from the control at the former air speeds (Section A.4.4). The reason for these differences in the manipulated animals is that the responses in the no-wind condition and at 1.5 $m.s^{-1}$ are stronger than in the intact controls. This finding implies, surprisingly, that under no-wind conditions and at intermediate air speeds, the input from the antennae *inhibits* the abdominal pitching that is observed in normal honeybees.

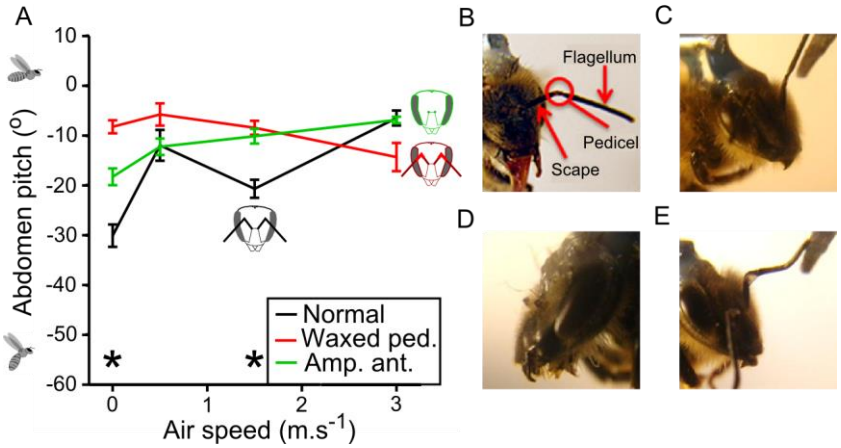

Figure 2-3: Comparison of honeybee's abdomen response across various experimental conditions. **A**, comparison showing the mean response across all optic flow levels at each air speed, for all conditions. A star (*****) denotes a significant difference between normal bees and both manipulations at the indicated air speed. Error bars show ± S.E.M. The sample size for each air speed and antenna condition are noted in the legends in Figure 2-2A, B and C. **B**, antenna morphology. **C**, flexibility of non-waxed antenna. **D**, amputated antennae. **E**, illustration of immobilisation and lack of flexibility of waxed pedicel joint.

2.5.3 Response to a tail wind

In a second set of experiments, we investigated how tethered honeybees respond to a tail wind by positioning the fan behind a tethered bee in the arena, and conducted experiments similar to those in the antennal manipulation case (at air speeds of -0, -0.5, -1.5, and -3 $m.s^{-1}$, corresponding to the points of interest in the positive air speed response). At these negative air speeds, bees still displayed their characteristic streamlining response to the visual stimulus (Figure 2-4). The responses at -1.5 and -3 $m.s^{-1}$ were close to the baseline 'no wind' condition, whilst the response at -0.5 $m.s^{-1}$ was slightly elevated. Overall the bees exhibited a reduced response to negative air speeds. ANOVA testing revealed that, with tail winds, the streamlining response depends weakly on airspeed ($F_{3,32}$=3.10, ***p*=0.041**), with significant differences being observed between the response at -0.5 and -1.5 $m.s^{-1}$ (Section A.4.5).

Whilst the observed response to a tail wind is clearly different from a honeybee's response to a head wind, it is not clear if this is because the honeybee is unable to sense the air speed (because its antenna are occluded by its body), or could sense the air flow, either with its antenna or with other sensory organs, and chooses not to respond. However, the results indicate that the streamlining response is functionally asymmetrical, with the response at positive air speeds differing from the response at negative air speeds, much as the streamlining response to optic flow (Luu et al., 2011).

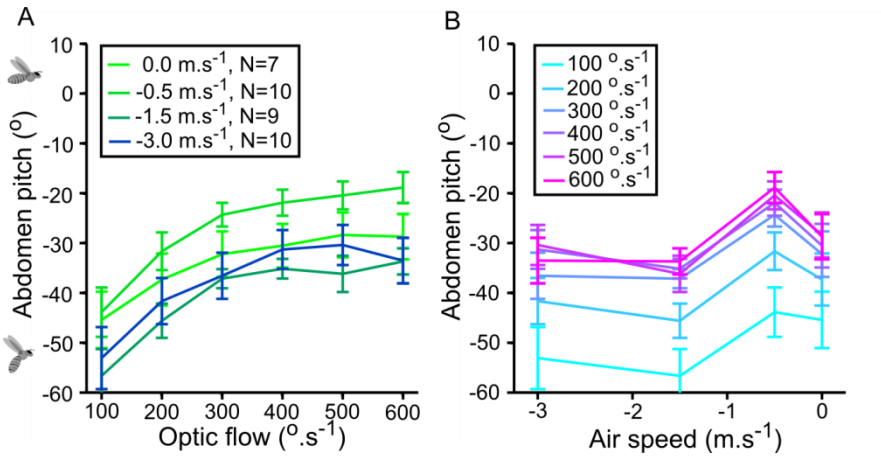

Figure 2-4: Response to a tailwind. Plotted as a function of optic flow with air speed as a parameter (**A**), and as a function of air speed with optic flow as a parameter (**B**). The box in A shows number of bees tested at each air speed. Error bars show ± S.E.M.

2.5.4 Invariance of the streamlining response to thorax orientation

During natural flight honeybees reorient their entire body as their flight speed increases (Nachtigall, Widmann, & Renner, 1971). In this situation, the head, thorax and abdomen are rotated forwards relative to the flight path, but the thorax–abdomen angle (which we describe as abdomen pitch in this study) remains relatively constant. Such a rotation would change the angle of the insect's head and the sensory structures on it, relative to the oncoming optic flow and air flow, which in this study are directed horizontally. To test if the angle of the thorax affected the abdominal pitch response to optic flow and air speed, we conducted experiments where bees were tethered with the thorax pitched up, simulating slow or hovering flight, and the thorax pitched down, a position that is not assumed during normal flight. These results were compared to those obtained for the usual experimental paradigm where bees were tethered with their thorax at 0°, simulating fast flight. These angles are of the thorax relative to the horizontal, and are analogous to the body angle measured for free flying insects (although in free flight the abdomen is usually held in line with the thorax). The effects of air speeds that would elicit a low, intermediate, and strong streamlining response were tested, these air speeds being 0, 1.5, and 3 $m.s^{-1}$ respectively.

The thorax angle of bees could only be set by changing the angle they were glued relative to the metal tether; it was not possible to adjust this during or between experiments. The insects often refused to participate in experiments if they were anesthetized a second time, and because of this, separate bees were tested for each thorax orientation. The average thorax angle of bees

with their thorax pitched down was -33 ± 4.6^{o}, and the average with their thorax pitch up was 36 ± 5.3^{o}. In addition, we used data collected with the thorax pitch horizontal (2 ± 4.2^{o}) from the standard experiments described in Chapter 2. Notably, bees with their thorax pitched down were very reluctant to fly (even more so than when antennal manipulations were performed); indeed, the flight attitude appears very unnatural (Figure 2-5). In these experiments the bees were only tested at a single air speed because there was an effect of presentation order on the response to air speed, as described in the following section.

Bees with their thorax pitched up show a similar response (Figure 2-5A and D) to optic flow and air speed, as do normal bees (Figure 2-5B and E). Increasing strengths of optic flow and air speed both act to increase the response, and they appear to interact via a non-linear, saturating function. Both main effects (air speed ($F_{2,25}$=11.10, ***p*<0.001**) and optic flow ($F_{1.6,41.0}$=28.31, ***p*<0.001**)), and their interaction ($F_{3.3,41.0}$=4.49, ***p*=0.007**), are significant (Section A.4.6). Furthermore, there is no statistical difference between bees in this condition and bees with their thorax tethered horizontally, neither as a main effect of tethering angle ($F_{1,57}$=0.17, p=0.678), nor as an interaction with any other factors (Section A.4.6). Hence, it appears that at the upper and lower limits of thorax angles that a bee might assume during natural flight (at the three wind speeds tested), the streamlining response persists, regardless of thorax angle. Because thoracic reorientation also rotates the honeybee's head, this implies the streamlining response is invariant to the perceived direction of optic flow and air movement (and also the direction of gravity) for head orientation angles between 0^{o} and 36^{o}.

Conversely, honeybees with their thorax pitched down show a qualitatively different behaviour (Figure 2-5C and F); noticeably, optic flow no longer acted to steadily increase the abdomen pitch to a plateau point. In fact, for all three air speeds, the response relative to optic flow reaches a peak value before the maximum optic flow rate tested, after which it begins to decrease. Furthermore, the responses at 0 and 1.5 m.s^{-1} air speed overlap substantially, suggesting that the response to air speed is also modified by pitching the thorax down. ANOVA shows there is no longer a significant main effect of optic flow ($F_{2.9,47.0}$=1.58, p=0.208), although it continues to interact with air speed ($F_{5.9,47.0}$=2.8, ***p*=0.021**), which does itself have significant main effect ($F_{2,16}$=8.19, ***p*=0.004**; Section A.4.7). Honeybees flying with their thorax pitched down are in a distinctly un-natural position, and it is perhaps unsurprising their response is fundamentally different.

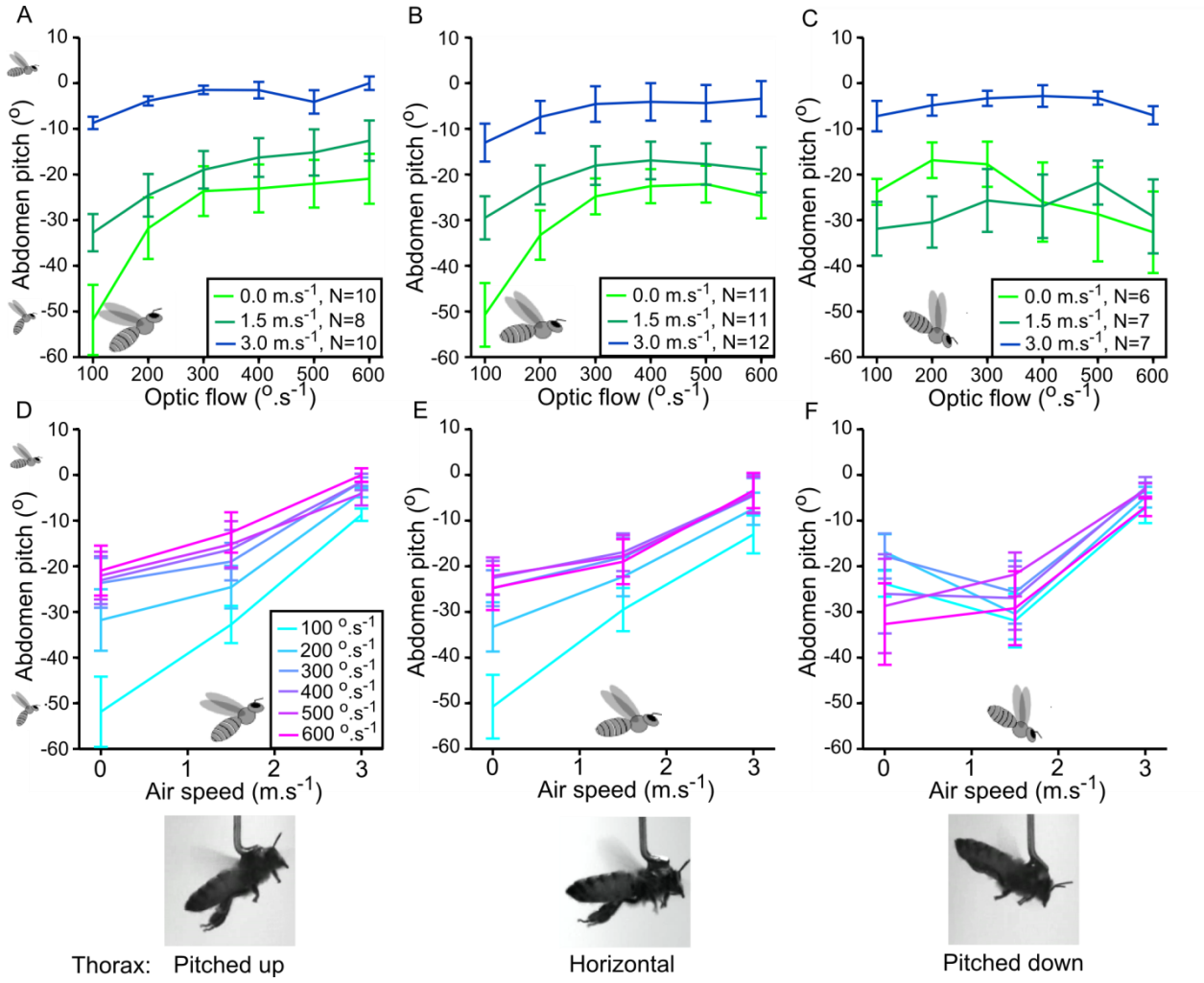

Figure 2-5: The honeybee's abdomen response when tethering angle of the thorax is varied. The response is plotted as a function of optic flow with air speed as a parameter (A, B and C), and as a function of air speed with optic flow as a parameter (C, D and E). **A** and **D** represent data from bees with their thorax pitched up. **B** and **E** represent data from bees with a horizontal thorax (re-plotted from Figure 2-2). **C** and **F** represent data from bees with their thorax pitched down. The legends (A, B and C) show the sample size of bees tested at each airspeed, for a particular thorax pitch. The legend in D is also used for E and F. The image at the bottom of the figure show representative images of bees at different thorax tethering angles, flying in a 3 $m.s^{-1}$ air stream. Error bars show ± S.E.M.

2.5.5 Passive lifting by air flow

It is possible that airflow from the fan acted to lift the abdomen passively, by causing a pitching moment about the thorax-abdomen joint (generated by aerodynamic force against the abdomen), to pivot it into a streamlined position. For this to occur, the aerodynamic pitching moment would have to exceed the opposing moment caused by the weight of the abdomen itself. Since aerodynamic forces increase as the square of the wind velocity, high air speeds could exert an appreciable force against an insect's abdomen.

The effect of drag force on passive abdomen lift was investigated by using honeybee bodies that would experience the same drag forces as living bees. Honeybees were collected from the same hive as the insects used in the other experiments. They were tethered as usual, and then euthanized by amputation of the head capsule before they had recovered from the cold anaesthesia. The thorax and abdomen were immediately tested using air speeds of 0, 1, 2, 3 and 4 $m.s^{-1}$. Prior to testing, the abdomen was manually positioned at approximately -90°, which should have exposed it to the maximal possible drag force for a given air speed. Reflexive motions of the legs were observed for up to an hour after decapitation, indicating that rigor mortis had not set in.

The results indicate that air flow over the abdomen of deceased bees causes a small increase (several degrees) in the abdomen posture (Figure 2-6). In addition to aerodynamic forces, the thoracic ganglia could have caused abdominal motion either randomly, or based on information from air speed sensing organs on the body that projected directly to it, and these motions would have been combined with those caused by external forces. However, ANOVA (Section 0) showed no significant effect of air flow ($F_{4,34}$=0.83, p=0.517) on abdomen posture, and the range of the response exhibited by live flying bees far exceeded that of the decapitated insects, even at the lowest speed of optic flow (Figure 2-6). The aerodynamic forces clearly play a minor role in lifting the abdomen and the streamlining response to air speed is a primarily active response.

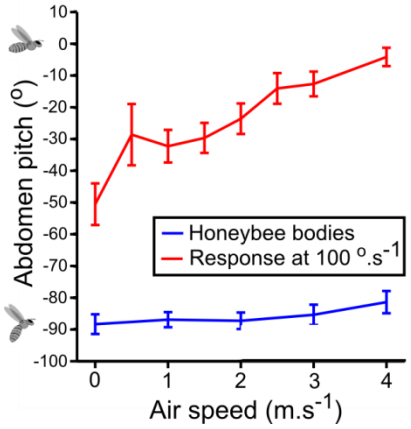

Figure 2-6: Passive forces acting on the abdomen. The effect of air speed on the abdomen pitch of deceased honeybee bodies, compared to the response of live tethered honeybees experiencing an optic flow of 100 $°.s^{-1}$ (the lowest optic flow condition). N=7 deceased bees. Error bars show ± S.E.M.

2.5.6 A model of the interaction between air speed and optic flow

Previous investigations of other flight control behaviours that are driven by visual as well as mechanosensory stimuli in *Drosophila* (Sherman & Dickinson, 2004) and *Manduca* (Hinterwirth & Daniel, 2010) have documented multimodal responses that can be accurately characterized as a linear, or weighted linear, summation of the visual and mechanosensory components of the response. We examined whether the abdomen response to the optic flow or to the wind could each be described by an input-output relationship that involved a saturating nonlinearity (Figure 2-7A and B). It was found that, in each case, the input versus output data were well fitted by a variable slope sigmoidal equation (Gibson, 1950), using least squares nonlinear regression (Figure 2-7F and G). Details of all models are in Section A.2.1.

How do optic flow and wind interact to generate the streamlining response? If the net response is a linear summation of the individual response to each stimulus, then it should be possible to predict the response to the combined stimuli by summing the (saturating) response to each stimulus. For example, it should be possible to predict the response to optic flow at 100 $^{o}.s^{-1}$ and an air speed of 5 $m.s^{-1}$ from the response to an optic flow at 100 $^{o}.s^{-1}$ (with zero air speed), and the response to wind at 5 $m.s^{-1}$ (with zero optic flow). However, when the two saturating responses are combined as a linear summation (Figure 2-7C), the result substantially overshoots the measured response for combinations of the two stimuli (Figure 2-7I and J).

A weighted sum of the two original saturating responses was also tested (Figure 2-7D). The optimal weightings for both saturation functions were found using a least squares fit across the entire response surface; optic flow was weighted by a factor of 0.45 and air speed by a factor of 0.74 (Figure 2-7D, G_1 and G_2 respectively). Whilst this weighted sum was found to perform well at predicting the air speed response curve for low and high optic flows (Figure 2-7F and I), it was less successful at predicting the entire response versus optic flow curve. Notably, the *range* of the optic flow response decreases between the 0 and 5 $m.s^{-1}$ air speed conditions, which is not captured by the weighted sum model (Figure 2-7G and J).

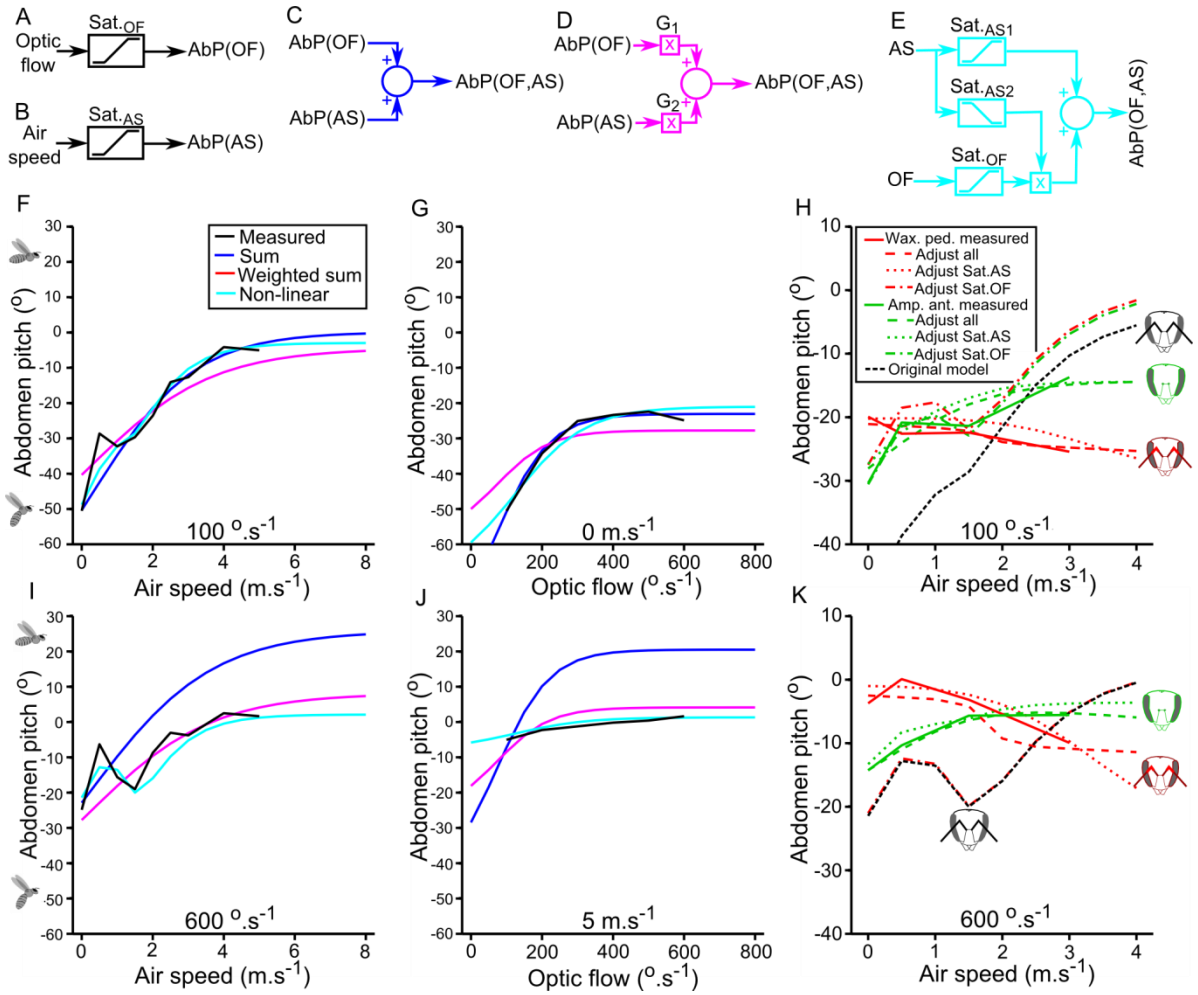

Figure 2-7: Model predictions of the abdomen pitch. Model types shown: **A** and **B**, abdomen pitch response as a function of each stimulus; **C**, Linear summation; **D**, linear weighted summation; **E**, non-linear combination. F, G, I and J, show response comparisons for all models at the boundaries of the measured response surface: **F**, response vs. air speed at 100 $^{o}.s^{-1}$ optic flow (the legend in this plot is used for F, G, I and J); **G**, response vs. optic flow at 0 $m.s^{-1}$ air speed; **I**, response vs. air speed at 600 $^{o}.s^{-1}$ optic flow and **J**, response vs. optic flow at 5 $m.s^{-1}$ air speed. H and K, response comparison of non-linear model refit to data from antenna manipulated bees, at low and high optic flow boundaries of the response surface (Model details and plots at the low and high air speed boundaries are shown in Section A.2.2). Some model parameters are refit (separately for each type of antennal manipulation), whilst others are held at the same values as those found for non-manipulated bees: **H**, response vs. air speed at 100 $^{o}.s^{-1}$ optic flow (the legend in this plot is used for H and K) and **K**, response vs. air speed at 600 $^{o}.s^{-1}$ (note that the curve for Adjust $Sat._{OF}$ for both manipulations overlap the curve for the original model). Abbreviations: AS – air speed, OF – optic flow, AbP – Abdomen pitch, G – Gain. Details of all model parameters are given in Section A.2.

Finally, the response was modelled as a non-linear combination of the two stimuli. Whilst there are many possible ways in which these responses could be combined nonlinearly, we found that a linear summation of the saturating response to each of the two stimuli, in conjunction with an interaction in which the magnitude of the response to optic flow was modulated by the

air speed (as shown in Figure 2-7E), was able to predict the observed ranges of the responses to the two stimuli, either in isolation or in combination (see Figure 2-8D and E). To modulate the optic flow response by air speed, a saturating function of air speed, $Sat._{AS2}$ (Figure 2-8B) was used to adjust the gain along the optic flow pathway, $Sat._{OF}$ (Figure 2-8C). While the output of $Sat._{AS1}$ (Figure 2-8A) increases as the air speed is increased, the output of $Sat._{AS2}$ decreases with increasing airspeed (Figure 2-8C). This interaction can be viewed as a gain control that is exerted by the airflow sensing pathway on the optic flow sensing pathway, in which the gain of the optic flow pathway is progressively reduced as the air speed increases. This postulated interaction successfully predicts the peak that is consistently observed at 0.5 $m.s^{-1}$ in the response to variation of air speed (Figure 2-7I), which arises from slight differences in the thresholds and slopes of the saturating functions $Sat._{AS1}$ and $Sat._{AS2}$.

A summary of the model, showing the block diagram and the exact profiles of the three nonlinearities is shown in Figure 2-8. This figure also shows a comparison of the experimentally measured two-dimensional response surface (Figure 2-8D) with that predicted by the model (Figure 2-8E). This model is designed to predict the response for positive air speeds and optic flows, the standard flight conditions for a honeybee.

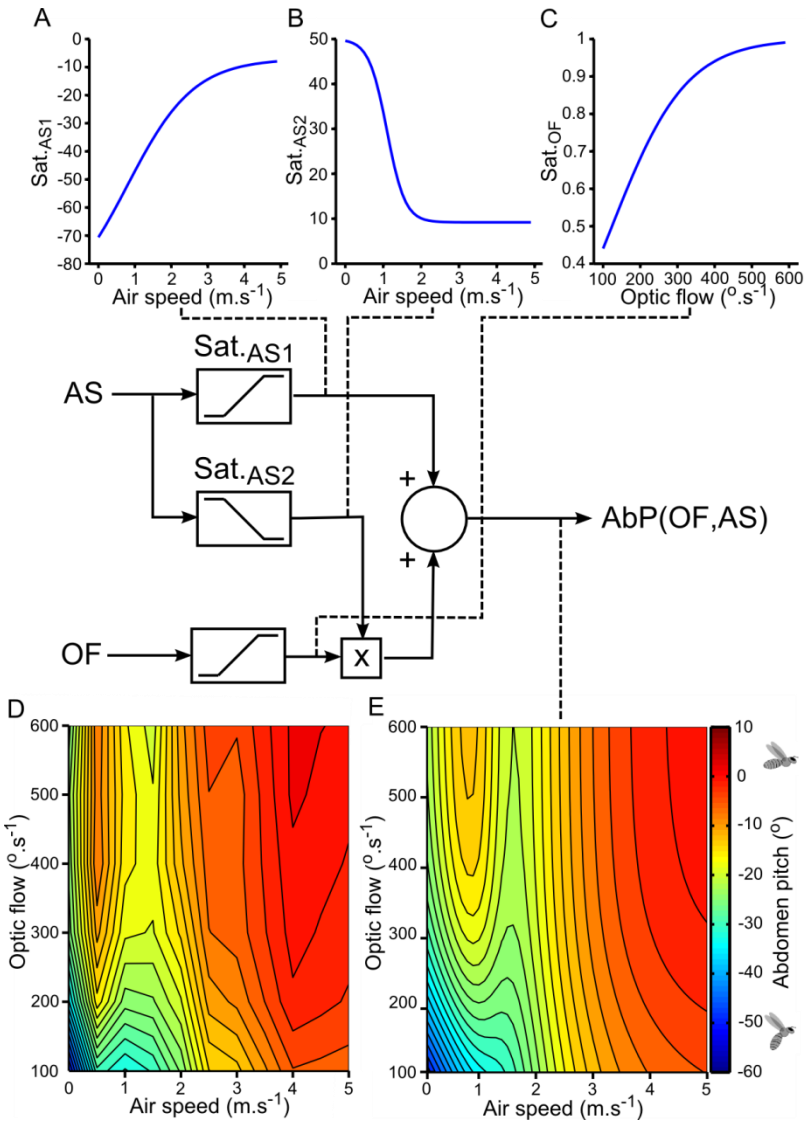

Figure 2-8: Model describing the non-linear interaction of air speed and optic flow. The plots indicated by dashed lines show the input-output relationships at various stages of the model. **A**, response to air speed. **B**, modulation of gain of the optic flow path way by air speed. **C**, response to optic flow. **D**, measured response surface. **E**, predicted response surface. Abbreviations: AS – air speed, OF – optic flow, AbP – Abdomen pitch. Model details are shown in Section A.2.1.

2.5.7 Streamlining in the absence of antennal information

Whilst this model captures the response of normally tethered honeybees, can one predict the honeybees' streamlining responses when they are deprived of air flow information from their antennae? From Figure 2-2 and 2-3 it is clear that whilst both antennal manipulations are significantly different from the control case, the response is also modulated by air speed to some extent, which in the case of antenna amputated bees is significant. From this, we might assume that streamlining is not only driven by optic flow following these manipulations, but

that the honeybee receives some measure of air speed from other sensory organs that would usually be combined with information from the antenna.

If all model parameters are refit (Section A.2.2), then the model is able to predict the bee's response to air speed after *either* type of antennal manipulations (Figure 2-7H and K, and Figure A-3). Notably, different model fits are required to capture the observation that streamlining is increased at high air speed when the antennae are amputated, but decreased at similar air speeds when the pedicels are waxed. It turns out that in both cases the response range, or gain, of both saturating functions is reduced (Table S2-1), which might be expected given that the honeybee's primary air speed sensor has been disabled. However, it is surprising that bees react differently to the two different manipulation cases, given that the same sensory information has been removed (waxing a honeybee's pedicel has been shown to completely remove any response to air speed from the antennal nerve, which would otherwise be present in intact antennae (Heran, 1959)). In both cases, they would presumably have the same remaining alternate, but unknown, mechanisms of sensing air speed. If the sensory systems are the same and the outputs are different, but our model can still predict the outcome, then it appears that the manipulated bees must have used different weightings at the neural level for combining the two sensory modalities. We comment on this further in the Section 2.6.

To further elucidate how honeybees made adaptations to use what air speed sense they had remaining after antennal manipulation, we tested if some model parameters could be held constant, at the level that fit the data for normal honeybees, whilst others were refit. In brief, if only the parameters in both saturating functions to air speed ($Sat._{AS1}$ and $Sat._{AS2}$) are allowed to vary, the model can be fit nearly as well as when all parameters are adjusted (Section A.2.2). Conversely, if only the parameters in the saturating response to optic flow ($Sat._{OF}$) are allowed to vary, the fit is qualitatively no better than the unadjusted model (Figure 2-7H and K, and Figure A-3). Further, if the terms in only one of $Sat._{AS1}$ or $Sat._{AS2}$ are recalculated, relatively good model fits are achievable, but they fail to capture the decrease in abdomen pitch at high air speeds and low optic flow rates for pedicel waxed bees (Figure A-3). Nevertheless, the model captures most of the observed response, particularly for the antennal amputation. In all cases, there is considerable flexibility in using this model to explain the behaviours that are observed under all of the experimental conditions (Table A-1).

2.6 Discussion

Our findings show that honeybees measure both air speed and optic flow to actively control their abdominal angle during tethered flight. The response to wind is asymmetrical, showing that honeybees differentiate between head and tail winds. This is in concordance with the effect of optic flow, which is also asymmetrical; honeybees respond by elevating their abdomen to progressive optic flow but not to regressive flow (Luu et al., 2011). Given the relatively small movements of the abdomen that are observed in tethered honeybee bodies, it seems likely that the raising of the abdomen is primarily an active response that is driven by sensing optic flow and air flow, rather than the passive mechanical lifting of the abdomen by air flow alone, which has previously been suggested (Nachtigall & Hanauer-Thieser, 1992; Nachtigall et al., 1971).

Luu et al. (2011) proposed that the raising of the abdomen serves to actively streamline an insect and reduce its energy consumption during flight. The present study lends support to this idea, as combining information from visual motion and airflow causes the abdomen to be raised into increasingly streamlined positions, further contributing to the energy savings of the insect in flight. The range of the air speed response curve at low optic flow is approximately 1.8 times that of the optic flow response curve with 'no wind'. In other words, wind appears to be more effective than optic flow at strengthening the streamlining response. The additional use of optic flow may increase the robustness of the response to fluctuations in air speed arising from turbulence during natural flight.

Our antennal manipulation experiments show that the antennae contribute to regulation of the insect's abdominal position in response to wind. When the antennae are either amputated or the Johnston's organs are immobilised, the modulation in response to air speed is clearly reduced. This supports previous findings from Heran (1959), which showed that the Johnston's organs are also responsible for regulating the bee's wingbeat amplitude in response to varying air speeds. Likewise, other studies have implicated the Johnston's organs in airflow sensing in butterflies (Niehaus, 1981), flies (Budick et al., 2007), dragonflies (Gewecke, Heinzel, & Philippe, 1974) and locusts (Gewecke, 1970) and have also suggested other mechanosensory roles (hearing (Dreller & Kirchner, 1993) and electric field perception (Greggers et al., 2013) in honeybees and inertial sensing in *Manduca* (Sane et al., 2007). Indeed the Johnston's organs, and antennae more generally, are recognized to provide insects with a wide range of sensory measurements. However, in both kinds of antennal manipulation, we find that there is still some

residual modulation in the abdominal response to airflow, and this activity can be predicted in both cases by our non-linear model if the insects are assumed to still have a mechanism to sense air speed. This suggests that other sensory receptors also contribute to the honeybee's perception of airflow, although these appear to have a reduced effect on the response compared to the information provided by the antennae. These additional sensory channels could be innervated hairs in various parts of the body, or wing load sensors, as are found in many orders of insects (Taylor & Krapp, 2007).

Our study indicates that the abdomen response to combinations of optic flow and air speed involves nonlinear interactions between the two sensory modalities. These interactions cannot be predicted accurately by using a weighted linear summation of the response to either stimulus. This is in contrast to other studies of visual and mechanosensory integration in insects, such as *Drosophila* (Sherman & Dickinson, 2004) and *Manduca* (Hinterwirth & Daniel, 2010), where multimodal responses have been found to combine as a linear or weighted sum to predict a response. We find that, in the case of the streamlining response, a non-linear combination of the saturating responses to wind and optic flow allows the model to predict the responses to various combinations of the two stimuli as well as the unexpected peak at 0.5 $m.s^{-1}$. Thus, a relatively simple, nonlinear combination of two stimuli can create an apparently complex behavioural response. Furthermore, this model can also be refit to predict the response after antennal ablations (assuming the bees have some other mechanism of sensing air speed), showing the model is capable of predicting some of the effects of manipulating the wind sense.

With the same information from the antenna being removed in both antennal manipulations, and likely the same alternate sensors providing air speed measurements, why does the response vary between bees with amputated antennae and waxed pedicels? The results of our non-linear model show that such results can be predicted if honeybees make different adjustments to the way in which they process air speed information in the two cases. We speculate that this may be a mechanism of adapting to uncertain sensory information. When a bee's antennae are amputated, it may be aware of this, and may then weight information from the correct, but possibly less sensitive, alternate sensors more strongly. When a bee's antennae are waxed it is less obvious they have been compromised, and the bee may not perform such reweighting, and even continue to use the erroneous air speed signals from its immobile Johnston's organs.

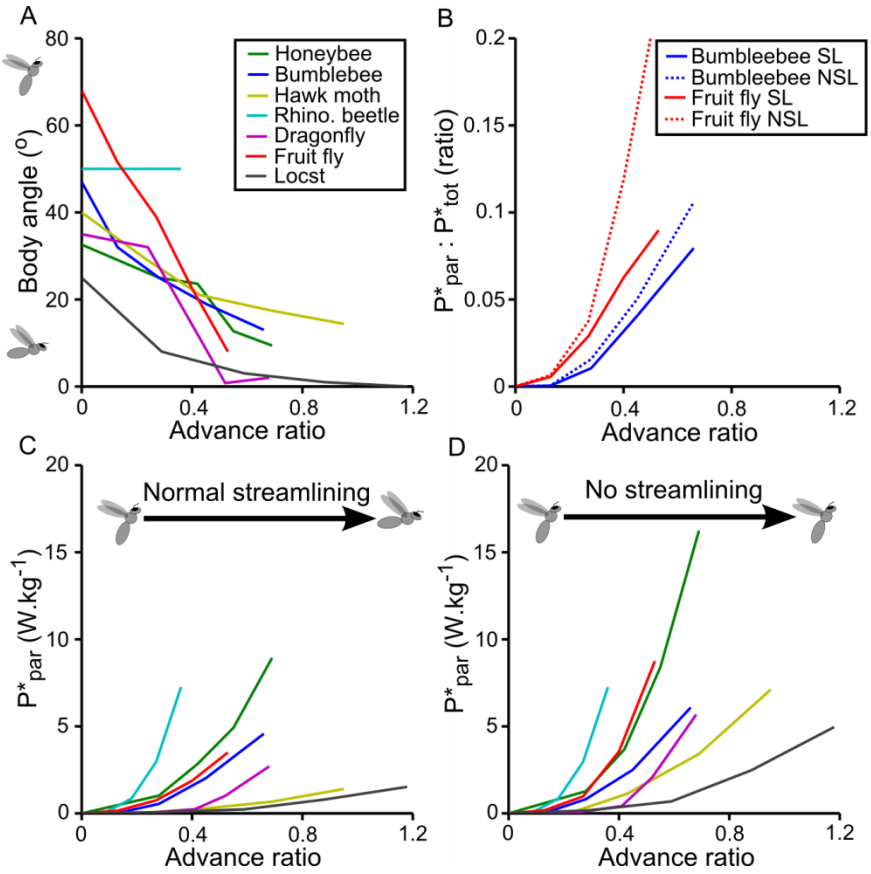

Figure 2-9: Streamlining reduces the power required for fast flight. **A**, body angle in free flight as a function of advance ratio for a variety of insect species (A, C and D use this legend). Note that this is a plot of body angle (the angle from the anterior tip of the head to the posterior point of the abdomen), rather than the abdomen pitch referred to elsewhere in this chapter. By convention, this is plotted with *positive* 90° indicating a non-streamlined flight position, rather than *negative* 90° as we used for the abdomen pitch. **B**, ratio of relative parasitic power (P^*_{par}) to relative total power (P^*_{tot}) required for flight at increasing advance ratios, when streamlined or not (SL: streamlined; NSL: not streamlined), for two species. **C**, parasitic power per unit body mass required for flight as a function of advance ratio when insects streamline as normal (using the body angles in A for each species). **D**, as for C, but the power is recalculated as if the insects had maintained the same body angle as for hovering (using the body angle at an advance ratio of zero for each species in A). The broken lines in B are calculated using the same approach. See Section A.3 for details on this data, and references.

Adjustments in body angle were first observed in free flying, rather than tethered insects. In free flight, the majority of insects have a similar response to what we have observed in tethered honeybees. Figure 2-9A shows body angle plotted against the advance ratio (the ratio between forwards velocity and mean flapping velocity of the wingtip), and as flight speed, and hence the advance ratio increase, the pitch angle of the body is adjusted until it is almost horizontal. However, in free flight the thorax and head are *also* rotated forwards, which a tethered insect cannot do. The insects we consider in the comparison shown in Figure 2-9A vary in size by

three orders of magnitude, as does the Reynolds number of their body during flight (Section A.3), yet most show a similar streamlining behaviour.

In this chapter, we focus on active, behavioural adjustment of the abdomen, which appears primarily to reduce body drag; however, insects also have some aspects of streamlining inherent to their morphology. This is the drag coefficient of an insect's body, which is usually compared between insects when the body is orientated with the long axis parallel to the air stream. This coefficient ranges from 0.25 in the case of *Manduca* (Willmott & Ellington, 1997b), which are very streamlined, to over 2.3 for small flies (Hocking, 1953), which are generally less streamlined. Yet, regardless of their inherent aerodynamic design, the majority of insect species make some attempt to streamline their flight. Does streamlining actually provide worthwhile benefits for insects? The comparison in Figure 2-9 (C and D) reveals that, when the insect streamlines in the left hand plot, the mass specific parasitic power (the power used to overcome drag against its body), increases with advance ratio, but for all the insects considered this would more than double at the equivalent advance ratio if it were not to streamline its body. This effect is most pronounced near the upper limits of the flight speed of each species.

Reduction in parasitic power is only meaningful if it represents a large contribution to the total power required for flight (a flying animal must also support its body weight which requires energy). The total power required for flight over a range of flight speeds has only been found, by simulation for two species; *Drosophila virilis* (Sun & Wu, 2003) and *Bombus terrestrius* (Wu & Sun, 2005). The ratio of parasitic to total power for these two species is similar over their flight speed ranges, and whilst parasitic power represents a negligible portion of the total power at low advance ratios, it rises rapidly to near a tenth of the total power at higher flight speeds (Figure 2-9B). If each species were to not streamline, and maintained their hovering abdomen angle across all flight speeds, parasitic power costs at high air speeds would be even larger, approaching one fifth of the total power required by *Drosophila* (the increase for bumblebees is not so severe, as they start at a body angle 20^{o} closer to horizontal). Although it has been suggested streamlining is of little benefit for small insects (Vogel, 1994), this statement appears to be only true when evolving an insect's body shape to be aerodynamically streamlined; regardless of their size or inherent drag coefficient, most of the insects considered here assume a streamlined body angle and benefit by reducing parasitic drag, which might otherwise be a factor that limits their maximum flight speed.

An exception to the general trend for streamlining is the order *Coleoptera*, the beetles. The rhinoceros beetle we include in Figure 2-9 do not streamline, and consequently they are likely to experience a body drag that is much higher than in for other insects at comparable advance ratios. These insects also reach maximum flight speed at lower advance ratios than other large insects in our comparison (hawk moth and locust), suggesting that body drag may be a limiting factor on the upper limit for the flight speed that beetles can attain. In some cases, other beetles adopt a peculiar looking posture where the thorax is not re-oriented, but the head is thrust forward, and the abdomen is partially lifted up into a streamlined position (Brackenbury, 1994). Beetle flight is somewhat different from the other insects we have considered: whilst they have only a single pair of true wings, like Diptera, their front wings, or elytra, are hardened and more like armour than wings. Elytra no doubt provide desirable protective benefits, and in flight may generate close to a fifth of the lift required to keep the insect aloft (much like a fixed wing aircraft), and even beat in time with the rear wings, albeit at a smaller amplitude (Schneider & Hermes, 1976). Thus whilst elytra may not have evolved to aid beetles in flight, their flight behaviours are probably optimized to make the most of their aerodynamic properties, possibly placing less emphasis on streamlining other body parts.

In theory, an insect should benefit from assuming a streamlined posture at any air speed above zero. Why, then, would a flying insect choose not to be streamlined at all flight velocities? When the abdomen is raised to a streamlined position it exerts the largest possible nose-up pitching moment on the insect. Whilst aerodynamic forces against the abdomen would act to raise the abdomen, our experiments, and calculations of the aerodynamic forces on free flying bumblebees (Dudley & Ellington, 1990b), show that this would be insufficient to sustain the abdomen in a streamlined position even at high air speeds. Much as they must support the insect's weight with a vertical force when hovering, it seems that insects' wings must also generate a nose-down pitching moment to allow streamlining. Hoverflies hover with 'streamlined' abdomen positions, and simulation studies have shown the power requirements for hover for these insects is only 10% more than when hovering with their abdomens lowered (Mou, Liu, & Sun, 2011). However, they do appear to have morphological adaptations that facilitate this; the relative distance from the centre of mass to their wing base is approximately half that of many other insects, including other Diptera (Ellington, 1984a), which would reduce the nose-up moment resulting from holding the abdomen up. Hovering with a raised abdomen

may be more energetically taxing for other insects, in which case the choice to streamline could be a compromise.

We previously mentioned that an insect in free flight rotates its entire body forwards. This does not necessarily imply that the net force vector (i.e. the angle between thrust and lift) produced by an insect's wings rotates with its body as the insect can also adjust its stroke plane. In fact, whilst both *Drosophila* (David, 1978) and bumblebees (Dudley & Ellington, 1990a) are observed to rotate their bodies by 40^{o} or more over the range of their free flight speeds, simulation studies show that the direction of the net force vector produced by the wings only varies by around 10^{o} for both insects (Sun & Wu, 2003; Wu & Sun, 2005), suggesting that changing the angle of the net force vector via thoracic reorientation may *not* be required for fast flight (although tethered *Drosophila* flying in still air show an angle of the net force vector which is fixed to the thorax (Gotz & Wandel, 1984)). The streamlining response (relative to the insect's body) of tethered honeybees is invariant to the pitch of the tethered insect's thorax, as least for positive thorax pitch angles varying from 0^{o} to 36^{o}. Thus, a complementary purpose for thoracic reorientation may be to allow the abdomen to freely move into a streamlined position relative to the opposing airflow; the reduction in energy expenditure from streamlining may make sustained fast flight more achievable for many insects.

Whilst minimising energy expenditure (or maximizing flight speed given an energy budget), is a compelling reason to streamline the abdomen, there may be other considerations for insect flight. One reason for maintaining a low abdominal position may be to improve aerodynamic stability. Besides decreasing the nose-up pitching moment on the body, lowering the abdomen would increase the moment of inertia about the insect's roll axis (enhancing roll stability), and bring the insect's centre of mass forward which would enhance longitudinal stability (Taylor & Thomas, 2002). This is not the only option available to insects; Combes and Dudley (2009) observed that tropical orchid bees extended their hind legs at high flight speeds to increase roll stability, at the cost of increased drag, but did not change their abdominal posture. Further, tethered *Drosophila* (Zanker, 1988b) and *Manduca* (Dyhr et al., 2013) have been observed to actively raise or lower their abdomen when shown a visual stimulus that indicates a pitch disturbance. This abdominal motion would both change the moment generated by the weight of the abdomen, and also create an inertial torque about the thorax-abdomen joint, both of which would act to adjust the pitch of the insect's thorax (assuming the wings did not modify

their generated pitching moment). In the case of *Manduca*, such a reaction has recently been calculated to be capable of providing pitch stability (Dyhr et al., 2013).

Clearly, by changing their body posture, flying insects trade benefits from reducing energy expenditure with increased aerodynamic stability and control, and possibly other, as yet undiscovered factors. One potential application of such a control scheme would be for dynamically reconfigurable small aerial vehicles. For instance, the battery pack on such a robot could be placed and actuated in a similar way to an insect's abdomen, and this type of device has recently been shown to provide pitch stability for a quadrotor helicopter, based on the control model discovered for *Manduca* (Demir et al., 2012). However, on long distance, cruising flights it would be critically important to ensure that such an aircraft is streamlined, as body drag accounts for the majority of power requirements in macro scale vehicles at higher velocities (Anderson, 2005).

Chapter 3 Walking honeybees adapt their behaviour to improve performance in virtual reality

3.1 Preamble

The chapter describes the finding that honeybees walking on a trackball change their behaviour depending on the properties of feedback sensor that is used to measure the bee's actions during a closed-loop visual fixation task. Specifically, honeybees exploit a systematic error that is present in optical motion sensors from computer mice (that are often used as feedback for virtual-reality experiments with walking animals) which allows bees to more accurately control the fixation stimulus. Preliminary results of this study were presented at the Australasian Society for the Study of Animal Behaviour Annual Conference (2013). This Chapter (and Appendix B) have been prepared and formatted as a publication, for submission to the journal 'PLoS One' authored by G. J. Taylor (the candidate), A. C. Paulk, T. W. L. Pearson, R. J. D. Moore, J. A. Stacey, D. Ball, B. van Swinderen, and M. V. Srinivasan. The contributions of each author are detailed in the preliminary pages of the thesis.

3.2 Abstract

Studying animals using tethered virtual reality paradigms can allow the neural mechanisms underlying their behaviours to be investigated, which is not always possible using unrestrained animals. Measurement of the animal's behaviour is an important aspect, particularly where its actions affect the visual stimuli, as in closed-loop experiments. Many different sensor types have been used to measure behaviour, and although some may produce more accurate measures than others, whether differences in accuracy between two separate sensors would affect the study animal's behaviour has not been considered. Here we find that honeybees change their behaviour by walking faster, depending upon whether a computer vision algorithm (FicTrac) or computer mice sensors are used to detect their behaviour when walking on an air-suspended ball in a closed-loop virtual reality arena. The bee's adaptation exploits a systematic error in the computer mice sensors, and this increases their control of the stimulus location. This shows honeybees can rapidly change their behaviour, even when coupling two normally separate motor outputs, walking forward and turning, in order to improve their performance.

3.3 Introduction

All animals use sensory information from the environment to guide their behaviour. To understand how animals use sensory information, researchers have designed virtual reality paradigms for tethered animals, which allow for tight control of sensory stimuli and detailed observation of behavioural responses from the animals interacting with the stimuli (Dombeck & Reiser, 2012). By fixing the animal in place, tethered experiments allow measurement of its reaction to precisely controlled stimuli. To study how the animal interacts with sensory stimuli, some motor output must be measured concurrently and fed back into the virtual reality system to adjust the animal's sensory environment, resulting in a closed-loop paradigm (Taylor et al., 2008). In particular, one of the best-studied closed-loop paradigms involves tethered flying flies orienting to objects in a circular arena (Poggio & Reichardt, 1973). In those studies, flies were shown to adjust their flight patterns to bring dark, vertical bars into their frontal visual field, a behaviour termed "fixation". This type of fixation has formed the groundwork for testing visual responsiveness, learning and memory, the neural mechanisms of visual processing, and how flies to adapt their motor patterns to improve fixation (Heisenberg & Wolf, 1984).

Closed-loop experimental paradigms with a tethered animal walking on an air-supported trackball, have increased in popularity over the last decade. In these experiments, optical motion sensors repurposed from consumer computer mice (CM) are often used to measure the angular velocity of the ball, which is then used to control the sensory environment, such as computer generated visual images (Harvey, Collman, Dombeck, & Tank, 2009; Seelig et al., 2010; Takalo et al., 2012). The CM sensors used in this study optically measure changes in ball position by acquiring sequential images of a surface and calculating the direction and magnitude of visual movement (Avago Technologies, 2009), which is integrated to determine the animal's instantaneous orientation in the virtual environment. However, CM sensors have been found to suffer from errors that alter the accuracy and precision of their measurements, for instance; inconsistent measurement of motion about both axes (Moore et al., 2014; Palacin, Valganon, & Pernia, 2006), effects of surface texture and pattern (Minoni & Signorini, 2006), and illumination (Tunwattana, Roskilly, & Norman, 2009). Despite such errors, animals have been shown to perform tasks including fixation (Bahl et al., 2013) and navigation (Harvey et al., 2009) with CM sensors.

Computer vision software (Moore et al., 2014), provides an alternative for measuring the angular velocity of a trackball, using video image sequences of the ball that are acquired and processed in real time. In contrast to CM sensors, FicTrac measures the absolute orientation, rather than the velocity, of the ball at each point in time. In addition, computer vision software measures this velocity with greater precision compared to CM sensors, and is also robust to a wide range of experimental conditions (Moore et al., 2014). When CM sensors and FicTrac were compared using the same animals, namely honeybees, the two systems produced differing results in open-loop (where the bees did not control the stimulus position). In addition, FicTrac could be used for closed-loop feedback, such that honeybees could reliably fixate on a single green bar in closed-loop (Moore et al., 2014), positioning it in their frontal visual field during an experiment, as has been demonstrated with the use of CM sensors (Paulk et al., 2014).

Classic experiments with tethered flies have measured their yaw torque (or wingbeat amplitude difference as a close proxy; Gotz et al., 1979) as behavioural output to control closed-loop fixation (Poggio & Reichardt, 1973) or their turning motions when walking on an air supported ball (Bahl et al., 2013). In addition, other experiments have shown *Drosophila* can learn to use a wide range of non-standard behavioural outputs to control a fixation stimulus, such as their flight thrust (Wolf & Heisenberg, 1991), and leg movements (Wolf et al., 1992). Insects have the capacity to adapt their motor commands to increase their performance in achieving their behavioural goal. Given the differences between measurements from CM sensors and FicTrac, would insects change their sensorimotor control depending on the feedback sensor used in closed-loop, particularly if this could optimise their performance? If insects did adapt, this would raise questions around how closely their behaviour in virtual-reality would correspond to behaviour in the real world.

To examine whether the feedback sensor used in closed-loop virtual-reality would affect an insect's behaviour, we tested the honeybees fixation behaviour (Moore et al., 2014; Paulk et al., 2014) using several feedback sensors conditions. Honeybees walked on a ball, the motion of which was measured as feedback by using FicTrac, CM sensors, or when the output from FicTrac was adjusted to mimic systematic errors that occurred in CM mice. In all cases bees could fixate the stimulus, but increased their walking speed if this reduced the sensitivity of the feedback sensor to their turning rate, which occurred when using the CM sensors and FicTrac's adjusted measurements. This behavioural change was made within two minutes, and the

reduction in turning rate sensitivity aided the honeybee as it could improve fixation performance.

3.4 Methods

3.4.1 Honeybee preparation

Honeybees (*Apis mellifera*) were captured exiting the hive in Brisbane, Australia. Bees were cold anesthetised and tethered to thin metal rods using wax and a cautery tool (Bovie; Figure 1A). The heads of the bees were fixed to the thorax using dental cement (Coltene Whaledent synergy D6 FLOW A3.5/B3) to ensure that they responded to visual stimulus by manipulating the trackball rather than making compensatory head movements. However, it should be noted that whether the head is fixed or free has been shown not to quantitatively alter the fixation behaviour of tethered bees (Paulk et al., 2014). Wax was also applied to the base of the wings to encourage walking behaviour. All bees were fed sucrose solution before being placed in a humidified chamber (~35˚C) for at least one hour to allow acclimatisation to the tether (Moore et al., 2014; Paulk et al., 2014).

3.4.2 Tethered virtual reality arena

The virtual reality arena consisted of a visual stimulus and a motion compensating trackball supported on a cushion of air. The visual stimulus was generated using four 32x32 tri-colour LED panels positioned panoramically around the tethered honeybee (Shenzchen Sinorad Medical Electronics Inc.; Zhou, Ji, Gong, Gong, & Liu, 2012), covering 360^{o} of the azimuthal and 54^{o} of the vertical field of view. A green bar 54^{o} high and 20^{o} wide was displayed to the tethered honeybee as the fixation stimulus. The peak wavelength and luminance (from the bee's location) for a single green bar were measured as 518 nm and 168 lux respectively. The angular orientation of the bar in the arena was controlled in closed-loop, where the bee could control the bar's orientation by rotating the ball around its vertical axis (Moore et al., 2014; Paulk et al., 2014). A Python script using Vision Egg software (Straw, 2008) updated the visual stimulus at 200 Hz (Figure 3-1A).

The trackball was a 50mm diameter Styrofoam ball (weight 1.4 g; Sullivans International) that was supported on a low friction air cushion and constrained in a custom designed 3D printed mould (Plastic Ink). Although the weight of the ball was substantially more than the honeybee,

they appeared to manipulate it easily, and were able to walk at comparable speeds to freely walking bees (Schone, 1996). A manipulator was used to position a tethered honeybee above the centre of the ball in a natural walking posture. The ball was textured with an irregular black and white pattern with a felt-tipped pen for use with camera tracking.

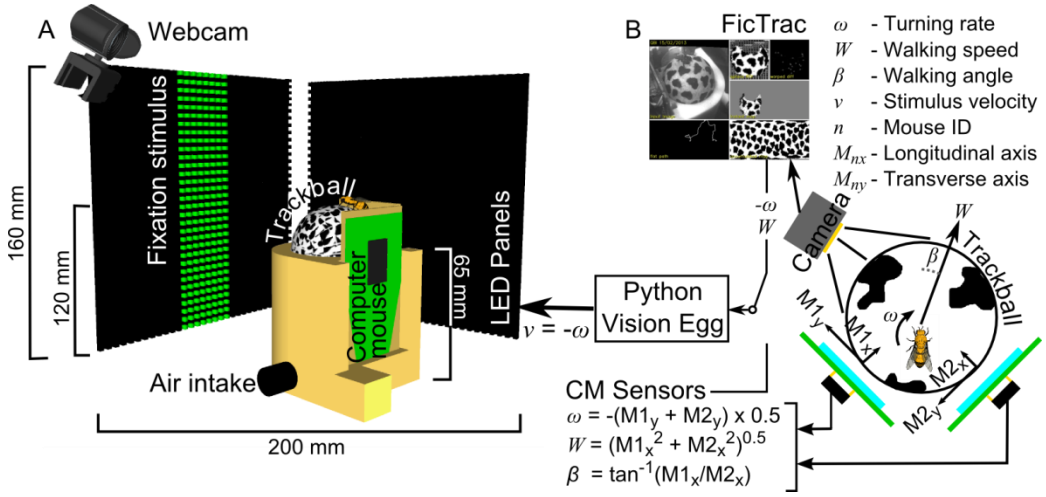

Figure 3-1: Virtual reality arena used for experiments. **A**, A honeybee is tethered (manipulator not shown) on an air supported trackball, whilst centrally positioned in rectangular arrangement of LED panels (only the two furthest panels in the rectangle are depicted in A). **B**, Two computer mice and two cameras record the motion of the trackball resulting from the honeybee's walking and turning actions (only one camera and one computer mouse are depicted in A). Both sets of measurements are converted to motion in the honeybee's reference frame, and used to control the fixation stimulus.

3.4.3 Trackball motion measurement

We used two methods of measuring the walking motions of bees, by tracking the movement of the ball either with computer mice (CM) sensors or by filming the movement of the ball and analysing it using a program called FicTrac (Moore et al., 2014). The measurements from either the CM sensors or FicTrac provide the position of the ball and were fed back to the Python script that updated the state of the visual stimulus.

The first method involved the use of sensor chips from commercial computer mice, in which a proprietary optoelectronic device is used to measure the visual motion of an image. Our implementation used two laser mice (Logitech MX400; sensing chips: Avago ADNS7050) aligned orthogonally to each another, such that their transverse measurement axes both measured the ball's rotation (Figure 3-1B). The CM sensors were placed approximately 3mm from the surface of the Styrofoam ball. The measurements from the sensors were used to

determine the rotation and translation rates of the ball in the bee's frame of reference, based on the two measurements of each mouse (Figure 3-1B). A custom C++ script sampled the accumulated movement of the computer mice sensors at 100 Hz on a computer running Windows XP SP3. A non-standard computer mouse driver, CPNMouse (Westergaard, 2002), was used to interface directly with the mice, bypassing the standard Windows interface. This system had a closed-loop latency of approximately 46 ms from the motion of the ball to the movement of the stimulus. This design is comparable to other systems that have been used to study invertebrates (fly, Clark, Bursztyn, Horowitz, Schnitzer, & Clandinin, 2011; honeybee, Paulk et al., 2014; cockroach, Takalo et al., 2012).

The second method tracked the motion of the ball from video images in close to real time (Moore et al., 2014). Images were recorded using a firewire camera (Point Grey, Firefly), which recorded the ball at 30 fps in grey scale on a computer running Ubuntu 12.04. FicTrac then calculated the orientation of the ball, with a resulting closed-loop latency of approximately of 87 ms. A webcam (Logitech Pro 9000) was used to film the ball when using the CM sensors in closed-loop. The video from this was analysed offline with FicTrac. The data from both cameras was time stamped along with the visual presentation program for synchronisation with the CM sensor data. In all cases, the shutter speed, camera gain, and brightness were set such that sharp images of the irregular ball pattern were taken, even when the bees were running at high speeds. FicTrac provided a direct measurement of the (negative) turning rate and walking speed in the bees' reference frame (Moore et al., 2014), so a coordinate transformation was not required. The relatively long closed-loop latency was a limitation for both measurement methods, as the visual stabilisation reflexes of insects such as flies can respond with latencies on the order of 30 ms (Warzecha & Egelhaaf, 2000).

3.4.4 Closed-loop experiments

All experiments were conducted in closed-loop. When the bee rotated the ball about the vertical axis, the visual display rotated the fixation stimulus (a green bar) around the bee by the same angle, but in the opposite direction. This represented a feedback gain of x1, which corresponded to walking under natural conditions. During each experiment, which ran for two minutes, bees had the opportunity to bring the green bar to their frontal visual field, thereby fixating on the stimulus. To ensure bees were attempting to control the visual cue, brief open-loop displacements were introduced, in which the bar was displaced abruptly by 90^{o} in either

direction (at random time intervals between 3 s and 15 s), to test if the bees were paying attention to the bar and compensating for these displacements (Heisenberg & Wolf, 1984; Moore et al., 2014; Paulk et al., 2014). Periods including displacements were excluded from all analysis. Individual bees were tested using both feedback sensors.

3.4.5 Systematic manipulation of rotation sensitivity

A second experimental condition was conducted where the rotational sensitivity of the measurement made by FicTrac was adjusted based on the instantaneous walking speed, *W*, (also measured by FicTrac), while the bees also fixated the bar in closed-loop. This manipulation was analogous to varying the gain between the honeybee's actions and their influence on the stimulus, and took two forms, the 'decrease' and 'increase' conditions respectively. The 'decrease' condition allowed bees to *reduce* the rotational sensitivity of FicTrac by walking faster,

$$Sensitvity_{Dec.}(W) = \begin{cases} 1 - W/5 & W \le 2.5 \\ 0.5 & W > 2.5 \end{cases} \quad (3\text{-}1)$$

Conversely, in the 'increase' condition, running faster *increased* sensitivity.

$$Sensitvity_{\mathrm{Inc.}}(W) = \begin{cases} 0.5 + W/5 & W \le 2.5 \\ 1 & W > 2.5 \end{cases} \quad (3\text{-}2)$$

In the above equations, walking speed is measured in rad.s^{-1} in the bee's reference frame; graphical representations of these functions are shown in Figure B-2. The effect of the 'decrease' condition was approximately equivalent to the relationship observed from the CM sensors (Figure B-2), whereas the 'increase' condition was considered to approximate the opposite relationship. Bees in this experiment were exposed to a pre-test control, where the sensitivity was uniformly one, followed by either the 'increase' or 'decrease' conditions.

3.4.6 Data acquisition and analysis

Data on the orientation of the bar and the bees' movements measured by the sensors were synchronously recorded from within the Python script. All data was down-sampled to 30 Hz for analysis, to provide a fair comparison between the computer mouse sensors and FicTrac (which had the lowest sampling frequency in the system, 30 Hz). Data analysis was conducted using custom Matlab (The Mathworks Inc.) scripts.

The fixation on the bar was quantified by calculating the frequency distribution at each possible bar orientation, mapped to 360° around the arena for each bee. These results are shown on radial distribution plots, calculated in 2.8° bins (which corresponded to the resolution of the LED display). As an additional comparison, a mean vector was determined using the Circular Statistics Toolbox in Matlab for the location of the bar around the arena for each bee (Berens, 2009). This vector is a representation of the strength of fixation (vector length) and the mean angle of fixation (direction of the vector). The mean vector directions for all bees in a group were tested for uniformity using Rayleigh's test for each condition (Batschelet, 1981; Berens, 2009).

Frequency distributions for the turning rate and walking speed were calculated for each condition. Turning rate distributions were calculated based on 5 $^{o}.s^{-1}$ bins ranging from -250 $^{o}.s^{-1}$ to 250 $^{o}.s^{-1}$, and walking speed distributions were calculated based on 1 $mm.s^{-1}$ bins ranging from 0 $mm.s^{-1}$ to 100 $mm.s^{-1}$. The mean values of walking speeds, and absolute mean values of turning rates were compared statistically as described below.

Statistical comparisons (besides Rayleigh's test), were made using repeated measures statistics in SPSS V20 (IBM). Data was tested for normality using the Shapiro-Wilk test, and, if it was found to be normal the comparison was made using a paired samples *t*-test. Otherwise a related-sample Wilcoxon signed rank test was used (for which the standardised test statistic is reported). The results are specified the *t* and *W* test statistics respectively (Rayleigh's test uses the *z* test statistic). All statistical tests used a significance level of 0.05.

3.5 Results

3.5.1 Honeybees can fixate on a single green bar using either feedback sensor

Honeybees were able to fixate a bringing a bright vertical green bar displayed on a LED array (Figure 3-1A) in frontal visual field using either feedback sensor in closed-loop (Figure 3-2A and B; Mean vector angles were non-uniformly distributed for both FicTrac (z_{10}=6.75, ***p*<0.001**), and computer mice (CM) sensors (z_{10}=4.62, ***p*=0.007**), Figure B-1). Although the distribution of bar positions appears to differ between feedback sensors (Figure 3-2B), a comparison of the mean vector lengths between groups revealed there was negligible difference

in fixation strength (Figure 3-2C, t_{10}=0.67, p=0.517). We conclude that honeybees perform similarly at fixating the bar regardless of whether their walking behaviour is measured using FicTrac or CM sensors to provide feedback.

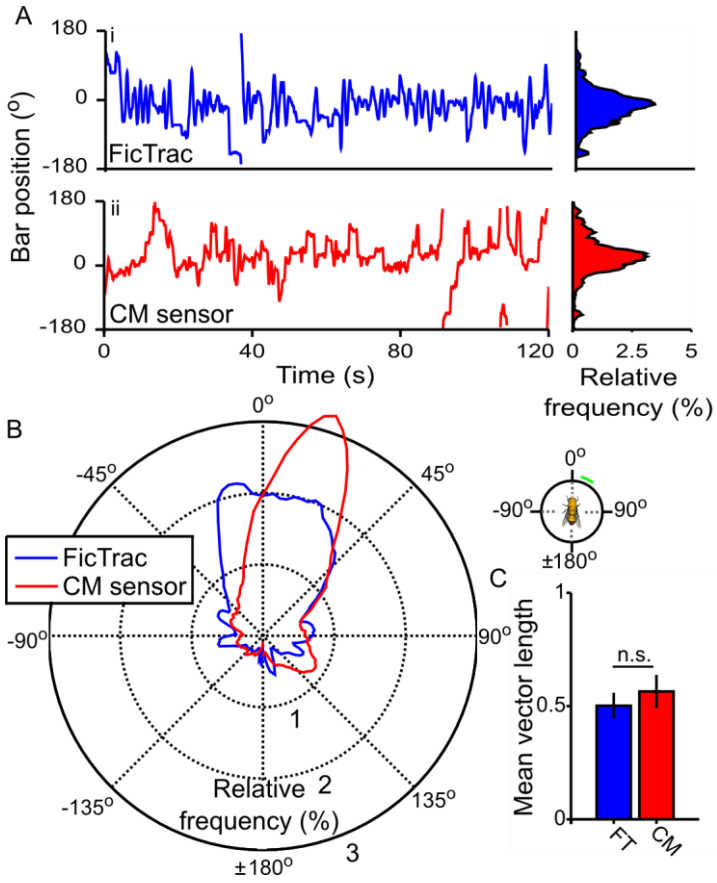

Figure 3-2: Honeybees fixate using both feedback sensors. **A**, Example of fixation using FicTrac (**i**), and CM sensors (**ii**) from a single bee. Plots show a time history of bar positions (left), and the resulting frequency distribution of bar positions around the arena (right). **B**, Average fixation performance for all bees tested with each feedback sensor, in terms of the frequency distribution of bar positions. **C**, Fixation performance quantified using mean vector length, actual mean vectors are shown in Figure B-1. N=11 repeated both conditions. Error bars show ±S.E.M.

3.5.2 Honeybees walk faster with computer mouse sensors

While honeybees were able to fixate equally well using either feedback sensor, we next examined whether they change other aspects of their behaviour depending upon which sensor was used. FicTrac provides a more accurate and precise measure of the balls rotation than the CM sensors, which were known to be noisier and suffer from systematic biases (Moore et al., 2014). Hence, for both feedback sensors, we considered the bee's turning rate, which was intended to control the stimulus position, and their walking speed, which could have affected

the biases present in the CM sensors. In both cases, the data measured using FicTrac as the feedback sensor was compared to the data measured by CM sensors when used for feedback, and also to FicTrac's simultaneous measurement of the movement of the ball for verification of the CM sensors recording. This allowed us to compare whether behavioural differences were observed using measurements of equivalent accuracy and precision for both feedback sensors, and also whether similar differences would have been detected using the measurements from both sensors directly.

When examining the honeybees' turning rate, symmetrical and zero biased distributions were observed which were qualitatively similar for all datasets (Figure 3-3A). The largest difference in turning rates was between the CM sensors and FicTrac's verification of this data, which were both measurements of the *same* ball movement (Figure 3-3A and B). However, neither the mean absolute turning rate measured using the CM sensors directly (t_{10}=1.38, p=0.197), nor their verification with FicTrac (t_{10}=0.76, p=0.468), were significantly different from when FicTrac was used as the feedback sensor (although the average turning rate measured by the CM sensors was notably lower). For the bee's walking speed, long tailed distributions with a prominent peak at or close to zero were observed for all datasets (Figure 3-3). Interestingly, both the CM sensors measurement and FicTrac's verification of this data both showed that bees were more likely to walk quickly using the CM sensors for feedback as compared to when FicTrac provided feedback. Comparison of the mean walking speeds (Figure 3-3D) using FicTrac as the feedback sensor and the verified measurements for CM sensors confirmed a significant increase in mean walking speed occurred when CM sensors provided feedback (W_{10}=2.13, $\boldsymbol{p}$**=0.033**). However, the difference would not be noted when using the data from the CM sensors directly (W_{10}=46, p=0.248). Despite the feedback sensor not affecting honeybee's fixation performance, it does affect their behaviour, as bees increased their walking speed when CM sensors were used.

One reason honeybees may have increased their walking speed when CM sensors provided feedback is a systematic error that affects these sensors (Moore et al., 2014; Palacin et al., 2006). This error results in inconsistent measurement of complex rotations, where the velocity measured along one axis can affect that measured along the other axis. In other words, CM sensors exhibit an interaction, or coupling, between the measurements of movement that they register along their two principal axes. Specifically, given the arrangement of CM sensors that we used, the honeybee could reduce the sensitivity of the CM sensors to its turning rate by

walking faster (Figure B-2). We therefore hypothesized that the bees may have increased their walking speed to adjust the sensitivity of CM sensors to their turning rate.

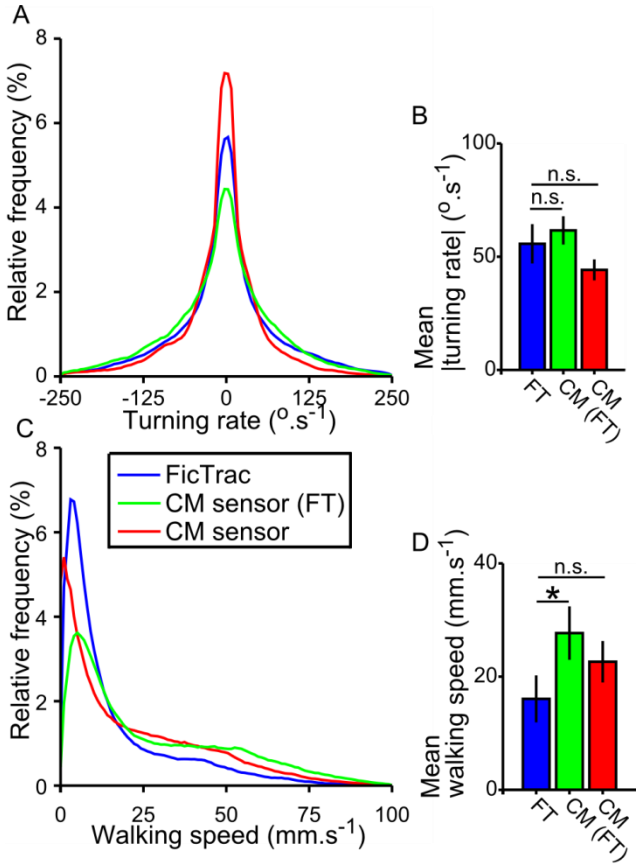

Figure 3-3: Honeybees maintain similar turning rates between feedback sensors, but vary their walking speed. **A**, turning rate frequency distribution, and **B**, mean absolute turning rates. **C**, walking speed frequency distribution, and **D**, mean walking speeds. Note that computer mice (CM) sensor (red), is a measurement directly from the sensors (when they were used for feedback), whereas CM sensor (FT), is the post-experiment verification measurement of the movement of the ball using FicTrac. N=11 repeated both conditions. Error bars show ±S.E.M. The star (*) denotes a statistically significant difference with $p<0.05$.

3.5.3 Honeybees walk faster to reduce rotational sensitivity

To test the hypothesis that honeybees would adjust their walking speed to modify the feedback sensitivity to turning rate, we conducted an experiment using FicTrac as the feedback sensor, and used two equations to couple walking speed to turning rate. The two conditions were 1) a 'decreasing' condition: turning sensitivity was *decreased* as walking speed increased (Eq. (3-1)), and 2) 'increasing' condition: turning sensitivity was *increased* as walking speed increased (Eq. (3-2)). The decreasing condition replicates the systematic error that we observed from the measurements of CM sensors (Moore et al., 2014). Prior to testing either condition,

bees were given a pre-test in which walking speed did not change rotational sensitivity with FicTrac operating as the feedback sensor. Thus, in this condition, there was no coupling between the translational and rotational movements that were registered. If bees varied their walking speed between the pre-test and the altered coupling condition, it would demonstrate their ability to exploit such relationships, and also their preference for decreased, or increased, feedback sensitivity. Importantly, as FicTrac was used to measure the ball motion for all conditions, the latency always 87 ms, whereas the latency was not matched when comparing FicTrac to the CM sensors in the previous section.

Regardless of the test condition – pre-test, 'decreasing', or 'increasing' – honeybees were able to position the fixation stimulus frontally (Mean vector angles were non-uniformly distributed for all conditions; Pre-test$_{Dec}$, z_9=6.47, ***p*<0.001**; 'decreasing', z_9=7.85, ***p*<0.001**; Pre-test$_{Inc}$, z_9=9.33, ***p*<0.001**; 'increasing', z_9=4.54, ***p*=0.008,** Figure B-1). However, when given the 'decrease' condition, honeybees achieved a qualitatively sharper fixation distribution (Figure 3-4A), and significantly longer mean vector lengths than in their pre-test (Figure 3-4B, t_9=2.51, ***p*=0.033**). Honeybees tested with the 'increase' condition did not alter their mean vector lengths or fixation distributions compared to their pre-test results (Figure 3-4B, t_9=0.28, p=0.787).

Analysing the behaviour further, we found that honeybees did not modify turning rate (Figure 3-4D, t_9=0.73, p=0.484), but significantly increased walking speed when tested in the 'decrease' condition relative to the pre-test (Figure 3-4F, W_9=2.29, ***p*=0.022**). Conversely, honeybees do not modify their walking speed in the 'increase' condition (Figure 3-4F, W_9=1.17, p=0.241), and whilst they do slightly decrease their turning rate (Figure 3-4C), the change in mean absolute turning rate was not significant (Figure 3-4D, t_9=1.41, p=0.191).These findings indicate that bees changed their locomotory behaviour in the 'decrease' (but not the 'increase') condition, by walking faster. In the 'decrease' condition, walking faster decreased the sensitivity of the feedback sensor to their turning rate, apparently aiding the bees in achieving more accurate fixation.

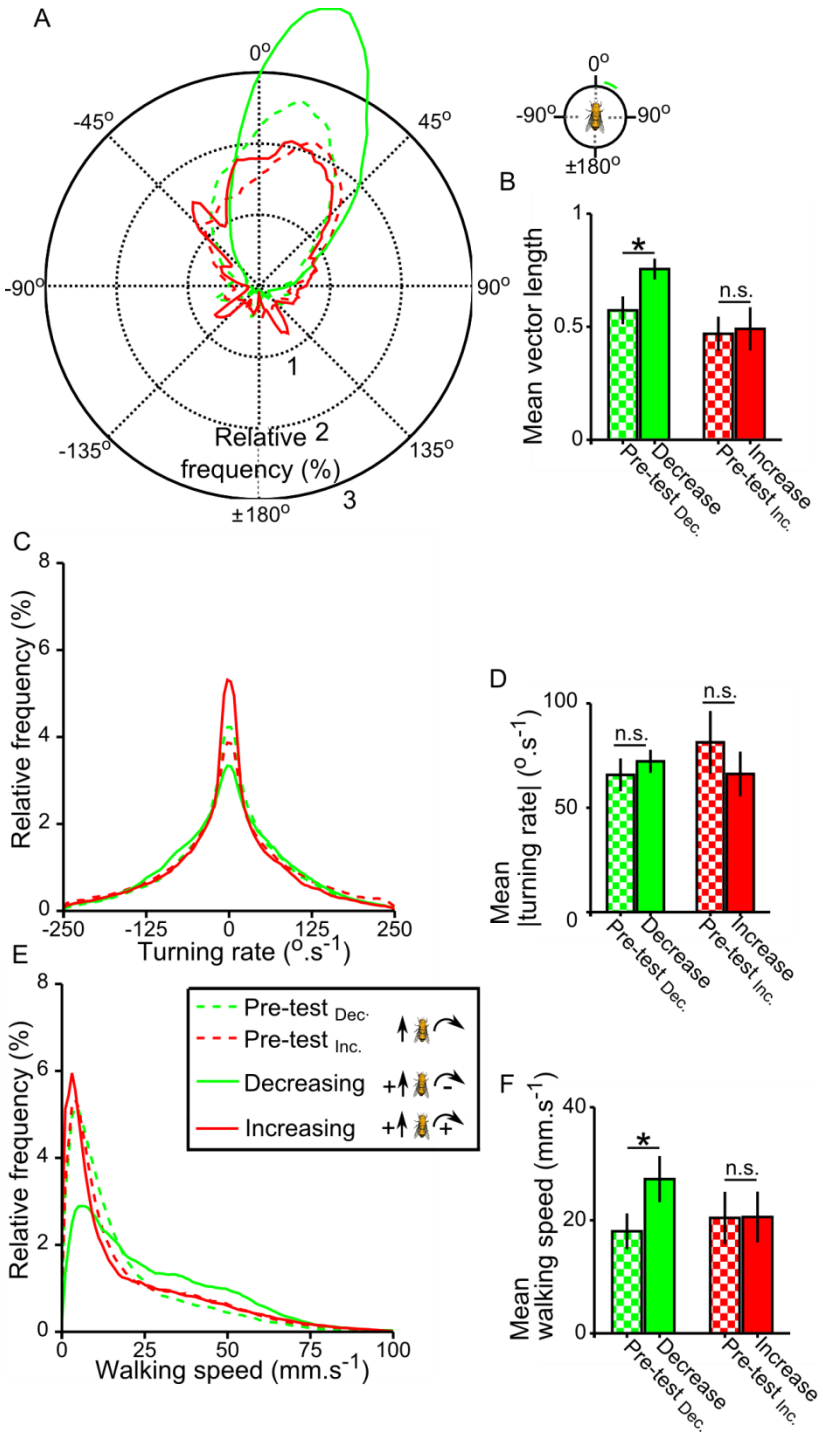

Figure 3-4: Honeybees walk faster to decrease the feedback sensitivity to rotational movement. **A**, Average fixation performance for bees tested with all conditions, in terms of the frequency distribution of bar positions. **B**, Fixation performance quantified using mean vector length, actual mean vectors are shown in Figure B-1. **C**, Turning rate frequency distribution, and **D**, mean absolute turning rates. **E**, walking speed frequency distribution, and **F**, mean walking speeds. Dashed lines in frequency distributions correspond to chequer bar plots throughout. N = 10 repeated the pre-test and either 'decreasing' or 'increasing'. Error bars show ±S.E.M. Stars (*) denote statistically significant differences with $p<0.05$.

3.6 Discussion

Closed-loop virtual reality systems are an important paradigm for studying the visuomotor mechanisms that underlie numerous types of behaviour, including learning and memory (Dill, Wolf, & Heisenberg, 1995), attention (Sareen, Wolf, & Heisenberg, 2011; van Swinderen, 2007), spatial navigation and place memory (Harvey et al., 2009), orientation behaviour (Schuster, Strauss, & Gotz, 2002; Strauss, Schuster, & Götz, 1997), and multimodal integration (Chow, Theobald, & Frye, 2011). The critical component of a closed-loop system is that some output from the animal produces a change in the sensory environment. In our experiments in which walking honeybees manipulate an air-supported ball to control the position of a visual stimulus, we find that the reliability of the sensors that are used to monitor the animal's behaviour and generate the visual feedback played an important role in determining the behaviour. Using two separate feedback sensors, namely optical motion sensors from computer mice (CM) and a novel computer vision approach, FicTrac, we find the bees use different, sensor-dependent strategies to fixate a single green bar. Apart from the differing feedback sensors, all other components of the virtual reality system are unchanged when comparing the two systems. In general, bees walk faster when feedback comes from the CM sensors, as compared to FicTrac, and similarly walk faster when we replicate a systematic error occurring in CM sensors in data measured using FicTrac. In both cases, when the bees walk faster, this systematic error has the effect of decreasing the rotational sensitivity of the feedback sensor to the bee's turning rate, which is the behavioural measurement that is used to control the bar position. Presumably, with decreased rotational sensitivity, the position of the bar is less affected by any accidental turning errors that the bees make, thus making it easier to accurately control the angular position of the bar.

Why does walking faster change the sensitivity of the CM sensors? Both feedback sensors measure the angular velocity of the ball resulting from the honeybee's walking and turning actions. When integrating a velocity signal, as in our experiments, any errors in the signal result in progressively larger errors in the estimated virtual position and heading direction of the bee, because the instantaneous velocity signals corresponding to walking speed and turning rate are integrated over time to estimate the position and heading direction (Britting, 2010). Whilst the motion sensing chips used in CM take measurements at a high sample rate, the measured values are surprisingly imprecise when compared to those delivered by FicTrac when the sample rate was matched (Moore et al., 2014). In addition, CM sensors can be affected by systematic and

biased errors, resulting in inaccurate measurements (Minoni & Signorini, 2006; Palacin et al., 2006; Tunwattana et al., 2009), whereas FicTrac's underlying measurement of the trackballs orientation is unbiased (Moore et al., 2014). By walking faster, bees exploited a systematic error present in CM sensors, which reduces the sensitivity of the devices when making simultaneous measurements of their turning movement. Systematic errors could also be present on other types of sensors used for feedback in virtual reality paradigms (Kröger, Kubus, & Wahl, 2008; Xu & Li, 2000). Thus, sensor calibration is an important consideration to establish how reliably an animal's motor output is measured, and also to establish whether an opportunity exists for the animal to improve its performance by exploiting any systematic errors that are present. Other characteristics besides sensitivity will also vary between sensors used in closed-loop paradigms, such as latency, response time, and frequency responses, which may also trigger an animal to modify aspects of its behaviour. Notably, in this study we could not have detected that honeybees changed their behaviour between sensor types by comparing measurements from FicTrac with biased CM sensor data directly; FicTrac was required to provide verification and detect the difference.

Experimental paradigms have measured behavioural outputs from flying and walking animals (Dombeck & Reiser, 2012), to enable the creation of an interface between the behaviour that the animal produces and the sensory cues that it experiences. For relatively simple tasks, like visual orientation and stabilization, animals quickly become accustomed to using their behavioural output to control the stimulus in virtual reality (Wolf & Heisenberg, 1991), although more complicated tasks, can require training (Harvey et al., 2009). Without any obvious reward, other than improving their fixation, the bees in this study rapidly change their walking speed to improve their control of the stimulus. The capacity of *Drosophila* to switch between using a linear and rotational behaviour, such as thrust force and yaw torque, when controlling a rotational stimulus has previously been observed (Wolf & Heisenberg, 1991). However, the bee's demonstrated ability to fine-tune behavioural performance using a coupling between two usually separate motor commands, walking and turning, does not appear to have been previously reported.

Honeybees can adapt to the feedback sensor in complex ways, which raises the question: depending on the measurement errors involved in the closed-loop system, what is the experimenter studying? Does the path an animal takes through a virtual reality arena match how the animal would move through a real space populated with similar stimuli, or are the

observed behaviours a result of the uniquely artificial set up? In addition, since bees quickly adapt to the different feedback sensors, do the changes in behaviour involve higher-order learning, or do they represent a basic type of sensorimotor adaptation involving operant conditioning?

Chapter 4 Turning towards the light: Honeybees adapt the control functions underlying their visual fixation

4.1 Preamble

The chapter describes how honeybees control their turning rate based on the position and motion of the stimulus during a closed-loop visual fixation task, which they adapt to improve their performance when the coupling between their actions and the environment is varied. Quantitative analysis of fixation behaviour is usually based on open-loop experiments, and a key component of this study is the development of an analysis method for use with closed-loop experimental data, which allows quantification of the adaptive components of honeybee behaviour. The contents of this Chapter (and Appendix C) are prepared and formatted as a publication, for submission to the journal 'PLoS Computational Biology' authored by G. J. Taylor (the candidate), A. C. Paulk, T. W. L. Pearson, B. van Swinderen, and M. V. Srinivasan. The work is intended for submission as two part publication with Chapter 5. The contributions of each author are detailed in the preliminary pages of the thesis.

4.2 Abstract

When an insect moves through the world, it must not only stabilise its path against transient disturbances, the but also occasionally adapt to fundamental changes in the way in which its motor actions alter its sensory environment. We used a closed-loop virtual reality paradigm to investigate how tethered walking honeybees adapted their performance in an object fixation task while varying the gain, a linear multiplier coupling the magnitude of their actions to the magnitude of the resulting effect on the stimulus. The bees' response could be modelled by separate non-linear functions of the position and motion of the fixation stimulus, and the insects adapted both of those functions depending on the gain condition. To determine position- and motion-dependent control functions from closed-loop data, we developed a novel analysis approach for data where the stimulus is non-uniformly sampled and the response is temporally correlated. Simulations with control functions measured from experimental data showed that these functions can predict the fixation behaviour observed. The simulations also suggest that by changing the control functions underlying fixation behaviour, bees can improve control of the stimulus at high gains.

4.3 Introduction

When an animal is moving through the environment it uses sensory feedback to guide its motor output. However, there is not always a consistent coupling between an animal's motor output and its effect; these relationships can change over different time scales. For example, insects would have to change their wingbeat kinematics if wing damage occurred (Dukas & Dukas, 2011; Haas & Cartar, 2008) or when flying in low density air when ascending to high altitude (Altshuler et al., 2005; Dillon & Dudley, 2014; Dudley, 1995). Similarly, walking insects may suffer leg damage (Götz & Wenking, 1973; Wittlinger et al., 2007), or encounter slippery or springy surfaces (Epstein & Graham, 1983; Spence et al., 2010). When these changes in coupling occur, and insect would likely be required to modify its locomotion control, to continue to move effectively under the new conditions.

A popular paradigm to study how insects respond to visual objects is to use a tethered insect's motor output, whether in flight or walking, to drive changes in the position of a vertical bar presented on a circular display surrounding the animal (Poggio & Reichardt, 1973; Reichardt, 1969; Reichardt & Poggio, 1976). When tethered flies are tested in such a 'closed-loop' paradigm, the insects typically 'rotate' left or right by either changing their yaw torque, or their walking patterns to position a vertical bar in their frontal visual field – behaviour termed 'fixation'. Flies (*Drosophila* and *Musca*) have been commonly used for quantitative studies of visual fixation, however, similar behaviour has been observed in other insects, including moths (Preiss & Kramer, 1984), beetles (Lönnendonker, 1991; Varjú, 1975), and honeybees (Moore et al., 2014; Paulk et al., 2014). The fixation paradigm has formed the basis for testing theories of visual responsiveness, learning and memory, the neural mechanisms of visual processing, and for understanding how insects adapt their motor patterns to view and track objects (Heisenberg & Wolf, 1984).

The visual fixation that is observed in flies is a robust behaviour; although the fixation stimulus is typically a dark vertical bar on a bright background, flies will fixate on a variety of different types of stimuli (Brembs & Heisenberg, 2001) and can distinguish patterned object when it moves in front of a similarly patterned background (Aptekar, Shoemaker, & Frye, 2012; Bülthoff, 1981; Reichardt, Egelhaaf, & Guo, 1989). Similar fixation has been observed for both flying (Heisenberg & Wolf, 1984; Heisenberg, Wonneberger, & Wolf, 1978) and walking *Drosophila* (Bahl et al., 2013). Furthermore, *Drosophila* can learn to use non-standard motor

outputs to fixate on a stimulus, for example, they can learn to use flight thrust (Wolf & Heisenberg, 1991) or leg forces (Wolf et al., 1992), even though these would not usually control the flies' rotation. Fixation behaviour is also robust to variations in the coupling, or gain, between the measured behavioural output and its effect on the movement of the stimulus (Poggio & Reichardt, 1973; Wolf & Heisenberg, 1990). However, performance degrades when the gain is very high (Poggio & Reichardt, 1973), indicating that the coupling of the fixation stimulus to motor output represents a performance constraint for fixation control.

In a standard fixation experiment an insect controls the position of the stimulus using its turning response. Open-loop experiments, where the insect cannot control the stimulus, have shown that the turning response depends on both the position and the motion, or angular velocity, of the stimulus (Figure. 4-1A; Reichardt & Poggio, 1976). Thus, the fixating insect can be modelled as a control system, which uses feedback from the state of the environment to modulate its motor output in order to control the state of the stimulus over time (Nise, 2008). Specifically, fixation control is similar to a proportional-derivative linear control system, which would produce a response proportional to the difference between the current position of the stimulus and its preferred position, as well as the rate of change of that difference. Fixation behaviour has been modelled as linear system after linearizing the fly's response when the stimulus is in its frontal visual field (Reichardt & Poggio, 1976; Roth, Reiser, Dickinson, & Cowan, 2012). However, if the insect's response to stimulus across its entire visual field is considered, fixation behaviour appears to be more complex, as the fly's response to the position and motion of a stimulus depend on the different non-linear functions of stimulus position (Aptekar et al., 2012; Bahl et al., 2013; Reichardt & Poggio, 1976).

Despite the apparent complexities of the control system underlying fixation, open-loop measurements of the control functions linking turning response to stimulus position and motion have been used to successfully predict fixation results in closed-loop experiments (Bahl et al., 2013; Reichardt & Poggio, 1976). However, other studies have shown that flies rapidly learn to adapt their motor output to control a stimulus (Wolf & Heisenberg, 1991; Wolf et al., 1992). Further, an insect's open-loop responses often saturate (Taylor et al., 2008), or are otherwise different compared to the responses measured during closed-loop behaviour (Heisenberg & Wolf, 1988; Paulk et al., 2014). Thus, the control functions measured in open-loop may not exactly correspond with those used by the insects to control fixation in closed-loop. The control functions are likely to be qualitatively similar, although they may be fine-tuned to optimize the

insect's fixation performance given the experimental conditions. One instance where closed-loop results cannot be predicted using control functions measured in open-loop occurs in experiments with flies where a high gain multiplier was used (Poggio & Reichardt, 1973); the measured control functions predicted more robust fixation than was observed in closed-loop. Whilst fixation degraded at high gains, did the flies attempt to compensate by modifying the control of their behaviour?

To investigate how insects adapt to varying gain conditions in closed-loop fixation, we performed experiments using tethered walking bees fixating on a bright vertical bar. The gain multiplier was randomly varied between low, normal and high gains in separate experiments. We developed a novel analysis method to extract control functions dependent on the position and motion of the fixation stimulus from the closed-loop data, which is described in Section 4.5. The analysis method was then applied to experimental data (Section 4.6) to reveal that, whilst fixation performance declines at high gain conditions, bees did compensate for the imposed gain changes by adapting their control functions. A simulated model, using the measured control functions, suggests that these adaptations do improve control at high gains.

4.4 Methods

4.4.1 Honeybee preparation

Honeybees (*Apis mellifera*) were captured exiting the hive in Brisbane, Australia. Cold anesthetised bees were tethered to a metal rod using wax and a cautery tool (Bovie). The heads of the bees were fixed to the thorax using dental cement (Coltene Whaledent synergy D6 FLOW A3.5/B3), and wax was also applied to the base of the wings. As bee's heads were fixed, this ensured their response to visual stimulus was represented in body centric coordinates, as compensatory head movements could not be made. Bees were fed a sucrose solution before being placed in a humidified chamber (~35 ^{o}C) for an hour to acclimatise to the tether (Paulk et al., 2014).

4.4.2 Tethered virtual reality apparatus

The virtual reality apparatus consisted of a visual stimulus and a motion-compensating ball supported on a cushion of air (Figure 4-1B). The visual stimulus, a bright green bar (54^{o} high and 20^{o} wide), was generated using four 32x32 tri colour LED panels (Shenzchen Sinorad

Medical Electronics Inc.; Zhou et al., 2012) positioned panoramically around the tethered insect (Moore et al., 2014; Paulk et al., 2014). The peak wavelength and luminance (from the bee's location) for a single green bar were measured as 518 nm and 168 lux respectively. The angular position of the bar in the arena was controlled in closed-loop, where the bee could control the bar's position by rotating the trackball. The trackball was patterned with an irregular black and white pattern using a felt-tipped pen to allow measurement of its motion using custom designed software (FicTrac, described below). In closed-loop, the measurement of the rotation of the ball about the vertical axis (yaw), as registered by FicTrac, was used to control the angular velocity of the bar at an update rate of 200 Hz by using a Python script to drive Vision Egg software (Straw, 2008).

The bee was positioned above the trackball, a 50 mm diameter Styrofoam ball (weight 1.4 g) that was supported on a low friction air cushion and constrained in a custom designed 3D printed mould (Plastic Ink). Whilst the dynamics of the ball were not matched for a honeybee (approximately perceived weight 580 mg (honeybee mass ~100 mg) and perceived rotational inertia 330 nkg.m^2 (honeybee inertia ~5 nkg.m^2) calculated using the methods of Weber, Thorson, and Huber (1981)), subjectively the bees appeared to manipulate the ball easily. The mean walking speed observed during undirected walking in the no stimulus control was approximately 30 mm.s^{-1}, frequently reaching 75 mm.s^{-1}. These speeds are approximately half the free walking speed observed in honeybees walking down a corridor when returning to their hive (Schone, 1996).

4.4.3 Trackball motion measurement

An image matching algorithm called FicTrac (Moore et al., 2014), was used to measure the rotation of the ball in real time. This provided a measurement of the honeybees turning rate, ω, walking speed, W, and walking angle, β ($-\omega$ and $\beta + 180^o$ were the values registered by FicTrac, which were transformed to the bee's reference frame), as shown in Figure 4-1A.

Images of the trackball were recorded in grey scale using a firewire camera (Point Grey, Firefly) at 30 fps on a computer running Ubuntu 12.04. FicTrac then calculated the position of the ball, which was used by Vision Egg to change the angular position of the fixation bar, with a resulting latency of approximately of 87 ms (Moore et al., 2014). Although the closed-loop latency of the feedback system may be longer than the latency of the visual stabilisation

reflexes of the bee (which can be 30 ms in flies; Warzecha & Egelhaaf, 2000), the ability of bees to control the stimulus under most gain conditions suggested the additional latency did not prevent fixation behaviour. Yet at increased gains the long latency would be expected to further decrease fixation performance (Nise, 2008), and is a limiting factor when relating the measured control functions in this study to natural behaviour. To account for this latency for analysis, the time series of the measured ω was shifted three frames back relative to the time series of stimulus positions, such that they were temporally aligned.

4.4.4 Closed-loop experiments

Experiments were conducted in closed-loop, and when the bee rotated the ball about the vertical axis the visual display rotated the fixation stimulus around the bee, to the angular position ψ. To test the honeybee's ability to adapt to varying control conditions, we varied the gain, a linear multiplier, coupling the measured rotation of the ball to the angular position of the green bar (Figure 4-1A). A x1 gain means that 1° of rotation of the ball results in 1° of rotation of the visual stimulus, such that $\psi(t) = \int(\omega(t-l)\times gain)dt$, where l is the closed-loop latency of the virtual reality system.

During two-minute experiments, bees could bring the green bar to their frontal visual field, thereby fixating on the stimulus. To test whether the bees were attempting to control the visual cue, brief open-loop displacements would intermittently move the bar by 90°, at 300 °.s^{-1}, requiring bees to correct the bar's position (Heisenberg & Wolf, 1984; Paulk et al., 2014). Displacements occurred randomly, with an interval of 3 to 15 s between each event. Bees were usually observed to successfully correct for disturbances at x2 gain and lower (data not shown; Moore et al., 2014), although these corrections were not analysed in detail. Periods including displacements were excluded from all analysis. The gains of closed-loop experiments were set at values ranging from x0.5 to x4 for the duration of each experiment.

A black bar on a black background (thereby rendering the bar 'invisible') was used as a control to test if the bees had clear directional running preferences. The black bar is referred to as the no stimulus, or NS, condition. Individual bees completed all test conditions across the range of gains and the control in a pseudo-randomized order.

4.4.5 Data acquisition and analysis

Data on the angular positions of the bar and the bees' movements as measured by FicTrac were synchronously recorded from within the Python script. All data was analysed at 30 Hz and data analysis was conducted using custom programs written in Matlab (The Mathworks Inc.).

Fixation ability was compared by calculating the frequency distribution at each possible bar position mapped to 360° around the arena for each bee. These results are shown as polar plots, calculated in 2.8^{o} bins (which corresponded to the resolution of the LED display). As an additional comparison, a mean vector was determined using a circular statistical toolbox (Berens, 2009) in Matlab for each bee's path. This vector is a representation of the strength of fixation (vector length) and the mean angle the bee faces (direction of the vector). A mean vector length of 1.0 would indicate perfect fixation, where the stimulus was maintained at a single position for the entire experiment, whereas a length of 0.0 would indicate random movement, from a uniform distribution of stimulus positions. The mean vector directions from all bees were tested for significant difference from a uniform distribution (with no preferred orientation) using Rayleigh's test for each condition (Batschelet, 1981; Berens, 2009).

Distributions of the turning rate, ω, were calculated for bees in each condition. ω distributions were calculated based on 5 $^{o}.s^{-1}$ bins between -250 and 250 $^{o}.s^{-1}$. The techniques described in Section 4.5 were implemented in custom Matlab scripts to calculate the position- and motion-dependent control functions in Figure 4-5 and Figure 4-6.

Statistical comparisons (besides Rayleigh's test) are detailed in Section C.5. All statistics were performed using SPSS V20 (IBM).

4.4.6 Modelling

The models in Figure 4-7 were simulated using custom Matlab scripts. In addition to the explanation in Section 4.6.4.1, the following details apply: for each experimental condition fifty simulations were run, with each simulation running for 120 s (3600 time points at 30 Hz), the duration of the actual experiments. Each simulation was initialized with the stimulus positioned at a random location, and the model bee had zero initial turning rate.

4.5 Analysis procedure

Previously a model has been used to predict an insect's turning responses during closed-loop fixation behaviour, which is based on responses as a function of the position and motion of a stimulus in open-loop (Poggio & Reichardt, 1973). Instead of using open-loop behaviour to derive an insect's response to the position and motion of a stimulus, we extract these functions directly from closed-loop experimental data. Before detailing the proposed closed-loop analysis method, we briefly review the methodology for characterising position and motion-dependent control functions from open-loop experiments. Although the control functions are nearly equivalent between open- and closed-loop analyses, deriving control functions from closed-loop experiments require additional factors to be considered. These factors are the non-uniform distribution of stimulus parameters and the temporal correlation of turning responses. In addition, the motion-dependent response could be affected by the direction of motion, which we take into consideration.

4.5.1 Open-loop control functions

In open-loop, a fly responds to the angular position, ψ, and motion, v, of a dark bar presented in a virtual reality arena (Reichardt & Poggio, 1976). This control system (Figure 4-1A), has been modelled using a 'phenomenological' or input-output equation that characterises an insect's expected turning response, as a function of ψ and v,

$$R(\psi, v) = P(\psi) + M(\psi)v + n \tag{4-1}$$

The elements of the phenomenological equation are the position, $P(\psi)$, and motion, $M(\psi)$, functions (originally termed $D(\psi)$ and $r(\psi)$ respectively by Poggio and Reichardt (1973)), are both dependent on the angular position (or bearing) of the stimulus, ψ, at any instant in time. $P(\psi)$ represents the turning response of the animal elicited by the stimulus position. In addition, the insect will usually turn in the same direction as the movement of the stimulus, a response to local-field motion (Bahl et al., 2013). $M(\psi)$ represents the modulation of the insect's response depending on the angular position of the stimulus movement across the visual field. The velocity of the stimulus motion, v, also influences the scale of this response, and the actual response elicited by bar motion (assumed to be proportional to v), is described as $M(\psi)v$. This model assumes that the response to motion in the front-to-back direction is equivalent to the response to back-to-front motion at the same location. The variable n represents random

endogenous movements generated by the animal (Heisenberg & Wolf, 1988), which can be considered a source of stochastic noise in the context of measuring deterministic control functions.

The elements of Eq. (4-1) have classically been reconstructed from open-loop data by observing the behaviour of flies responding to a vertical bar presented in a virtual reality arena (Poggio & Reichardt, 1973; Reichardt & Poggio, 1976). Firstly, the turning response is measured whilst moving the bar completely around the insect in a clockwise (CW) and then in a counter-clockwise (CCW) direction. Whilst both rotations cover the same range of ψ, the polarity of v is inverted between them. $P(\psi)$ and $M(\psi)v$ can then be determined (neglecting n, and assuming no latency either in experimental apparatus, or in the insect physiological measurement of stimulus parameters) as,

$$P(\psi) = \big(R(\psi, v) + R(\psi, -v)\big)/2 \tag{4-2}$$

and,

$$M(\psi)v = \big(R(\psi, v) - R(\psi, -v)\big)/2 \tag{4-3}$$

An insect's response in closed-loop can be predicted using Eq. (4-1) and the control functions, $P(\psi)$ and $M(\psi)$, as measured in open-loop. These control functions abstract a set of underlying processes, involving the non-linear responses and dynamics of visual receptors, neural circuits and motor units, which are embedded in the calculation of each function. Simulations show that these control functions predict similar fixation to that observed in closed-loop experiments (Bahl et al., 2013; Reichardt & Poggio, 1976). However, we extend this approach by using closed-loop data to characterise the control functions underlying insect fixation using analogous position- and motion-dependent functions.

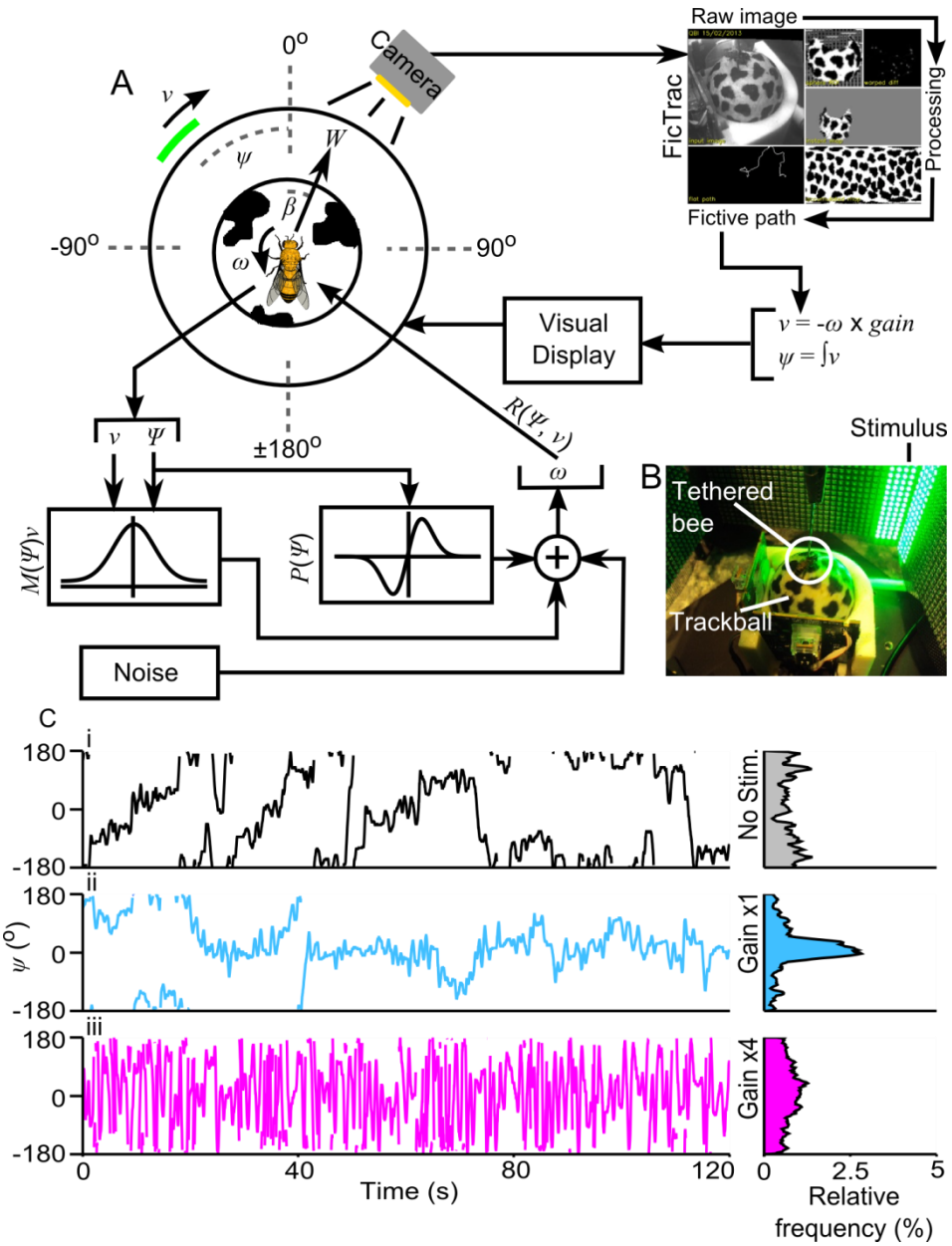

Figure 4-1: Honeybees control the position of a fixation stimulus in closed-loop. **A**, Schematic diagram of the closed-loop interaction between the walking honeybee and the fixation stimulus (central portion). FicTrac (Moore et al., 2014) measures the movement of the trackball, resulting in a measurement of the turning rate, ω, walking speed, W, and walking angle, β, in the bee's reference frame. The measured ω is used to update the state of stimulus (right portion, further described in Section 4.4.3). An insect's turning response, $R(\psi,v)$, depends on the position, ψ, and motion, v, of the stimulus; the sum of non-linear functions of both of those variables ($P(\psi)$ and $M(\psi)v$ respectively), and noise, produce a turning response that can explain fixation behaviour in C (Section 4.5.1). **B**, Photograph of a tethered honeybee walking in the virtual reality arena and the fixation stimulus. **C**, Example time series of stimulus position, ψ, (left), and the resulting distribution (right) over two minute trials from a single bee, with no stimulus – **i**, x1 gain – **ii**, and x4 gain – **iii** conditions. Fixation behaviour produces the peaked distribution of bar positions directly in front of the bee (0^o) in ii.

4.5.2 Considerations for closed-loop analysis

Although an identical stimulus can be used for open- and closed-loop experiments, the spatial and temporal statistics of the stimulus would usually be quite different, making the derivation of comparable control functions difficult. This arises because the insect actively controls the stimulus in order to achieve a particular aim, such as positioning the stimulus when fixating, or stabilising its visual motion when producing the optomotor response (Götz, 1964; Kunze, 1961). If the insect can successfully control the stimulus, its position and movement will not deviate from the stable set points for these parameters in the insect's control system.

In contrast, open-loop experiments have an important property, in that the distribution of any stimulus parameter is controlled by the experimenter. In the usual experiment for determining the position, $P(\psi)$, and motion, $M(\psi)$ functions, the probability of the bar being in a given angular position, ψ, is uniformly distributed over the range of possible ψ values around the arena, and furthermore the number of observations made of the stimulus rotating clockwise (CW) matches those for counter-clockwise (CCW) rotation of equal velocity. Such uniform distributions do not occur in closed-loop when the insect is successfully fixating the stimulus, as a bee will usually bias the ψ distribution to the front of the arena (Figure 4-1C; Moore et al., 2014; Paulk et al., 2014). Furthermore, in controlling the stimulus position, a honeybee will be biased towards turning the stimulus in different directions depending on its position, for example, when the stimulus is positioned to the bee's right (+90°), it preferentially turns rightwards and experiences CCW image motion (Figure 4-2B), and the opposite occurs when the stimulus is positioned to the bee's left (-90°). Non-uniform stimulus distributions occurring in closed-loop experiment are the first consideration in calculating control functions, as an imbalanced number of CW and CCW rotations, at any ψ, will result in an inaccurate calculation of $P(\psi)$ using Eq. (4-2).

Our second consideration is the temporal structure of the turning rate, ω, over time, which can be examined using autocorrelation. The average autocorrelation of ω when no stimulus is displayed indicates that the bee's spontaneous turning motions are temporally structured, and show an exponentially decaying autocorrelation curve (Figure 4-2A). When a fixation stimulus is shown, at any gain condition, the autocorrelation was similar to when the stimulus was not shown (albeit at higher gains the autocorrelation exhibits some periodicity). Intuitively, the exponentially decaying autocorrelation of ω indicates that, regardless of the state of the

stimulus, a bee will likely keep doing much the same as what it was doing in the recent past, implying that the temporal dynamics of the bee's turning behaviour involved low-pass filtered dynamics.

Because a bee's turning rate is low-pass filtered, the relationship between ω and the stimulus velocity is what differentiates the analysis for open- and closed-loop conditions. In closed-loop, when a bee turns in a CW direction, it will simultaneously experience CCW visual motion. The optomotor response describes an insect's strong tendency to turn in the same direction as the wide-field visual motion it experiences (Gotz, 1975; Reichardt, 1973). The ω autocorrelation indicates that it will then likely continue turning CW for some time, contrary to our expectations from the optomotor response. The motion function, $M(\psi)$, quantifies the strength of the response to local-field motion, depending on its angular position in the visual field. If Eq. (4-3) were then directly used to calculate $M(\psi)v$ from closed-loop data, this function will have the opposite polarity to our expectations, and indicate that the bee turned away from the visual motion. This would be in contradiction to findings from open-loop experiments on the bee's response to wide field motion (Kunze, 1961), and is unlikely to occur. A similar autocorrelation of ω would undoubtedly be present in open-loop experiments. However, autocorrelation in open-loop is not as problematic because the insect cannot control the stimulus. Therefore we see that, with non-uniform distributions and temporally correlated data, the $P(\psi)$ and $M(\psi)$ functions cannot be determined accurately using open-loop analysis of closed-loop data with Eqs. (4-2) and (4-3).

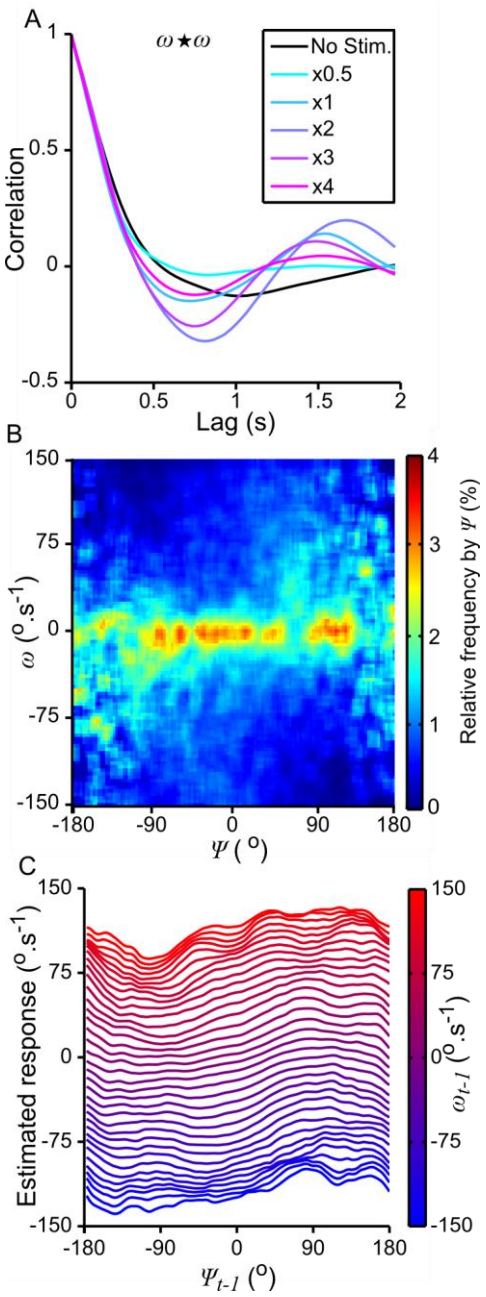

Figure 4-2: Non-uniform stimulus distributions and autocorrelated behaviour are confounding factors for modelling using closed-loop data. **A**, Autocorrelation of turning rate, ω, for all gain conditions. **B**, Heat map of ω distribution for each stimulus position, ψ. **C**, The expected response, $E(\omega_t|\psi_{t-1},\omega_{t-1})$, plotted against ψ_{t-1}, parameterised by ω_{t-1} (Curves are parameterised at 8.5 $^{o}.s^{-1}$ increments). B and C show example data for x2 gain. N=11 repeated all gain conditions.

4.5.3 Uniformly estimating data using Gaussian kernel regression

Gaussian kernel regression (GKR) is a non-parametric statistical technique to estimate the conditional expectation of a random variable, $E(Z|Y,X,\ldots) = F(Y,X,\ldots)$, using noisy observations (Bowman & Azzalini, 1997). The estimation for a set of predictor variables is made based on

a locally weighted average of all observed combinations of predictors, where a Gaussian kernel is used as a weighting function. We used this technique to estimate the expected turning response, ω_t, based on the immediate time history of turning response and stimulus position, ω_{t-1} and ψ_{t-1}, as $E(\omega_t \mid \psi_{t-1}, \omega_{t-1})$. The inclusion of ω_{t-1} as a predictor variable in the regression incorporates both the strongly autocorrelated structure of ω as an autoregression, but also the effect of stimulus velocity, v, on the honeybee's response, as ω and v are directly coupled. $E(\omega_t \mid \psi_{t-1}, \omega_{t-1})$ was calculated based on uniformly distributed ω (0.42 $^{o}.s^{-1}$) and ψ (2.8^{o}) increments (Cao, 2008). The result of such a regression shows the influence of autocorrelation of ω_t strongly offsets the predicted response at all ω_{t-1} parameterisations; however, some of the variation in the curve also appears to depend on ψ_{t-1} (Figure 4-2C).

With ω_{t-1}, the autoregressive component, being the dominant predictor of the estimated value ω_t, $E(\omega_t \mid \psi_{t-1}, \omega_{t-1})$ is not directly useful for calculating the honeybee's response in terms of position- and motion-dependent functions. To remove the immediate effect of autocorrelation from the estimate, the mean value dependent on ω_{t-1} was subtracted, such that the estimated function was now zero-mean for any ω_{t-1} level (a diacritic tilde (~) is used to denote that function has had its mean level subtracted,

$$\tilde{E}(\omega_t \mid \psi_{t-1}, \omega_{t-1}) = E(\omega_t \mid \psi_{t-1}, \omega_{t-1}) - \overline{E(\omega_t \mid -180 < \psi_{t-1} < 180, \omega_{t-1})} \qquad (4\text{-}4)$$

After this operation, the variation in the expected value of ω_t, depending on ψ_{t-1}, is clear across all ω_{t-1} parameterisations and maintains a consistent scale (Figure 4-3B). There does appear to be a distortion of the curve at larger ω_{t-1} parameterisations, suggesting that v, affects the shape of curve. In addition to ensuring that the response is uniformly estimated across the ranges of ψ and ω, Eq. (4-4) provides insight as to how an insect will vary its turning rate in response to the stimulus conditions, and removes the effect of the autocorrelation in ω.

4.5.4 Open-loop control functions from zero-mean responses

In open-loop experiments, where the fixation stimulus is rotated around an insect, the measured response function, $R(\psi, v)$, would not have a mean level of zero because of the insect's response to stimulus motion (Figure 4-3Aii). However, for closed-loop data, subtracting the mean value from the estimated turning response is necessary to prevent the autocorrelation of ω from interfering with the calculation of the insect's response to stimulus motion (Eq. (4-4)).

For open-loop data, if the mean of $R(\psi,v)$ was subtracted, what would the effect on reconstructing the position, $P(\psi)$, and motion, $M(\psi)v$, functions be?

Eq. (4-1) predicts ω based on the underlying $P(\psi)$ and $M(\psi)v$ functions. Subtracting the mean level of this function is equivalent to subtracting the mean level of both the underlying functions,

$$\tilde{R}(\psi,v) = P(\psi) - \overline{P(\psi)} + \left(M(\psi) - \overline{M(\psi)}\right)v \tag{4-5}$$

Reconstructing the underlying functions would then be accomplished by combining the response to CW and CCW motion as in Eqs. (4-2) and (4-3). Reconstruction from zero-mean responses leads to both $P(\psi)$ and $M(\psi)v$ having their mean levels subtracted,

$$\tilde{P}(\psi) = \left(\tilde{R}(\psi,v) + \tilde{R}(\psi,-v)\right)/2 = P(\psi) - \overline{P(\psi)} \tag{4-6}$$

$$\tilde{M}(\psi)v = \left(\tilde{R}(\psi,v) - \tilde{R}(\psi,-v)\right)/2 = \left(M(\psi) - \overline{M(\psi)}\right)v \tag{4-7}$$

This process is illustrated in Figure 4-3A using an example pair of $P(\psi)$ and $M(\psi)$ functions[1] (Figure 4-3Ai), that are summed using Eq. (4-1) to find $R(\psi,v)$ (Figure 4-3Aii). Subtracting the mean level of the function removes information from $\tilde{R}(\psi,v)$ (Figure 4-3Aiii). However, provided each function varies over ψ, information on the shape and scale of this variation is retained (Figure 4-3Aiv-v) when reconstructing $\tilde{P}(\psi)$ and $\tilde{M}(\psi)$ using Eqs. (4-6) and (4-7).

Open-loop functions (with zero-mean) depend on ψ and v, and closed-loop responses (with zero-mean), are also observed to depend on ψ and ω. As such, we propose that zero-mean closed-loop responses and classic open-loop functions, both with their mean level subtracted, are treated as functionally equivalent when analysing fixation control, that is (given $v = -\omega \times gain$),

$$\tilde{R}(\psi,v) = \tilde{E}\left(\omega_t \mid \psi_{t-1}, v_{t-1}\right) = \tilde{E}\left(\omega_t \mid \psi_{t-1}, -\omega_{t-1} \times gain\right) \tag{4-8}$$

[1] The example functions used are $P(\psi) = -50 \times \frac{d}{d\psi} e^{-(\psi/50)^2}$ and $M(\psi) = 0.75 \times e^{-(\psi/70)^2}$.

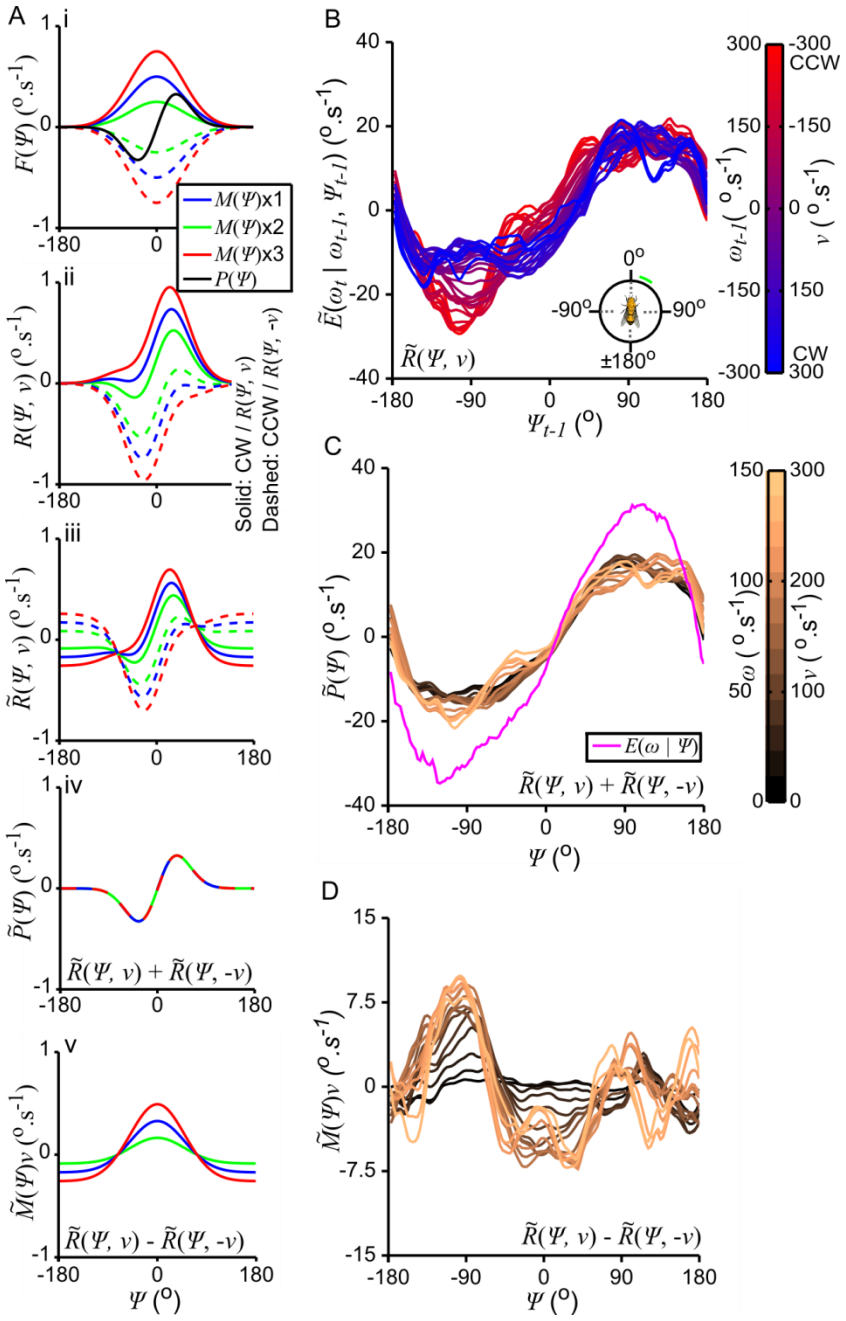

Figure 4-3: Reconstruction of zero-mean functions is possible from zero-mean responses. **A**, Graphical example of reconstructing position, $\tilde{P}(\psi)$, and motion, $\tilde{M}(\psi)v$, dependent functions, using responses where the mean level is subtracted (Section 4.5.4). **i**, functions of stimulus position ($P(\psi)$), and motion ($M(\psi)$) at different stimulus velocities (v). **ii**, the response ($R(\psi,v)$) to CW or CCW motion from the functions in i (Eq. (4-1)). **iii**, zero-mean responses ($\tilde{R}(\psi,v)$) from ii. **iv**, calculation of $\tilde{P}(\psi)$ using the curves in iii (Eq. (4-6), the curves overlap exactly). **v**, calculation of $\tilde{M}(\psi)v$ using the curves in iii (Eq. (4-7)). **B**, The zero-mean expected response, ω_t (from Eq. (4-8)), plotted against past stimulus position, ψ_{t-1}, parameterised by past stimulus velocity, ω_{t-1}. The reconstructed, $\tilde{P}(\psi)$, **C**, and $\tilde{M}(\psi)v$, **D**, functions (from Eqs. (4-6) and (4-7) respectively), plotted against ψ, parameterised by v. B, C, D show an example based on x2 gain. Curves are parameterised in 8.5 $^{o}.s^{-1}$ increments. N=11 repeated all gain conditions.

4.5.5 Closed-loop control functions from zero-mean responses

The standard method of reconstructing position- and motion-dependent functions from open-loop data can then be applied to closed-loop data, by substituting $\tilde{E}(\omega_t|\psi_{t-1},\omega_{t-1})$ in place of $\tilde{R}(\psi,v)$ in both Eqs. (4-6) and (4-7). Reconstruction of the position-dependent function, $\tilde{P}(\psi)$, from the responses for x2 gain (Figure 4-3B) yields a function (Figure 4-3C) that is of a qualitatively consistent scale and shape over a wide range of *v*, although it starts to deform slightly at high *v*. The motion-dependent function, $\tilde{M}(\psi)v$, also displays a relatively consistent shape, the scale of which increases as *v* increases. Notably, the central portion of the function drops below zero, whilst both lateral portions remain above zero. This observation does not require that the bee's response to motion be inverted for motion in its frontal visual field. Rather, the mean level of all curves has been subtracted, and whilst such inversion could be the case, there is likely to be an unknown offset to the original motion function, $M(\psi)v$, such that the response to motion in this region would be zero or positive.

Instead of using Eq. (4-6) to calculate the position-dependent function, $\tilde{P}(\psi)$, an alternative approach to calculating a similar function from closed-loop data would be to take the mean value of ω for each value of ψ. This approach yields an expected value for ω, or $E(\omega|\psi)$, for each value of ψ (Figure C-2). How does this compare to the response calculated using uniformly re-estimated zero-mean data? The $E(\omega|\psi)$ curve is substantially larger in amplitude than those obtained using zero-mean functions (Figure 4-3C). This disparity arises because Eq. (4-6) predicts how the honeybee will change her behaviour from the autoregressive expectation, based on the immediate history ψ and ω, whereas $E(\omega|\psi)$ measures the expected ω after integrating a series of such changes. The expected ω at any ψ will then depend on the average time series of stimulus conditions leading to that ψ, which varies depending on ψ (Figure 4-2B). Both methods provide a representation of the underlying control system (in response to ψ), although Eq. (4-6) provides a representation that can be more easily generalised across all combinations of ψ and *v*. Qualitatively similar curves are observed between $\tilde{P}(\psi)$ and $E(\omega|\psi)$, for all gain levels (in Figure 4-5A and Figure C-2 respectively), although the amplitude of $E(\omega|\psi)$ is always larger than the equivalent $\tilde{P}(\psi)$ function. There is not an obvious alternative to Eq. (4-7) for measuring $M(\psi)v$ from closed-loop data.

4.5.6 Calculating a motion function that depends on motion direction

Studies have shown that the response of a fly to visual motion depends upon the direction of visual motion (Götz, 1975; Götz & Buchner, 1978). The magnitude of the response to stimulus motion was also found to vary at any stimulus position, depending upon whether the motion was from front-to-back or back-to-front (Bahl et al., 2013; Heisenberg & Wolf, 1984; Reichardt, 1973), in other words, that $M(\psi)\times v \neq -M(\psi)\times -v$. This means that to calculate the position function (Eq. (4-2)), which relies on direction invariance of $M(\psi)$, at any ψ, will introduce inaccuracies into the calculation of the $P(\psi)$. When calculating the motion function (Eq. (4-3)), there will also be ambiguities, as $M(\psi)$ will represent an intermediate between $M(\psi)\times v$ and $M(\psi)\times -v$. In this section, we show that is possible to expand the traditional method of calculation $P(\psi)$ and $M(\psi)$ to correctly calculate both, even though front-to-back and back-to-front motion may not elicit equivalent responses.

To do this, we must first include a function describing the insect's response that depends on the direction of motion. This is termed[2] $M_D(\psi)$, and modifies Eq. (4-1) such that,

$$R(\psi,v) = P(\psi) + \left(M(\psi) + M_D\left(\psi \times \mathrm{sgn}(v)\right)\right)v + n \tag{4-9}$$

In this, $M(\psi)$ continues to represent a function modulating the response to motion that is independent of motion direction (although the polarity of the response depends on the direction of motion). However, as well as changing the polarity of $M_D(\psi)$, the direction of motion also reflects this function about $\psi = 0$. $R(\psi,v)$ now allows for the response to motion in the right visual field, during clockwise (CW) motion, to be modulated in the same way as motion in the left visual field, during counter-clockwise (CCW) motion, both of which represent motion from front-to-back. The implicit assumption is then that $M_D(\psi)\times v = -M_D(-\psi)\times -v$, rather than the broader assumption that $M(\psi)\times v = -M(\psi)\times -v$.

This representation of $R(\psi,v)$ is now able to describe the directional dependency of an insect's response to visual motion; however, isolating $P(\psi)$ and $M(\psi)v$ becomes more complicated.

[2] Although $M_D(\psi)$ is expressed as $M_D(\psi \times \mathrm{sgn}(v))$ in Eq. (9), for brevity, the result of the signum function is calculated and written as either ψ or $-\psi$ in the argument for the M_D function in the following equations.

If Eqs. (4-2) and (4-3) are rewritten using Eq. (4-9), then these functions are now reconstructed as,

$$\left(R(\psi,v)+R(\psi,-v)\right)/2 = P(\psi)+\left(M_D(\psi)-M_D(-\psi)\right)v/2 \neq P(\psi) \tag{4-10}$$

and,

$$\left(R(\psi,v)-R(\psi,-v)\right)/2 = \left(M(\psi)+\left(M_D(\psi)+M_D(-\psi)\right)/2\right)v \neq M(\psi)v \tag{4-11}$$

Thus, position and motion functions will be incorrectly represented if Eq. (4-9) underlies an insect's response, rather than Eq. (4-1).

It is possible to fully separate the insect's response for further decomposing Eq. (6) and separating all functions into components that are mirror symmetric or anti-symmetric about $\psi = 0$. Any function can be decomposed such that,

$$F(\psi) = F^M(\psi)+F^A(\psi) \tag{4-12}$$

where $F(\psi)$ is the original function, $F^M(\psi)$ is the mirror symmetric component and $F^A(\psi)$ is the anti-symmetric component, and the axis of symmetry is $\psi = 0$. These component functions are easily found, as,

$$F^A(\psi) = \left(F(\psi)-F(-\psi)\right)/2 \tag{4-13}$$

and,

$$F^M(\psi) = \left(F(\psi)+F(-\psi)\right)/2 \tag{4-14}$$

$F(\psi)$ can be reconstructed by summing Eqs. (4-13) and (4-14). Additionally two useful identities arise from this definition: for anti-symmetric functions,

$$F^A(\psi) = -F^A(-\psi) \tag{4-15}$$

and for mirror symmetric functions,

$$F^M(\psi) = F^M(-\psi) \tag{4-16}$$

Using the function decomposition above, Eq. (4-9) can be re-written as,

$$R(\psi,v) = P^A(\psi)+P^M(\psi)+\left(M^A(\psi)+M^M(\psi)+M_D^A\left(\psi\times\mathrm{sgn}(v)\right)+M_D^M\left(\psi\times\mathrm{sgn}(v)\right)\right)v+n \tag{4-17}$$

Whilst not immediately obvious, the advantage of this decomposition is that all terms in $R(\psi,v)$ can always be expressed as functions of positive ψ using the identities in Eqs. (4-15) and (4-16) . Furthermore, we can now add and subtract the measured responses to CW, $R(\psi,v)$, and CCW

motion, $R(\psi,-v)$, and reflections about ψ = 0 of those responses (these being $R(-\psi,v)$ and $R(-\psi,-v)$ respectively), whilst still expressing all equations as functions of ψ. Four equations provide additional insight, which are (further described in Section C.2),

$$\big(R(\psi,v)+R(\psi,-v)+R(-\psi,v)+R(-\psi,-v)\big)/4 = P^M(\psi) \tag{4-18}$$

$$\big(R(\psi,v)+R(\psi,-v)-R(-\psi,v)-R(-\psi,-v)\big)/4 = P^A(\psi)+M_D^A(\psi)v \tag{4-19}$$

$$\big(R(\psi,v)-R(\psi,-v)+R(-\psi,v)-R(-\psi,-v)\big)/4 = \big(M^M(\psi)+M_D^M(\psi)\big)v \tag{4-20}$$

$$\big(R(\psi,v)-R(\psi,-v)-R(-\psi,v)+R(-\psi,-v)\big)/4 = M^A(\psi)v \tag{4-21}$$

Three of these equations contain terms arising from either a position or motion response, although it is not possible to completely separate these components, as Eq. (4-19) has terms dependent on both. However, when $v \approx 0$, Eq. (4-19) will result in function describing a position response,

$$\big(R(\psi,\sim 0)+R(\psi,\sim 0)-R(-\psi,\sim 0)-R(-\psi,\sim 0)\big)/4 \approx P^A(\psi) \tag{4-22}$$

The motion response for any v can now be determined. The sum of Eqs. (4-19) to (4-21), minus (4-22), will provide the complete response to stimulus motion in a CW direction, $M_{CW}(\psi)v$ (see Section C.2 for the derivation of $M_{CCW}(\psi)v$),

$$\begin{aligned}&\big(3R(\psi,v)-R(\psi,-v)-R(-\psi,v)-R(-\psi,-v)\big)/4-P^A(\psi)\\&=\big(M^A(\psi)+M^M(\psi)+M_D^A(\psi)+M_D^M(\psi)\big)v = M_{CW}(\psi)v\end{aligned} \tag{4-23}$$

The sum of $P^M(\psi)$ (from Eq. (4-18)) and $P^A(\psi)$ (from Eq. (4-22)) will also provide the complete response to stimulus position in either direction, $P(\psi)$, although this can also be calculated using Eq. (4-2) when $v \approx 0$. This procedure uses function symmetry to separate the position- and motion-dependent components of an insect's response to a fixation stimulus when the motion-dependent component is fully or partially directionally dependent. Although we have used the classic function notation for $P(\psi)$ and $M(\psi)v$ through this section, the procedure is also applicable to zero-mean responses.

We have outlined three separate analysis procedures as follows: 1) Gaussian kernel regression to uniformly estimate non-uniformly sampled closed-loop data, 2) zero-mean functions for removing the immediate effect of autoregression, and 3) calculation of a motion-dependent

function for each direction of motion. In combination, this yields functions that depend on the position, $\tilde{P}(\psi)$, and motion, $\tilde{M}(\psi)$, of a fixation stimulus that can be calculated from closed-loop experimental data. This provides a new method of characterising the control functions that underlie an insect's fixation behaviour from closed-loop data.

4.6 Results

Walking honeybees have been shown to orient towards bright visual objects (Moore et al., 2014; Paulk et al., 2014; Zolotov, Frantsevich, & Falk, 1975), however, it is not known how robust this behaviour is to varying gains. To examine this, we tested walking honeybees with a task in which they could fixate a vertical bright green bar on a black background in closed-loop (Figure 4-1B), using their turning rate to control its angular position. The coupling between the measured turning rate and the angular velocity of the bar (i.e. the gain of the feedback coupling), was randomly varied across five conditions, representing gains of x0.5, x1 x2, x3 and x4, as well as a no stimulus control condition, where the fixation stimulus was not presented. The results revealed that honeybees were able to fixate the stimulus at lower gains, although their performance degraded at high gain conditions (Figure 4-4A). To both derive and analyse the control system underlying the bee's fixation behaviour, we used the closed-loop analysis procedures outlined in the preceding section.

4.6.1 Honeybees fixate a visual stimulus over a range of gains

Honeybees attempted to position the fixation stimulus, a vertically oriented bright green bar, in their frontal visual field. At a x1 gain (Figure 4-1Cii), which means that for every 1° rotation of the ball there is a 1° rotation of the stimulus, the bee is clearly able to fixate on the stimulus, resulting in a single major peak in the distribution of bar positions in front of the bee (around 0^o). This behaviour was less pronounced at higher gains, such as at x4 gain where the distribution shows a much shallower peak in frontal region (Figure 4-1Ciii). However, without a visual cue, the position of the stimulus was scattered, demonstrating that presence of the visual stimulus clearly had an effect on the bee's behaviour (Figure 4-1Ci).

Bees fixated the stimulus frontally over varying gain conditions, as observed in radial histograms (Figure 4-4A). However, at higher gains the stimulus positions become less frontally distributed, and the distributions at very high gains were similar to those for the no

stimulus control. To quantify the sharpness of these directional distributions, we calculated the mean vector of the bar positions over the experiment (Figure C-1). The length of the mean vector (which is a measure of the sharpness of an angular distribution) was generally larger at lower gains compared to those at higher gains, and for the no stimulus condition, indicating that fixation was more robust at the low gains (Figure 4-4B). The gain condition had a significant effect on mean vector length (χ^2_5=32.20, ***p*<0.001**), and *post-hoc* tests showed that the x0.5 gain condition, which had the longest mean vectors, was significantly different from the x4 gain and the no stimulus conditions. In addition, the mean vector *directions* for x4 gain and the no stimulus conditions were not significantly different from random (Figure C-1, Rayleigh's test – NS: z_{10}=0.80, p<0.459, and x4: and z_{10}=0.11, p=0.902). This confirms that a bee's ability to position the stimulus in its frontal field of view degrades progressively as the gain is increased, as bees could not maintain preferred angular position for the stimulus at x4 gain. However, the fixation results do not distinguish between two possibilities: 1) bees may not have adapted their behaviour at different gains, and been unable to control the stimulus at high gain, or 2) the bees may have adapted their behaviour, even though the adaptions were insufficient to control the stimulus at high gains. Since these two possibilities cannot be separated by measuring fixation performance alone, we must further analyse the characteristics of the underlying control system used by bees for the various gain conditions.

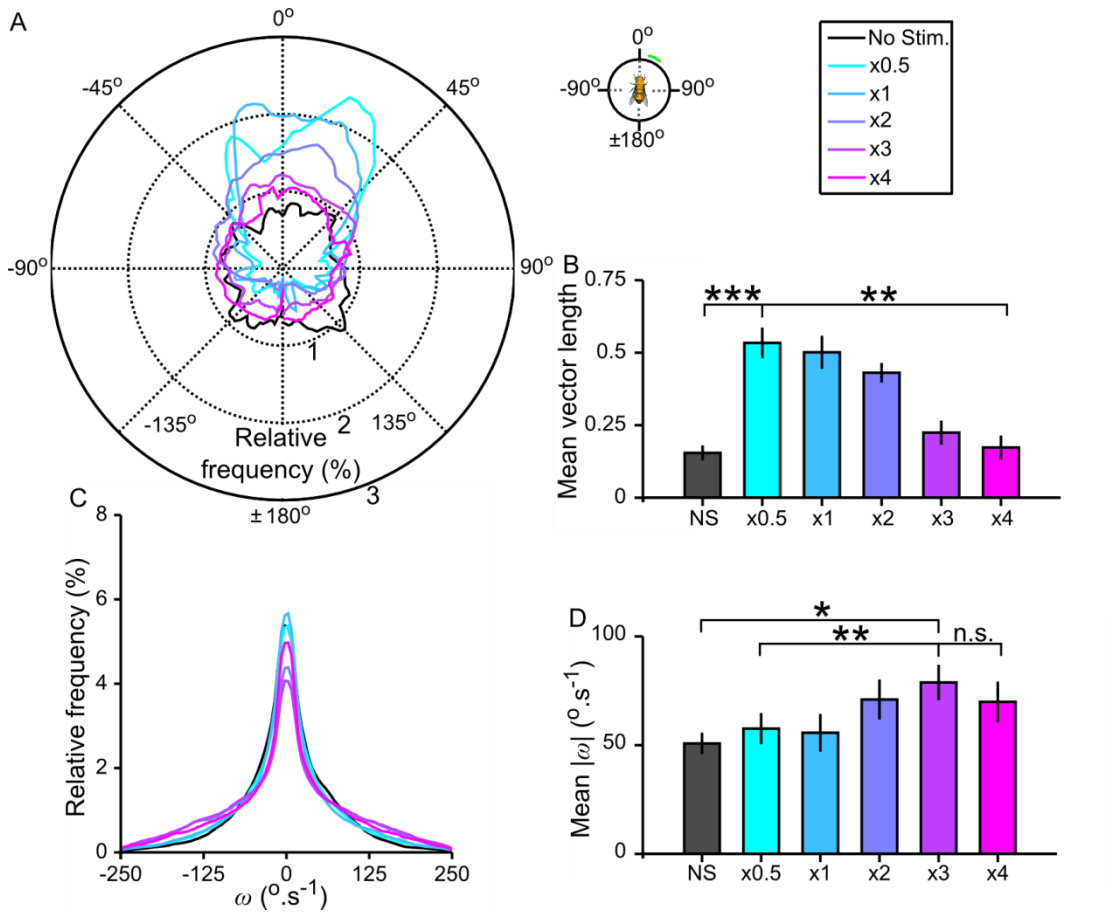

Figure 4-4: Honeybee's fixation performance degrades at high gain conditions. **A**, Radial histograms of stimulus position, ψ, showing distributions for each gain condition. **B**, Average mean vector lengths for all conditions (Actual mean vectors are shown in Figure C-1). **C**, Distributions of turning rate, ω. **D**, Mean $|\omega|$ for all conditions. Error bars show ± S.E.M. N=11 repeated all gain conditions. Stars (n.s.: $p>0.05$, *: $p<0.05$, **: $p<0.01$, ***: $p<0.001$) denote a statistically significant differences between groups, with full statistical in Section C.5.1.

4.6.2 Average turning rate increases with gain

Did the bees attempt to modify the way in which they controlled the stimulus at higher gains in order to improve performance? An initial test for such adaption was to investigate the distribution of turning rates, ω, which is the bee's motor output used to control the stimulus (Figure 4-4C). The results show that the shapes of the ω distributions are qualitatively similar across all of the gain conditions, but that the mean $|\omega|$ significantly increased as gain increased (Figure 4-4D, $F_{5,50}=6.08$, $\mathbf{p<0.001}$). Given that increased gain increases angular velocity of the bar for a given turning rate of the bee, one might intuitively expect that the honeybee would reduce the magnitude of its turning motions to control the stimulus more effectively. Surprisingly, we found the opposite effect.

Yet the distributions of bar position or turning rate provide limited information on whether the bees are adapting their behaviour to gain changes, because they do not specifically link the bee's motor output, ω, to specific control inputs, such as stimulus position, ψ, and velocity, v. Furthermore, at the different gain conditions, the bees experienced very different combinations of ψ and v. For example, at x0.5 gain, ω distributions are the result of a control system operating when the stimulus is positioned predominantly in the frontal visual field. This is in contrast with the situation at x4 gain, where the stimulus position is more widely distributed (Figure 4-4A). To understand how bees adapt to each of these gain conditions, we must examine the control functions linking the stimuli to the motor actions.

4.6.3 Comparison of control functions at varying gains

To quantify how the bees adapted the control functions underlying their fixation at various gain conditions, we characterised their responses to the fixation stimulus in terms of position, $\tilde{P}(\psi)$, and motion, $\tilde{M}(\psi)$, dependent functions. The functions were calculated from closed-loop data using the methods described in the Section 4.5 to uniformly estimate the data, remove the immediate effects of autocorrelation, and separate the motion responses dependent on motion direction.

4.6.3.1 Position-dependent function

Honeybees were found to vary the scale of their response to stimulus position, depending upon the gain condition. The stimulus position, $\tilde{P}(\psi)$, was calculated using Eq. (4-3) when the bee's turning rate, ω, was close to zero (specifically, for $|\omega| < 5\ ^{o}.s^{-1}$ at all gain conditions). $\tilde{P}(\psi)$ generally has an anti-symmetric shape for all gain conditions (Figure 4-5A). For x2 gain and above, this appears to approximate a single period of a sine function. The amplitude, or scale, of the $\tilde{P}(\psi)$ in Figure 4-5A varies depending on the gain condition. To objectively compare the scale (*Sc.*) of $\tilde{P}(\psi)$, the mean of the function for $\psi < 0$ was subtracted from the mean for $\psi > 0$, that is,

$$\tilde{P}^{Sc.} = \overline{\tilde{P}(0 < \psi < 180)} - \overline{\tilde{P}(-180 < \psi < 0)} \qquad (4\text{-}24)$$

$\tilde{P}^{Sc.}$ values for gain conditions above x1 were significantly different from zero, indicating that honeybees modulated ω such that it was generally positive for $\psi > 0$ and negative for $\psi < 0$

(Figure 4-5B). Further, $\tilde{P}^{Sc.}$ peaked at x2 gain, and varied significantly depending on gain condition ($F_{1.71,\ 17.06}$=3.78, ***p*=0.047**). *Post-hoc* tests showed that $\tilde{P}^{Sc.}$ for x2 gain was significantly higher than for the x0.5 or the x4 gain, indicating that the bees varied the scale of their response to a given stimulus position, depending on the gain condition. In contrast, in the no stimulus condition, the predicted $\tilde{P}(\psi)$ does not vary depending on ψ (Figure 4-5A), and $\tilde{P}^{Sc.}$ is not significantly different from zero (Figure 4-5B), confirming that $\tilde{P}(\psi)$ represents the response to a stimulus. Bees modulated their turning rate depending upon the angular position of the stimulus, and the scale of this modulation varies depending on the gain condition.

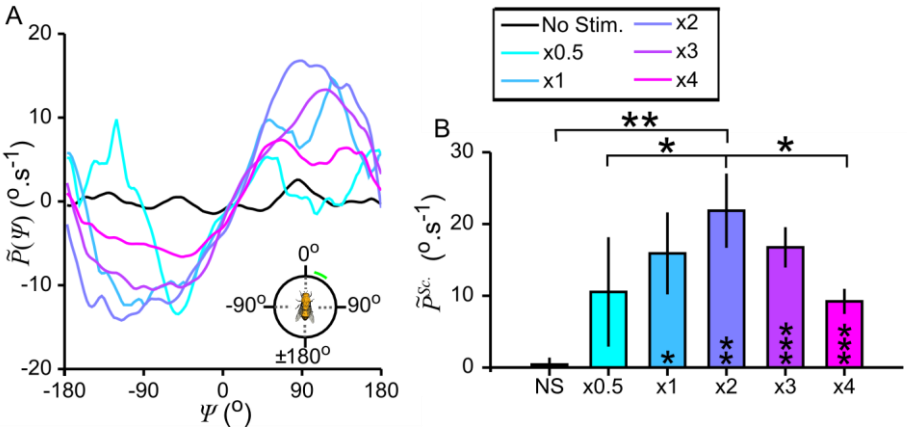

Figure 4-5: The scale of the position-dependent response function varied depending on the gain condition. **A**, The average position-dependent function, for various gain conditions. **B**, The scale of $\tilde{P}(\psi)$ as indicated by $\tilde{P}^{Sc.}$ (from Eq. (4-24)). N=11 repeated all gain conditions. Error bars show ± S.E.M. Stars (*: p<0.05, **: p<0.01) in bars denote factor averages that are statistically different from zero, otherwise stars denote a statistically significant difference between the indicated groups, with full statistical details in Section C.5.2.

4.6.3.2 Motion-dependent function

Honeybees were found to adjust the shape of their response to motion, which depended on the direction of motion. $\tilde{M}(\psi)v$ for clockwise (CW) motion was calculated using Eq. (4-23), and for counter-clockwise (CCW) motion using Eq. (C-11), over the limited range[3] $|\omega| < 50\ ^{o}.s^{-1}$, for all gain conditions (the motivation for limiting the range of ω is discussed in Section C.3). For all gain conditions, increasing ω increased the scale of the motion-dependent response (Figure 4-6A for $\tilde{M}_{CW}(\psi)v$ and Figure C-3 for $\tilde{M}_{CCW}(\psi)v$).

[3] $P^{M}(\psi)$ in these equations was calculated using Eq. (4-18) when $|\omega| < 5\ ^{o}.s^{-1}$.

The amplitude, or scale, of $\tilde{M}_{CW}(\psi)v$ varies for the no stimulus condition (Figure 4-6Ai). This could indicate that ω affects the scale of this function in the absence of a fixation stimulus, which potentially arises due to the slight periodicity observed in the autocorrelation of turning responses observed during the no stimulus condition (Figure 4-2A). This is confounding for comparing the scale of the motion response between gain conditions, because the stimulus velocity, *v*, is always proportional to ω (with the gain determining the proportionality). As such, different gain conditions cannot be compared with simultaneously equivalent ω and *v* levels, and we cannot draw conclusions based on variation in scale between gain conditions.

On the other hand, the shape (*Sh.*) of $\tilde{M}_{CW}(\psi)v$, appears to vary depending on gain condition. Because the scale of the function obviously changes with *v*, comparing the typical shape between gain conditions is difficult. To facilitate this comparison, we calculated a scale invariant shape of the motion-dependent response, as $\tilde{M}^{Sh.}(\psi)$. Firstly $\tilde{M}(\psi)v$ measured for any ω was divided by its root-mean-square (RMS) value, $\tilde{M}^{RMS}(\psi)v$, resulting in a function that would have an RMS value of 1. $\tilde{M}^{Sh.}(\psi)$ was calculated as the average of these RMS normalized functions, across the range $20 < |\omega| < 50$ $^{o}.s^{-1}$ (the lower limit was imposed as $\tilde{M}(\psi)v$ may be poorly attenuated at low ω, Section C.3),

$$\tilde{M}^{Sh.}(\psi) = 1/30 \int_{20}^{50} \frac{\left(\tilde{M}(\psi)v\right)|\omega}{\left(\tilde{M}^{RMS}(\psi)v\right)|\omega} .d\omega \tag{4-25}$$

This procedure was performed for both CW and CCW motion, to find $\tilde{M}^{Sh.}_{CW}(\psi)$ and $\tilde{M}^{Sh.}_{CCW}(\psi)$ respectively.

In this form, $\tilde{M}^{Sh.}(\psi)$ clearly varies depending on stimulus position, ψ, for all gain conditions, and also between motion directions (Figure 4-6D). An initial observation is that the elevated responses of these functions tend to occur when the stimulus is moving from front-to-back, for CW motion this is when $\psi > 0$, and for CCW motion $\psi < 0$. Further, these regions of elevated response appear to occur when the bar is positioned laterally to the bee, at $\psi \approx \pm 90^{o}$, for all gain conditions. A second observation is that the difference in amplitude between these elevated regions, and the response when the stimulus is positioned centrally, at $\psi \approx 0^{o}$, increases as gain increases. At x2 gain or higher, the response to motion in the frontal field is clearly diminished for motion in both directions, suggesting that varying the relative response of the motion response across the visual field is an adaption to varying gain conditions.

For each gain condition, two comparisons were made for motion in each direction, at each gain condition. These comparisons were measurements of the difference in the response of $\tilde{M}^{Sh.}(\psi)$ in various visual regions. These regions were: left lateral; -135 < ψ < -45º, frontal; -45 < ψ < 45º, and right lateral; 45 < ψ < 135º. We compared the difference between mean response in the left lateral region and the mean response in the frontal region,

$$\overline{\tilde{M}^{Sh.}(L)} - \overline{\tilde{M}^{Sh.}(F)} = \overline{\tilde{M}^{Sh.}(-45 < \psi < -135)} - \overline{\tilde{M}^{Sh.}(-45 < \psi < 45)} \quad (4\text{-}26)$$

and, also the difference between the mean response in the right lateral region and the mean response in the frontal region,

$$\overline{\tilde{M}^{Sh.}(R)} - \overline{\tilde{M}^{Sh.}(F)} = \overline{\tilde{M}^{Sh.}(45 < \psi < 135)} - \overline{\tilde{M}^{Sh.}(-45 < \psi < 45)} \quad (4\text{-}27)$$

These differences in the motion function corresponding to frontal and side bar positions confirm that at all gain conditions, for both bar motion directions, the strength of $\tilde{M}^{Sh.}(\psi)$ in the lateral visual field corresponding to front-to-back motion is larger than the response in the frontal visual field (Figure 4-6C and D). This results in a positive difference that is significantly larger than zero for the majority of gain levels. Furthermore, this difference in the motion function varies significantly depending on gain condition, tending to increase as gain increases. In contrast, the difference in $\tilde{M}^{Sh.}(\psi)$ between the lateral and frontal visual fields for back-to-front motion is only significantly larger from zero in one case (Figure 4-6C), and in some cases falls below zero. It does not vary significantly depending on gain condition. This indicates that the strength of $\tilde{M}^{Sh.}(\psi)$ in the lateral visual field is generally comparable to that in the frontal visual field for back-to-front motion. Bees modulated their turning rate in response to stimulus motion depending on where in their visual field it occurs. The relative strength of the response in any given area of the visual field changes depending on the gain condition, and it also differs depending on whether the stimulus motion is from front-to-back, or from back-to-front.

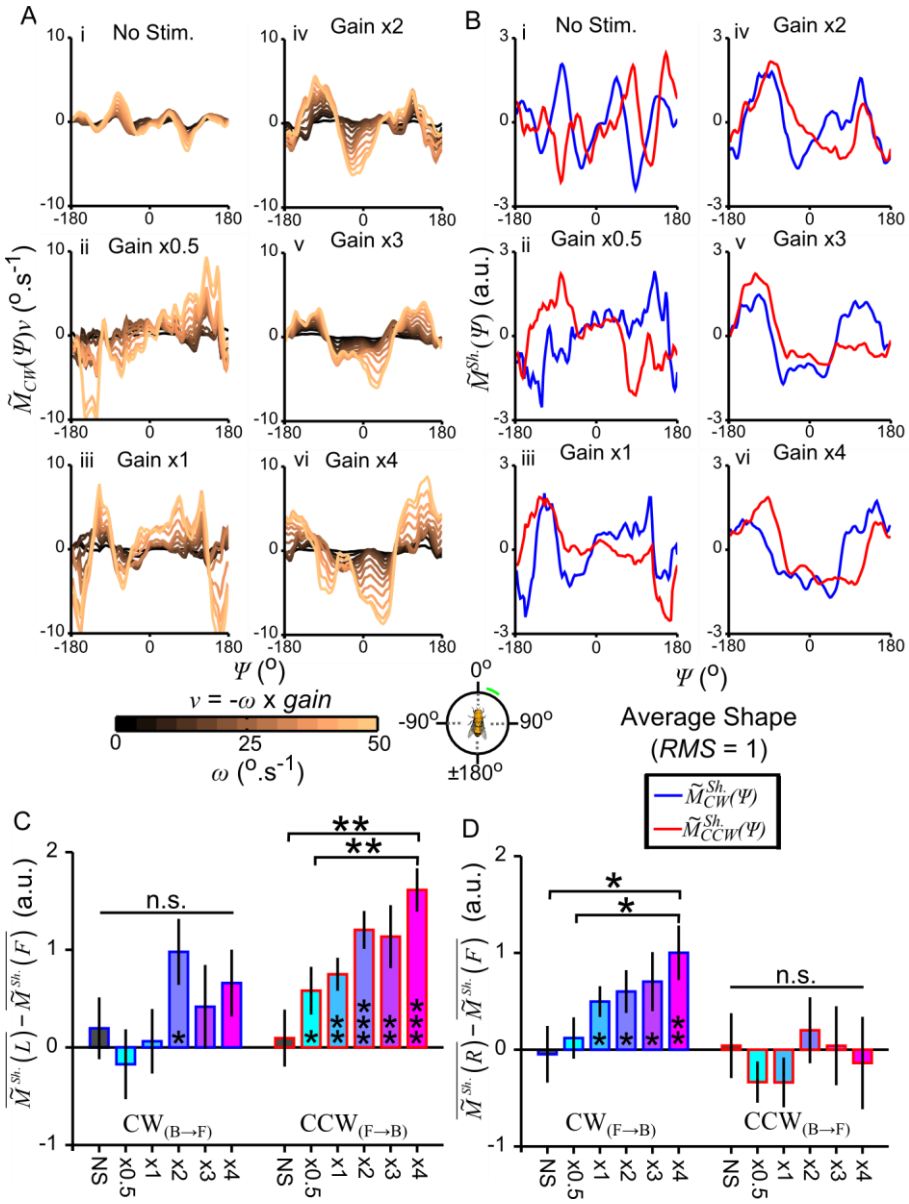

Figure 4-6: The shape of the motion-dependent function varies depending on gain condition. **A**, The clockwise motion-dependent function, $\tilde{M}_{CW}(\psi)$, for all gain conditions, parameterised by turning rate, ω, ($v = -\omega \times gain$, see Figure C-3 for $\tilde{M}_{CCW}(\psi)$ curves) in 4.2 °.s^{-1} increments. **B**, The scale invariant motion function, $\tilde{M}^{Sh.}(\psi)$ (from Eq. (4-25)), for rotation in both directions, for each gain condition. All curves in B have an RMS scale of one. **C**, comparison of relative strength of $\tilde{M}^{Sh.}(\psi)$ in the left ($-135 < \psi < -45°$) and frontal ($-45 < \psi < 45°$) visual fields, across all gain conditions for both motion directions using Eq. (4-26). **D**, as for C, with the comparison between the right and frontal visual fields using Eq. (4-27). N=11 repeated all gain conditions. a.u. = arbitrary units. Error bars show ± S.E.M. Stars (n.s.: $p>0.05$, *: $p<0.05$, **: $p<0.01$, ***: $p<0.001$) in bars denote factor averages that are statistically different from zero, otherwise stars denote a statistically significant difference between the indicated groups, with full details in Section C.5.3.

4.6.4 Model simulations using control functions

To assess how well the control functions predicted bee behaviour, we used these functions to computationally simulate the fixation behaviour of a 'model' honeybee under various gain conditions. This model was used to test how the position or motion-dependent functions would respond in isolation, and also how the control functions would perform when tested using simulation gains that were different from the experimental gain for which they were calculated.

4.6.4.1 Model details

The model (Figure 4-7A), uses the instantaneous stimulus position, ψ, and instantaneous velocity, v, to predict the simulated bee's turning response, ω, using position- and motion-dependent functions calculated from the experimental data for each gain condition. By incorporating temporal dynamics, noise, and stimulus displacements, the model mimics the conditions experienced during actual behavioural experiments.

The position-dependent response was predicted using $\tilde{P}(\psi)$, as in Figure 4-5. The motion-dependent response was predicted using $\tilde{M}^{Sh.}(\psi)$ (further separated into $\tilde{M}^{Sh.}_{CW}(\psi)$, and $\tilde{M}^{Sh.}_{CCW}(\psi)$) as in Figure 4-6. Both $\tilde{P}(\psi)$ and $\tilde{M}^{Sh.}(\psi)$ were calculated as zero-mean functions. Hence, $\tilde{M}^{Sh.}(\psi)$ must have a negative magnitude at some ψ values. If $\tilde{M}^{Sh.}(\psi)$ was left as is, the stimulated honeybee's response to stimulus motion would change polarity depending on stimulus position; at some ψ it would turn in the same direction as stimulus motion, at others it would turn in the opposite direction. This is unlikely to occur; hence to correct this, each calculated $\tilde{M}^{Sh.}(\psi)$ curve was offset such that its minimum was zero,

$$\tilde{M}\uparrow^{Sh.}(\psi) = \tilde{M}^{Sh.}(\psi) + \min\left(\tilde{M}^{Sh.}(\psi)\right) \tag{4-28}$$

A linear function of v was used as a multiplier to scale $\tilde{M}\uparrow^{Sh.}(\psi)$; the coefficients, a_M and b_M, of this function were found using a linear regression on the average RMS scale between $\tilde{M}_{CW}(\psi)$ and $\tilde{M}_{CCW}(\psi)$, over the ω range 0 to 150°.s^{-1}, from experimental data for each gain condition (Figure C-4). The simulated honeybee's response to visual motion was then,

$$M(\psi)F(v) = \tilde{M}\uparrow^{Sh.}(\psi) \times (a_M + b_M v) \tag{4-29}$$

The sum of $\tilde{P}(\psi)$, $M(\psi)F(v)$, and a source of Gaussian noise predicted the change in the simulated honeybees turning rate, ω, from its past state. The Gaussian noise represented the

random actions made by a honeybee, and the average standard deviation for the no stimulus condition, 71.5 $^{o}.s^{-1}$, was used as the standard deviation of the noise term. The amplitude of the noise may have varied between experimental gain conditions; however it was not possible to use our data to measure if such changes occurred. A saturation limit of ± 500 $^{o}.s^{-1}$ was imposed on ω, as turning rates reaching this were very rarely observed (Figure 4-4C). The stimulus velocity, v, experienced by the honeybee, was $v = -\omega \times gain$.

To ensure that the simulation replicated the experimental conditions, forced displacements were incorporated that followed the same randomized pattern as for the actual experiments (described in Section 4.4.4), were included in the simulation (these did not noticeably influence fixation performance, Figure C-5). A three time point delay was also included between the simulated bee's action affecting the stimulus position, representing the latency between the honeybees' actions and a change in the stimulus position under experimental conditions. The results from this configuration of the model overestimated the bees' fixation ability at most gain conditions (Figure C-5), exhibiting more accurate fixation than observed in experiments (Figure 4-4A).

To include an approximation of the temporal dynamics underlying the response, we fitted a six-step (200 ms) autoregression (AR) filter to the ω time series from the no stimulus condition[4]. The AR filter implements the low-pass dynamics observed in the exponentially decaying autocorrelation of ω (Figure 4-2A), this may be limited to describing the dynamics of a bee's actuation signal, rather than the sensorimotor dynamics. Incorporating the AR low-pass filter resulted in similar simulated fixation performance (Figure 4-7B and Figure C-5) to experimental results (Figure 4-4A). Hence, it is possible to qualitatively replicate honeybee fixation with a simulation model by using control functions calculated from closed-loop experiments combined with temporal dynamics. Fixation results can be replicated from all experimental gain conditions, when matched to the appropriate simulation gain, which validates the measurement of position- and motion-dependent functions from closed-loop data.

[4] $\omega(t) = 0.67\omega(t-1) + 0.26\omega(t-2) + 0.03\omega(t-3) + 0.04\omega(t-4) - 0.05\omega(t-5)$
$-0.08\omega(t-6) + M(\psi)F(v) + \tilde{P}(\psi) + n$

4.6.4.2 Model results

When the simulation gain matched the experimental gain used for deriving control functions, simulations of the model honeybee showed fixation performance (Figure 4-7Bi) that was similar to that observed in the actual behavioural experiments (Figure 4-4A) across all gain conditions. At low gains the simulated honeybee concentrated the distribution of the stimulus position into its frontal visual field and these distributions were less concentrated at high gains. The simulations showed exponentially decaying and periodic autocorrelations (Figure 4-7Bii), which were again similar to observations from behavioural experiments (Figure 4-2A), although shorter oscillation periods were found for the simulated data. Un-modelled dynamics in the bee's response may be responsible for the observed difference in the autocorrelation periods, although this does not appear to affect the fixation results.

To assess the robustness of the control functions calculated for each experimental gain condition, we ran the simulation using the normal x1 gain (Figure 4-7C), and the highest gain, x4 (Figure 4-7F). At a simulation x1 gain, the control functions calculated from all experimental gains could bee used to to fixate the stimulus, although the efficacy varied; control functions calculated for x3 and x4 gains performed worse than those calculated for x0.5 and x1 gains (Figure 4-7C). At a simulation x4 gain, the model honeybee could not fixate the stimulus regardless of which experimental gain the control functions were calculated from (Figure 4-7F). Furthermore, the autocorrelations when using control functions calculated at experimental x0.5 and x1 gains showed that unstable oscillations of ω occurred (Figure 4-7Fii), whereas the autocorrelations when using control functions calculated at experimental x2, x3, and x4 gains produced ω oscillations that were damped (Figure 4-7Fii). This indicates that, despite having limited success in fixating the stimulus at higher gains, the control strategy adopted by honeybees allowed them to retain some stability at these gains, was not achieved using the control functions calculated for lower gains.

The efficacy of either position or motion-dependent functions at providing fixation control, in isolation, was tested using a x1 gain. When the simulated honeybee only used the position-dependent function (Figure 4-7D), fixation was noticeably impaired, with the function calculated at experimental x0.5 gain performing worst. Surprisingly, when the simulated honeybee only used the motion-dependent function, weak fixation appeared possible using the function calculated for experimental x0.5 and x1 gains, although not when the function was calculated from data for higher gains (Figure 4-7E). When using either the position or motion-

dependent functions in isolation, regardless of the gain condition, fixation performance was worse than when the control functions were used in combination (Figure 4-7C).

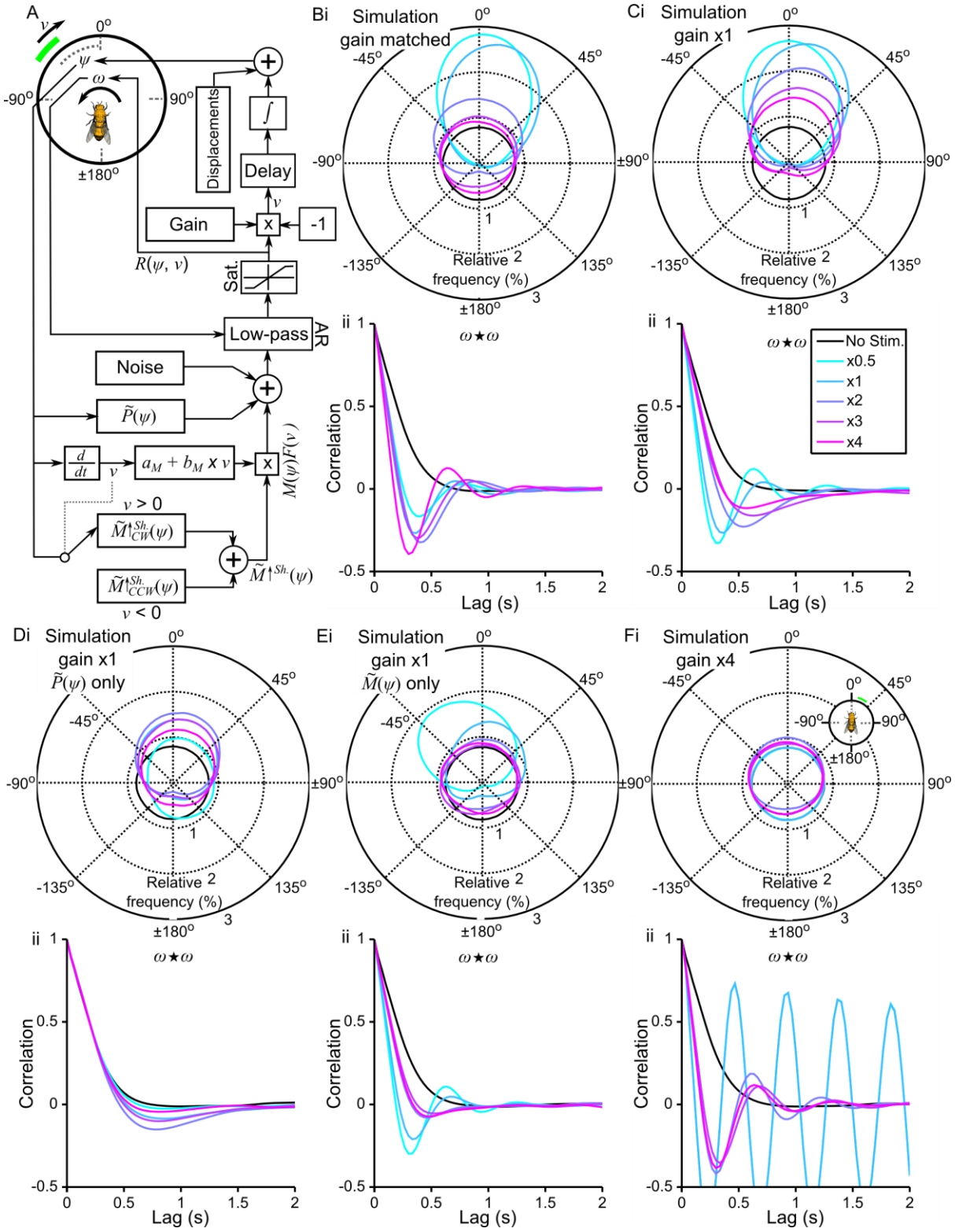

Figure 4-7: Position- and motion-dependent functions can qualitatively predict fixation performance across all gain settings. **A**, Block diagram of fixation model (Section 4.6.4.1). Position- and motion-dependent functions are calculated based on experimental data for each

gain setting. **B**, Simulation gain matches experimental gains. **C**, Simulation is x1 gain regardless all experimental gains. **D**, As for C, however, only the position-dependent function, $\tilde{P}(\psi)$, is used for fixation control. **E**, As for C, however, only the motion-dependent function, $\tilde{M}(\psi)$, is used for fixation control. **F**, Simulation is x4 gain regardless of experimental gain. For B, C, D, E, and F; **i** shows radial histograms of stimulus position, ψ, distributions, and **ii** shows the corresponding autocorrelations of turning rate, ω. Results from experimental data for fixation are displayed in Figure 4-4A, and for autocorrelation in Figure 4-2A.

4.7 Discussion

Tethered visual fixation, where an insect uses a motor output to control the angular position of a fixation stimulus, represents a relatively constrained behavioural experiment compared to flying or walking in the natural world. However, given that an insect combines non-linear responses to the position and motion of the stimulus, and also generates random turning fluctuations, quantifying the underlying control scheme from closed-loop data is a non-trivial task (Wolf et al., 1992). Using novel analysis techniques, we find that the position- and motion-dependent functions, $\tilde{P}(\psi)$ and $\tilde{M}(\psi)$, that describe a honeybee's turning response can be reconstructed from a quantitative analysis of closed-loop behaviour in which bees fixated a vertical bar. These functions are similar to the classic position and motion functions, $P(\psi)$ and $M(\psi)$ that have been derived for flies (Bahl et al., 2013; Heisenberg & Wolf, 1984; Reichardt & Poggio, 1976), except that they represent how a honeybee will change her turning rate, given the current state of the stimulus, rather directly predicting the turning rate. Honeybees adapt both the position- and motion-dependent functions underlying their control of the stimulus. Whilst the bee's ability to fixate the stimulus deteriorates as gain increases, the simulation studies suggest that their adaptations do improve their control of the stimulus at high gain.

4.7.1 Closed-loop analysis techniques

In order to examine these control functions, we used Gaussian kernel regression (GKR) to uniformly estimate the honeybee's response to all combinations of stimulus position and velocity from data that was originally non-uniformly sampled over these variables. Non-uniform stimulus distributions could result from any closed-loop behaviours, particularly those based on an orientation task such as navigation or prey pursuit. Whilst some control systems identification techniques can be applied directly to data from closed-loop experiments (Ljung, 1999; Westwick & Kearney, 2003), uniform stimulus distributions are required to reconstruct $\tilde{P}(\psi)$ and $\tilde{M}(\psi)$ for use with the classic phenomenological equation (Poggio & Reichardt,

1973) in Eq. (4-1). Uniformly resampling closed-loop data using GKR alleviates the problem of non-uniformly sampled data, and could enable systems identification using closed-loop data for other behaviours.

One consideration when resampling with GKR is that the signal to noise ratio (SNR) across the range of predictor variables may not be constant, as a non-equal number of points contribute to any estimate. As every estimate is based on a locally weighted average, increasing the number of contributing observations will decrease the SNR. When reconstructing $\tilde{P}(\psi)$ from x0.5 gain data, low SNR may have been problematic when the stimulus position approached $\pm 180^{o}$, as most bees rarely position the stimulus to their rear. Tellingly, the reconstructed $\tilde{P}(\psi)$ for x0.5 gain appears qualitatively noisier than those for higher gains. When characterising a highly stable control system in closed-loop, as bees were for the x0.5 gain condition, open-loop displacements should be applied to ensure that the insect's response can be measured multiple times across the full range of all stimulus parameters (Ljung, 1999). Obviously it is a fine distinction between conducting a closed-loop experiment with regular open-loop disturbances, and an experiment where too many disturbances may influence how the insect adapts its control.

4.7.2 Control functions

The position-dependent function, $\tilde{P}(\psi)$, defines how the honeybee's response will change depending on the angular position of the stimulus relative to the insect. The function follows an approximately sinusoidal curve, peaking in the bee's lateral visual field, which results in the bee turning towards the stimulus. Whilst a similar analysis has not been undertaken for flying honeybees, the function we have obtained is qualitatively similar to the position function, $P(\psi)$, observed for both walking (Bahl et al., 2013) and flying *Drosophila* (Heisenberg & Wolf, 1984; Heisenberg et al., 1978) in open-loop experiments. Our results indicate that, in adapting to different gain conditions bees adjust the scale, but not the shape, of their response to stimulus position. The position-dependent function has the largest scale at x2 gain, with the lowest scales occurring at gains of x0.5 and x4. As has been found in motion-blind *Drosophila* (Bahl et al., 2013), simulations show that the measured position-dependent function on its own would allow a bee to fixate. However, both the position- and motion-dependent components of the

honeybee's response are required to predict the characteristics of the experimentally observed fixation behaviour.

The motion-dependent function, $\tilde{M}(\psi)$, specifies how a bee's response to stimulus motion varies, depending on where in its visual field that motion occurs. Varying the gain condition caused honeybees to change the shape of the motion-dependent function. As gain increased, honeybees tended to *decrease* their response to forwards motion in their frontal visual field relative to their lateral visual field. This difference was present across all gains, but the difference was largest at x4 gain. A similar reduction in the response to visual motion occurring in the frontal visual field has not been observed for flies, where the response has been found to be uniform across the visual field for *Musca* (Poggio & Reichardt, 1973), or elevated in the frontal visual field in *Drosophila* (Aptekar et al., 2012; Bahl et al., 2013). In linear control system theory, the motion-dependent response is similar to the derivative term of a proportional-derivative (PD) controller, although here it generates a non-linear function of stimulus position and velocity, rather than a linear derivative function of an error term (Nise, 2008). In a high-gain system, it is well known that the derivative term can cause unstable oscillations (Ljung, 1999; Nise, 2008). Hence, reducing the response to visual motion in the frontal visual field should be a beneficial control strategy for the insect at high gain.

The honeybee's motion-dependent response was found to vary depending on the direction of motion of the stimulus. Motion in the front-to-back direction generally elicits a larger response than motion in the back-to-front direction, particularly at high gain. A similar phenomenon has been observed in *Drosophila's* response to fixation stimulus motion (Bahl et al., 2013), although it has not previously been incorporated into analysis methods for calculating the motion function. It is not clear if this particular aspect of the motion-dependent response represents a desirable feature of its control system, or simply reflects constraints in the physiological mechanisms that underlie the detection of stimulus motion. We developed a novel analysis procedure to calculate a separate motion function to be calculated for motion in either direction, which allows the directional dependency of the motion response to be determined in future open- or closed-loop experiments with fixation stimuli.

These position- and motion-dependent functions outline the non-linear functions linking stimulus position and motion to a honeybee's response. However, the methodology we propose

does not measure the temporal dynamics of how the insect responds to either the stimulus position or motion; it is possible that the honeybees also adapt this aspect of their response depending on the gain condition. Systems analysis techniques have been used to separately determine the temporal dynamics of flies' responses to both stimulus position and motion in open-loop (Aptekar et al., 2012; Theobald, Ringach, & Frye, 2010), and similar techniques could potentially be used to analyse closed-loop experiments.

4.7.3 Mechanisms underlying adaptation

Fundamental questions that arise from these experiments concern the nature of the mechanism that enables a honeybee to recognize changes in gain and the realisation of these mechanisms at the neural level. A proposed method for adaption is to correlate changes in motor output with changes in the velocity of the stimulus to be controlled (Wolf & Heisenberg, 1990; Wolf & Heisenberg, 1991). Based on this correlation, the coupling coefficient between motor actions and the stimulus can be determined, which can explain how *Drosophila* adjust their flight patterns in response to inverted or increased gain conditions during fixation (Heisenberg & Wolf, 1988; Wolf & Heisenberg, 1990). The bees in this study had to modify their behaviour based on subtle changes in the magnitude of the correlation between their motor output and its effect on the fixation stimulus. When walking speed is coupled to rotational gain in an identical fixation task, honeybees were also found to adjust their walking speed to improve their fixation (Chapter 3). This observation, taken together with the present study, suggests that honeybees possess a sensitive mechanism for detecting and optimising the results of their motor output, based on the sensory feedback they receive. These mechanisms may involve the use of a forwards model, where the intended results of an action are predicted and compared to the actual results, which would allow the bee to update its motor commands if discrepancies arrive (Miall & Wolpert, 1996).

The neural mechanisms that underlie the gain adaptation for complex visual behaviours have yet to be discovered for any insect. Given that separate regions of the brain are responsible for processing stimulus motion and position in *Drosophila* (Bahl et al., 2013; Seelig & Jayaraman, 2013), adaptation to varying gains could depend on the insect's comparison of its motor output to the visual objects position, or its motion, or a combination of both. Recent findings from a vertebrate organism, zebra fish larva, have found that separate brain areas function during adaptation to conditions of decreased and increased gain (Ahrens et al., 2012). Similar

specialisation could also be present in insects. Taken at the behavioural level, fixation is a robust, yet surprisingly complex behaviour and the underlying neural mechanisms, particularly when adapting to changes in gain, are probably similarly complex. Further insight could be provided by behavioural experiments that use compound stimuli to separately stimulate an insect's position and motion responses (Aptekar et al., 2012).

4.7.4 Conclusion

Novel analysis methods are described that enable characterisation of closed-loop fixation behaviour in terms of position- and motion-dependent functions, for a number of different feedback gains. These functions provide insight into the choices, at the behavioural level, made by an adaptive biological control system to increase its efficacy. Similar control schemes could be used to guide adaptive behaviours for a robotic agent, and optimise its ability to orient towards visual features in the environment.

Chapter 5 Walking towards the light: Honeybees modulate their walking speed to move effectively towards a visual landmark

5.1 Preamble

This chapter describes how honeybees modulate their walking speed as a function of the angular position of a visual fixation stimulus, when also actively controlling its position in closed-loop. Bees were found to modulate their forwards and sideways walking speed to effectively move towards the stimulus, providing a new insight into how insects control their translation from a paradigm designed to study orientation. The contents of this Chapter (and Appendix D) have been prepared and formatted as a publication, for submission to the journal 'PLoS Computational Biology' authored by G. J. Taylor (the candidate), A. C. Paulk, T. W. L. Pearson, B. van Swinderen, and M. V. Srinivasan. The work is intended for submission as two-part publication with Chapter 4. The contributions of each author are detailed in the preliminary pages of the thesis.

5.2 Abstract

Honeybees use vision to control their orientation towards objects, though the influence of both motion and position of the stimulus in the visual field can be complex. We analysed the walking speeds of honeybees as they oriented towards a visual fixation stimulus in a virtual-reality arena. In these closed-loop experiments, tethered bees walked on a trackball where yaw rotation was measured and used to control the azimuthal position of a bar presented on a panoramic visual display. Although the bee's walking speed had no direct effect on the movement of the visual stimulus, bees modulated both their forward and sideways walking speeds depending on the angular position of the stimulus. The bee's forwards, or longitudinal, speed was highest when the stimulus was positioned in their frontal visual field, whereas their sidestepping, or transverse, speed was modulated such that the bees would step towards the stimulus when it was positioned in their lateral visual field. In the experiments analysed, the gain condition, a linear coupling between the insect's turning rate and the stimulus velocity, was varied by a factor of eight. Although bees have been found to adapt the control of their turning rate depending on the gain condition, we find here the control of walking speed is similar across all

gain conditions. Simulations indicate that the strategy used by bees to modulate both forward and sideways walking speeds can be effective when attempting to move towards a distant landmark, particularly if its angular position is unstable. The study and modelling of translatory movements can provide new insights into how insects intend to control their locomotion, even in paradigms designed to study rotational control.

5.3 Introduction

Many insects orient towards visual objects in their environment. This behaviour can serve a variety of purposes, as insects orient with respect to prey, predators, food sources, their nests, or conspecifics. However, behaviour when orienting towards a visual object also depends on the translational speed of the insect's locomotion, as translation changes the insect's position and also its orientation with respect to the object of interest. For example, during prey pursuit (Boeddeker et al., 2003; Gilbert, 1997; Land & Collett, 1974), or navigation (Robie, Straw, & Dickinson, 2010; Srinivasan, 2011; Wehner, Michel, & Antonsen, 1996), an insect will move towards an object or location until it is reached. In other situations a constant distance may be maintained towards the object, such as when hovering in front of a flower whilst feeding from it (Farina, Varjú, & Zhou, 1994; Kern & Varjú, 1998; Sprayberry & Daniel, 2007), during mating flights (Land, 1993; van Praagh et al., 1980), or courtship rituals (Cook, 1979, 1980; Frantsevich & Gorb, 2006). The insect may even orient towards an object whilst remaining in place, such as when reacting to the presence of a predator (Kelber & Zeil, 1990; Kevan, Cant, & Kevan, 1983). How an insect modulates both its translatory and rotational motions will therefore determine how it interacts with the stimulus.

Behaviours that involve simultaneous orientation and movement towards an object have primarily been studied in experiments with freely moving animals, where specific features of the visual cue have been shown to control locomotion. Forwards speed can be controlled based on the perceived retinal size of the object (Boeddeker et al., 2003; Collett & Land, 1975; Cook, 1979; Schuster et al., 2002; Wehrhahn et al., 1982), which can allow an insect to follow a moving object at a fixed distance, or decelerate during interception. Cues from the visual expansion of an object (Baird et al., 2013; Borst, 1986; van Breugel & Dickinson, 2012) can also be used to control deceleration during flight and initiate leg movements for landing. When the animal is nearing the target, the location of the object in the visual field can be used to control either sideways or vertical motions that correct an insect's alignment (Collett & Land,

1975; Wagner, 1986; Wehrhahn & Reichardt, 1975; Zhang, Wang, Liu, & Srinivasan, 1990), or to allow it to maintain a stable hovering position (Sprayberry & Daniel, 2007; Wijngaard, 2010). However, in some instances changes in alignment are desirable, such as during peering behaviour, where intentional lateral (or vertical) motion provides depth information, through motion parallax, to assess an objects distance (Voss & Zeil, 1998; Wallace, 1959). These methods of controlling translational movements appear to be primarily used when the insect is already close to a visual object.

Insects also use visual information to control their orientation towards an object. A classic paradigm for studying visually guided orientation towards a specific object is exemplified by the so-called 'fixation' experiments that have been conducted with tethered flies in virtual-reality arenas. Flies use their turning actions to control the azimuthal position of a dark bar against a bright background, and to position the bar in their frontal visual field, a behaviour called 'fixation' (Bahl et al., 2013; Heisenberg & Wolf, 1984; Reichardt & Poggio, 1976). Behaviourally, control of fixation appears to be based on non-linear functions that use information on the azimuthal position and angular velocity of the fixation stimulus to control turning rates (Aptekar et al., 2012; Bahl et al., 2013). Similar behaviour involving orientation towards visual cues been observed in other insects, including moths (Preiss & Kramer, 1984), beetles (Lönnendonker, 1991; Varjú, 1975), and honeybees (Chapter 4; Moore et al., 2014; Paulk et al., 2014). Yet, fixation in virtual-reality is an inherently artificial scenario, as the insect can never change its perceived distance the stimulus (Heisenberg & Wolf, 1984). However, could the insect's translational movements during fixation provide further information on how it attempts to interact with the visual object?

To answer this question, we examined the behaviour of tethered walking honeybees as they modulated both their longitudinal (forward) and transverse (sideways) walking speed when controlling the angular position of a fixation stimulus (a vertical bright green bar). The linear coupling, or gain, between the bee's turning rate and the stimulus velocity was systematically varied by a factor of eight between experiments. We analysed closed-loop behavioural data on the bee's walking speed by estimating the current speed as a function of the prior value of the stimulus position, and the bee's turning rate and walking speed, and also compensating for the effects of the autocorrelation of the response on the estimation. Our analysis indicates that bees modulate both their longitudinal and transverse walking speed depending on the angular position of the fixation stimulus, regardless of the gain. Even though fast walking is negatively

correlated with fixation performance, we find that the observed strategy of modulating walking speeds would result in effective movement towards a visual object at all but the highest gain condition. Simulations of fixation behaviour and control of walking speed indicate that modulating either longitudinal or transverse walking speed is important when approaching an unstably orientated object.

5.4 Methods

This chapter further investigates walking speeds measured from honeybees performing a fixation task in virtual-reality. Chapter 4 describes the experimental conditions in detail, and analyses the turning motions made during this task. An abridged description of the methods is described in Sections 5.4.1 and 5.4.2. The analysis and the modelling that are specific to this chapter is described in Sections 5.4.3 and 5.4.4.

5.4.1 Animal preparation, apparatus and experiments

Honeybees (*Apis mellifera*) were captured exiting the hive in Brisbane, Australia. Bees were anesthetised before being tethered to a metal rod using wax and a cautery tool (Bovie). The heads of the bees were fixed to the thorax using dental cement (Coltene Whaledent synergy D6 FLOW A3.5/B3), and wax was also applied to the base of the wings. Bees were fed with a sucrose solution before being placed in a humidified chamber (~35 ^{o}C) to acclimatise for one hour (Moore et al., 2014; Paulk et al., 2014).

Tethered honeybees were placed an arena consisting of four 32x32 LED panels (Shenzchen Sinorad Medical Electronics Inc.; Zhou et al., 2012) that displayed a fixation stimulus, a bright green vertical bar (54^{o} high, 20^{o} wide, peak wavelength 518 nm and luminance 168 lux) against a background of unlit LEDs. In the arena, the bees walked on a light Styrofoam ball supported on an air cushion. The dynamics of the ball (approximate perceived weight 580 mg and rotational inertia 330 nkg.m^2; calculated using the methods described in (Weber et al., 1981)) were not matched for a honeybee (mass ~100 mg and rotational inertia ~5 nkg.m^2). However, the bees appeared to manipulate the ball easily.

Measurements of the bee's movements were made using FicTrac (Moore et al., 2014), a computer vision algorithm that tracks the motion of the ball on which an insect walks. FicTrac

used images from a firewire camera (Point Grey, Firefly), which were processed in real time at 30 fps. The bee's walking speed, W, walking angle, β, and turning rate, ω, were calculated concurrently, and the turning rate was used to update the position of the stimulus, using a Python script running at 200 Hz incorporating Vision Egg software (Straw, 2008). The latency from the bee's movements to a change in the visual display was approximately 87 ms (Moore et al., 2014), hence the time series of measured values from FicTrac was shifted three frames back relative to the time series of stimulus positions in order to ensure the temporal alignment of the data.

Bees had closed-loop control of the visual stimulus, so that as they rotated the ball the position of the stimulus on the LEDs was updated in real time. To study how the insects reacted to changes in the coupling of their action-perception loop, the gain conditions were altered. Gain refers to the linear multiplier coupling the insect's turning action to the movement of the stimulus. A gain of x1 meant that 1° of rotation of the ball resulted in 1° of rotation of the visual stimulus in the same direction, which corresponds to natural, free locomotion. Five gain conditions were used, x0.5, x1, x2, x3, and x4, as well as a 'no stimulus' control condition which displayed a black, unlit bar on a black, unlit arena to record behaviour in the absence of the visual stimulus. During the experimental runs, the angular position of the stimulus was displaced by 90° at random intervals as described in Chapter 4. The displacement periods were excluded from all analysis. Individual experiments lasted two minutes, and all bees were tested with all stimulus conditions in a pseudo-randomised order.

5.4.2 Data analysis

All data on the orientation of the bar and the bee's movements were recorded within the Python script controlling the visual stimulus. Data was analysed at 30 Hz using custom programs written in Matlab (The Mathworks Inc.). The walking speed, W, and walking angle, β, measured by FicTrac were used to calculate the bee's speed in terms of longitudinal, W^L, and transverse components, W^T, as $W^L = W \times \cos(\beta)$ and $W^T = W \times \sin(\beta)$ (see Figure 1A; Moore et al., 2014).

Distributions of longitudinal speed were calculated using one hundred 2 mm.s^{-1} bins spanning the range between -100 and 100 mm.s^{-1}. Distributions of transverse speed were calculated using one hundred 1 mm.s^{-1} bins spanning the range between -50 and 50 mm.s^{-1}.

The stimulus position, ψ, was calculated based on the bee's turning rate, ω, and the gain condition, such that $\psi(t) = \int(\omega(t) \times gain)dt$. The path, P, that a bee would have taken across a 2D surface was reconstructed in Cartesian coordinates based on the time series of W^L, W^T and ψ, as,

$$P(W^L(t), W^T(t), \psi(t)):$$

$$P^X(t) = \int_0^t \sqrt{W^L(t)^2 + W^T(t)^2} \cos\left(\psi(t) + \tan^{-1}\left(W^L(t) / W^T(t)\right)\right).dt \quad (4\text{-}30)$$

$$P^Y(t) = \int_0^t \sqrt{W^L(t)^2 + W^T(t)^2} \sin\left(\psi(t) + \tan^{-1}\left(W^L(t) / W^T(t)\right)\right).dt$$

For brevity, the notation (t) is omitted through the remainder of the chapter. ψ represented the angle to a distant, fixed visual landmark that was aligned with the bee's starting point, essentially having (x, y) coordinates at (0, ∞). Comparisons of the distance moved towards the stimulus during an experiment were calculated based on the final value P^Y from Eq. (4-30) for each experiment.

Statistical comparisons are detailed in Section D.2. All statistics were performed using SPSS V20 (IBM).

5.4.3 Gaussian kernel regression estimations

The initial analysis of both longitudinal and transverse walking speeds in Section 5.5.1 indicated that the past stimulus position, turning rate (or stimulus velocity) and autocorrelations influence both components of walking speed. Because measurements were made during closed-loop behaviour, there were two considerations for the analysis.

The first consideration is that the observed combinations of predictor variables were non-uniformly distributed. The honeybee's control of its turning rate resulted in the fixation stimulus usually being positioned in their frontal visual field, and also in its turning rate being biased to be either positive or negative when the stimulus was positioned to either their right or left respectively (Chapter 4). Thus, simply calculating walking speed as an average, given the concurrent value of stimulus position could produce misleading results, as it would be influenced by the relationship between stimulus position and turning rate combined with the relationship between turning rate and walking speed. To compensate for the non-uniform stimulus distributions, Gaussian kernel regression (GKR; Bowman & Azzalini, 1997; Cao,

2008) was used to uniformly estimate the bee's longitudinal and transverse walking speeds across the range of all predictor variables (Eqs. (4-31) and (4-32)). We decided not to use either component of walking speed as a predictor for the other, as their cross-correlation indicated they were only weakly coupled (Figure D-1), and adding dimensionality to the GKR estimation would increase the noise at every estimation point.

The second consideration is that walking speed was strongly autocorrelated; hence, the most influential predictor variable for walking speed any time point is its own past value, regardless of the state of the other predictors at that time point. The autocorrelation would then mask the effects of the other predictor variables in the analysis. The effect of autocorrelation was compensated for by subtracting the mean level of the estimation when analysing the effect turning rate of stimulus position as predictor variables (Eq. (4-33)).

The considerations associated with closed-loop data and both methods of analysis are discussed in further detail in Chapter 4. This section describes the analysis procedure used to determine the influence of each predictor variable on the behavioural response, and the metrics used for making statistical comparisons. The control functions, relating the influence of predictor variables to motor output, embed the non-linear responses and dynamics of the underlying physiological mechanisms in the function calculated for each variable.

Current longitudinal speed, W^L_t, was estimated using GKR as function of past stimulus position, ψ_{t-1}, past turning rate, ω_{t-1}, and past longitudinal speed, W^L_{t-1},

$$E\left(W_t^L \mid \psi_{t-1}, \omega_{t-1}, W_{t-1}^L\right) \tag{4-31}$$

The estimation was based on increments in W^L_{t-1} of 0.25 mm.s^{-1} (between -12.5 and 65 mm.s^{-1}), 1.43 ^{o}.s^{-1} increments in ω_{t-1}, (between -150 and 150 ^{o}.s^{-1}), and 2.8^{o} increments in ψ_{t-1} (between -180 and 180^{o}). The current transverse speed, W^T_t, was similarly estimated using GKR as function of past stimulus position, ψ_{t-1}, past turning rate, ω_{t-1}, and past transverse speed, W^T_{t-1},

$$E\left(W_t^T \mid \psi_{t-1}, \omega_{t-1}, W_{t-1}^T\right) \tag{4-32}$$

The estimation was based on increments in W^T_{t-1} of 0.25 mm.s^{-1} (between -20 and 20 mm.s^{-1}), 1.43 ^{o}.s^{-1} increments in ω_{t-1}, (between -150 and 150 ^{o}.s^{-1}), and 2.8^{o} increments in ψ_{t-1} (between -180^{o} and 180^{o}). The range for estimating longitudinal and transverse speeds both encompassed approximately 95% of the range of measured data for both variables respectively. The

following analysis procedures were applied to estimates of both $W^L{}_t$ and $W^T{}_t$ from Eqs. (4-31) and (4-32) respectively, hence, the superscript L/T is used for brevity in Eqs. (4-33) to (4-35).

Both W^L and W^T were strongly autocorrelated (Figure D-1), which could mask the effect of other predictor variables. To compensate for this, the mean level of the estimation given the prior walking speed was subtracted,

$$\tilde{W}_t^{L/T}\left(\psi_{t-1},\omega_{t-1}\right)=E\left(W_t^{L/T}\middle|\psi_{t-1},\omega_{t-1},W^{L/T}{}_{t-1}\right)-E\left(W_t^{L/T}\middle|-180<\psi_{t-1}<180,-150<\omega_{t-1}<150,W^{L/T}{}_{t-1}\right) \tag{4-33}$$

The resulting function has zero-mean which is denoted with a diacritic tilde (~). The zero-mean function indicates how the bee's walking speed would vary from the mean level predicted by the autoregression, as a 2D function of both ψ_{t-1} and ω_{t-1}. The role of an individual predictor variable in modulating walking speed can be examined by averaging the surface represented by Eq. (4-33) over the range of the other variable. To examine the role of turning rate, ω_{t-1}, in modulating walking speed Eq. (4-33) was averaged over the range of ψ_{t-1}:

$$\tilde{W}_t^{L/T}\left(\omega_{t-1}\right)=1/360\int_{-180}^{180}\tilde{W}_t^{L/T}\left(\psi_{t-1},\omega_{t-1}\right).d\psi_{t-1} \tag{4-34}$$

To examine the role of ψ_{t-1}, in modulating walking speed, Eq. (4-33) was averaged over the estimated range of ω_{t-1}:

$$\tilde{W}_t^{L/T}\left(\psi_{t-1}\right)=1/300\int_{-150}^{150}\tilde{W}_t^{L/T}\left(\psi_{t-1},\omega_{t-1}\right).d\omega_{t-1} \tag{4-35}$$

Additionally, the autoregressive component of walking speed can be examined using Eqs. (4-31) or (4-32), where mean levels were not subtracted. In this case, both ψ_{t-1} and ω_{t-1} were averaged over their complete range as,

$$W_t^{L/T}\left(W_{t-1}^{L/T}\right)=1/300\int_{-150}^{150}\left(1/360\int_{-180}^{180}E\left(W_t^{L/T}\middle|\psi_{t-1},\omega_{t-1},W_{t-1}^{L/T}\right).d\psi_{t-1}\right).d\omega_{t-1} \tag{4-36}$$

Using Eqs. (4-34) to (4-36), both longitudinal and transverse walking speed can be plotted as functions of their individual predictor variables, as in Figure 5-2, Figure 5-3 and Figure D-3. For statistical comparisons (Section D.2), a single feature of interest that characterised the relationship of longitudinal or transverse speed with a predictor variable was chosen. This was quantified as a difference between the average values over two ranges of the predictor variable, and provided an indication of the magnitude and the variance aspects of the response.

The longitudinal walking speed was observed to either increase or decrease (depending on the stimulus condition) as a function of the absolute turning rate (Figure 5-2). We quantified this

relationship using the average difference between estimations of W^L_t for fast (*Fa.*;100 < $|\omega_{t-1}|$ < 150 $^o.s^{-1}$) and slow (*Sl.*; $|\omega_{t-1}|$ < 25 $^o.s^{-1}$) turning rates, calculated as,

$$\overline{W^L\left(\omega(Fa.)\right)} - \overline{W^L\left(\omega(Sl.)\right)} = \overline{\tilde{W}^L_t(100 < |\omega_{t-1}| < 150)} - \overline{\tilde{W}^L_t(0 < |\omega_{t-1}| < 25)} \quad (4\text{-}37)$$

When considering the relationship between longitudinal speed and stimulus position, W^L_t was typically highest when the stimulus was positioned in the frontal visual field, and decreased as the stimulus moved behind the bee (Figure 5-2). To quantify the relationship, the average difference between estimations of W^L_t for front (*Fr.*; -45 < ψ_{t-1} < 45^o) and rear (*Re.*; 135 < $|\psi_{t-1}|$ < 180^o) stimulus positions was calculated as,

$$\overline{W^L\left(\psi(Fr.)\right)} - \overline{W^L\left(\psi(Re.)\right)} = \overline{\tilde{W}^L_t(-45 < \psi_{t-1} < 45)} - \overline{\tilde{W}^L_t(135 < |\psi_{t-1}| < 180)} \quad (4\text{-}38)$$

The transverse walking speed was observed to vary as an approximately linear function of turning rate (Figure 5-3). We quantified this relationship using the average difference between estimations of W^T_t for positive (0 < ω_{t-1} < 150 $^o.s^{-1}$) and negative (-150 < ω_{t-1} < 0 $^o.s^{-1}$) turning rates, calculated as,

$$\overline{W^T\left(\omega(+)\right)} - \overline{W^T\left(\omega(-)\right)} = \overline{\tilde{W}^T_t(0 < \omega_{t-1} < 150)} - \overline{\tilde{W}^T_t(-150 < \omega_{t-1} < 0)} \quad (4\text{-}39)$$

When considering the relationship between transverse speed and stimulus position, W^T_t was typically positive when the stimulus was positioned to the bee's right, and negative when stimulus was positioned to the bee's left. To quantify this relationship, the average difference between estimations of W^T_t for right (0 < ψ_{t-1} < 180^o) and left (-180 < $|\psi_{t-1}|$ < 0^o) stimulus positions was calculated as,

$$\overline{W^T\left(\psi(+)\right)} - \overline{W^T\left(\psi(-)\right)} = \overline{\tilde{W}^T_t(0 < \psi_{t-1} < 180)} - \overline{\tilde{W}^T_t(-180 < \psi_{t-1} < 0)} \quad (4\text{-}40)$$

When comparing the effect of longitudinal or transverse walking speed as an autoregressive function (Eq. (4-33)), a similar function appeared to be present for all stimulus conditions, with varying vertical offsets between each curve (Figure D-3). To compare this relationship, a 'base curve' was computed, which was the average of Eq. (4-36) for all stimulus conditions, and offset such that $W^{L/T}_t(0) = 0$. Comparisons with the average vertical offset of Eq. (4-33) from any stimulus condition from the base curve provided an indication of any constant bias present in the bee's walking speed.

5.4.4 Modelling paths towards an object

The modelling of a bee's path towards an object is divided into two parts, as in Figure 5-5A. First, a model of fixation behaviour uses turning rate, as a function of the position and velocity of the fixation stimulus, to predict control of the fixation stimulus (Chapter 4). The second part is a model of walking speed control simultaneously predicts values for longitudinal, W^L, and transverse, W^T, walking speeds which are used to calculate the path taken by a simulated bee walking on a 2D surface towards a distant object.

For each walking speed component, the current value is the sum of the functions (for each gain condition) of stimulus position, $\tilde{W}^{L/T}(\psi)$, and turning rate, $\tilde{W}^{L/T}(\omega)$, (Figure 5-2: W^L and Figure 5-3: W^T). Both W^L and W^T are low-pass filtered using a three point autoregressive model fit to observations from the no stimulus condition[5]. Furthermore, random noise is added to both W^L and W^T. Based on data from the no stimulus condition the standard deviation of the derivative of both W^L and W^T was found to vary as a function of the value of W^L_{t-1} or W^T_{t-1} (Figure D-4), which indicates that the random variation in walking speed did not follow a Gaussian distribution. This is incorporated into the noise for the model, such that the standard deviation of Gaussian noise injected into both W^L and W^T is parameterised depending on W^L_{t-1} and W^T_{t-1} (Figure D-4). As a positive mean was observed in W^L, an offset was added to W^L such that the population mean for each simulation gain matched the population mean for data at the equivalent gain (Figure D-4). An offset combined with low-pass filtering and noise (where the standard deviation depends on W^L_{t-1}) can produce long tailed distributions that are similar to those observed from experimental data (Figure D-4). A limitation of this model is that turning rate influences both W^L and W^T, where as in an actual insect, bi-directional interaction would be likely to occur. (Full, Kubow, Schmitt, Holmes, & Koditschek, 2002).

The model was implemented using custom written Matlab scripts. Fifty simulations of fixation were calculated for each gain condition, each lasting 3600 time steps, or 120 s as in the real experiments (each time step represented 30 ms). All W^L and W^T models were calculated based on the same set of simulations, and thus shared common stimulus position and turning rate inputs. Simulated W^L, W^T and ψ were used to calculate path, $P(W^L, W^T, \psi)$, using Eq. (4-30).

[5] $W^L(t) = 0.58W^L(t-1) + 0.11W^L(t-2) + 0.16W^L(t-3) + \tilde{W}^L(\psi) + \tilde{W}^L(\omega) + n(W^L(t-1)) + offset$
$W^T(t) = 0.71W^T(t-1) - 0.29W^T(t-2) + 0.13W^T(t-3) + \tilde{W}^T(\psi) + \tilde{W}^T(\omega) + n(W^T(t-1))$

5.5 Results

Tethered walking honeybees can turn an air-supported ball to bring a bright vertical bar to their front, a behaviour we term 'fixation' (Chapter 4; Moore et al., 2014; Paulk et al., 2014). However, bees can also modulate their forward (longitudinal) and sidestepping (transverse) movements during fixation. We analysed both the longitudinal and transverse components of walking speeds in the absence of a stimulus, as well as when bee's controlled a fixation stimulus at different gain conditions ranging from x0.5 to x4.

5.5.1 Walking with and without a stimulus

Bees would walk either with or without a visual stimulus. We measured their longitudinal, W^L, and transverse, W^T, walking speeds for the no stimulus condition and also when the fixation stimulus was presented, at a variety of gain conditions (Chapter 4). Without the stimulus, honeybees would often stand stationary (Figure 5-1C and E). However, the distribution of W^L indicated that the bees tended to walk forwards rather than backwards, frequently at speeds up to approximately 50 mm.s^{-1} when the visual stimulus was not present (Figure 5-1C). When the visual stimulus was introduced, the bias towards positive W^L decreased, resulting in lower mean W^L, regardless of the gain condition. Mean W^L did vary significantly depending on stimulus condition (χ^2_5 =14.58, ***p*=0.012**), although speeds were only significantly faster when the stimulus was absent when compared to x1 gain (Figure 5-1D). On the other hand, the distribution of W^T was unbiased and symmetrical about zero, and the mean absolute W^T did not vary significantly depending on stimulus condition (Figure 5-1F, $F_{5,50}$ =1.73, p=0.145).

Next, we examined whether the stimulus position or the bee's turning rate during fixation may influence either the longitudinal or transverse walking speed. When the average value for either component of walking speed was calculated at each stimulus position, ψ, it appeared that both W^L and W^T were modulated based on ψ (Figure D-1). The cross-correlation between walking speed and the honeybee's physical turning rate, ω, also indicated that that both W^L and W^T changed with ω (Figure D-1). However, ω is directly coupled to the stimulus velocity, v, since $v = \omega \times gain$, and the cross-correlation results did vary depending on gain condition. Hence, v may also influence walking speed. The relationship between the two components of walking speed was examined by calculating the average value of W^L across the range of W^T, which indicated an approximately linear relationship between the walking speed components (Figure 5-1B). However, a weak cross-correlation was found between W^L and absolute W^T (Figure

D-1). Hence, the linear relationship between W^L and absolute W^T may arise because both variables are influenced by the stimulus position and also the turning rate of the honeybee, rather than being directly coupled themselves. Finally, the auto-correlation of both W^L and W^T was found to decay exponentially (Figure D-1). The strong influence of autoregression – whereby the bee's current longitudinal and transverse walking speed depend upon their previous values – bee's walking speeds also depended on the stimulus position and the bee's turning rate. We further investigated how the two components of walking speed depend on these predictor variables.

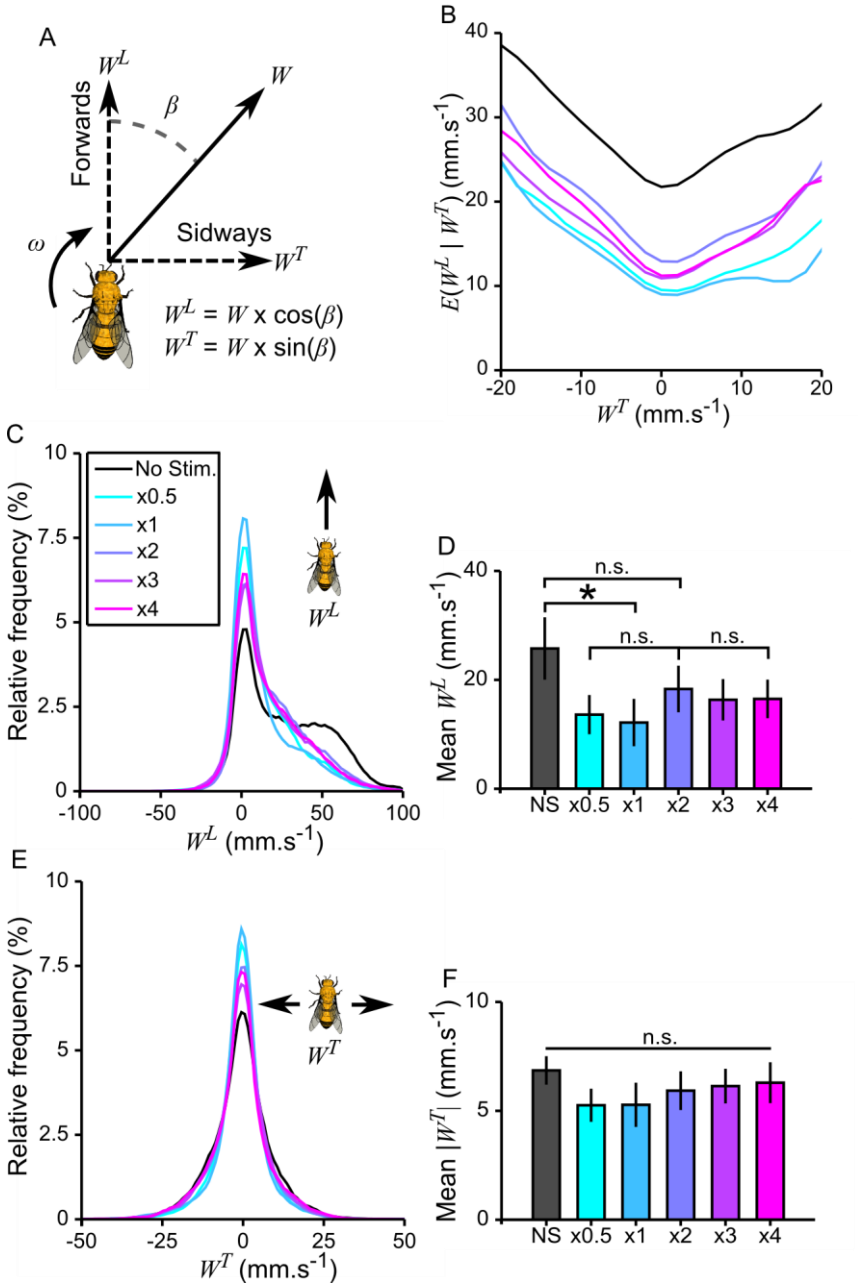

Figure 5-1: Longitudinal and transverse components of the bee's walking speed. **A**, A honeybees movement is measured in terms of its turning rate, ω, walking speed, W, and walking angle, β. Walking speed can also be expressed in longitudinal, W^L, and transverse, W^T, components. **B**, The expected W^L given W^T. **C**, Frequency distributions of W^L. **D**, Mean W^L for each condition. **E**, Frequency distributions of W^T. **D**, Mean absolute W^T for each condition. All plots show each gain condition as a separate curve. N=11 bees repeated all gain conditions. Error bars show ± S.E.M. Bars denotes a statistically significant difference (n.s.: p>0.05, *: p<0.05) between the indicated groups. Full statistical details are provided in Section D.2.1.

5.5.2 Predictors of longitudinal walk speed

The honeybee's predicted longitudinal walking speed, W^L_t, was estimated using Eq. (4-31). The influence of past longitudinal speeds, W^L_{t-1} on the W^L_t (essentially the autoregression; Eq.

(4-36)), indicated an approximately linear relationship between past and current longitudinal speed. However, the autoregressive relationship had a positive bias, or offset, for all stimulus conditions, the magnitude of which was significant for both the no stimulus and x4 gain conditions (Figure D-3). Further, the bias was significantly higher without the stimulus as compared to when the stimulus was visible at any gain condition (Section D.2.5, $F_{5,50}$=4.43, ***p*=0.002**).

Investigation of the influence of the bee's past turning rate, $\omega_{t-1,}$ on W^L_t (Eq. (4-34)) revealed that, in the absence of a stimulus, W^L_t decreased as the absolute value of ω_{t-1} increased (Figure 5-2A). However, the opposite was true when the stimulus was visible, at any gain condition: honeybees tended to maintain or increase W^L_t as the absolute value of ω_{t-1} increased. The relationship between longitudinal speed and turning rate was quantified using Eq. (4-37), which indicated the average difference in W^L_t between periods when the bee was turning slowly, versus when it was turning quickly (Figure 5-2B); a positive value indicated that W^L_t was higher when turning quickly, or vice versa. With no stimulus displayed, W^L_t was significantly lower when honeybees were turning rapidly, as compared to when they were turning slowly. Yet, when the fixation stimulus was displayed, W^L_t was generally higher when the bees turned rapidly. Although significant variation in the difference occurred depending on whether the stimulus was displayed ($F_{2.20,21.98}$ =7.05, ***p*=0.004**), there was not significant variation between the gain conditions (Section D.2.2). The modulation appears unlikely to be a function of stimulus velocity, which varied by a factor of eight depending on gain condition.

We then examined whether the past stimulus position, $\psi_{t-1,}$ predicted W^L_t (Eq. (4-35)). When the stimulus was visible, W^L_t was highest when the fixation stimulus was positioned in the frontal visual field, particularly compared to when it was positioned at the rear (Figure 5-2C). This was true at all gain conditions. In the absence of a stimulus, the bee's orientation had no effect on W^L_t, as would be expected. The relationship between longitudinal speed and stimulus position was quantified using Eq. (4-38), which indicated the average difference in W^L_t between when the bee had the stimulus positioned to its front versus when it was positioned to the rear (Figure 5-2D). A positive value indicated that W^L_t was higher when the stimulus was positioned to the bee's front, or vice versa. For all gain conditions W^L_t was higher when the stimulus was positioned in the honeybee's frontal visual field, as opposed to its rear visual field. Although this difference progressively decreased as gain increased, there was no significant variation between the highest and lowest gain conditions (x0.5 vs. x4, W_{10}=-1.33, p=0.182). Both the

stimulus position and the turning rate were factors that influenced the modulation of longitudinal walking speed under different conditions.

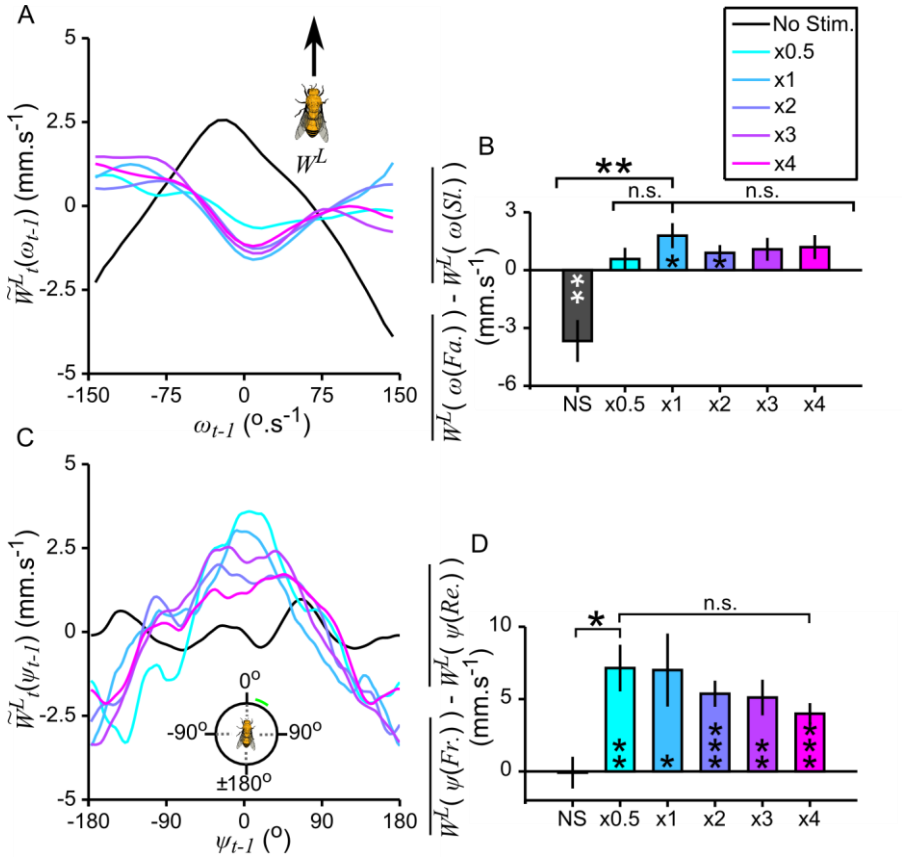

Figure 5-2: Longitudinal walking speed is modulated by stimulus position and turning rate. **A**, modulation of longitudinal speed, W^L_t, as a function of prior turning rate, ω_{t-1}. **B**, the difference in W^L_t between fast ($100 < |\omega_{t-1}| < 150$ °.s^{-1}) and slow ($-25 < \omega_{t-1} < 25$ °.s^{-1}) prior turning rates, from Eq. (4-37). **C**, modulation of W^L_t as a function of prior stimulus position, ψ_{t-1}. **D**, the difference in W^L_t between front ($-45 < \psi_{t-1} < 45^o$) and rear ($135 < |\psi_{t-1}| < 180^o$) stimulus positions, from Eq. (4-38). All plots show each gain condition as a separate curve. N=11 bees repeated all gain conditions. Error bars show ± S.E.M. Bars denote statistical significance (n.s.: $p>0.05$, *: $p<0.05$, **: $p<0.01$, ***: $p<0.001$) of the difference between the indicated groups, whereas stars in bars denote statistically significant difference from a value of zero. Full statistical details are provided in Section D.2.2.

5.5.3 Predictors of transverse walking speed

We have seen above that bee's longitudinal speed is influenced by both the turning rate and the stimulus location. The next question is whether the bee's transverse speed, W^T_t (Eq. (4-32)) is also predicted by these variables. The autoregressive influence of past transverse speed, W^T_{t-1}, on W^T_t (Eq. (4-36)) indicated a linear relationship between the two variables. For the majority of conditions (besides x3 gain, Figure D-3) there was no significant bias in the regression line,

and biases did not vary significantly depending on stimulus condition (Section D.2.5, χ^2_5 =0.76, p=0.979).

The past turning rate of a bee, ω_{t-1}, had a proportional relationship with W^T_t (Eq. (4-34)), in the absence of the stimulus as well as in in the x0.5 gain condition (Figure 5-3A). At gains of x1 and above, W^T_t was generally inversely proportional to ω_{t-1}, though the relationship was inconsistent. The relationship between transverse speed and turning rate was quantified using Eq. (4-39), which indicated the average difference in W^T_t between periods when the bee was turning right, versus when it was turning left (Figure 5-3B); a positive value indicated that W^T_t was positive when bees turned right, and vice versa. Although the difference did vary significantly depending on the gain condition ($F_{5,50}$ =3.42, ***p*=0.010**), it was not significantly different from zero for any condition. This suggests that the bee's turning rate, and by extension the stimulus velocity, has a negligible or inconsistent influence on the transverse speed.

On the other hand, the stimulus position, ψ_{t-1}, predicted W^T_t (Eq. (4-35)) for all gain conditions to exhibit a periodic relationship that peaked when the stimulus was positioned in the lateral visual field. This indicates bees would step towards the side of their body at which the stimulus was located (Figure 5-3C). In the no stimulus condition, the 'phantom' position of the stimulus had no effect on W^T_t, as expected. The relationship between transverse speed and stimulus position was quantified using Eq. (4-40), which indicated the average difference in W^T_t between when the stimulus was positioned to its left versus when it was positioned to the right (Figure 5-3D); a positive value indicated that W^T_t was positive when the stimulus was positioned to the bee's right, or vice versa. For all gain conditions, W^T_t was modulated such that bees would step towards the stimulus (Figure 5-3D). The magnitude of this relationship varied significantly depending on the stimulus condition (χ^2_5 =15.41, ***p*=0.009**). However, although x2 gain had the largest magnitude, the relationship was not significantly different from that for x0.5 gain, which had the lowest magnitude (W_{10}=-1.42, p=0.155). The honeybee's transverse speed was only modulated by the angular position of the stimulus.

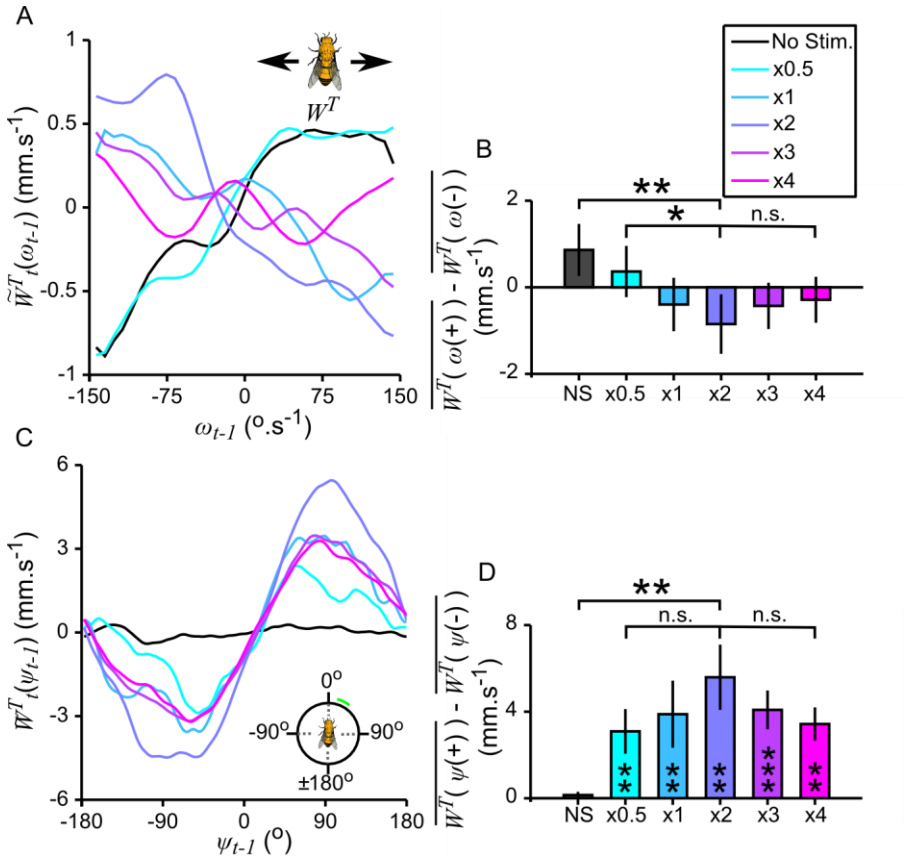

Figure 5-3: Transverse walking speed is modulated by stimulus position. **A**, modulation of longitudinal speed, W^T_t, as a function of prior turning rate, ω_{t-1}. **B**, the difference in W^T_t between positive ($0 < \omega_{t-1} < 150$ °.s^{-1}) and negative ($-150 < \omega_{t-1} < 0$ °.s^{-1}) prior turning rates, from Eq. (4-39). **C**, modulation of W^T_t as a function of prior stimulus position, ψ_{t-1}. **D**, the difference in W^T_t between right ($0 < \psi_{t-1} < 180$°) and left ($-180 < |\psi_{t-1}| < 0$°) stimulus positions, from Eq. (4-40). All plots show each gain condition as a separate curve. N=11 bees repeated all gain conditions. Error bars show ± S.E.M. Bars denote statistical significance (n.s.: $p>0.05$, *: $p<0.05$, **: $p<0.01$, ***: $p<0.001$), of the difference between the indicated groups, whereas stars in bars denote a statistically significance difference from a value of zero. Full statistical details are provided in Section D.2.3.

5.5.4 Walking speed can influence fixation performance

Both longitudinal and transverse walking speeds are modulated depending on the stimulus position, yet, the design of our experimental paradigm was such that their measured values do not influence the movement of the fixation stimulus in any way. To better understand why bees modulated their walking speed, we tested whether walking speed was related to fixation perfromance. To do this, we quantified the relationship between the duration of fixation periods and mean longitudinal, W^L, or absolute transverse speed, $|W^T|$, during such periods. Fixation periods were defined as a period of at least 100 ms in which the bee positioned the stimulus in

its frontal visual field, $45 < \psi < 45^{o}$ (for the no stimulus condition, ψ represents the calculated angle of the black bar that is not visible to the bees).

Surprisingly, in the absence of a visual stimulus, honeybees could maintain relatively long periods of constant orientation when walking quickly (Figure 5-4A). When the fixation stimulus was visible, the relationship between W^L and fixation duration depended on the gain condition. At x0.5 gain, the fixation duration peaked during periods of fast walking (at approximately 50 $mm.s^{-1}$) although bees could also fixate for nearly as long when walking slowly. Hence, fast walking may have some inherent benefits for maintaining a straight course, at least in our experimental paradigm. In contrast, at x1 gain and above, fixation durations generally declined as bees walked faster, to the extent where, for gains of x3 and x4, average durations greater than 1 s only occurred when W^L was lower than 10 $mm.s^{-1}$ (Figure 5-4A). Conversely, increasing $|W^T|$ rapidly decreased the expected duration for periods of constant orientation or fixation, regardless of the gain condition (Figure 5-4B). These results suggest that fast walking generally made fixation difficult, potentially causing errors or otherwise reducing the precision of the bee's turning control. At gains of x2 and higher, these difficulties in fixation appeared to outweigh any passive stability provided by fast walking. Indeed, bees were likely to be more successful in fixation at higher gain levels if they walked slowly, therefore improving their control of turning the ball. Yet, bees maintained similar walking speeds across all gain conditions (Figure 5-1). Therefore, we further considered how the bees' observed walking speeds would affect how far they could move towards the fixation stimulus if their path was calculated considering the assumption that the stimulus was a distant visual landmark.

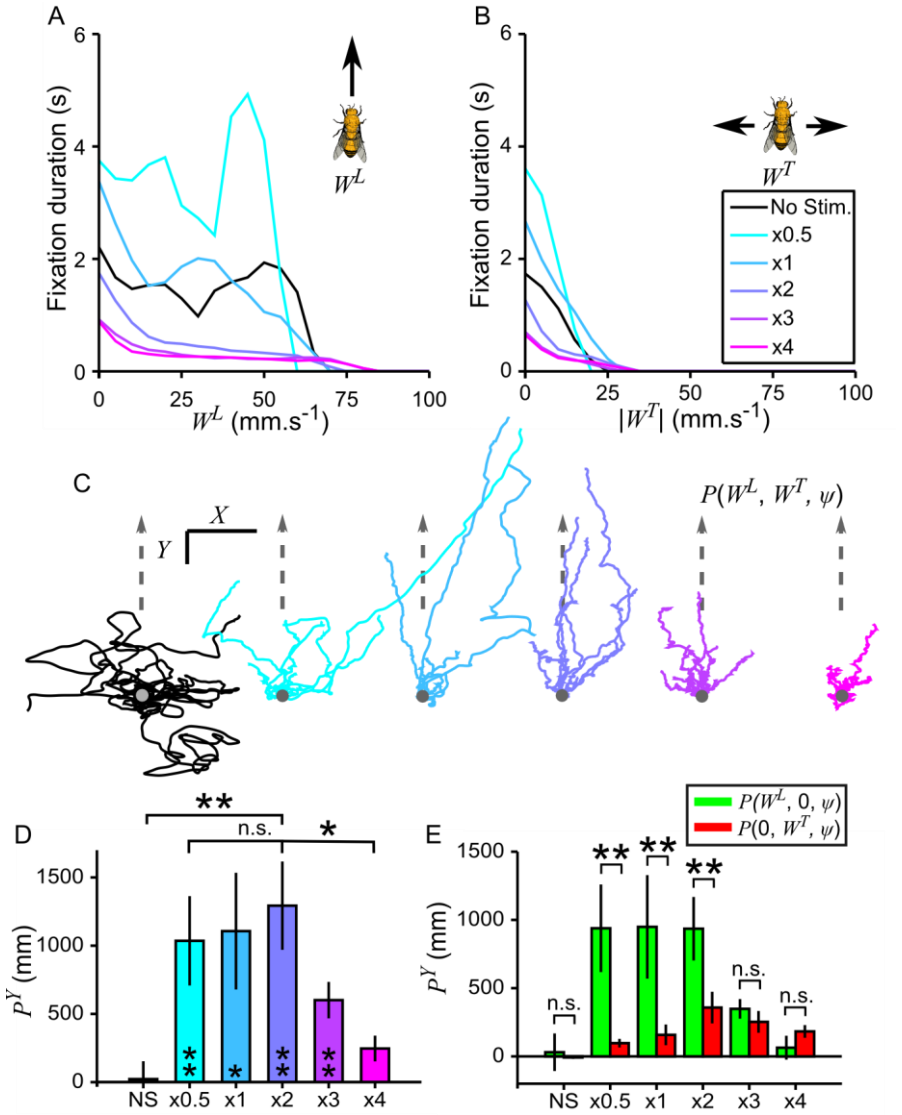

Figure 5-4: Walking speed influences fixation performance, and allows bees to approach the stimulus. **A**, Relationship between longitudinal walking speed, W^L, and fixation duration. **B**, Relationship between transverse walking speed, W^T, and fixation duration. In both A and B, fixation duration refers to the duration of periods greater than 100 ms where the stimulus is positioned in the region $-45 < \psi < 45^o$. **C**, Path reconstructions from each bee's movement using Eq. (4-30). A grey dot denotes the start point of all trajectories for a given condition and the arrow represents the direction to the distant landmark represented by the fixation stimulus. All scale bars represent 500 mm. **D**, Final distance moved towards the stimulus location in the *Y*-direction, P^Y. **E**, Average P^Y based only on either W^L or W^T. All plots show each gain condition as a separate curve. N=11 bees repeated all gain conditions. Error bars show ± S.E.M. Bars denote statistical significance (n.s.: $p>0.05$, *: $p<0.05$, **: $p<0.01$), of the difference between the indicated groups, whereas stars in bars denote the statistical significance from zero. Full statistical details are provided in Section D.2.4.

5.5.5 Reconstructed paths would take honeybees towards the stimulus

During actual walking, the bee's speed and orientation over time define the path of its movement through the world. The stimulus could be considered to be a distant landmark, as

translatory motion towards or away from it results in no change to its apparent size. The bee's path for the entire duration of the experiment can be reconstructed using Eq. (4-30) based in its longitudinal, W^L, and transverse, W^T, speeds, and by treating the stimulus position, ψ, as the idiothetic bearing of the external landmark.

In the absence of a visual stimulus, the reconstructed paths of bees meander in random directions from the starting point (Figure 5-4C). However, in the presence of an external orientation cue, in this case the fixation bar, the reconstructed paths indicate that the bees would have moved towards the fixation stimulus given their turning rate and longitudinal and transverse walking speeds (Eq. (4-30)). This is true for all gain conditions to varying extents. Progress towards the fixation stimulus was quantified as the final distance moved towards the stimulus in the *Y*-direction, P^Y. The distance moved varied significantly depending on the gain condition (Figure 5-4D, $\chi^2_5 = 19.94$, $\boldsymbol{p=0.001}$), with x2 gain resulting in the largest P^Y, although the distances for gains x0.5 and x1 were comparable. P^Y decreased sharply at x3 gain, and bees did not move a significant distance towards the stimulus at x4 gain. As expected, bees did not move a significant distance from the starting point in the no stimulus condition on average.

The path that a bee takes reflects a vector summation of the path resulting from W^L and W^T, that is,

$$P\left(W^L, W^T, \psi\right) = P\left(W^L, 0, \psi\right) + P\left(0, W^T, \psi\right) \tag{4-41}$$

Thus, it is possible to compare how either W^L or W^T individually contributes to P^Y, by calculating either $P\left(W^L, 0, \psi\right)$ or $P\left(0, W^T, \psi\right)$. These calculations indicated that at gains x0.5, x1 and x2, the bees walked significantly further based on W^L than W^T (Figure 5-4E and Supp. Figure 2). However, W^T does result in movement towards the stimulus for all gain conditions, and P^Y based on both W^L and W^T is statistically similar at gains x3 and x4. Both longitudinal and transverse walking speeds can contribute to a bee's movement towards an object in the environment. Next, we use a simulation to identify how the bee's method of modulation its longitudinal and transverse speed components contributes to progress towards the stimulus.

5.5.6 Simulated paths from modelled fixation and walking speed

To assess how the variables modulating a bee's locomotion would influence its path towards an object, we used a previously developed model to simulate honeybee fixation (Chapter 4,

Figure 5-5Ai) and simultaneously calculated the longitudinal, W^L, and transverse, W^T, walking speeds to construct the simulated path (Figure 5-5Aii). Both components of walking speed are predicted as autoregressive low-pass filtered functions of stimulus position, ψ, and turning rate, ω. We also included noise and offset terms (described in Section 5.4.4). The simulation predicted paths that a bee would take towards a distant visual landmark when fixating on it, and was used to test how various methods of modulating both W^L and W^T contributed to a bee's displacement towards the stimulus P^Y. Four different types of modulation were examined: 1) no modulation, 2) modulation as a function of ψ, 3) modulation as a function of ω, or 4) modulation as a function of ψ and ω. All types of modulation included the injection of random noise (Figure D-4). The simulation was conducted for gain conditions varying from x0.5 to x4, as used in experimental conditions. As gain increased, control of the angular position of the stimulus became progressively less stable (Figure 5-5Aii). The functional dependence of walking speed on ψ and ω for each gain condition, as measured in real bees, was used in the simulation, in order to directly evaluate their role in shaping paths under stable and un-stable fixation conditions. The results of the simulations were quantified by computing the final distance moved towards the stimulus location in the *Y*-direction, P^Y, as was done for the measured paths shown in Figure 5-4.

When considering the paths resulting from unmodulated longitudinal speed, the injection positively biased noise resulted in simulated trajectories that exhibited progress towards the stimulus at all gain conditions. Similar P^Y values, which are the final distance moved towards the stimulus, were found for both simulated (Figure 5-5B and C - red) and measured data (Figure 5-5C - black). Substantially longer paths occurred at lower gains (x0.5, x1 and x2) than at higher gains (x3 and x4). When longitudinal speed was modulated as a function of turning rate and injected noise, there was negligible difference on simulated paths or P^Y values (Figure 5-5B and C - green) from the simulations where the longitudinal speed was not modulated. When W^L was modulated as a function of the stimulus position and injected noise, simulated paths progressed *further* towards the stimulus (Figure 5-5B and C - blue) than seen for other simulation configurations and for measured data (Figure 5-5C). Although this made only a small relative contribution at lower gains, when P^Y was large for all simulations, at higher gains the relative contribution was much larger (Figure 5-5C). Modulating longitudinal speed by ψ allowed the simulated bee to progress more than twice as far towards the stimulus at high gains than in other conditions.

If paths resulting from transverse speed are considered, it is apparent only injecting unbiased noise does not result in movement towards the stimulus (Figure 5-5D and E - red), and nor does modulation of W^T based on turning rate and injected noise. However, modulation of W^T by stimulus position did result in progress towards the stimulus at all gain conditions (Figure 5-5D and E - blue). At all gain conditions, the average P^Y was marginally longer for the simulated data than for the measured data, although both followed a qualitatively similar trend, peaking at x2 gain. Evidentially, the manner in which both longitudinal and transverse speed are modulated by stimulus position contributes to the bee's progress towards a fixation stimulus, particularly when its angular position is unstable. For both longitudinal and transverses speeds, modulation due to turning rate has negligible effect on the bee's progress, either when used alone, or in combination with modulation due to the stimulus position (Figure 5-5B to E - cyan).

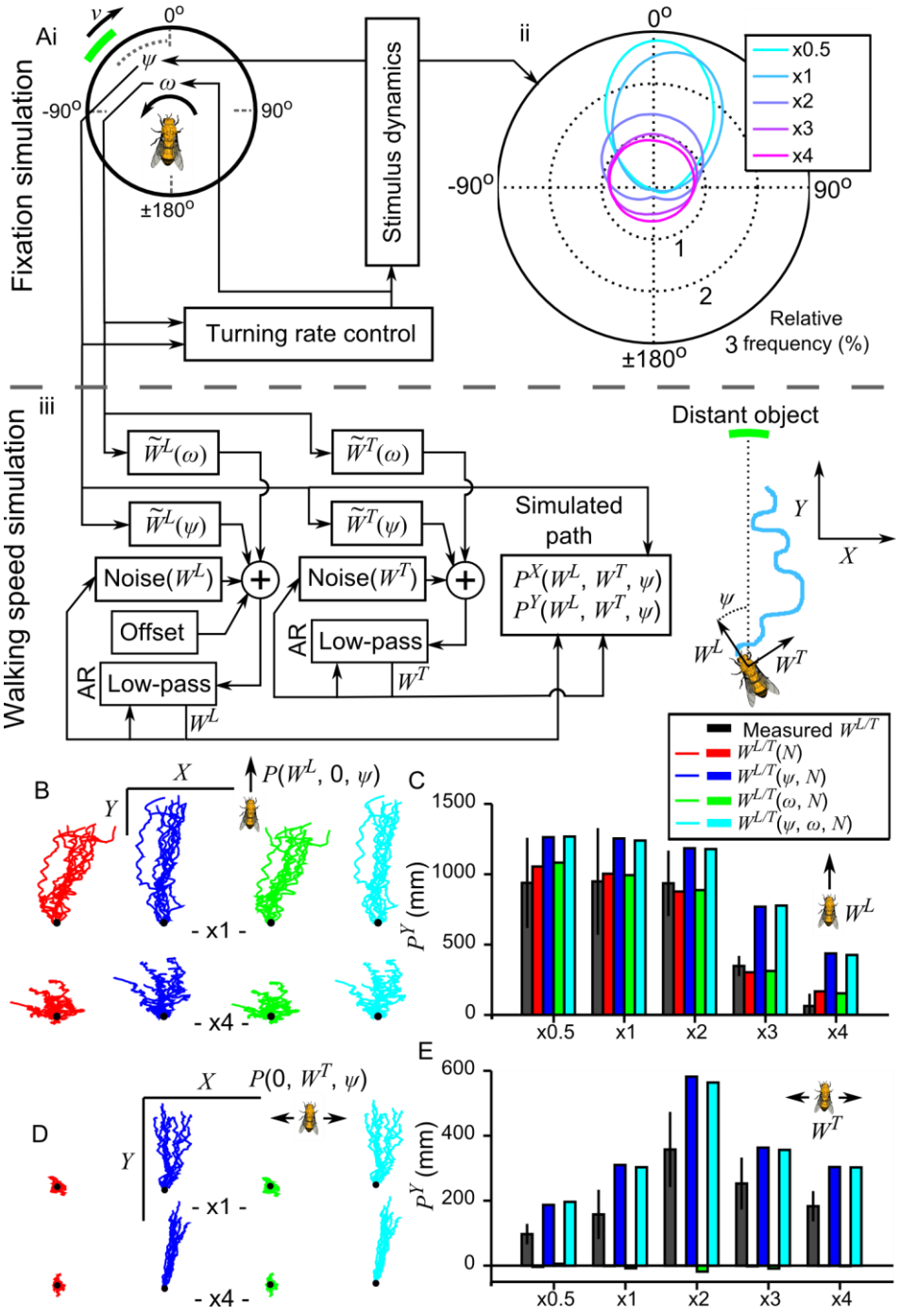

Figure 5-5: Simulated paths progress further when walking speed is modulated by stimulus position. **A**, Schematic diagram of stimulation: honeybee fixation (**i**), and the stimulations distribution of stimulus positions, ψ, (**ii**; Section 4.6.4), (**iii**) simulation of longitudinal, W^L, and transverse, W^T, walking speeds and calculation of simulated path (Section 5.4.4). In B, C, D and E, paths and bars are coloured depending on the functions used to modulate both components of walking speed in a particular simulation: **red** – walking speed is low-pass filtered noise, and in addition to noise, **blue** – walking speed is a function of stimulus position (ψ), **green** – walking speed is a function of turning rate (ω), and **cyan** – walking speed is a function of both ψ and ω. The black bars in D and F show the measured data from Figure 5-4E for comparison. **B**, ten example paths based on longitudinal speed ($P(W^L, 0, \psi)$) from each modulation condition. The dot denotes the starting point of all trajectories for a given condition. All scale bars represent 500 mm. **C**, the average final displacement towards the stimulus, P^Y,

of paths based on W^L for all gain conditions. **D** and **E,** as for B and C, however calculated from transverse speed ($P(0,W^T,\psi)$). In both B and D, the top row of paths represents x1 gain, and the bottom row x4 gain. Distributions and autocorrelations for both W^L and W^T relating to the cyan lines are shown in Figure D-5.

5.6 Discussion

During a fixation task, insects use their turning actions to position a visual stimulus to their front. This study shows that when honeybees are actively controlling the fixation stimulus (a vertical green bar), they also concurrently modulate both their longitudinal and transverse walking speeds as functions of the stimulus position. If the fixation stimulus were considered as a static visual landmark, the observed modulation of walking speed would result in movement towards the object. Modulation is particularly important when the bee had minimal control of the stimulus position at high gain conditions, as might occur if it attempted to approach a flower moving unpredictably in the wind. Modulation of walking speed occurs despite bees receiving no cues indicating movement towards the stimulus, which is would normally be present during natural movement. During movement through the environment, speed control based on stimulus position presumably interacts with other sensory cues that are also used to control speed.

5.6.1 Control dependent on stimulus position

Flying insects are frequently observed to regulate their forward movement speed depending on visual information. Speed can be controlled depending on optic flow from the environment, allowing insects to maintain a consistent, presumably safe ground speed (Baird et al., 2005; David, 1979; Fry et al., 2009), and to perform smooth landings (Srinivasan et al., 2000). Movement speed may also be controlled depending on the apparent size of a visual object that is being approached (Boeddeker et al., 2003; Cook, 1979; Land, 1993; Schuster et al., 2002; van Praagh et al., 1980). We observe that walking bees control their longitudinal speed to walk fastest when the fixation stimulus is positioned in their frontal visual field. This strategy promotes efficient progress towards the object, because the walking speed is higher when moving towards an object and lower when moving away from it. When the fixation stimulus can be held in a stable position, the modulation of longitudinal speed has a small influence on how far the bee would progress towards the stimulus location, although at higher gains (x3 and above), this method of speed modulation appears to allow honeybees to progress at least twice

as far towards the stimulus than without it. Therefore, the method of controlling longitudinal speed could be important when moving towards an unstable object. Importantly, this method of controlling walking speed is not detrimental when moving towards a stable object.

Insects have previously been shown to use side-to-side movements to control their alignment with respect to a visual object during flight, either to adjust their lateral position relative to a target (Sprayberry & Daniel, 2007; Zhang et al., 1990) or to centre the insect with respect to the environment (Kirchner & Srinivasan, 1989). In our fixation task, bees step sideways towards the visual stimulus when it is in their lateral visual field. This method of controlling transverse speed would result in similar alignment adjustments as those observed in free flight. Our findings indicate that when the angular position of the fixation stimulus cannot be accurately controlled, such as during high gain conditions, modulation of transverse speed would also allow them to progress further towards the stimulus location, as compared to the situation when only longitudinal speed is modulated. Thus, the bee's method of controlling transverse speed also assists movement towards an unstable object.

In their natural environment, honeybees inside a hive orient and walk towards the exit which is often brightly illuminated during the day (Tautz, 2008), and use non-visual cues to track other bees during the waggle dance (Judd, 1994; Rohrseitz & Tautz, 1999). Although the orientation and tracking tasks performed by walking bees do not appear particularly demanding, their methods of modulating both longitudinal and transverse walking speeds are robust. When flying, honeybees are known to use side-slip to adjust their alignment to a visual object that is being approached (Zhang et al., 1990), and can maintain a fixed distance relative to the visual objet they are following (van Praagh et al., 1980). Optic flow from the apparent motion of the environment also regulates forwards movement speed in flying bees (Baird et al., 2005), and has a similar influence when walking (Schone, 1996). Honeybees appear to control transverse speed depending on stimulus position in a similar manner when walking and as well as flying, and commonalities may also be found in how flying honeybees control their longitudinal speed when approaching an object.

5.6.2 Conclusion

If an insect cannot maintain a stable orientation with respect to a visual object, use of the target's angular position as a parameter for controlling the speed of movement towards it

appears to be an important factor in ensuring an efficient approach. Although we cause target instability in our experiments by using a high gain value, analogous instability could occur if the target actively evades capture, or if both the insect and its target, such as a flower, are displaced by turbulent airflow. The target's angular position is a variable that is already used to control an insect's turning rate (Chapter 4; Aptekar et al., 2012; Bahl et al., 2013), so the control of longitudinal and transverse speeds, as observed in bees, suggests an effective mechanism to further utilize an already measured variable to expedite the progress towards the object. Indeed, incorporating a mechanism for controlling the speed of locomotion based on the angular position of a target could be an effective strategy for a robot designed to intercept a moving object, and may reduce the performance requirements for the control system underlying object fixation.

Chapter 6 General discussion

Understanding the roles of multi-sensory integration and adaptive control can provide insights into insect behaviour under general and varied environmental conditions. In this thesis, I have used virtual-reality paradigms to investigate how honeybees utilize both multi-sensory information and adaptive control to increase the efficacy and robustness of their behaviours.

6.1 Summary of results

Chapter 2 describes the streamlining response of flying honeybees to combinations of translational optic flow and air speed. As optic flow or air speed increases, bees raise their abdomen into alignment with their thorax, which would act to reduce energy expenditure during actual flight. The Johnston's organ in the antennae was primarily responsible for measurement of air speed, although minor residual wind sensing capacity remains after its ablation. A model in which optic flow and air speed interact in a non-linear fashion predicts the movement of the abdomen. A brief review, considering insects ranging in size from *Drosophila* to locusts, indicates that streamlining by raising the abdomen would generally benefit the insects considered by reducing their energy expenditure during flight. The honeybee's method of multi-sensory integration between air speed and optic flow appears to ensure the streamlining response is primarily mediated by sensing air speed, with optic flow acting to make the response robust to transient disturbances.

Chapter 3 describes how honeybees perform a visual fixation task where they walk on a ball, and the measurement of their turning rate is used to control the azimuthal position of the fixation stimulus in closed-loop. In this paradigm, honeybees usually position the fixation stimulus in their frontal visual field; however, if the feedback sensor measuring the ball's movement is coupled to the bee's walking speed, such that increased walking speed reduces the sensitivity of the turning rate sensor, bees walk faster. This phenomenon is demonstrated using the FicTrac sensor, which is capable of measuring the movements of the ball accurately. However, the study also shows that such a coupling can occur as an artefact when the motion of the ball is measured using optical motion sensors from a consumer computer mouse. In both situations, the presence of the coupling induces a change in the bee's behaviour, which increases their success when fixating the stimulus.

Chapter 4 further explores adaption during fixation, in this case examining how honeybees change their behaviour when the gain condition, which is the coupling between their turning rate and the movement of the fixation stimulus, is varied. An analysis method is described that allows for calculation of an insect's response to both the position, and directionally dependent motion of the fixation stimulus. Although the bee's fixation deteriorates at high gains, they adapt to increased gains by reducing the magnitude of their response to the stimulus position, and also by changing their response to stimulus motion such that the response to motion was weakest when the stimulus is in the frontal visual field. Simulations show that these adaptions increased the stability of fixation at elevated gain.

Chapter 5 characterises how bees vary their walking speed during the closed-loop fixation task described in Chapter 4. Bees modulate both their longitudinal (forwards) and transverse (sideways) speeds as a function of the position of the fixation stimulus, but are not significantly influenced by the gain condition coupling their turning rate to the movement of the fixation stimulus. Fast walking appears to make fixation difficult, however, honeybees progressed towards the stimulus at all but the highest gain. Simulations indicated that the control of longitudinal and transverse components of walking speed represent an effective strategy for moving towards an object, even if its angular position is unstable.

6.2 Implications of results

These studies shed light on the mechanisms honeybees use to control their behaviour. In addition to the discussions in each results chapter, several points relating virtual-reality paradigms and insect sensorimotor control are considered further here.

6.2.1 Honeybees in virtual-reality

In this thesis all experimental work used tethered bees. Freely flying bees have long been used as a model organism for the study of higher order cognitive tasks such as visual navigation, learning and memory (Frisch & Lindauer, 1956; Menzel & Giurfa, 2001; Zhang et al., 2012). However, studies with restraiend honeybees have largely focused on classical conditioning (Giurfa & Malun, 2004; Menzel & Bitterman, 1983; Vergoz, Roussel, Sandoz, & Giurfa, 2007) or physiological aspects of flight performance (Esch, Nachtigall, & Kogge, 1975; Hanauer-

Thieser & Nachtigall, 1995); learning experiments investigating restrained visual conditioning typically require antennal amputation and show relatively low learning rates (Hori et al., 2006; Niggebruegge, Leboulle, Menzel, Komischke, & de Ibarra, 2009). This thesis indicates that sustained flight and walking can be elicited from intact, tethered bees, during which they respond with flight control reflexes (Chapter 2) and also orientation behaviour (Chapters 3 and 4) that involves adaptation. A recent study, using the same apparatus, demonstrated that neural recordings are possible from walking tethered honeybees that are actively fixating a stimulus (Paulk et al., 2014). In the future, virtual-reality paradigms may allow investigation of the neural processing mechanisms of honeybees performing a range of behavioural tasks.

6.2.2 Closed-loop virtual-reality

The technical specifications of the equipment used to implement virtual-reality arenas for insects may present limitations. For instance, the LCD monitors used to display visual stimulus in Chapter 2 to provided adequate visual stimulation to elicit flight in honeybees, but unfortunately, the monitors refresh rate of 60Hz was well below the flicker fusion frequency of honeybees (Srinivasan & Lehrer, 1984). A bee could have perceived a series steps in the tunnels position, rather than the smooth motion a human observer observed. The low measurement frequent (30 Hz) of FicTrac would have resulted in similar artefacts for closed-loop experiments. Control experiments could be conducted to determine whether this experimental artefact influences an insect by measuring its behaviour or the activity of motion sensitive neurons, when stimulated using a display system with a faster refresh rate to display identical stimulus with different update frequencies. Closed-loop latency, that is the delay between the insect making an action and its influence on the sensory environment during closed-loop experiments, is another potential confound of using the CM sensors (46 ms delay) and FicTrac (87 ms delay) feedback systems for measuring trackball motion in Chapters 3, 4 and 5. Ideally feedback latency should be minimised in virtual-reality studies, as long latency will negatively influence control (Nise, 2008). Dipteran neurons sensitive to visual motion have been shown to respond to within 30 ms (Warzecha & Egelhaaf, 2000), hence it is likely that the closed-loop latency in our system exceeded the latency of measurements by the bee's nervous system. Still, honeybees were still evidentially able to control the visual stimulus (Chapter 4). Again, further behavioural studies could be conducted using behavioural and physiological paradigms by incorporating different latencies into a closed-loop task, which would elucidate how latency influences the bees control of a stimulus and whether insects make

adaptations if latency varies. Lacking control experiments regarding the influence of update frequency or latency, a safe consideration would be to avoid analysing temporal and transient components of an insect's response where slow update speeds or latencies are present in the virtual-reality apparatus; these temporal nonlinearities in the visual environment are most likely to influence transient, rather than steady state responses (Nise, 2008).

The cross-motor adaption between walking speed and turning rate described in Chapter 3 has the potential to produce misleading results regarding behavioural control during closed-loop experiments. Although the experiments in Chapter 3 are motivated by errors occurring when using a computer mouse sensor to measure a trackball's motion, conceivably similar errors could occur using other sensors, such as multi-axis force/torque transducers (Kröger et al., 2008; Xu & Li, 2000). While the bee's adaptation improves their performance in virtual reality, cross-motor adaption could lead to observations of unexpected couplings between motor outputs that do not represent activity occurring during normal movement. Such adaptions could also prove confounding when investigating the neural mechanisms underlying behaviour. Recent findings show that many neural functions are context dependent (Maimon, 2011), and that separate brain regions in vertebrates are active during reflexive motor action compared to when adapting to increased and decreased gain (Ahrens et al., 2012). Thus, different neural activity may well be expected if the insect is performing cross-motor adaptation as compared to when behaving under normal conditions.

Likewise, the influence of selectively breaking aspects of the action perception loop when cross-motor adaptation occurs is unknown. To illustrate this point, consider fixation experiments. Typically the ideal scenario is that an insect's yawing actions (either aerodynamic forces in flight, or leg motions when walking) will be selectively measured and used to control the stimulus, with other motor actions being completely ignored. However, the insect is still likely to vary all motor outputs to determine the most efficacious for the given task (Wolf & Heisenberg, 1991), and would conclude that motor actions other than yaw have no influence on the sensory environment. If the insect must then adapt to changes in the coupling between its yaw torque and the angular position of the stimulus, would it do so in the same manner as if its other motor commands still influenced its perception as expected? This is a difficult question to probe using current virtual-reality apparatus, as almost all selectively measure some aspect of an insect's motor output while aiming to disregard others (Roth et al., 2014), but this

is a core question to answer for closed-loop virtual reality studies aiming to address issues of motor control.

Adaptive behaviours are measured by taking the average of the bee's behaviour over the two-minute duration of a particular test condition (Chapters 3, 4 and 5). Behavioural variability during the fixation task is typically large. Therefore, a long average is beneficial for accurately estimating the bee's response to stimulus position and motion using many samples (Bowman & Azzalini, 1997). The use of many samples also increased the likelihood of observing many combinations of the predictor variables. However, the insect's mechanisms of detecting that adaptation is required and making behavioural changes undoubtedly takes some time, and the analysis method averages the adaption period with the eventual adapted state in this study. *Drosophila* typically require several hundred milliseconds to adapt to changes in the coupling multiplier between their turning rate and the stimulus motion (Wolf & Heisenberg, 1990), and several seconds when switching to use alternate motor outputs, such as thrust, to control the stimulus (Wolf & Heisenberg, 1991); the adaption period for bees could be similarly brief. The dynamics of adaptive behaviour in *Drosophila* were determined by measuring the insect's responses over many repetitions where the closed-loop coupling was altered after the fly had voluntarily moved the fixation stimulus to a single predetermined position. The method used with flies to measure the dynamics of adaption is then not well suited for also describing the resulting response to the fixation stimulus over the insect's entire visual field. Knowledge of both of these aspects of adaption is useful, as dynamics are informative about the mechanisms used to adapt, whereas the response is informative about the eventual, control strategy after adaptation. There does not appear to be a standardised systems identification methodology for adaptive controllers in biological or engineered systems, and the study of adaptive behaviour would benefit from further research in this area.

6.2.3 Multi-sensory integration

The findings in Chapter 2 show that honeybees use a non-linear combination of information from optic flow and air speed to control the streamlining response. Specifically, air speed appears to adjust the sensitivity of the streamlining response to optic flow. This differs from other multi-sensory interactions involving air speed (Haag et al., 2010) and contrasts with studies on bee and fly flight, where flight speed is controlled exclusively by optic flow (Baird et al., 2005; David, 1979), and is largely invariant to air speed (Barron & Srinivasan, 2006; Fry

et al., 2009). However, in tethered flight, air speed acts to reduce the insect's wingbeat amplitude, which would influence flight speed in free flight (Gewecke, 1967; Heran, 1959). Thus, whilst air speed influences wingbeat kinematics, it appears that the set point for flight speed is determined by optic flow and determining how both senses interact to control flight speed is difficult. Streamlining is evidence that aspects of honeybee flight are directly mediated by both optic flow and air speed, which presents the possibility that both senses could also interact in other sensorimotor control tasks. A beneficial (although unconfirmed) control scheme for insects could be to use air speed as a scaling factor for aspects of visually guided control that respond to disturbances, which is similar to the multiplicative role air speed plays in the streamlining response. For instance, air speed could scale the transient changes in thrust that correct for disturbances away from the preferred rate of optic flow (Fry et al., 2009; Theobald et al., 2010), or could be used to scale abdominal ruddering motions that produce a yaw torque in response to disturbances in rotational optic flow (Camhi, 1970b; Zanker, 1988a). Such a scheme is commonly used in aeronautical control and stability augmentation, where control gains are scheduled depending on the measured air speed (Cook, 2012).

6.2.4 Adaptive control

The experiments in Chapter 4 indicated that bees adapt their behaviour by modifying their response to fixed stimulus parameters to improve their performance at a fixation task. Testing adaptive mechanisms of motor control in insects often involves severely altering the coupling in the usual action-perception loop (Möhl, 1988; Wolf & Heisenberg, 1991; Wolf et al., 1992). The fine tuning of behavioural responses, as seen in Chapters 3 and 4, have rarely been examined (but see Hesselberg & Lehmann, 2009; Wolf & Heisenberg, 1990), and would likely to be beneficial. Events that occur during an insect's life, such as leg damage (Götz & Wenking, 1973; Wittlinger et al., 2007) or encountering slippery or springy terrain (Epstein & Graham, 1983; Spence et al., 2010), change the usual coupling in the action-perception loop when walking. Arguably, the numerous mechanoreceptors providing feedback from an insect's legs (Schmitz, 1993; Zill et al., 2004) could adjust the control of these body parts so that movements elicited in response to external stimuli remain largely unchanged; providing robust control that does not require higher order adaptive processes for fine tuning. This blurs the line between robust and adaptive behaviour, as highly robust control with many pre-defined motor routines for different scenarios could be hard to distinguish from changing the parameters of a smaller number of general motor routines (Dickinson, 2013; Ritzmann & Büschges, 2007). Hence, the

adaption observed in this study could result not from an adaptive, but rather a highly robust control system. The reality is probably somewhere between the two standpoints, supporting the previous assertions of Wolf et al. (1992), that despite having evolved a range of relatively fixed sensorimotor reflexes, insects retain the ability to adapt these if necessary.

Classically, it has been proposed that an organism must compare the predicted consequences and actual effects of its actions to detect changes in feedback coupling (Webb, 2004), either by using a full predictive model (von Holst & Mittelstaedt, 1950), or by determining the correlation between changes of reafferent and afferent signals (Wolf & Heisenberg, 1990; Wolf & Heisenberg, 1991). Experiments have shown that both supressing stabilisation reflexes (Payne et al., 2010) and initiating compensatory head movements (Schwyn et al., 2011; Viollet & Zeil, 2013) during voluntary movement are both explained by the presence of a forward model. The ability to adapt suggests that honeybees must make some estimation as to the effect of their actions and compare this to reality, although these experiments do not provide clarification on the mechanism that detects adaption is required. Once the need for adaption is detected, however, it is evident that honeybees do not simply scale their responses depending on gain, which is a mechanism that explains *Drosophila's* responses when stabilising wide field motion (Wolf & Heisenberg, 1990). Rather, bees scale their response to the position of the fixation stimulus, but change the underlying function of their response to stimulus motion by reducing their sensitivity to motion in their frontal visual field. This could form part of a pre-programmed reaction to elevated gain, or result from testing various responses to stimulus motion, and selecting the response that is most appropriate for the fixation task. Detailed examination of the temporal structure of responses during adaption may be required to differentiate these two adaptive mechanisms, and has proven informative for studies on motor adaption with vertebrates (Mehta & Schaal, 2002; Wolpert et al., 1995).

Honeybees control their turning rate as a function of stimulus position, and vary the magnitude of this response significantly depending on the gain condition (Chapter 4). Although their longitudinal and transverse walking speeds are also modulated depending on stimulus position (Chapter 5), the magnitude of these responses did not vary significantly depending on gain condition. Given that walking speed does not directly affect the stimulus, the absence of any significant variation is unsurprising; however, small variation between gain conditions is observed and merits a brief consideration. There is a striking similarity between how honeybees control both their turning rate and transverse speed depending on stimulus position, as the

amplitude of both responses peaks at x2 gain, and decreases at higher and lower gains. Transverse speed is not significantly influenced by turning rate, ruling out a direct biomechanical coupling. Hence, the responses from both motor outputs may share a common control pathway, with adaptations to varying gain changing the magnitude of both responses. Conversely, modulation of longitudinal speed due to stimulus position peaks at x0.5 gain and steadily decreases as gain increases. Although all three motor outputs use a similar sensory measurement, it is evident that a different control system utilises this information to modulate longitudinal speed. However, the two control systems also interact, as bees learn to vary their forward speed when it influences rotational control of the fixation stimulus (Chapter 3), and similar cross-motor adaptions have been observed in flies (Wolf & Heisenberg, 1991; Wolf et al., 1992). Cross-motor adaptions would require convergence of reafferent signals from many of the insect's muscles with multiple sources of afferent information, which suggests that higher order neural processing would underlie adaption (Webb, 2004). Such a convergence of reafferent and afferent signals occurs in the insect central complex, which is suggested to play a supervisory role in controlling locomotion (Ritzmann, Ridgel, & Pollack, 2008; Strausfeld, 1999)

To further understand insect adaptive sensorimotor control, the obvious suggestion would be to investigate the structure and function of the neural mechanisms underpinning adaptive sensorimotor control. However, explicitly designed behavioural studies may provide additional insight as to how insects adapt to multi-sensory combinations of stimuli with multiple motor outputs. When fixating a stimulus in free flight, an insect visually perceives the position and motion of the object of interest, the motion of the background, its own rotations based on mechanoreception, and can potentially exert aerodynamic control in six degrees of freedom. Consider that it is possible to display a two component visual stimulus, part of which elicits a response to image position, and part which elicits a response to image motion (Aptekar et al., 2012), as well as separate visual and mechanosensory cues to tethered insects in virtual-reality (Budick et al., 2007; Sherman & Dickinson, 2004). A paradigm that allows the closed-loop coupling between an insect's motor output and its effect on each sensory parameter to be arbitrarily manipulated could test: 1) which sensory parameters are prioritised during adaptation, 2) whether similar mechanisms are involved when adapting control for each parameter, and 3) how multiple motor outputs could contribute to adaption. Although this situation would represent more elaborate sensorimotor coupling changes than an insect would ever experience whilst freely moving, it would define the limits of sensorimotor adaption, and

may suggest where in the nervous system adaption occurs based on the required convergence of specific afferent and reafferent signals.

6.3 Conclusions and perspective

Consistent with observations of freely moving insects, this thesis finds that honeybees robustly use sensory information to control their behaviour. Specifically, they achieve this by using non-linear responses to multi-sensory stimuli, and by adapting control parameters to changes in the coupling of the action-perception loop during closed-loop behaviour. Given that the majority of studies involving insects treat them as static control systems, responding with a pre-programmed set of reactions to a given stimulus, the study of adaption may provide fruitful avenues for investigating the complexity of insect control systems. Although insects appear to be genetically pre-programmed for movement (Hesselberg & Lehmann, 2009), the ability to adapt sensorimotor programs would be advantageous. For instance, adaptation could allow insects to survive longer after sustaining injuries and enable them to better exploit changes in environmental conditions, relaxing the requirements for the evolution of well-matched filters in the sensory system. The benefits of higher order of learning for insects is already well established (Menzel & Giurfa, 2001; Srinivasan, 2009).

Besides contributing to knowledge of insect control strategies, understanding effective adaptive mechanisms may prove useful for micro-scale robotics. As scale decreases, small errors during manufacturing can have relatively large impacts on system dynamics; manufacturing variations in a recently developed 80 mg flapping robot required individual control systems to be tuned for each prototype (Ma, Chirarattananon, Fuller, & Wood, 2013). A direct application of robust adaptive control schemes could be to supplement or replace factory calibrations when producing small robotic devices.

List of References

Ahrens, M.B., Li, J.M., Orger, M.B., Robson, D.N., Schier, A.F., Engert, F., & Portugues, R. (2012). Brain-wide neuronal dynamics during motor adaptation in zebrafish. *Nature, 485*(7399), 471–477.

Altshuler, D.L., Dickson, W.B., Vance, J.T., Roberts, S.P., & Dickinson, M.H. (2005). Short-amplitude high-frequency wing strokes determine the aerodynamics of honeybee flight. *Proc. Natl. Acad. Sci. USA, 102*(50), 18213-18218.

Anderson, J.D. (2005). *Introduction to flight*. New York: McGraw-Hill.

Aptekar, J.W., Shoemaker, P.A., & Frye, M.A. (2012). Figure tracking by flies is supported by parallel visual streams. *Curr. Biol., 22*(6), 482-487.

Arbas, E.A. (1986). Control of hindlimb posture by wind-sensitive hairs and antennae during locust flight. *J. Comp. Physiol. A, 159*(6), 849-857.

Avago Technologies. (2009). ADNS-7050 laser mouse sensor datasheet.

Azuma, A., & Watanabe, T. (1988). Flight performance of a dragonfly. *J. Exp. Biol., 137*(1), 221-252.

Baddeley, R., Ingram, H., & Miall, R. (2003). System identification applied to a visuomotor task: near-optimal human performance in a noisy changing task. *J. Neurosci., 23*(7), 3066-3075.

Bahl, A., Ammer, G., Schilling, T., & Borst, A. (2013). Object tracking in motion-blind flies. *Nat. Neurosci., 16*(6), 730-738.

Baird, E., Boeddeker, N., Ibbotson, M.R., & Srinivasan, M.V. (2013). A universal strategy for visually guided landing. *Proc. Natl. Acad. Sci. U.S.A., 110*(46), 18686-18691.

Baird, E., Kornfeldt, T., & Dacke, M. (2010). Minimum viewing angle for visually guided ground speed control in bumblebees. *J. Exp. Biol., 213*(10), 1625.

Baird, E., Srinivasan, M.V., Zhang, S.W., & Cowling, A. (2005). Visual control of flight speed in honeybees. *J. Exp. Biol., 208*(20), 3895-3905.

Bao, P., & Ananda, M.M.A. (2001). Performance of two-way ANOVA procedures when cell frequencies and variances are unequal. *Commun. Stat. Simulat., 30*(4), 805-829.

Barron, A., & Srinivasan, M.V. (2006). Visual regulation of ground speed and headwind compensation in freely flying honey bees (*Apis mellifera* L.). *J. Exp. Biol., 209*(5), 978-984.

Batschelet, E. (1981). *Circular statistics in biology*. New York: Academic Press.

Berens, P. (2009). CircStat: a MATLAB toolbox for circular statistics. *J. Stat. Soft., 31*(10), 1-21.

Blondeau, J., & Heisenberg, M. (1982). The three-dimensional optomotor torque system of *Drosophila melanogaster*. *J. Comp. Physiol. A, 145*(3), 321-329.

Boeddeker, N., & Hemmi, J.M. (2010). Visual gaze control during peering flight manoeuvres in honeybees. *Proc. R. Soc. B, 277*(1685), 1209-1217.

Boeddeker, N., Kern, R., & Egelhaaf, M. (2003). Chasing a dummy target: smooth pursuit and velocity control in male blowflies. *Proc. R. Soc. B, 270*(1513), 393-399.

Böhm, H., Heinzel, H.-G., Scharstein, H., & Wendler, G. (1991a). The course control system of beetles walking in an air-current field. *J. Comp. Physiol. A, 169*(6), 671-683.

Böhm, H., Schildberger, K., & Huber, F. (1991b). Visual and acoustic course control in the cricket *Gryllus bimaculatus*. *J. Exp. Biol., 159*(1), 235-248.

Borst, A. (1986). Time course of the houseflies' landing response. *Biol. Cybern., 54*(6), 379-383.

Borst, A., Flanagin, V.L., & Sompolinsky, H. (2005). Adaptation without parameter change: Dynamic gain control in motion detection. *Proc. Natl. Acad. Sci. U.S.A., 102*(17), 6172-6176.

Borst, A., Haag, J., & Reiff, D.F. (2010). Fly motion vision. *Ann. Rev. Neurosci., 33*, 49-70.

Bowman, A.W., & Azzalini, A. (1997). *Applied smoothing techniques for data analysis*. Oxford: Oxford University Press Inc.

Brackenbury, J.H. (1994). Wing folding and free-flight kinematics in Coleoptera (Insecta): a comparative study. *J. Zool., 232*(2), 253-283.

Brembs, B., & Heisenberg, M. (2001). Conditioning with compound stimuli in *Drosophila melanogaster* in the flight simulator. *J. Exp. Biol., 204*(16), 2849-2859.

Brinkworth, R.S., & O'Carroll, D.C. (2009). Robust models for optic flow coding in natural scenes inspired by insect biology. *PLoS Comput. Biol., 5*(11), e1000555.

Britting, K.R. (2010). *Inertial navigation systems analysis*. Norwood: Artech House Publishers.

Budick, S.A., Reiser, M.B., & Dickinson, M.H. (2007). The role of visual and mechanosensory cues in structuring forward flight in *Drosophila melanogaster*. *J. Exp. Biol., 210*(23), 4092-4103.

Bülthoff, H. (1981). Figure-ground discrimination in the visual system of *Drosophila melanogaster*. *Biol. Cybern., 41*(2), 139-145.

Bülthoff, H. (1982). *Drosophila* mutants disturbed in visual orientation. II. Mutants affected in movement and position computation. *Biol. Cybern., 41*(1), 71-77.

Camhi, J., & Johnson, E. (1999). High-frequency steering maneuvers mediated by tactile cues: antennal wall-following in the cockroach. *J. Exp. Biol., 202*(5), 631-643.

Camhi, J.M. (1970a). Sensory control of abdomen posture in flying locusts. *J. Exp. Biol., 52*(3), 533-537.

Camhi, J.M. (1970b). Yaw-correcting postural changes in locusts. *J. Exp. Biol., 52*(3), 519-531.

Campan, R. (1997). Tactic components in orientation. In M. Lehrer (Ed.), *Orientation and communication in arthropods* (pp. 1-40). Basel: Birkhäuser Verlag.

Cao, Y. (2008). Efficient Kernel Smoothing Regression using KD-Tree. *MATLAB Central File Exchange.* Retrieved July, 2013

Cardé, R.T., & Willis, M.A. (2008). Navigational strategies used by insects to find distant, wind-borne sources of odor. *J. Chem. Ecol., 34*(7), 854-866.

Chahl, J.S., Srinivasan, M.V., & Zhang, S.-W. (2004). Landing strategies in honeybees and applications to uninhabited airborne vehicles. *Int. J. Robot. Res., 23*(2), 101-110.

Chan, W.P., Prete, F., & Dickinson, M.H. (1998). Visual input to the efferent control system of a fly's "gyroscope". *Science, 280*(5361), 289-292.

Cheung, A., Zhang, S., Stricker, C., & Srinivasan, M.V. (2007). Animal navigation: the difficulty of moving in a straight line. *Biol. Cybern., 97*(1), 47-61.

Chiappe, M.E., Seelig, J.D., Reiser, M.B., & Jayaraman, V. (2010). Walking modulates speed sensitivity in *Drosophila* motion vision. *Curr. Biol., 20*(16), 1470-1475.

Chiel, H.J., & Beer, R.D. (1997). The brain has a body: adaptive behavior emerges from interactions of nervous system, body and environment. *Trends Neurosci., 20*(12), 553-557.

Chow, D.M., & Frye, M.A. (2008). Context-dependent olfactory enhancement of optomotor flight control in *Drosophila*. *J. Exp. Biol., 211*(15), 2478-2485.

Chow, D.M., Theobald, J.C., & Frye, M.A. (2011). An olfactory circuit increases the fidelity of visual behavior. *J. Neurosci., 31*(42), 15035-15047.

Christensen, T.A. (Ed.). (2005). *Methods in Insect Sensory Neuroscience*. Boca Raton: CRC Press.

Clark, D.A., Bursztyn, L., Horowitz, M.A., Schnitzer, M.J., & Clandinin, T.R. (2011). Defining the computational structure of the motion detector in *Drosophila*. *Neuron, 70*(6), 1165-1177.

Collett, M. (2009). Spatial memories in insects. *Curr. Biol., 19*(24), 1103-1108.
Collett, T., & Land, M. (1975). Visual control of flight behaviour in the hoverfly, *Syritta pipiens* L. *J. Comp. Physiol., 99*(1), 1-66.
Collett, T.S. (1996). Insect navigation en route to the goal: Multiple strategies for the use of landmarks. *J. Exp. Biol., 199*(1), 227-235.
Combes, S., & Dudley, R. (2009). Turbulence-driven instabilities limit insect flight performance. *Proc. Natl. Acad. Sci. USA, 106*(22), 9105-9108.
Cook, M.V. (2012). *Flight dynamics principles: a linear systems approach to aircraft stability and control*. Oxford: Butterworth-Heinemann.
Cook, R. (1979). The courtship tracking of *Drosophila melanogaster*. *Biol. Cybern., 34*(2), 91-106.
Cook, R. (1980). The extent of visual control in the courtship tracking of *D. melanogaster*. *Biol. Cybern., 37*(1), 41-51.
Cowan, N., Lee, J., & Full, R. (2006). Task-level control of rapid wall following in the American cockroach. *J. Exp. Biol., 209*(9), 1617-1629.
Dacke, M., Byrne, M.J., Scholtz, C.H., & Warrant, E.J. (2004). Lunar orientation in a beetle. *Proc. R. Soc. B, 271*(1537), 361-365.
Dahanukar, A., Hallem, E.A., & Carlson, J.R. (2005). Insect chemoreception. *Curr. Opin. Neurobiol., 15*(4), 423-430.
David, C. (1979). Optomotor control of speed and height by free-flying *Drosophila*. *J. Exp. Biol., 82*(1), 389-392.
David, C.T. (1978). The relationship between body angle and flight speed in free-flying *Drosophila*. *Physiol. Ent., 3*(3), 191-195.
David, C.T. (1982). Compensation for height in the control of groundspeed by *Drosophila* in a new, 'barbers pole' wind-tunnel. *J. Comp. Physiol. A, 147*(4), 485-493.
Demir, A., Ankarali, M.M., Dyhr, J.P., Morgansen, K.A., Daniel, T.L., & Cowan, N.J. (2012). *Inertial redirection of thrust forces for flight stabilization.* Paper presented at the Proc. 15th Int. Conf. Climb. Walk. Rob. Supp. Tech. Mob. Mach.
Dickinson, M.H. (2013). Death Valley, *Drosophila*, and the Devonian Toolkit. *Ann. Rev. Entom., 59*, 51-72.
Dickinson, M.H., Farley, C.T., Full, R.J., Koehl, M., Kram, R., & Lehman, S. (2000). How animals move: an integrative view. *Science, 288*(5463), 100-106.
Dill, M., Wolf, R., & Heisenberg, M. (1995). Behavioral analysis of *Drosophila* landmark learning in the flight simulator. *Learn. Mem., 2*, 152-160.
Dillon, M.E., & Dudley, R. (2014). Surpassing Mt. Everest: extreme flight performance of alpine bumble-bees. *Biol. Lett., 10*(2), 20130922.
Dombeck, D.A., & Reiser, M.B. (2012). Real neuroscience in virtual worlds. *Curr. Opin. Neurobiol., 22*(1), 3-10.
Dreller, C., & Kirchner, W.H. (1993). Hearing in honeybees: localization of the auditory sense organ. *J. Comp. Physiol. A, 173*(3), 275-279.
Dudley, R. (1995). Extraordinary flight performance of orchid bees (*Apidae: Euglossini*) hovering in heliox (80% He/20% O_2). *J. Exp. Biol., 198*(4), 1065-1070.
Dudley, R., & Ellington, C.P. (1990a). Mechanics of forward flight in bumblebees. 1. Kinematics and morphology. *J. Exp. Biol., 148*, 19-52.
Dudley, R., & Ellington, C.P. (1990b). Mechanics of forward flight in bumblebees. 2. Quasi-steady lift and power requirements. *J. Exp. Biol., 148*, 53-88.
Duistermars, B.J., Chow, D.M., & Frye, M.A. (2009). Flies require bilateral sensory input to track odor gradients in flight. *Curr. Biol., 19*(15), 1301-1307.
Dukas, R., & Dukas, L. (2011). Coping with nonrepairable body damage: effects of wing damage on foraging performance in bees. *Anim. Behav., 81*(3), 635-638.

Dyhr, J.P., Morgansen, K.A., Daniel, T.L., & Cowan, N.J. (2013). Flexible strategies for flight control: an active role for the abdomen. *J. Exp. Biol, 216*(9), 1523-1536.

Egelhaaf, M. (1987). Dynamic properties of two control systems underlying visually guided turning in house-flies. *J. Comp. Physiol. A, 161*(6), 777-783.

Ejaz, N., Krapp, H.G., & Tanaka, R.J. (2013). Closed-loop response properties of a visual interneuron involved in fly optomotor control. *Front. Neural Circuits, 7*(50).

Ellington, C.P. (1984a). The aerodynamics of hovering insect flight. 2. Morphological parameters. *Phil. Trans. R. Soc. B, 305*(1122), 17-40.

Ellington, C.P. (1984b). The aerodynamics of hovering insect flight. 3. Kinematics. *Phil. Trans. R. Soc. B, 305*(1122), 41-78.

Epstein, S., & Graham, D. (1983). Behaviour and motor output of stick insects walking on a slippery surface: I. Forward walking. *J. Exp. Biol., 105*(1), 215-229.

Erber, J., Kierzek, S., Sander, E., & Grandy, K. (1998). Tactile learning in the honeybee. *J. Comp. Physiol. A, 183*(6), 737-744.

Esch, H., Nachtigall, W., & Kogge, S.N. (1975). Correlations between aerodynamic ouput, electrical-activity in indirect flight muscles and wing positons of bees flying in a servomechanically controlled wind-tunnel. *J. Comp. Physiol., 100*(2), 147-159.

Etheredge, J.A., Perez, S.M., Taylor, O.R., & Jander, R. (1999). Monarch butterflies (*Danaus plexippus* L.) use a magnetic compass for navigation. *Proc. Natl. Acad. Sci. U.S.A., 96*(24), 13845-13846.

Evangelista, C., Kraft, P., Dacke, M., Labhart, T., & Srinivasan, M. (2014). Honeybee navigation: critically examining the role of the polarization compass. *Phil. Trans. R. Soc. B, 369*(1636), 20130037.

Farina, W., Varjú, D., & Zhou, Y. (1994). The regulation of distance to dummy flowers during hovering flight in the hawk moth *Macroglossum stellatarum*. *J. Comp. Physiol. A, 174*(2), 239-247.

Faruque, I., & Humbert, S.J. (2010). Dipteran insect flight dynamics. Part 1 Longitudinal motion about hover. *J. Theor. Biol., 264*(2), 538-552.

Fraenkel, G., & Pringle, J. (1938). Halteres of flies as gyroscopic organs of equilibrium. *Nature, 141*, 919-920.

Frantsevich, L., & Gorb, S. (2006). Courtship dances in the flies of the genus lispe (Diptera: Muscidae): From the fly's viewpoint. *Arch. Insect Biochem. Physiol., 62*(1), 26-42.

Frisch, K., & Lindauer, M. (1956). The" language" and orientation of the honey bee. *Ann. Rev. Entom., 1*, 45-58.

Fry, S., Rohrseitz, N., Straw, A., & Dickinson, M. (2009). Visual control of flight speed in *Drosophila melanogaster*. *J. Exp. Biol., 212*(8), 1120-1130.

Frye, M.A. (2001). Effects of stretch receptor ablation on the optomotor control of lift in the hawkmoth *Manduca sexta*. *J. Exp. Biol., 204*(21), 3683-3691.

Frye, M.A., & Dickinson, M.H. (2004). Motor output reflects the linear superposition of visual and olfactory inputs in *Drosophila*. *J. Exp. Biol., 207*(1), 123-131.

Full, R.J., Kubow, T., Schmitt, J., Holmes, P., & Koditschek, D. (2002). Quantifying dynamic stability and maneuverability in legged locomotion. *Integrative and comparative biology, 42*(1), 149-157.

Galizia, C.G., & Rössler, W. (2010). Parallel olfactory systems in insects: anatomy and function. *Ann. Rev. Entom., 55*, 399-420.

Gettrup, E. (1966). Sensory regulation of wing twisting in locusts. *J. Exp. Biol., 44*(1), 1-16.

Gewecke, M. (1967). Die Wirkung von Luftströmung auf die Antennen und das Flugverhalten der blauen Schmeissfliege (*Calliphora erythrocephala*). *J. Comp. Physiol. A, 54*(2), 121-164.

Gewecke, M. (1970). Antennae: Another wind-sensitive receptor in locusts. *Nature, 225*(5239), 1263-1264.
Gewecke, M. (1974). The antennae of insects as air-current sense organs and their relationship to the control of flight. In L. B. Browne (Ed.), *Experimental analysis of insect behaviour* (pp. 100-113). Berlin: Springer-Verlag.
Gewecke, M., Heinzel, H.G., & Philippe, J. (1974). Role of antennae of the dragonfly *Orthetrum cancellatum* in flight control. *Nature, 249*(5457), 584-585.
Gibson, J.J. (1950). *The perception of the visual world*. Oxford: Houghton Mifflin Company.
Gilbert, C. (1997). Visual control of cursorial prey pursuit by tiger beetles (*Cicindelidae*). *J. Comp. Physiol. A, 181*(3), 217-230.
Giurfa, M., & Malun, D. (2004). Associative mechanosensory conditioning of the proboscis extension reflex in honeybees. *Learn. Mem., 11*(3), 294-302.
Goodman, L. (2003). *Form and function in the honeybee*. Cardiff: International Bee Research Association.
Götz, K. (1964). Optomotorische Untersuchung des visuellen Systems einiger Augenmutanten der Fruchtfliege *Drosophila*. *Biol. Cybern., 2*(2), 77-92.
Gotz, K.G. (1975). Optomotor Equilibrium of *Drosophila* navigation system. *J. Comp. Physiol., 99*(3), 187-210.
Götz, K.G. (1975). Hirnforschung am Navigationssystem der Fliegen. *Naturwissenschaften, 62*(10), 468-475.
Götz, K.G., & Buchner, E. (1978). Evidence for one-way movement detection in the visual system of *Drosophila*. *Biol. Cybern., 31*(4), 243-248.
Gotz, K.G., Hengstenberg, B., & Biesinger, R. (1979). Optomotor control of wing beat and body posture in *Drosophila*. *Biol. Cybern., 35*(2), 101-112.
Gotz, K.G., & Wandel, U. (1984). Optomotor control of the force of flight in *Drosophila* and *Musca*. 2. Covariance of lift and thrust in still air. *Biol. Cybern., 51*(2), 135-139.
Götz, K.G., & Wenking, H. (1973). Visual control of locomotion in the walking fruitfly *Drosophila*. *J. Comp. Physiol., 85*(3), 235-266.
Goyret, J. (2010). Look and touch: multimodal sensory control of flower inspection movements in the nocturnal hawkmoth *Manduca sexta*. *J. Exp. Biol., 213*(21), 3676-3682.
Greggers, U., Koch, G., Schmidt, V., Dürr, A., Floriou-Servou, A., Piepenbrock, D., . . . Menzel, R. (2013). Reception and learning of electric fields in bees. *Phil. Trans. R. Soc. B, 280*(1759), 20130528.
Haag, J., Wertz, A., & Borst, A. (2007). Integration of lobula plate output signals by DNOVS1, an identified premotor descending neuron. *J. Neurosci., 27*(8), 1992-2000.
Haag, J., Wertz, A., & Borst, A. (2010). Central gating of fly optomotor response. *Proc. Natl. Acad. Sci. U.S.A., 107*(46), 20104-20109.
Haas, C., & Cartar, R. (2008). Robust flight performance of bumble bees with artificially induced wing wear. *Canada. J. Zoo., 86*(7), 668-675.
Hanauer-Thieser, U., & Nachtigall, W. (1995). Flight of the honey bee 6. Energetics of wind tunnel exhaustion flights at defined fuel content, speed adaptation and aerodynamics. *J. Comp. Physiol. B, 165*(6), 471-483.
Harvey, C.D., Collman, F., Dombeck, D.A., & Tank, D.W. (2009). Intracellular dynamics of hippocampal place cells during virtual navigation. *Nature, 461*(7266), 941-946.
Hassenstein, B., & Reichardt, W. (1956). Systemtheoretische Analyse der Zeit-, Reihenfolgen- und Vorzeichenauswertung bei der Bewegungsperzeption des Rüsselkäfers *Chlorophanus*. *Z. Naturforsch. B, 11*, 513-524.
Haykin, S.S. (2001). *Kalman filtering and neural networks*. Hoboken: John Wiley & Sons, Inc.

Hedwig, B., & Poulet, J. (2005). Mechanisms underlying phonotactic steering in the cricket *Gryllus bimaculatus* revealed with a fast trackball system. *J. Exp. Biol., 208*(5), 915-927.

Hedwig, B., & Poulet, J.F. (2004). Complex auditory behaviour emerges from simple reactive steering. *Nature, 430*(7001), 781-785.

Heinzel, H.-G., & Gewecke, M. (1979). Directional sensitivity of the antennal campaniform sensilla in locusts. *Naturwissenschaften, 66*(4), 212-213.

Heinzel, H., & Böhm, H. (1989). The wind-orientation of walking carrion beetles. *J. Comp. Physiol. A, 164*(6), 775-786.

Heisenberg, M., & Wolf, R. (1979). On the fine structure of yaw torque in visual flight orientation of *Drosophila melanogaster*. *J. Comp. Physiol. A, 130*(2), 113-130.

Heisenberg, M., & Wolf, R. (1984). *Vision in Drosophila: Genetics of microbehaviour*. Berlin: Springer-Verlag.

Heisenberg, M., & Wolf, R. (1988). Reafferent control of optomotor yaw torque in *Drosophila melanogaster*. *J Comp. Physiol. A, 163*(3), 373-388.

Heisenberg, M., Wonneberger, R., & Wolf, R. (1978). Optomotor-blind^{H31} - a *Drosophila* mutant of the lobula plate giant neurons. *J. Comp. Physiol., 124*(4), 287-296.

Hengstenberg, R. (1984). Roll-stabilization during flight of the blowfly's head and body by mechanical and visual cues. In D. Varju & H. U. Schnitzler (Eds.), *Localization and orientation in biology and engineering* (pp. 121-134). Berlin: Springer-Verlag.

Hengstenberg, R. (1993). Multisensory control in insect oculomotor systems. *Rev. Oculomot. Res., 5*, 285-298.

Hengstenberg, R., Sandeman, D., & Hengstenberg, B. (1986). Compensatory head roll in the blowfly *Calliphora* during flight. *Proc. R. Soc. B, 227*(1249), 455-482.

Heran, H. (1959). Wahrnehmung und Regelung der Flugeigengeschwindigkeit bei *Apis mellifica* L. *Z. Vergl. Physiol., 42*(2), 103-163.

Hesselberg, T., & Lehmann, F.-O. (2009). The role of experience in flight behaviour of *Drosophila*. *J. Exp. Biol., 212*(20), 3377-3386.

Hinterwirth, A.J., & Daniel, T.L. (2010). Antennae in the hawkmoth *Manduca sexta* (Lepidoptera, Sphingidae) mediate abdominal flexion in response to mechanical stimuli. *J. Comp. Physiol. A, 196*(12), 947-956.

Hocking, B. (1953). The intrinsic range and speed of flight of insects. *Trans. R. Ent. Soc. Lond., 104*, 223-345.

Homberg, U. (2005). Multisensory processing in the insect brain. In T. A. Christensen (Ed.), *Methods in Insect Sensory Neuroscience* (pp. 3-25). Boca Raton: CRC Press.

Hori, S., Takeuchi, H., Arikawa, K., Kinoshita, M., Ichikawa, N., Sasaki, M., & Kubo, T. (2006). Associative visual learning, color discrimination, and chromatic adaptation in the harnessed honeybee *Apis mellifera* L. *J. Comp. Physiol. A, 192*(7), 691-700.

Hoy, R., & Robert, D. (1996). Tympanal hearing in insects. *Ann. Rev. Entom., 41*(1), 433-450.

Huston, S.J., & Krapp, H.G. (2009). Nonlinear integration of visual and haltere inputs in fly neck motor neurons. *J. Neurosci., 29*(42), 13097-13105.

Jander, R. (1975). Ecological aspects of spatial orientation. *Ann. Rev. Ecol. Syst., 6*, 171-188.

Judd, T.M. (1994). The waggle dance of the honey bee: which bees following a dancer successfully acquire the information? *Journal of insect behavior, 8*(3), 343-354.

Kanzaki, R. (1998). Coordination of wing motion and walking suggests common control of zigzag motor program in a male silkworm moth. *J. Comp. Physiol. A, 182*(3), 267-276.

Kanzaki, R., Arbas, E., & Hildebrand, J. (1991). Physiology and morphology of descending neurons in pheromone-processing olfactory pathways in the male moth *Manduca sexta*. *J. Comp. Physiol. A, 169*(1), 1-14.

Kawato, M. (1999). Internal models for motor control and trajectory planning. *Curr. Opin. Neurobiol., 9*(6), 718-727.
Keil, T.A. (1997). Functional morphology of insect mechanoreceptors. *Microsc. Res. Tech., 39*(6), 506-531.
Kelber, A., & Zeil, J. (1990). A robust procedure for visual stabilisation of hovering flight position in guard bees of *Trigona* (*Tetragonisca*) *angustula* (Apidae, Meliponinae). *J. Comp. Physiol. A, 167*(4), 569-577.
Kern, R., & Varjú, D. (1998). Visual position stabilization in the hummingbird hawk moth, *Macroglossum stellatarum* L. I. Behavioural analysis. *J. Comp. Physiol. A, 182*(2), 225-237.
Kevan, P.G., Cant, J.G., & Kevan, D. (1983). Predator avoidance posturing of grasshoppers (Orthoptera: Acrididae) from the colorado alpine and plains. *Can. Entomol., 115*(02), 115-122.
Kirchner, W.H., & Srinivasan, M.V. (1989). Freely flying honeybees use image motion to estimate object distance. *Naturwissenschaften, 76*(6), 281-282.
Körding, K.P., & Wolpert, D.M. (2006). Bayesian decision theory in sensorimotor control. *Trends Cogn. Sci., 10*(7), 319-326.
Kral, K. (2003). Behavioural–analytical studies of the role of head movements in depth perception in insects, birds and mammals. *Behav. Process., 64*(1), 1-12.
Krapp, H.G. (2000). Neuronal matched filters for optic flow processing in flying insects. *Int. Rev. Neurobiol., 44*, 93-120.
Krapp, H.G., Taylor, G.K., & Humbert, J.S. (2012). The mode-sensing hypothesis: matching sensors, actuators and flight dynamics. In F. G. Barth, J. A. C. Humphrey & M. V. Srinivasan (Eds.), *Frontiers in Sensing*. Berlin: Springer-Verlag.
Kress, D., & Egelhaaf, M. (2012). Head and body stabilization in blowflies walking on differently structured substrates. *J. Exp. Biol., 215*(9), 1523-1532.
Kröger, T., Kubus, D., & Wahl, F.M. (2008). *12d force and acceleration sensing: A helpful experience report on sensor characteristics.* Paper presented at the Proc. Int. Conf. Rob. Auto.
Krutchkoff, R.G. (1988). One—way fixed effects analysis of variance when the error varianes may be unequal. *J. Stat. Comp. Sim., 30*(4), 259-271.
Kunze, P. (1961). Untersuchung des Bewegungssehens fixiert fliegender Bienen. *J. Comp. Physiol. A, 44*(6), 656-684.
Land, M. (1993). Chasing and pursuit in the dolichopodid fly *Poecilobothrus nobilitatus*. *J. Comp. Physiol. A, 173*(5), 605-613.
Land, M.F., & Collett, T.S. (1974). Chasing behaviour of houseflies (*Fannia canicularis*). *J. Comp. Physiol., 89*(4), 331-357.
Land, M.F., & Nilsson, D.-E. (2002). *Animal eyes*. Oxford: Oxford University Press.
Lehrer, M., & Srinivasan, M.V. (1992). Freely flying bees discriminate between stationary and moving objects: performance and possible mechanisms. *J. Comp. Physiol. A, 171*(4), 457-467.
Lin, S. (2011). NGPM -- A NSGA-II program in Matlab v1.4. *MATLAB Central File Exchange.*
Ljung, L. (1999). *System identification* (2 ed.). Upper Saddle River: Prentice-Hall, Inc.
Lönnendonker, U. (1991). Dynamic properties of orientation to a visually fixated target by walking Colorado beetles. *J. Exp. Biol., 158*(1), 149-164.
Luu, T., Cheung, A., Ball, D., & Srinivasan, M.V. (2011). Honeybee flight: a novel 'streamlining' response. *J. Exp. Biol., 214*(13), 2215-2225.
Ma, K.Y., Chirarattananon, P., Fuller, S.B., & Wood, R.J. (2013). Controlled flight of a biologically inspired, insect-scale robot. *Science, 340*(6132), 603-607.

Maimon, G. (2011). Modulation of visual physiology by behavioral state in monkeys, mice, and flies. *Curr. Opin. Neurobiol., 21*(4), 559-564.

Maimon, G., Straw, A., & Dickinson, M. (2010). Active flight increases the gain of visual motion processing in *Drosophila*. *Nat. Neurosci., 13*(3), 393-399.

Mappes, M., & Homberg, U. (2004). Behavioral analysis of polarization vision in tethered flying locusts. *J. Comp. Physiol. A, 190*(1), 61-68.

Maye, A., Hsieh, C.-h., Sugihara, G., & Brembs, B. (2007). Order in spontaneous behavior. *PLoS One, 2*(5), e443.

McCullough, E.L., & Tobalske, B.W. (2013). Elaborate horns in a giant rhinoceros beetle incur negligible aerodynamic costs. *Proc. R. Soc. B, 280*(1758), 20130197.

McCullough, E.L., Weingarden, P.R., & Emlen, D.J. (2012). Costs of elaborate weapons in a rhinoceros beetle: how difficult is it to fly with a big horn? *Behav. Ecol., 23*(5), 1042-1048.

Mehta, B., & Schaal, S. (2002). Forward models in visuomotor control. *J. Neurophysiol., 88*(2), 942-953.

Menzel, R., & Bitterman, M.E. (1983). Learning by honeybees in an unnatural situation. In F. Huber & H. Markl (Eds.), *Neuroethology and behavioral physiology*. Berlin: Springer-Verlag.

Menzel, R., & Giurfa, M. (2001). Cognitive architecture of a mini-brain: the honeybee. *Trends Cogn. Sci., 5*(2), 62-71.

Merkle, T., Knaden, M., & Wehner, R. (2006). Uncertainty about nest position influences systematic search strategies in desert ants. *J. Exp. Biol., 209*(18), 3545-3549.

Miall, R., & Wolpert, D.M. (1996). Forward models for physiological motor control. *Neural networks, 9*(8), 1265-1279.

Minoni, U., & Signorini, A. (2006). Low-cost optical motion sensors: An experimental characterization. *Sens. Actuator A-Phys., 128*(2), 402-408.

Mitchell, B., Itagaki, H., & Rivet, M.-P. (1999). Peripheral and central structures involved in insect gustation. *Microsc. Res. Tech., 47*(6), 401-415.

Möhl, B. (1988). Short-term learning during flight control in *Locusta migratoria*. *J. Comp. Physiol. A, 163*(6), 803-812.

Möhl, B. (1989). 'Biological noise'and plasticity of sensorimotor pathways in the locust flight system. *J. Comp. Physiol. A, 166*(1), 75-82.

Moore, R.J., Taylor, G.J., Paulk, A.C., Pearson, T., van Swinderen, B., & Srinivasan, M.V. (2014). FicTrac: a visual method for tracking spherical motion andgenerating fictive animal paths. *Journal of Neuroscience Methods, 225*(1), 106-119.

Mou, X.L., Liu, Y.P., & Sun, M. (2011). Wing motion measurement and aerodynamics of hovering true hoverflies. *J. Exp. Biol, 214*(17), 2832-2844.

Nachtigall, W., & Hanauer-Thieser, U. (1992). Flight of the honeybee. 5. Drag and lift coefficients of the bee's body; implications for flight dynamics. *J. Comp. Physiol. B, 162*(3), 267-277.

Nachtigall, W., Widmann, R., & Renner, M. (1971). Über den « ortsfesten » freien Flug von Bienen in einem Saugkanal. *Apidologie, 2*(3), 271-282.

Nalbach, G. (1994). Extremely non-orthogonal axes in a sense organ for rotation: behavioural analysis of the dipteran haltere system. *Neurosci., 61*(1), 149-163.

Neese, V. (1965). Zur Funktion der Augenborsten bei der Honigbiene. *Z. Vergl. Physiol. , 49*(6), 543-585.

Newland, P.L., Hunt, E., Sharkh, S.M., Hama, N., Takahata, M., & Jackson, C.W. (2008). Static electric field detection and behavioural avoidance in cockroaches. *J. Exp. Biol., 211*(23), 3682-3690.

Niehaus, M. (1981). Flight and flight control by the antennae in the small tortoiseshell (*Aglais urticae* L., Lepidoptera). II. Flight mill and free flight experiments. *J. Comp. Physiol. A, 145*(2), 257-264.

Niggebruegge, C., Leboulle, G., Menzel, R., Komischke, B., & de Ibarra, N.H. (2009). Fast learning but coarse discrimination of colours in restrained honeybees. *J. Exp. Biol., 212*(9), 1344-1350.

Nise, N.S. (2008). *Control systems engineering* (4 ed.). Hoboken: John Wiley & Sons, Inc.

Oie, K.S., Kiemel, T., & Jeka, J.J. (2002). Multisensory fusion: simultaneous re-weighting of vision and touch for the control of human posture. *Cogn. Brain Res., 14*(1), 164-176.

Okada, J., & Toh, Y. (2006). Active tactile sensing for localization of objects by the cockroach antenna. *J. Comp. Physiol. A, 192*(7), 715-726.

Palacin, J., Valganon, I., & Pernia, R. (2006). The optical mouse for indoor mobile robot odometry measurement. *Sens. Actuator A-Phys., 126*(1), 141-147.

Parsons, M.M., Krapp, H.G., & Laughlin, S.B. (2006). A motion-sensitive neurone responds to signals from the two visual systems of the blowfly, the compound eyes and ocelli. *J. Exp. Biol., 209*(22), 4464-4474.

Paulk, A.C., Stacey, J.A., Pearson, T.W., Taylor, G.J., Moore, R.J., Srinivasan, M.V., & van Swinderen, B. (2014). Selective attention in the honeybee optic lobes precedes behavioral choices. *Proc. Natl. Acad. Sci. U.S.A., 111*(13), 5006-5011.

Payne, M., Hedwig, B., & Webb, B. (2010). Multimodal predictive control in crickets. In S. Doncieux, B. Girard, A. Guillot, J. Hallam, J.-A. Meyer & J.-B. Mouret (Eds.), *From animals to animats 11*. Berlin: Springer-Verlag.

Poggio, T., & Reichardt, W. (1973). A theory of the pattern induced flight orientation of the fly *Musca domestica*. *Kybernetik, 12*(4), 185-203.

Pollack, G.S., & Plourde, N. (1982). Directionality of acoustic orientation in flying crickets. *J. Comp. Physiol. A, 146*(2), 207-215.

Portelli, G., Ruffier, F., Roubieu, F.L., & Franceschini, N. (2011). Honeybees' speed depends on dorsal as well as lateral, ventral and frontal optic flows. *PloS one, 6*(5), e19486.

Preiss, R., & Kramer, E. (1984). The interaction of edge-fixation and negative phototaxis in the orientation of walking gypsy moths, *Lymantria dispar*. *J. Comp. Physiol. A, 154*(4), 493-498.

Price, P.W. (1997). *Insect ecology*. Hoboken: John Wiley & Sons, Inc.

Pringle, J.W.S. (1948). The gyroscopic mechanism of the halteres of Diptera. *Phil. Trans. R. Soc. B, 233*(602), 347-384.

Reichardt, W. (1969). Movement perception in insects. In W. Reichardt (Ed.), *Processing of optical data by organisms and machines*. New York: Academic Press.

Reichardt, W. (1973). Musterinduzierte Flugorientierung der Fliege *Musca domestica*. *Naturwissenschaften, 60*(3), 122-138.

Reichardt, W., Egelhaaf, M., & Guo, A. (1989). Processing of figure and background motion in the visual system of the fly. *Biol. Cybern., 61*(5), 327-345.

Reichardt, W., & Poggio, T. (1976). Visual control of orientation behaviour in the fly: Part I. A quantitative analysis. *Q. Rev. Biol., 9*(3), 311-375.

Reinhard, J., Srinivasan, M.V., Guez, D., & Zhang, S.W. (2004). Floral scents induce recall of navigational and visual memories in honeybees. *J. Exp. Biol., 207*(25), 4371-4381.

Reiser, M.B., & Dickinson, M.H. (2013). Visual motion speed determines a behavioral switch from forward flight to expansion avoidance in *Drosophila*. *J. Exp. Biol., 216*(4), 719-732.

Ritzmann, R.E., & Büschges, A. (2007). Adaptive motor behavior in insects. *Curr. Opin. Neurobiol., 17*(6), 629-636.

Ritzmann, R.E., Ridgel, A.L., & Pollack, A.J. (2008). Multi-unit recording of antennal mechano-sensitive units in the central complex of the cockroach, *Blaberus discoidalis*. *J. Comp. Physiol. A, 194*(4), 341-360.

Robert, D., & Göpfert, M.C. (2002). Novel schemes for hearing and orientation in insects. *Curr. Opin. Neurobiol., 12*(6), 715-720.

Robie, A.A., Straw, A.D., & Dickinson, M.H. (2010). Object preference by walking fruit flies, *Drosophila melanogaster*, is mediated by vision and graviperception. *J. Exp. Biol., 213*(14), 2494-2506.

Rohrseitz, K., & Tautz, J. (1999). Honey bee dance communication: waggle run direction coded in antennal contacts? *J. Comp. Physiol. A, 184*(4), 463-470.

Roth, E., Reiser, M.B., Dickinson, M.H., & Cowan, N.J. (2012). *A task-level model for optomotor yaw regulation in Drosophila melanogaster: a frequency-domain system identification approach.* Paper presented at the Proc. 51st Ann. Conf. Proc. Deci. Cont.

Roth, E., Sponberg, S., & Cowan, N. (2014). A comparative approach to closed-loop computation. *Curr. Opin. Neurobiol., 25*, 54-62.

Rowell, C. (1988). Mechanisms of flight steering in locusts. *Cell. Mol. Life Sci., 44*(5), 389-395.

Rowell, C.H.F., & Reichert, H. (1986). Three descending interneurons reporting deviation from course in the locust. *J. Comp. Physiol. A, 158*(6), 775-794.

Ruffier, F., & Franceschini, N. (2005). Optic flow regulation: the key to aircraft automatic guidance. *Robot. Auton. Syst., 50*(4), 177-194.

Ruxton, G.D., & Beauchamp, G. (2008). Time for some a priori thinking about post hoc testing. *Behav. Ecol., 19*(3), 690-693.

Sandeman, D.C., & Markl, H. (1980). Head movements in flies (*Calliphora*) produced by deflexion of the halteres. *J. Exp. Biol., 85*(1), 43-60.

Sane, S.P., Dieudonne, A., Willis, M.A., & Daniel, T.L. (2007). Antennal mechanosensors mediate flight control in moths. *Science, 315*(5813), 863-866.

Sareen, P., Wolf, R., & Heisenberg, M. (2011). Attracting the attention of a fly. *Proc. Natl. Acad. Sci. U.S.A., 108*(17), 7230-7235.

Schmitz, J. (1993). Load-compensating reactions in the proximal leg joints of stick insects during standing and walking. *J. Exp. Biol., 183*(1), 15-33.

Schneider, P., & Hermes, M. (1976). Die Bedeutung der Elytren bei Vertretern des *Melolontha*-Flugtyps (Coleoptera). *J. Comp. Physiol. A, 106*(1), 39-49.

Schone, H. (1996). Optokinetic speed control and estimation of travel distance in walking honeybees. *J. Comp. Physiol. A, 179*(4), 587-592.

Schuster, S., Strauss, R., & Gotz, K.G. (2002). Virtual-reality techniques resolve the visual cues used by fruit flies to evaluate object distances. *Curr. Biol., 12*(18), 1591-1594.

Schütz, C., & Dürr, V. (2011). Active tactile exploration for adaptive locomotion in the stick insect. *Phil. Trans. R. Soc. B, 366*(1581), 2996-3005.

Schwyn, D.A., Heras, F.J., Bolliger, G., Parsons, M.M., Krapp, H.G., & Tanaka, R.J. (2011). *Interplay between feedback and feedforward control in fly gaze stabilization.* Paper presented at the Proc. 18th Int. Fed. Aut. Con. Wor. Cong., Milano.

Seelig, J., Chiappe, M., Lott, G., Dutta, A., Osborne, J., Reiser, M., & Jayaraman, V. (2010). Two-photon calcium imaging from head-fixed *Drosophila* during optomotor walking behavior. *Nat. Meth., 7*(7), 535–540.

Seelig, J.D., & Jayaraman, V. (2013). Feature detection and orientation tuning in the *Drosophila* central complex. *Nature*, Advance online publication. doi: 10.1038/nature12601

Sherman, A., & Dickinson, M. (2003). A comparison of visual and haltere-mediated equilibrium reflexes in the fruit fly *Drosophila melanogaster*. *J. Exp. Biol., 206*(2), 295-302.
Sherman, A., & Dickinson, M.H. (2004). Summation of visual and mechanosensory feedback in *Drosophila* flight control. *J. Exp. Biol., 207*(1), 133-142.
Spence, A.J., Revzen, S., Seipel, J., Mullens, C., & Full, R.J. (2010). Insects running on elastic surfaces. *J. Exp. Biol., 213*(11), 1907-1920.
Sperry, R.W. (1950). Neural basis of the spontaneous optokinetic response produced by visual inversion. *J. Comp. Physiol. Psychol., 43*(6), 482-489.
Sprayberry, J.D.H., & Daniel, T.L. (2007). Flower tracking in hawkmoths: behavior and energetics. *J. Exp. Biol., 210*(1), 37-45.
Srinivasan, M.V. (2009). Honey bees as a model for vision, perception, and cognition. *Ann. Rev. Entom., 55*, 267-284.
Srinivasan, M.V. (2011). Honeybees as a model for the study of visually guided flight, navigation, and biologically inspired robotics. *Physiol. Rev., 91*(2), 413-460.
Srinivasan, M.V., & Bernard, G.D. (1975). The effect of motion on visual acuity of the compound eye: a theoretical analysis. *Vision Res., 15*(4), 515-525.
Srinivasan, M.V., & Bernard, G.D. (1977). Fly can discriminate movement at signal-noise ratios as low as 1/8. *Vision Res., 17*(5), 609-616.
Srinivasan, M.V., & Lehrer, M. (1984). Temporal acuity of honeybee vision: behavioural studies using moving stimuli. *J. Comp. Physiol. A, 155*(3), 297-312.
Srinivasan, M.V., Lehrer, M., Kirchner, W.H., & Zhang, S.W. (1991). Range perception through apparent image speed in freely flying honeybees. *Visual Neurosci., 6*(5), 519-535.
Srinivasan, M.V., Thurrowgood, S., & Soccol, D. (2010). From visual guidance in flying insects to autonomous aerial vehicles. In D. Floreano, J.-C. Zufferey, M. V. Srinivasan & C. Ellington (Eds.), *Flying Insects and Robots*. Berlin: Springer-Verlag.
Srinivasan, M.V., Zhang, S.W., Chahl, J.S., Barth, E., & Venkatesh, S. (2000). How honeybees make grazing landings on flat surfaces. *Biol. Cybern., 83*(3), 171-183.
Srinivasan, M.V., Zhang, S.W., & Chandrashekara, K. (1993). Evidence for two distinct movement-detecting mechanisms in insect vision. *Naturwissenschaften, 80*(1), 38-41.
Srinivasan, M.V., Zhang, S.W., Lehrer, M., & Collett, T.S. (1996). Honeybee navigation en route to the goal: Visual flight control and odometry. *J. Exp. Biol., 199*(1), 237-244.
Srygley, R.B., & Dudley, R. (2008). Optimal strategies for insects migrating in the flight boundary layer: mechanisms and consequences. *Integr. Comp. Biol., 48*(1), 119-133.
Stange, G., & Howard, J. (1979). An ocellar dorsal light response in a dragonfly. *J. Exp. Biol., 83*(1), 351-355.
Steck, K., Hansson, B.S., & Knaden, M. (2011). Desert ants benefit from combining visual and olfactory landmarks. *J. Exp. Biol., 214*(8), 1307-1312.
Strausfeld, N., & Seyan, H. (1985). Convergence of visual, haltere, and prosternai inputs at neck motor neurons of *Calliphora erythrocephala*. *Cell Tissue Res, 240*(3), 601-615.
Strausfeld, N.J. (1999). A brain region in insects that supervises walking. *Prog. Brain Res., 123*, 273-284.
Strauss, R., Schuster, S., & Götz, K.G. (1997). Processing of artificial visual feedback in the walking fruit fly *Drosophila melanogaster*. *J. Exp. Biol, 200*(9), 1281-1296.
Straw, A., Lee, S., & Dickinson, M. (2010). Visual control of altitude in flying *Drosophila*. *Curr. Biol., 20*(17), 1550–1556.
Straw, A.D. (2008). Vision egg: an open-source library for realtime visual stimulus generation. *Front. Neuroinform., 2*(4).

Sun, M., Wang, J., & Xiong, Y. (2007). Dynamic flight stability of hovering insects. *Acta Mech. Sinica, 23*(3), 231-246.

Sun, M., & Wu, J.H. (2003). Aerodynamic force generation and power requirements in forward flight in a fruit fly with modeled wing motion. *J. Exp. Biol., 206*(17), 3065-3083.

Sun, M., & Xiong, Y. (2005). Dynamic flight stability of a hovering bumblebee. *J. Exp. Biol., 208*(3), 447-459.

Takalo, J., Piironen, A., Honkanen, A., Lempea, M., Aikio, M., Tuukkanen, T., & Vahasoyrinki, M. (2012). A fast and flexible panoramic virtual reality system for behavioural and electrophysiological experiments. *Sci. Rep., 2*, 324.

Tammero, L.F., & Dickinson, M.H. (2002). Collision-avoidance and landing responses are mediated by separate pathways in the fruit fly, *Drosophila melanogaster*. *J. Exp. Biol., 205*(18), 2785-2798.

Tanaka, K., & Kawachi, K. (2006). Response characteristics of visual altitude control system in *Bombus terrestris*. *J. Exp. Biol., 209*(22), 4533-4545.

Tautz, J. (2008). *The buzz about bees: biology of a superorganism*. Berlin: Springer-Verlag.

Taylor, C.P. (1981). Contribution of compound eyes and ocelli to steering of locusts in flight: I. Behavioural analysis. *J. Exp. Biol., 93*(1), 1-18.

Taylor, G.K., Bacic, M., Bomphrey, R.J., Carruthers, A.C., Gillies, J., Walker, S.M., & Thomas, A.L.R. (2008). New experimental approaches to the biology of flight control systems. *J. Exp. Biol, 211*(2), 258-266.

Taylor, G.K., & Krapp, H.G. (2007). Sensory systems and flight stability: What do insects measure and why? *Adv. Insect Physiol., 34*, 231-316.

Taylor, G.K., & Thomas, A.L.R. (2002). Animal flight dynamics. II. Longitudinal stability in flapping flight. *J. Theor. Biol., 214*(3), 351-370.

Theobald, J.C., Greiner, B., Wcislo, W.T., & Warrant, E.J. (2006). Visual summation in night-flying sweat bees: a theoretical study. *Vision Res., 46*(14), 2298-2309.

Theobald, J.C., Ringach, D.L., & Frye, M.A. (2010). Dynamics of optomotor responses in Drosophila to perturbations in optic flow. *J. Exp. Biol., 213*(8), 1366-1375.

Trischler, C., Kern, R., & Egelhaaf, M. (2010). Chasing behavior and optomotor following in free-flying male blowflies: flight performance and interactions of the underlying control systems. *Front. Behav. Neurosci., 4*(20).

Tunwattana, N., Roskilly, A., & Norman, R. (2009). Investigations into the effects of illumination and acceleration on optical mouse sensors as contact-free 2D measurement devices. *Sens. Actuat. A, 149*(1), 87-92.

van Breugel, F., & Dickinson, M.H. (2012). The visual control of landing and obstacle avoidance in the fruit fly *Drosophila melanogaster*. *J. Exp. Biol., 215*(11), 1783-1798.

van Praagh, J.P., Ribi, W., Wehrhahn, C., & Wittmann, D. (1980). Drone bees fixate the queen with the dorsal frontal part of their compound eyes. *J. Comp. Physiol. A, 136*(3), 263-266.

van Swinderen, B. (2007). Attention-like processes in *Drosophila* require short-term memory genes. *Science, 315*(5818), 1590-1593.

van Truong, T., Le, T.Q., Byun, D., Park, H.C., & Kim, M. (2012). Flexible wing kinematics of a free-flying beetle (Rhinoceros beetle *Trypoxylus dichotomus*). *J. Bionic Eng., 9*(2), 177-184.

Vance, J., Faruque, I., & Humbert, J. (2013). Kinematic strategies for mitigating gust perturbations in insects. *Bioinspir. Biomim., 8*(1), 016004.

Varjú, D. (1975). Stationary and dynamic responses during visual edge fixation by walking insects. *Nature, 255*(5506), 330-332.

Vergoz, V., Roussel, E., Sandoz, J.C., & Giurfa, M. (2007). Aversive learning in honeybees revealed by the olfactory conditioning of the sting extension reflex. *PloS One, 2*(3), e288.

Vickers, N.J. (2000). Mechanisms of animal navigation in odor plumes. *Biol. Bull., 198*(2), 203-212.

Viollet, S., & Zeil, J. (2013). Feed-forward and visual feedback control of head roll orientation in wasps (*Polistes humilis*, Vespidae, Hymenoptera). *J. Exp. Biol., 216*(7), 1280-1291.

Vogel, S. (1966). Flight in *Drosophila.* I. Flight performance of tethered flies. *J. Exp. Biol., 44*(3), 567-578.

Vogel, S. (1994). *Life in moving fluids: the physical biology of flow*. Princeton: Princeton University Press.

von Helversen, D., & Wendler, G. (2000). Coupling of visual to auditory cues during phonotactic approach in the phaneropterine bushcricket *Poecilimon affinis*. *J. Comp. Physiol. A, 186*(7-8), 729-736.

von Holst, E., & Mittelstaedt, H. (1950). Das Reafferenzprinzip. *Naturwissenschaften, 37*(20), 464-476.

Voss, R., & Zeil, J. (1998). Active vision in insects: an analysis of object-directed zig-zag flights in wasps (*Odynerus spinipes*, Eumenidae). *j. Comp. Physiol. A, 182*(3), 377-387.

Wagner, H. (1986). Flight performance and visual control of flight of the free-flying housefly (*Musca domestica* L.) II. Pursuit of targets. *Phil. Trans. R. Soc. B, 312*(1158), 553-579.

Wakeling, J.M., & Ellington, C.P. (1997a). Dragonfly flight. I. Gliding flight and steady-state aerodynamic forces. *J. Exp. Biol., 200*(3), 543-556.

Wakeling, J.M., & Ellington, C.P. (1997b). Dragonfly flight. II. Velocities, accelerations and kinematics of flapping flight. *J. Exp. Biol., 200*(3), 557-582.

Wallace, G. (1959). Visual scanning in the desert locust *Schistocerca gregaria*, Forskal. *J. Exp. Biol, 36*, 512-525.

Warrant, E.J. (1999). Seeing better at night: life style, eye design and the optimum strategy of spatial and temporal summation. *Vision Res., 39*(9), 1611-1630.

Warzecha, A.K., & Egelhaaf, M. (2000). Response latency of a motion-sensitive neuron in the fly visual system: dependence on stimulus parameters and physiological conditions. *Vision Res., 40*(21), 2973–2983.

Wasserman, S., Lu, P., Aptekar, J.W., & Frye, M.A. (2012). Flies dynamically anti-track, rather than ballistically escape, aversive odor during flight. *J. Exp. Biol., 215*(16), 2833-2840.

Webb, B. (2004). Neural mechanisms for prediction: do insects have forward models? *Trends Neurosci., 27*(5), 278-282.

Webb, B., Harrison, R.R., & Willis, M.A. (2004). Sensorimotor control of navigation in arthropod and artificial systems. *Arth. Struct. & Dev., 33*(3), 301-329.

Webb, B., & Reeve, R. (2003). Reafferent or redundant: Integration of phonotaxis and optomotor behavior in crickets and robots. *Adapt. Behav., 11*(3), 137-158.

Weber, T., Thorson, J., & Huber, F. (1981). Auditory-behavior of the cricket 1. Dynamics of compensated walking and discrimination paradigms on the kramer treadmill. *J. Comp. Physiol., 141*(2), 215-232.

Wehner, R. (1981). *Spatial vision in arthropods*. Berlin: Springer-Verlag.

Wehner, R. (1987). 'Matched filters'—neural models of the external world. *J. Comp. Physiol. A, 161*(4), 511-531.

Wehner, R., Michel, B., & Antonsen, P. (1996). Visual navigation in insects: Coupling of egocentric and geocentric information. *J. Exp. Biol., 199*(1), 129-140.

Wehrhahn, C., Poggio, T., & Bülthoff, H. (1982). Tracking and chasing in houseflies (*Musca*). *Biol. Cybern., 45*(2), 123-130.

Wehrhahn, C., & Reichardt, W. (1975). Visually induced height orientation of the fly *Musca domestica*. *Biol. Cybern., 20*(1), 37-50.

Weir, P.T., Schnell, B., & Dickinson, M.H. (2014). Central complex neurons exhibit behaviorally gated responses to visual motion in *Drosophila*. *J. Neurophysiol., 111*(1), 62-71.

Weis-Fogh, T. (1949). An aerodynamic sense organ stimulating and regulating flight in locusts. *Nature, 164*(4177), 873-874.

Weis-Fogh, T. (1956). Biology and physics of locust flight. II. Flight performance of the desert locust (*Schistocerca gregaria*). *Phil. Trans. R. Soc. B, 239*(667), 459-510.

Weis-Fogh, T. (1972). Energetics of hovering flight in hummingbirds and in *Drosophila*. *J. Exp. Biol., 56*(1), 79-104.

Westergaard, M. (2002). *Supporting Multiple Pointing Devices in Microsoft Windows*. Paper presented at the Proc. Microsoft Sum. Work.

Westwick, D.T., & Kearney, R.E. (2003). *Identification of Nonlinear Physiological Systems*. Hoboken: John Wiley & Sons, Inc.

Wijngaard, W. (2010). *Accuracy of insect position control as revealed by hovering male Eristalis nemorum.* Paper presented at the Proc. 20th Neth. Ent. Soc. Meet.

Willis, M.A., Ford, E., & Avondet, J. (2013). Odor tracking flight of male *Manduca sexta* moths along plumes of different cross-sectional area. *J. Comp. Physiol. A, 199*(11), 1015-1036.

Willmott, A.P., & Ellington, C.P. (1997a). The mechanics of flight in the hawkmoth *Manduca sexta*. I. Kinematics of hovering and forward flight. *J. Exp. Biol., 200*(21), 2705-2722.

Willmott, A.P., & Ellington, C.P. (1997b). The mechanics of flight in the hawkmoth *Manduca sexta*. II. Aerodynamic consequences of kinematic and morphological variation. *J. Exp. Biol., 200*(21), 2723-2745.

Wittlinger, M., Wehner, R., & Wolf, H. (2007). The desert ant odometer: A stride integrator that accounts for stride length and walking speed. *J. Exp. Biol., 210*(2), 198-207.

Wolf, H., & Wehner, R. (2005). Desert ants compensate for navigation uncertainty. *J. Exp. Biol., 208*(22), 4223-4230.

Wolf, R., & Heisenberg, M. (1990). Visual control of straight flight in *Drosophila-melanogaster*. *J. Comp. Physiol. A, 167*(2), 269-283.

Wolf, R., & Heisenberg, M. (1991). Basic organization of operant behaviour as revealed in *Drosophila* flight orientation. *J. Comp. Physiol. A, 169*(6), 699-705.

Wolf, R., Voss, A., Hein, S., & Heisenberg, M. (1992). Can a fly ride a bicycle? *Phil. Trans. R. Soc. B, 337*(1281), 261-269.

Wolpert, D.M., Ghahramani, Z., & Jordan, M.I. (1995). An internal model for sensorimotor integration. *Science, 269*(5232), 1880-1882.

Wolpert, D.M., & Kawato, M. (1998). Multiple paired forward and inverse models for motor control. *Neural Networks, 11*(7), 1317-1329.

Wu, J., & Sun, M. (2005). Unsteady aerodynamic forces and power requirements of a bumblebee in forward flight. *Acta Mechanica Sinica, 21*(3), 207-217.

Xu, K.-J., & Li, C. (2000). Dynamic decoupling and compensating methods of multi-axis force sensors. *IEEE Trans. Instrum. Meas., 49*(5), 935-941.

Zanker, J.M. (1988a). How does lateral abdomen deflection contribute to flight control in *Drosophila-melanogaster*. *J. Comp. Physiol. A, 162*(5), 581-588.

Zanker, J.M. (1988b). On the mechanism of speed and altitude control in *Drosophila-melanogaster*. *Physiol. Ent., 13*(3), 351-361.

Zanker, J.M., & Collett, T.S. (1985). The optomotor system on the ground: on the absence of visual control of speed in walking ladybirds. *J. Comp. Physiol. A, 156*(3), 395-402.

Zhang, S., Si, A., & Pahl, M. (2012). Visually guided decision making in foraging honeybees. *Front. Neurosci., 6*(88).
Zhang, S., Wang, X., Liu, Z., & Srinivasan, M. (1990). Visual tracking of moving targets by freely flying honeybees. *Visual Neurosci., 4*(4), 379-386.
Zhou, Y., Ji, X., Gong, H., Gong, Z., & Liu, L. (2012). Edge detection depends on achromatic channel in *Drosophila melanogaster*. *J. Exp. Biol., 215*(19), 3478-3487.
Zill, S., Schmitz, J., & Büschges, A. (2004). Load sensing and control of posture and locomotion. *Arth. Struct. & Dev., 33*(3), 273-286.
Zollikofer, C. (1994). Stepping patterns in ants - Influence of speed and curvature. *J. Exp. Biol., 192*(1), 95-106.
Zolotov, V., Frantsevich, L., & Falk, E. (1975). Kinematik der phototaktischen Drehung bei der Honigbiene *Apis mellifera* L. *J. Comp. Physiol., 97*(4), 339-353.
Zufferey, J.-C., & Floreano, D. (2006). Fly-inspired visual steering of an ultralight indoor aircraft. *IEEE Trans. Robot., 22*(1), 137-146.

Appendix A **Supplementary material for Chapter 2**

A.1 The influence of stimulus presentation order

Initial experiments showed that honeybees exhibited a hysteresis-like effect when exposed to different air speeds. Qualitatively, it appeared that when the bees were initially exposed to a high air speed, they were reluctant to fly when the air flow was reduced or removed. This effect was observed to occur regardless of whether the lower air speed was presented to a bee during the same flight trial as the higher air speed, or during a later trial. To test this apparent effect of presentation order, or hysteresis, we presented bees with air speed in a stepped triangle function of increasing and then decreasing air speeds, at several optic flows. Whilst no dependence of the response to optic flow on presentation order had been observed, we also tested separate bees with a similar function of increasing then decreasing optic flows, at several air speeds.

A.1.1 Air speed

Honeybees were exposed to a stimulus pattern of progressively increasing series of air speeds, from 0 to 5 $m.s^{-1}$ (in 1 $m.s^{-1}$ increments of 10 s duration), followed by a decreasing series of air speeds that mirrored the initial increase. Honeybees were tested at optic flow levels that would elicit low, intermediate and strong streamlining responses, these being 100, 300, and 500 $^{o}.s^{-1}$. This was similar to the standard protocol of presenting a progressively increasing series of optic flow levels, except here optic flow was held constant during the flight whilst air speed was systematically varied. Bees were exposed to all optic flow levels twice in random order, and their responses averaged.

When exposed to this triangular function of air speed levels, bees typically maintained their abdomens at a higher level during the decreasing portion of the response function, regardless of optic flow level (Figure A-1). The sole exception is at the end of the ramp when there is no wind, or at 3 $m.s^{-1}$ air speed, at which point honeybees dropped their abdomens to lower positions than at the beginning. Generally, this phenomenon appears to approximate a classic hysteresis function. The effects of optic flow ($F_{2,18}$=5.46, ***p*=0.014**), air speed ($F_{1.8,15.8}$=64.41, ***p*<0.001**) and their interaction ($F_{2.4,21.4}$=5.81, ***p*=0.007**) in these trials were significant, and

agreed with other results. The effect of air speed presentation order was not itself significant as a main effect ($F_{1,9}$=0.76, p=0.407), but showed a significant interaction with air speed ($F_{1.6,14.4}$=11.44, ***p*=0.002**), and also a three factor interaction with air speed and optic flow ($F_{2.0,17.7}$=5.41, ***p*=0.015**). Thus, it appears the order in which a tethered bee experienced air speeds modified its response to the following air speeds, and further how this response interacts with the response to optic flow.

It is unclear what causes presentation order to affect the observed abdomen pitch in this manner. The response itself does not display hysteresis when bees are exposed to a triangular function of optic flow (see the following section), and a similar effect was initially observed when air speed was changed between trials, suggesting that the response does not arise from short term habituation of the mechanoreceptors. We speculate that tethered bees rapidly become accustomed to higher air speeds in the flight arena, and are reluctant to assume a posture associated with low flight speed. They may even modulate their flight forces during the decreasing section of the triangular function, in an attempt to accelerate to faster flight speeds. Regardless of the cause, such hysteresis may be a consideration in the design of experiments investigating flight control of insects in response to varying air speeds and understanding the underlying mechanosensory cues.

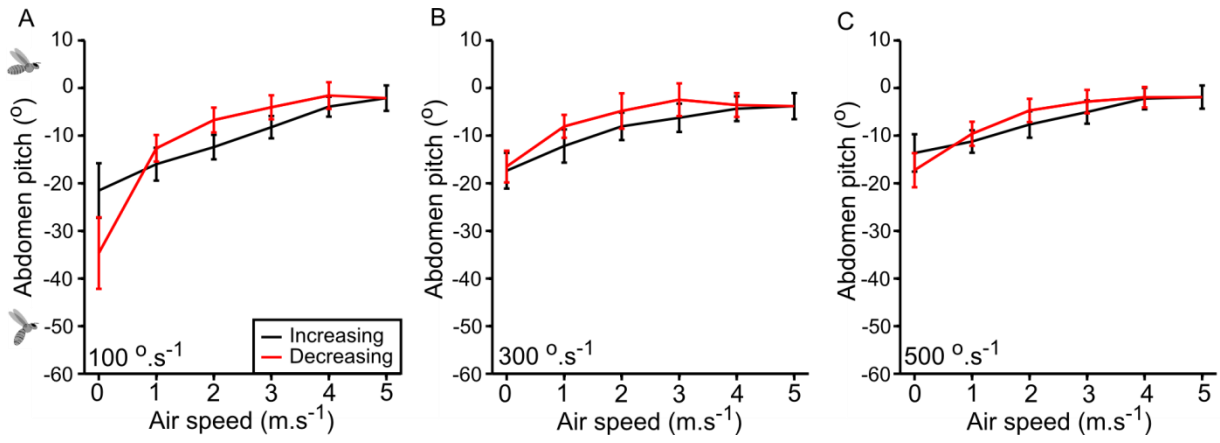

Figure A-1: Air speed presentation order affects the streamlining response. Response to a triangular air speed function at various optic flow levels: **A**, 100 °.s^{-1}; **B**, 300 °.s^{-1}, and **C**, 500 °.s^{-1}. Presentation order is indicated as increasing (black line), followed by decreasing (red line) air speed. 10 bees participated in all conditions. Error bars show ± S.E.M.

A.1.2 Optic flow

Honeybees were exposed to a standard stimulus of progressively increasing optic flows, going from 100 to 600 ^{o}.s^{-1} (in 100 ^{o}.s^{-1} increments of 10 s duration), followed by a decreasing series of optic flows that mirrored the initial increase. As air speed presentation order was already suspected to affect the response, separate bees were tested without air flow and with airflow at intermediate and high speeds with respect to their effect on the streamlining response (Figure A-2). These air speeds were 0, 1.5, and 3 m.s^{-1} respectively.

Whilst there is some variation of the response with the increasing and decreasing side of the triangular optic flow function, this variation appears to be inconsistent and varies qualitatively between air speeds. Again, optic flow ($F_{1.8,40.8}$=22.81, ***p*<0.001**) and air speed ($F_{2,32}$=8.79, ***p*=0.001**) show a significant effect on abdomen position, and these are the only significant effects detected (Section A.4.10). The presentation order of optic flow has no significant effect on streamlining *per se* ($F_{1,32}$=0.10, p=0.750), nor does it show any significant interaction with other parameters. Thus, we conclude that the order of presentation of optic flow does not need to be controlled when designing experiments to examine its effects.

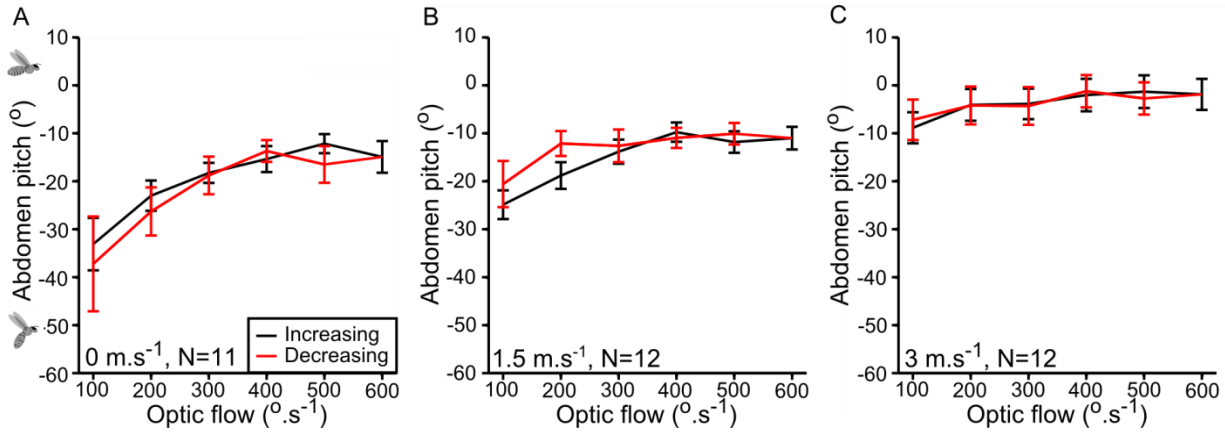

Figure A-2: Optic flow presentation order does not affect the streamlining response. Response to a triangular optic flow function at various air speed levels: **A**, 0 m.s^{-1}; **B**, 1.5 m.s^{-1}, and **C**, 3 m.s^{-1}. Presentation order is indicated as increasing (black line), followed by decreasing (red line) optic flow. The number of bees tested for each air speed is indicated in the bottom right corner of each plot. Error bars show ± S.E.M.

A.2 Models of interaction between air speed and optic flow (Figure 2-7)

A.2.1 Details of models

All of the saturating functions are characterized by a 4 parameter variable slope sigmoidal function, represented by the equation:

$$Y(x) = p(1) + \frac{p(2)}{1 + e^{(p(3)-x)\times p(4)}} \quad \text{(A-42)}$$

In Eq. (A-42), x represents input and $Y(x)$ represents the output at a particular value of x. $p(1)$ represents the minimum value of the function (or vertical offset), $p(2)$ the response range of the function, $p(3)$ the x value where the function is halfway between its minimum and maximum values (or, equivalently, the horizontal offset), and $p(4)$ a measure of the slope of the curve at this point.

The best-fitting values of these parameters for the first four models were found using the least squares fitting tool 'nlinfit' in Matlab R2009b. The parameters of the non-linear combination model were found using a genetic algorithm optimisation approach, the function 'nsga2' (Lin, 2011), where an artificial population size of 100 was used for 100 generations to optimise the 10 free variables using a least squares fit. The range of the parameters were not constrained in either fitting algorithm.

The values of these parameters for each of the saturating functions are given below:

Figure 2-7B. Optic flow saturation function (the minimum of this function, $p(1)$, was constrained to -90°),

$$\text{Sat.}_{\text{OF}} : AbP(OF) = -90 + \frac{66.9}{1 + e^{(74.3-OF)\times 0.01}} \quad \text{(A-43)}$$

Figure 2-7B. Air speed saturation function (the minimum of this function, $p(1)$, was constrained to -90°),

$$\text{Sat.}_{\text{AS}} : AbP(AS) = -90 + \frac{90.1}{1 + e^{(0.34-AS)\times 0.7}} \quad \text{(A-44)}$$

Figure 2-7C. Abdomen pitch as a linear summation of the saturating response to optic flow and air speed, $AbP(OF,AS) = \text{Sat.}_{\text{OF}} + \text{Sat.}_{\text{AS}} + 90$,

$$AbP(OF,AS) = -90 + \frac{66.9}{1 + e^{(74.3-OF)\times 0.01}} + \frac{90.1}{1 + e^{(0.34-AS)\times 0.7}} \quad \text{(A-45)}$$

Figure 2-7D. Abdomen pitch as a weighted linear summation of the saturating response to optic flow and air speed, $AbP(OF,AS) = \mathrm{G}_1 \times \mathrm{Sat.}_{\mathrm{OF}} + \mathrm{G}_2 \times \mathrm{Sat.}_{\mathrm{AS}} + 90$ (where G_1 = 0.45 and G_2 = 0.74),

$$AbP(OF,AS) = -90 + \frac{30.1}{1+e^{(74.3-OF)\times 0.01}} + \frac{66.7}{1+e^{(0.34-AS)\times 0.7}} \quad \text{(A-46)}$$

Figure 2-7E. Abdomen pitch as a non-linear combination of saturating responses to optic flow and air speed, $AbP(OF,AS) = \mathrm{Sat.}_{\mathrm{AS1}} + \mathrm{Sat.}_{\mathrm{AS2}} \times \mathrm{Sat.}_{\mathrm{OF}}$. Note that there appeared to be considerable 'play' in the optimiser's results, as the majority of variables could vary by some amount whilst still producing similar model results, indicating that the effect of various interacting variables could produce multiple similar solutions. The air speed saturation function is,

$$\mathrm{Sat.}_{\mathrm{AS1}} : -7.1 + \frac{-90.2}{1+e^{(0.8-AS)\times -1.1}} \quad \text{(A-47)}$$

The air speed saturating function that modulates optic flow gain is,

$$\mathrm{Sat.}_{\mathrm{AS2}} : 9.2 + \frac{40.8}{1+e^{(1.1-AS)\times -4.2}} \quad \text{(A-48)}$$

The optic flow saturating function is,

$$\mathrm{Sat.}_{\mathrm{OF}} : \frac{1}{1+e^{(124-AS)\times 0.01}} \quad \text{(A-49)}$$

A.2.2 Antennal manipulation comparison

The model using a non-linear combination of saturating responses was tested against the results found for the two antenna manipulation cases. As these abdomen positions for antenna manipulated bees were different from those observed in normal bees, the model would obviously have to be adjusted to fit this data. It is of interest to find if an entirely new model would be required, or if the same method of combining air speed and optic flow could be used with adjusted parameters, and if that was the case, which parameters should be adjusted.

We refit the following model parameters, whilst keeping the other parameters at the same level as found for normal bees (the data was refit for antenna amputated and pedicel waxed bees separately, $p(\ldots)$ refers to components of Eq. (A-42)):

- All parameters: ($\mathrm{Sat.}_{\mathrm{AS1}}$ – $p(1)$, $p(2)$, $p(3)$, $p(4)$; $\mathrm{Sat.}_{\mathrm{AS2}}$ – $p(1)$, $p(2)$, $p(3)$, $p(4)$; $\mathrm{Sat.}_{\mathrm{OF}}$ – $p(3)$, $p(4)$)
- Both saturating responses to air speed ($\mathrm{Sat.}_{\mathrm{AS1}}$ – $p(1)$, $p(2)$, $p(3)$, $p(4)$; $\mathrm{Sat.}_{\mathrm{AS2}}$ – $p(1)$, $p(2)$, $p(3)$, $p(4)$)

- Saturating response to optic flow ($Sat._{OF}$ –$p(3)$, $p(4)$)
- Saturating response to air speed ($Sat._{AS1}$ – $p(1)$, $p(2)$, $p(3)$, $p(4)$)
- Saturating response to air speed that modulates optic flow gain ($Sat._{AS2}$ – $p(1)$, $p(2)$, $p(3)$, $p(4)$)

The results of refitting these parameters are shown in Table A-1. Qualitative comparison between the various models and the corresponding data is performed using plots of the models' output, as shown in Figure 2-7 and Figure A-3. Similar to the model fit for data from non-manipulated bees, there appeared to be considerable 'play' in the parameters fit by the optimiser, further highlighting the interaction of variables in determining the best fit.

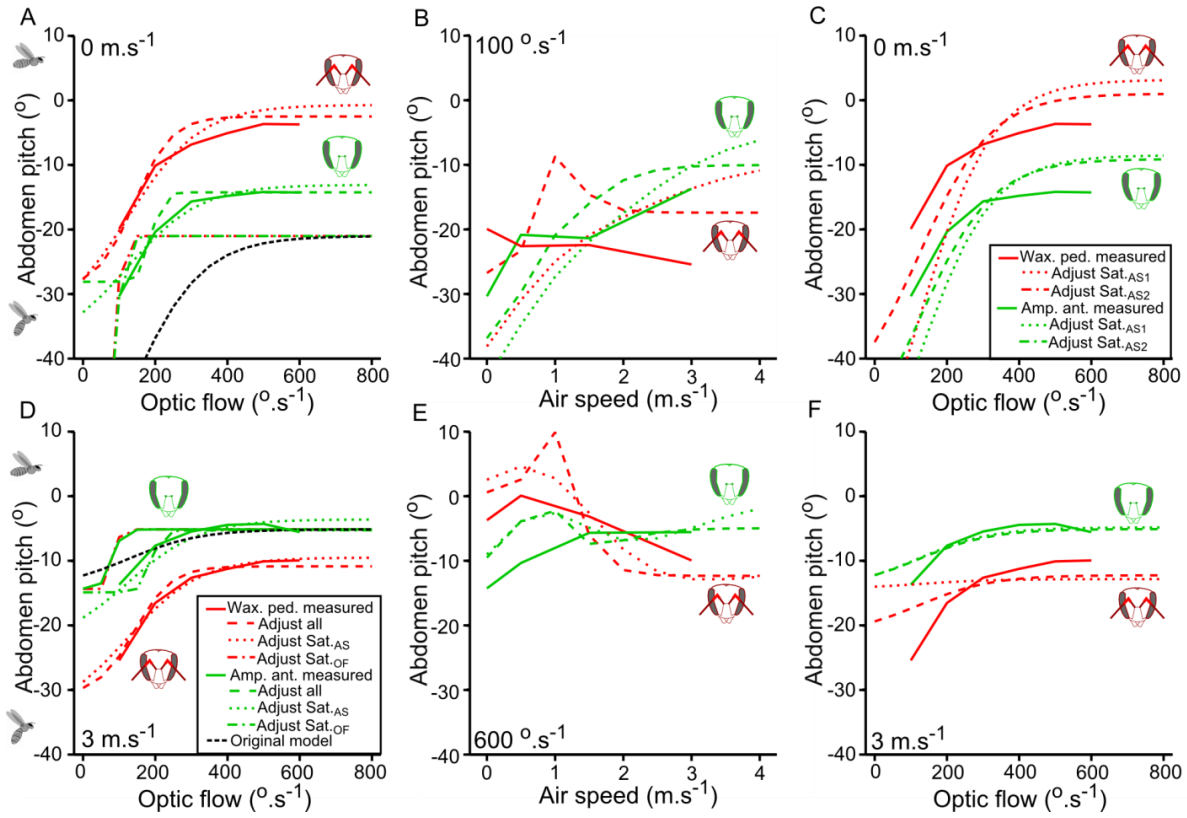

Figure A-3: Adaptability of a non-linear combination of saturating response model to antennal manipulations. A and D, comparisons of the model fits for the manipulated antennae shown in Figure 2-7 at the low and high air speed boundaries of the tested response surface (plots of the low and high optic flow boundaries are shown in Figure 2-7): **A**, response vs. air speed at 0 $m.s^{-1}$ air speed and **D**, response vs. air speed at 3 $m.s^{-1}$ air speed. B, C, E and F, comparison of other model fits (the legend in this plot is used for A and D) for manipulated antenna, at the boundaries of the measured response surface. Different combinations of parameters are refit (for each manipulation case separately) whilst some are held constant with those found for non-manipulated bees (Section A.2.2): **B**, response vs. air speed at 100 $°.s^{-1}$ optic flow; **C**, response vs. optic flow at 0 $m.s^{-1}$ air speed (the legend in this plot is used for B, C, E and F); **E**, response vs. air speed at 600 $°.s^{-1}$ optic flow and **F**, response vs. optic flow at 3 $m.s^{-1}$ air speed.

Table A-1: Comparison of model results for the various cases of antennal manipulation, and various constraints. For brevity the antennal manipulation cases are indicated in the left most column based on the following colour scheme: black, normal bees; green, antenna amputated; red, pedicel waxed. Model parameters that were fixed (at the value found for model fit for normal bees), are italicized, whereas those that were allowed to vary are shown in bold.

Model	$Sat._{AS1}$				$Sat._{AS2}$				$Sat._{OF}$	
	Vertical offset ***p*(1)**	**Vertical range** ***p*(2)**	**Horizontal offset** ***p*(3)**	**Slope** ***p*(4)**	**Vertical offset** ***p*(1)**	**Vertical range** ***p*(2)**	**Horizontal offset** ***p*(3)**	**Slope** ***p*(4)**	**Horizontal offset** ***p*(3)**	**Slope** ***p*(4)**
Original model (all points)	**-7.1**	**-90.2**	**0.8**	**-1.1**	**9.2**	**40.8**	**1.1**	**-4.2**	**124**	**0.01**
Original model (reduced set)	*-7.1*	*-90.2*	*0.8*	*-1.1*	*9.2*	*40.8*	*1.1*	*-4.2*	*124*	*0.01*
Original model	*-7.1*	*-90.2*	*0.8*	*-1.1*	*9.2*	*40.8*	*1.1*	*-4.2*	*124*	*0.01*
Original model	*-7.1*	*-90.2*	*0.8*	*-1.1*	*9.2*	*40.8*	*1.1*	*-4.2*	*124*	*0.01*
Adjust all terms	**-14.3**	**-25.3**	**0.1**	**-1.3**	**4.8**	**17.0**	**0.3**	**-0.4**	**190**	**0.07**
Adjust all terms	**-38.9**	**16.7**	**0.8**	**-0.1**	**20.0**	**6.7**	**1.8**	**-7.3**	**142**	**0.02**
Adjust $Sat._{AS}$ (both)	**-23.1**	**-21.9**	**0.45**	**-1.9**	**19.6**	**5.8**	**1.0**	-20.9	*124*	*0.01*
Adjust $Sat._{AS}$ (both)	**-30.6**	**-9.7**	**0.4**	**-0.2**	**9.2**	**26.1**	**3.3**	-1.3	*124*	*0.01*
Adjust $Sat._{OF}$	*-7.1*	*-90.2*	*0.8*	*-1.1*	*9.2*	*40.8*	*1.1*	*-4.2*	**81**	**0.07**
Adjust $Sat._{OF}$	*-7.1*	*-90.2*	*0.8*	*-1.1*	*9.2*	*40.8*	*1.1*	*-4.2*	**92**	**0.23**
Adjust $Sat._{AS1}$	**-14.1**	**-48.8**	**0.9**	**-2.6**	*9.2*	*40.8*	*1.1*	*-4.2*	*124*	*0.01*
Adjust $Sat._{AS1}$	**-21.5**	**-27.2**	**0.7**	**-8.0**	*9.2*	*40.8*	*1.1*	*-4.2*	*124*	*0.01*
Adjust $Sat._{AS2}$	*-7.1*	*-90.2*	*0.8*	*-1.1*	**7.4**	**59.4**	**1.3**	**-1.9**	*124*	*0.01*
Adjust $Sat._{AS2}$	*-7.1*	*-90.2*	*0.8*	*-1.1*	**-4.1**	**87.7**	**1.3**	**-1.5**	*124*	*0.01*

A.3 Comparison of streamlining benefits across insect orders (Figure 2-9)

Figure 2-9 is the result of a meta-analysis of the drag forces incurred during flights at a range of forward air speeds for a collection of seven insect species, across six orders. These are:

1. Hymenoptera - *Apis mellifera* (honeybee – female worker)
2. Hymenoptera - *Bombus terrestris* (bumblebee – female worker)
3. Lepidoptera - *Manduca sexta* (hawk moth – male)
4. Coleoptera - *Trypoxylus dichotomus* (rhinoceros beetle – male)
5. Odonata - *Sympetrum sanguineum* (dragon fly)
6. Diptera - *Drosophila viralis* (fruit fly)
7. Orthoptera - *Schistocherca gregaria* (locust)

For each species, data was taken from several sources (detailed in Table A-2 and Table A-3) and used to compute the drag when streamlining normally, or alternatively, and if the insect had maintained the body angle that it used when hovering across its range of flight speed. In many cases values were found from interpolating or extrapolating from published figures, and the studies from which data has been collected span seven decades, during which technological advances may have improved measurement accuracy for some variables. Hence the data in this section aims to provide a general indication that streamlining benefits flying animals, rather than to make precise comparisons between their power requirements.

Figure 2-9 uses the advance ratio of each insect species as the independent variable when plotting data from multiple species on the same plot. Whilst the insects examined here span three orders of magnitude in terms of mass, and also in terms of body Reynolds number over their flight range, their advance ratios during fast forward flight all fall within the range 0.4 to 1, making this a useful measure with which to compare flight power.

The values for the advance ratio (J), Reynolds number (Re), body drag (D^*) and parasitic power (P^*_{par}) were calculated from measured morphological and kinematic parameters (mass (m), wing (r) and body length (l), wingbeat frequency (n), wingbeat amplitude (Φ), body angle (χ),

coefficient of drag (C_d, dependent on body angle and Reynolds number) and body plan area (A)) at each flight speed (U) using the following equations (Ellington, 1984a, 1984b):

Advance ratio: $J = U/(2\phi nR)$

Reynolds number: $Re = Ul/\nu$ ν = 1.46 x 10^{-5} $m^2 \cdot s^{-1}$ (kinematic viscosity of air)

Body drag: $D^* = 0.5\rho C_d A U^2/m$ ρ = 1.23 $kg.m^{-3}$ (density of air)

Parasitic power: $P^*_{par} = D^* U$

Both parasitic power and body drag are expressed relative to the insect's body mass, m, as such they are labelled P^*_{par} and D^* respectively. The values for all parameters are shown in the following two tables, with the exception of the coefficient of drag, body plan areas, and parasitic power. Some sources provided drag measurements and not values for the coefficient of drag or body plan areas, hence we include only the value for body drag, whether calculated or taken directly from a source. The values for parasitic power are plotted in Figure 2-9.

Table A-2: Morphological details. The superscripted number denotes the source of data, and superscripted letters denote a footnote following the table. Values separate by commas are for the forewings and hindwings respectively.

Insect	Mass (mg)	Body length (mm)	Wing length (mm)
Apis	100 (Ellington, 1984a)	14.2 (Ellington, 1984a)	9.5 (Ellington, 1984a)
Bombus	175 (Dudley & Ellington, 1990a)	18.6 (Dudley & Ellington, 1990a)	13.5 (Dudley & Ellington, 1990a)
Manduca	1199 (Willmott & Ellington, 1997b)	45.6 (Willmott & Ellington, 1997b)	47.3 (Willmott & Ellington, 1997b)
Trypoxylus	5050 (McCullough, Weingarden, & Emlen, 2012)	40.0 (McCullough et al., 2012)	50.0 (McCullough et al., 2012)
Sympetrum	127 (Wakeling & Ellington, 1997a)	35.4 (Wakeling & Ellington, 1997a)	27.3, 26.5 (Wakeling & Ellington, 1997a)
Drosophila	2 (Weis-Fogh, 1972)	3.3 [r]	3.0 (Weis-Fogh, 1972)
Schistocherca	1850 (Weis-Fogh, 1956)	46.0 (Weis-Fogh, 1956)	48.5, 44.4 (Weis-Fogh, 1956)

[r] Assuming a wing to body length ratio of 1.1 as for *Drosophila melanogaster* (Ellington, 1984a)

Table A-3: Flight kinematics and power requirement details. The superscripted number denotes the source of data, and superscripted letters denote a footnote following the table. Unless followed by further superscripts, those at the lowest air speed for each species apply to the values for the following air speeds of that parameter. Drag NSL indicates the drag value was calculated assuming the insect had maintained the same body angle for hovering for all air speeds.

Insect	Air speed ($m.s^{-1}$)	Advance ratio	Reynolds number	Wingbeat freq. (Hz)	Wingbeat amp. (º)	Body angle (º)	Drag (% mass)	Drag NSL (% mass)
Apis	0	0	0	230 (Altshuler et al., 2005), h	91 (Altshuler et al., 2005), h	33 (Nachtigall et al., 1971)	0	0
	2	0.3	1775	230	91	25	3.3 (Nachtigall & Hanauer-Thieser, 1992)	6.5 (Nachtigall & Hanauer-Thieser, 1992), e
	3	0.4	2662	230	91	24	6.3	12.5 [e]
	4	0.6	3550	230	91	13	10.7	21.4 [e]
	5	0.7	4437	230	91	9	16.6	33.2 [e]
Bombus	0	0	0	155 (Dudley & Ellington, 1990a)	116 (Dudley & Ellington, 1990a)	47 (Dudley & Ellington, 1990a)	0	0
	1.5	0.1	1250	145	112	32	0.2 (Dudley & Ellington, 1990b)	0.2 (Dudley & Ellington, 1990b)
	2.5	0.3	3125	152	125	25	2.2	3.3
	3.5	0.5	4375	148	114	19	5.9	7.3
	4.5	0.7	5625	144	103	13	10.4	13.8
Manduca	0	0.0	0	26 (Willmott & Ellington, 1997a)	114 (Willmott & Ellington, 1997a)	40 (Willmott & Ellington, 1997a)	0	0
	1	0.2	4596	25	106	29	0.5 (Willmott & Ellington, 1997b)	0.6 (Willmott & Ellington, 1997b)
	2	0.4	5970	26	110	21	1.3	5.8
	3	0.7	8221	27	100	17	2.3	11.6
	4	1.0	10699	25	102	14	3.6	18.2
Trypoxylus	0	0	0	37 (van Truong, Le, Byun, Park, & Kim, 2012), h	170 (van Truong et al., 2012), h	50 (McCullough & Tobalske, 2013)	0	0
	1	0.1	2500	37	170	50	0.9 (McCullough & Tobalske, 2013), p	0.9 (McCullough & Tobalske, 2013), p
	2	0.2	5000	37	170	50	4.3	4.3
	3	0.3	7500	37	170	50	10.1	10.1
	4	0.4	10000	37	170	50	18.5	18.5

Insect	Air speed ($m.s^{-1}$)	Advance ratio	Reynolds number	Wingbeat freq. (Hz)	Wingbeat amp. (º)	Body angle (º)	Drag (% mass)	Drag N (% mass)
Sympetrum	0.7	0.2 [fw]	1536	38 (Wakeling & Ellington, 1997b), fw	80 (Wakeling & Ellington, 1997b), fw	32 (Azuma & Watanabe, 1988), da	0.4 (Wakeling & Ellington, 1997a), da, e	0.5 (Wakeling & Ellington, 1997a), da, e
	1.5	0.4	3293	38	100	13	1.6	2.8
	2.3	0.5	5049	38	120	1	2.5	9.1
	3.2	0.7	7025	38	130	2	8.6	18.1
Drosophila	0	0	0	240 (Weis-Fogh, 1972), h	150 (Weis-Fogh, 1972), h	68 (Sun & Wu, 2003)	0	0
	0.5	0.13	103	240	150	52	3.1 (Vogel, 1966)	3.6 (Vogel, 1966), e
	1	0.27	206	240	150	39	7.7	10.0 [e]
	1.5	0.4	309	240	150	22	12.8	24.2 [e]
	2	0.53	412	240	150	8	17.9	44.6 [e]
Schistocherca	0	0 [hw]	0	20 (Weis-Fogh, 1956), h, hw, t	109 (Weis-Fogh, 1956), h, hw, t	25 (Camhi, 1970a), t	0	0
	1	0.3	2813	20	109	8	0.7 (Weis-Fogh, 1956)	1.8 (Weis-Fogh, 1956)
	2	0.6	5625	20	109	3	1.2	3.5
	3	0.9	8438	20	109	1	2.7	8.4
	4	1.2	11250	20	109	0	3.9	12.7
	5	1.5	14063	20	109	0	6.5	21.1

[da] Body angles were from *Anax parthenope julius*, a larger species of dragon fly. A body angle of 35º was assumed for hovering when calculating non-streamlined body drag, slightly less horizontal than the 32º observed for 0.7 $m.s^{-1}$ flight.

[e] Value found by extrapolating beyond bounds of plot.

[fw] Value for forewings, the hindwings have a similar measurement.

[h] Value was only found for this parameter at hover, and was assumed equal to that for other flight speeds.

[hw] Value for hindwings; the value for the forewings appears un-representatively large.

[p] Data from personal communications.

[t] Measurements are from tethered animals

A.4 Statistical tests

Common abbreviations used when reporting statistical tests in this appendix are: Sum of squares (SS), degrees of freedom (df), mean squares (MS), F-value (F), *p*-value (*p*), χ^2-value (χ^2) and epsilon (test statistic for sphericity tests, ε). The subscripted number following χ^2 values denotes the degrees of freedom, and for F values, the first and second subscripted values denote the between subjects and within subjects (error) degrees of freedom respectively. If the degrees of freedom were adjusted based on Greenhouse-Geisser correction for non-spherical data in ANOVA, the unadjusted degrees of freedom are shown in brackets.

A.4.1 Figure 2-2 details (normal bees)

Two factor ANOVA was conducted with one within subjects factor (optic flow), and one between subjects factor (air speed) in SPSS using Type III sum of squares (used for all ANOVA comparisons). The number of bees included for each level of the between subjects factor were 11 (0 $m.s^{-1}$), 11 (0.5 $m.s^{-1}$), 11 (1 $m.s^{-1}$), 12 (1.5 $m.s^{-1}$), 11 (2 $m.s^{-1}$), 12 (2.5 $m.s^{-1}$), 12 (3 $m.s^{-1}$), 13 (4 $m.s^{-1}$), and 11 (5 $m.s^{-1}$). Of the 54 factor combinations, only two combinations were found to be non-normal (3 $m.s^{-1}$ at 100 $^{o}.s^{-1}$ and 0 $m.s^{-1}$ at 400 $^{o}.s^{-1}$) using a Shapiro-Wilk test. It is unlikely that these relatively minor deviations from normality will adversely influence an ANOVA's results.

The between subjects factors were found to be heteroscedastic at each of the within subjects factors levels (Table A-4). Heteroscedasticity can result in the F-statistic being non-conservative (an increase in Type 1 error), particularly in an unbalanced design where the group with the smaller number of samples has increased variance, or when the change in group means is small (Bao & Ananda, 2001; Krutchkoff, 1988). Simulation studies suggest that Type 1 error rates are unlikely to exceed 7% for normal, but heteroscedastic data (Bao & Ananda, 2001). Outside of those constraints, the F-statistic for heteroscedastic data is usually conservative (an increase in Type 2 error), however performance is improved when the number of groups are large (greater than ten; Bao & Ananda, 2001; Krutchkoff, 1988). Notably, the variance of between subjects groups in our data does not appear to be directly proportional to the group mean (for example the variance at 0.5 $m.s^{-1}$ air speed is larger than 0 and 1 $m.s^{-1}$), even though this air speed results in a reduced average

abdomen angle, whilst higher air speeds have both reduced averages and variances (Figure 2-2), so a transformation will not alleviate the issue (Krutchkoff, 1988), nor would a non-parametric test. We suggest that the effect of heteroscedasticity may make tests slightly more conservative, but will not adversely affect the conclusions we draw from our data. Note that heteroscedasticity only effects the between subjects factor (air speed), as its equivalent for the within subjects factor (optic flow) can be corrected for.

Table A-4: Leven's test of equality of variances for normal bees.

Factor ($^o.s^{-1}$)	**100**	**200**	**300**	**400**	**500**	**600**
Result	$F_{8,95}$=3.42, ***p*=0.002**	$F_{8,95}$=3.18, ***p*=0.003**	$F_{8,95}$=4.00, ***p*<0.001**	$F_{8,95}$=2.67, ***p*=0.011**	$F_{8,95}$=2.38, ***p*=0.022**	$F_{8,95}$=3.14, ***p*=0.003**

Mauchly's test of sphericity indicated that the assumption of sphericity was violated for this data, χ^2_{14}=542.5, ***p*<0.001**, and as ε=0.31, Greenhouse-Geisser correction was used to adjust degrees of freedom for the within subjects factor (Table A-5) after conducting the ANOVA. Both main effects and the interaction are highly significant. Based on Figure 2-2 it appears that the interaction effect occurs because the range of group means is reduced over the within subjects factor (optic flow) at high levels of the between subjects factor (air speed).

Table A-5: Repeated measures ANOVA results for normal bees.

Within subjects	**SS**	**df**	**MS**	**F**	***p***
Optic flow (OF)	15222.1	1.6 (5)	9819.5	141.39	**<0.001**
OF x AS	42109	12.4 (40)	399.6	4.89	**<0.001**
Error(OF)	10227.4	147.3 (475)	69.5		
Between subjects	**SS**	**df**	**MS**	**F**	***p***
Air speed (AS)	55248.4	8	6906.1	6.35	**<0.001**
Error	103359.8	95	1088.0		

Post-hoc comparisons were made between main effects by computing *p*-values for each pairwise comparison. Family wise error control is provided by using the Dunn-Sidak pairwise comparison for within subjects comparisons, and the Games-Howell comparison

(specifically for heteroscedastic data) for between subjects comparisons. Low optic flow levels are significantly different from all others up to 400 $^{o}.s^{-1}$ after which optic flow is no longer significantly different from higher levels (Table A-6). This indicates that a plateau, or saturation, of the response has been reached.

Table A-6: *Post-hoc* comparisons of optic flow levels for normal bees.

Optic flow ($^{o}.s^{-1}$)	**200**	**300**	**400**	**500**	**600**
100	***p*<0.001**	***p*<0.001**	***p*<0.001**	***p*<0.001**	**p<0.001**
200		***p*<0.001**	***p*<0.001**	***p*<0.001**	**p<0.001**
300			**p<0.001**	***p*<0.001**	***p*<0.001**
400				*p*=0.625	*p*=0.991
500					*p*=1.000

As apparent from Figure 2-2, the response to air speed is more complicated, and divides itself into four groups (Table A-7). *First***,** a plateau or saturation is again reached at 2.5 $m.s^{-1}$, after which air speed levels are no longer significantly different. *Second***,** the 0 $m.s^{-1}$ air speed is significantly different from these air speeds in the plateau region, but not from flow rates lower than 2.5 $m.s^{-1}$; 0 $m.s^{-1}$ representing the global minimum of the response. *Third*, the speed range 1 to 2 $m.s^{-1}$ represents an intermediate local minimum, which whilst not different from 0 $m.s^{-1}$ air speed and is different from the highest points on the plateau (4 and 5 $m.s^{-1}$), suggesting it represents slightly higher values than the 0 $m.s^{-1}$ minimum. *Fourth*, the 0.5 $m.s^{-1}$ air speed, as it is not significantly different from any other air speed. Figure 2-2 shows that at high optic flow the response at the 0.5 $m.s^{-1}$ air speed approaches the level the plateau, whilst at low optic flow levels the response is similar to the local minimum centred at 1.5 $m.s^{-1}$ air speed. 0.5 $m.s^{-1}$ represents a local maximum although its strength of its response is largely dependent on the interaction with optic flow.

Table A-7: *Post-hoc* comparisons of air speed levels for normal bees.

Air speed ($m.s^{-1}$)	**0.5**	**1**	**1.5**	**2**	**2.5**	**3**	**4**	**5**
0	p=0.485	p=0.614	p=0.834	p=0.102	***p*=0.019**	***p*=0.012**	***p*<0.001**	***p*=0.001**
0.5		p=0.981	p=0.977	p=1.000	p=0.999	p=0.998	p=0.781	p=0.855
1			p=1.000	p=0.864	p=0.259	p=0.180	***p*=0.001**	***p*=0.002**
1.5				p=0.907	p=0.357	p=0.283	***p*=0.012**	***p*=0.018**
2					p=0.830	p=0.736	***p*=0.011**	***p*=0.011**
2.5						p=1.000	p=0.803	p=0.899
3							p=0.808	p=0.905
4								p=1.000

A.4.2 Figure 2-2 details (antenna amputated bees)

Two factor ANOVA was conducted with one within subjects factor (optic flow), and one between subjects factor (air speed). The number of bees included for each level of the between subjects factor were 9 (0 $m.s^{-1}$), 9 (0.5 $m.s^{-1}$), 8 (1.5 $m.s^{-1}$), and 12 (3 $m.s^{-1}$). Of the 24 factor combinations none were found to be non-normal (using a Shapiro-Wilk test). However, as for the normal bees, between subjects factors were found to be heteroscedastic at most of the within subjects factors levels (Table A-8). Heteroscedasticity is not as severe as for normal bees, with five of the within subjects factor levels now displaying non-equal variances. From simulation studies (Bao & Ananda, 2001), it still seems unlikely Type 1 error will noticeably exceed 5%, although the test of effects for the between subjects factor may be reduced in power.

Table A-8: Leven's test of equality of variances for antenna amputated bees.

Factor ($^o.s^{-1}$)	**100**	**200**	**300**	**400**	**500**	**600**
Result	$F_{3,34}$=2.75, p=0.058	$F_{3,34}$=4.17, ***p*=0.013**	$F_{3,34}$=3.08, ***p*=0.041**	$F_{3,34}$=4.18, ***p*=0.013**	$F_{3,34}$=4.55, ***p*=0.009**	$F_{3,34}$=4.43, ***p*=0.010**

Mauchly's test of sphericity indicated that the assumption of sphericity was violated for this data, χ^2_{14}=196.8, ***p*<0.001**, and as ε=0.31, Greenhouse-Geisser correction was used to adjust degrees of freedom for the within subjects factor (Table A-9). The main effect of the

within subjects factor (optic flow) is highly significant, and the interaction term is not significant. The between subjects factor (air speed) remains significant, but not strongly so, although the power of the test (and thus the strength of the statistical conclusion) is likely reduced due to heteroscedasticity as discussed previously. Nonetheless, it is reasonable to conclude that air speed has less effect on these bees with their amputated antenna than their un-manipulated compatriots (Section A.4.1).

Table A-9: Repeated measures ANOVA results for antenna amputated bees.

Within subjects	**SS**	**df**	**MS**	**F**	***p***
Optic flow (OF)	4632.2	1.5 (5)	3011.3	52.04	**<0.001**
OF x AS	300.2	4.6 (15)	65.1	1.12	0.358
Error(OF)	3026.5	52.3 (170)	89.0		
Between subjects	**SS**	**df**	**MS**	**F**	***p***
Air speed (AS)	4152.1	3	1384.0	3.11	**0.039**
Error	15129.8	34	445.0		

Post-hoc comparisons are made between main effects by computing *p*-values for each pairwise comparison, using Dunn-Sidak and Games-Howell tests performed for within and between subjects comparisons respectively. The response to optic flow for antenna amputated bees plateaued (Table A-10) in a similar way to bees with normal antennas (Section A.4.1), except that the plateau level now occurs at 300 rather than 400 $^{o}.s^{-1}$. When comparing the effects of air speed (Table A-11), it now appears to follow a similar plateau or saturation response to the optic flow component. Only the 0 $m.s^{-1}$ air speed condition is significantly different from the highest air speed tested (3 $m.s^{-1}$). The local minimum at 1.5 $m.s^{-1}$ does not occur, as the response at this point is now close to the plateau, and the response at 0.5 $m.s^{-1}$ is now generally between the response for 0 and 1.5 $m.s^{-1}$ (Figure 2-2), without the obvious interaction with optic flow observed for normal bees.

Table A-10: *Post-hoc* comparisons of optic flow levels for antenna amputated bees.

Optic flow ($^o.s^{-1}$)	**200**	**300**	**400**	**500**	**600**
100	***p*<0.001**	***p* <0.001**	***p* <0.001**	***p* <0.001**	***p*<0.001**
200		***p* <0.001**	***p*<0.001**	***p*<0.001**	***p*<0.001**
300			*p*=0.919	*p*=0.863	*p*=0.989
400				*p*=0.997	*p*=1.000
500					*p*=1.000

Table A-11: *Post-hoc* comparisons of air speed levels for antenna amputated bees.

Air speed ($m.s^{-1}$)	**0.5**	**1.5**	**3**
0	*p*=0.658	*p*=0.299	***p*=0.049**
0.5		*p*=0.968	*p*=0.554
1.5			*p*=0.693

A.4.3 Figure 2-2 details (antenna waxed bees)

Two factor ANOVA was conducted with one within subjects factor (optic flow), and one between subjects factor (air speed). The number of bees included for each level of the between subjects factor were 12 (0 $m.s^{-1}$), 6 (0.5 $m.s^{-1}$), 12 (1.5 $m.s^{-1}$), and 7 (3 $m.s^{-1}$). Of the 24 factor combinations one was found to be non-normal (0 $m.s^{-1}$ at 100 $^o.s^{-1}$), using a Shapiro-Wilk test. As for previous comparisons, between subjects factors were found to be heteroscedastic at most of the within subjects factors levels (Table A-12). Heteroscedasticity is further reduced from the previous comparisons, with only four of the six within subjects factor levels now displaying non-equal variances. It still seems unlikely Type 1 error will noticeably exceed 5%, although the test of effects for the between subjects factor may be somewhat reduced in power.

Table A-12: Leven's test of equality of variances for antenna waxed bees.

Factor ($^{o}.s^{-1}$)	**100**	**200**	**300**	**400**	**500**	**600**
Result	$F_{3,33}$=0.78, p=0.512	$F_{3,33}$=2.42, p=0.084	$F_{3,33}$=4.29, ***p*=0.012**	$F_{3,33}$=4.12, ***p*=0.014**	$F_{3,33}$=5.05, ***p*=0.005**	$F_{3,33}$=5.67, ***p*=0.003**

Mauchly's test of sphericity indicated that the assumption of sphericity was violated for this data, χ^2_{14}=305.8, ***p*<0.001**, and as ε=0.23, Greenhouse-Geisser correction was used to adjust degrees of freedom for the within subjects factor (Table A-13). The main effect of the within subjects factor (optic flow) is highly significant, and the interaction and between subjects factor (air speed) are both insignificant. This shows that waxing the antenna has removed variability due to varying air speed.

Table A-13: Repeated measures ANOVA results for antenna waxed bees.

Within subjects	**SS**	**df**	**MS**	**F**	***p***
Optic flow (OF)	8184.8	1.1 (5)	7158.3	52.49	**<0.001**
OF x AS	196.1	3.4 (15)	57.2	0.42	0.766
Error(OF)	5145.7	37.7 (165)	136.4		
Between subjects	**SS**	**df**	**MS**	**F**	***p***
Air speed (AS)	1628.7	3	542.9	0.72	0.546
Error	24802.1	33	751.6		

Post-hoc comparisons are made between main effects by computing *p*-values for each pairwise comparison, using the Dunn-Sidak test for within subjects comparisons. The response to optic flow for antenna amputated bees plateaus (Table A-14) in a similar way to bees with normal antennae (Section A.4.1), except that the plateau level now occurs at 500 rather than 400 $^{o}.s^{-1}$.

Table A-14: *Post-hoc* comparisons of optic flow for antenna waxed bees.

Optic flow ($^{o}.s^{-1}$)	**200**	**300**	**400**	**500**	**600**
100	***p*<0.001**	***p*<0.001**	***p*<0.001**	***p*<0.001**	***p*<0.001**
200		***p*<0.001**	***p*<0.001**	***p*<0.001**	***p*<0.001**
300			***p*<0.001**	***p*<0.001**	***p*<0.001**
400				***p*=0.047**	***p*=0.020**
500					*p*=0.726

A.4.4 Figure 2-3 details (antennal manipulation comparison)

Two factor ANOVA was conducted with one within subjects factor (optic flow), and one between subjects factor (antennal manipulation) at each of the air speeds 0, 0.5, 1.5, and 3 $m.s^{-1}$. In this comparison we are not particularly interested in the effect of optic flow, as its effect has already been investigated for each antennal manipulation, but include it as a main effect to permit the use of repeated measures analysis. The number of subjects and normality tests are presented in the preceding three sections, and whilst several groups do not have normal distributions, this should not affect the outcome of our analysis. Likewise, between subjects groups are heteroscedastic, which will make our ANOVA more conservative, and non-spherical, which is corrected for using Greenhouse-Geisser correction.

The main effect of the within subjects factor (optic flow) is highly significant at all air speeds, while the interaction effect with antenna manipulation is only significant at 3 $m.s^{-1}$ (Table A-15). Figure 2-2 shows that the range of response to optic flow increases when the antenna is manipulated at this air speed, accounting for the significant interaction at that air speed. The between subjects factor (antenna manipulation), is only significant at 0 and 1.5 $m.s^{-1}$, not 0.5 or 3 $m.s^{-1}$. The antennae must provide information to regulate abdomen at those two air speeds.

Table A-15: Repeated measures ANOVA results for antennal manipulations at different air speeds.

0 m.s^{-1}	**Within subjects**	**SS**	**df**	**MS**	**F**	***p***
	Optic flow (OF)	9591.9	1.4 (5)	7074.9	56.06	**<0.001**
	OF x AM	818.1	2.7 (10)	301.7	2.39	0.089
	Error(OF)	4961.6	39.3 (145)	126.2		
	Between subjects	**SS**	**df**	**MS**	**F**	***p***
	Antenna Manipulation (AM)	16466.5	2	8233.3	10.43	**<0.001**
	Error	22887.0	29	789.2		
0.5 m.s^{-1}	**Within subjects**	**SS**	**df**	**MS**	**F**	***p***
	OF	6436.8	1.5 (5)	4181.9	40.41	**<0.001**
	OF x AM	601.7	3.1 (10	195.4	1.88	0.148
	Error(OF)	3663.7	35.4 (115)	103.5		
	Between subjects	**SS**	**df**	**MS**	**F**	***p***
	AM	1109.9	2	555.0	0.29	0.752
	Error	44178.8	23	1920.8		
1.5 m.s^{-1}	**Within subjects**	**SS**	**df**	**MS**	**F**	***p***
	OF	5262.6	1.4 (5)	3829.3	40.87	**<0.001**
	OF x AM	259.7	2.7 (10)	94.5	1.01	0.394
	Error(OF)	3734.1	39.9 (145)	93.7		
	Between subjects	**SS**	**df**	**MS**	**F**	***p***
	AM	6104.3	2	3052.1	41.19	**0.030**
	Error	22291.1	29	768.7	3.97	
3 m.s^{-1}	**Within subjects**	**SS**	**df**	**MS**	**F**	***p***
	OF	2615.8	2.0 (5)	1303.6	64.70	**<0.001**
	OF x AM	210.4	4.0 (10)	52.4	2.60	0.045
	Error(OF)	1132.1	56.2 (140)	20.2		
	Between subjects	**SS**	**df**	**MS**	**F**	***p***
	AM	1907.9	2	953.9	1.12	0.339
	Error	23735.4	28	847.7		

Post-hoc tests were conducted using least significant difference tests. These tests do not provide Type 1 error control, but as we are testing are pre-existing hypothesis that manipulated bees would be different from normal bees, rather than a full set of pairwise comparisons family wise error rate control is not critical (Ruxton & Beauchamp, 2008). Significant differences between normal bees and both antennal manipulations occur at 0 and 1.5 $m.s^{-1}$ (Table A-16).

Table A-16: *Post-hoc* comparisons of normal antenna to both manipulations. Pairwise comparisons were performed regardless of the significance of main effects to provide consistency cross air speeds.

Air speed ($m.s^{-1}$)	**Normal vs. antenna amputated**	**Normal vs. antenna waxed**
0	***p*=0.029**	***p*<0.001**
0.5	p=0.972	p=0.502
1.5	***p*=0.050**	***p*=0.013**
3	p=0.937	p=0.176

A.4.5 Figure 2-4 details (response to a tailwind)

Two factor ANOVA was conducted with one within subjects factor (optic flow), and one between subjects factor (air speed). The number of bees included for each level of the between subjects factor were 7 (0 $m.s^{-1}$), 10 (-0.5 $m.s^{-1}$), 9 (-1.5 $m.s^{-1}$), and 10 (-3 $m.s^{-1}$). Of the 24 factor combinations one was found to be non-normal (-1.5 $m.s^{-1}$ at 300 $^{o}.s^{-1}$) using a Shapiro-Wilk test. The between subjects factors were found to be slightly heteroscedastic at only one of the within subjects factors levels (Table A-17), and it is unlikely this would have affected the results of the ANOVA.

Table A-17: Leven's test of equality of variances for bees experiencing a tail wind.

Factor ($^{o}.s^{-1}$)	**100**	**200**	**300**	**400**	**500**	**600**
Result	$F_{3,32}$=0.73, p=0.541	$F_{3,32}$=0.50, p=0.683	$F_{3,32}$=3.4, ***p*=0.030**	$F_{3,32}$=1.47, p=0.242	$F_{3,32}$=0.67, p=0.574	$F_{3,32}$=1.3, p=0.291

Mauchly's test of sphericity indicated that the assumption of sphericity was violated for this data, χ^2_{14}=145.93, ***p*<0.001**, and as ε=0.33, Greenhouse-Geisser correction was used to adjust degrees of freedom for the within subjects factor (

Table A-18). The main effect of the within subjects factor (optic flow) is highly significant, and the between subjects factor (air speed) is weakly significant, and the interaction term is not.

Table A-18: Repeated measures ANOVA results for bees experiencing a tail wind.

Within subjects	**SS**	**df**	**MS**	**F**	***p***
Optic flow (OF)	12170.0	1.7 (5)	7316.4	52.11	**<0.001**
OF x AS	341.9	5.0 (15)	68.5	0.49	0.783
Error(OF)	7473.4	53.2 (16)	140.4		
Between subjects	**SS**	**df**	**MS**	**F**	***p***
Air speed (AS)	6267.6	3	2089.2	3.10	**0.041**
Error	21583.8	32	675.5		

Post-hoc comparisons are made between main effects by computing *p*-values for each pairwise comparison, using the Dunn-Sidak test for both main effects comparisons. The response to optic flow for bees experiencing a tail wind (Table A-19) plateaus in the same way to bees experiencing forwards air flow (Section A.4.1), at 400 $^{o}.s^{-1}$. The only significant difference in pairwise test of air speeds occurs between -0.5 and -1.5 $m.s^{-1}$ (Table A-20). These air speeds have the largest difference in abdomen pitch responses (Figure 2-4B), and it appears that the response at 0.5 $m.s^{-1}$ may be slightly elevated, as for bees experiencing forwards air speed (Figure 2-2).

Table A-19: *Post-hoc* comparisons of optic flow for bees experiencing a tail wind.

Optic flow ($^{o}.s^{-1}$)	**200**	**300**	**400**	**500**	**600**
100	***p*<0.001**	***p* <0.001**	***p* <0.001**	***p* <0.001**	***p*<0.001**
200		***p*<0.001**	***p*<0.001**	***p*<0.001**	***p*<0.001**
300			***p*=0.001**	***p*=0.040**	***p*=0.012**
400				*p*=0.991	*p*=0.980
500					*p*=1.000

Table A-20: *Post-hoc* comparisons of air speed for bees experiencing a tail wind.

Air speed ($m.s^{-1}$)	**-0.5**	**-1.5**	**-3**
-0	p=0.727	p=0.740	p=0.973
-0.5		***p*=0.044**	p=0.157
-1.5			p=0.991

A.4.6 Figure 2-5 details (bees with their thorax pitched upwards)

Two factor ANOVA was conducted with one within subjects factor (optic flow) and one between subjects factor (air speed) using data for bees tethered with their thorax pitched up. The number of bees included for each level of the between subjects factor were 10 (0 $m.s^{-1}$), 8 (1.5 $m.s^{-1}$), and 10 (3 $m.s^{-1}$). Of the 18 factor combinations for each level of the thorax pitch factor, none were non-normal (Shapiro-Wilk test). Whilst the between subjects factor was heteroscedastic at most of the within subjects factors levels (Table A-21), as for bees tethered with their thorax horizontal (Section A.4.1), we suggest that this will make our ANOVA conservative.

Table A-21: Leven's test of equality of variances for bees with their thorax pitched upwards. All bar one group are heteroscedastic.

Factor ($^o.s^{-1}$)	**100**	**200**	**300**	**400**	**500**	**600**
Result	$F_{2,25}$=17.04, ***p*<0.001**	$F_{2,25}$=5.00, ***p*=0.015**	$F_{2,25}$=7.10, ***p*=0.004**	$F_{2,25}$=4.16, ***p*=0.028**	$F_{2,25}$=2.59, p=0.095	$F_{2,25}$=6.65, ***p*=0.005**

Mauchly's test of sphericity indicated that the assumption of sphericity was violated for this data, χ^2_{14}=130.35, ***p*<0.001**, and as ε=0.33, the Greenhouse-Geisser correction was used to adjust degrees of freedom for the within subjects factor (Table A-22). Both main effects, optic flow and air speed, including their interaction, are significant, matching our findings for bees with their thorax tethered horizontally (Section A.4.1), and suggesting their behaviour is qualitatively similar.

Table A-22: Repeated measures ANOVA results for bees with their thorax pitched upwards.

Within subjects	**SS**	**df**	**MS**	**F**	***p***
Optic flow (OF)	7222.2	1.6 (5)	4403.9	28.31	**<0.001**
OF x AS	2290.0	3.3 (10)	698.2	4.49	**0.007**
Error(OF)	6378.6	41.0 (125)	155.6		
Between subjects	**SS**	**df**	**MS**	**F**	***p***
Air speed (AS)	20781.0	2	10390.5	11.10	**<0.001**
Error	23396.2	25	935.8		

Whilst bees appear to react in a similar manner to both stimuli when their thorax is pitched up, to make a direct comparison we conducted three factor ANOVA, with an additional between subjects factor, the thorax pitch. Data from Figure 2-2 for bees with a horizontal thorax (at 0, 1.5 and 3 $m.s^{-1}$ air speeds) and those with their thorax pitched up comprised the two levels of the new factor. The number of subjects, normality and equality of variance tests for bees with a horizontal thorax are listed previously in Section A.4.1. Whilst heteroscedasticity is not corrected for, the Greenhouse-Geisser correction is used for within-subjects factors. Air speed, optic flow and their interaction are significant, whereas the thorax angle does not have a significant main effect or interactions (Table A-23). This confirms that bees with their thoraxes pitched up exhibit a streamlining response to optic flow and air speed that is statistically indistinguishable from those with their thorax horizontal.

Table A-23: Repeated measures ANOVA results for comparison between bees with their thorax pitched upwards and horizontally.

Within subjects factors	**SS**	**df**	**MS**	**F**	***p***
Optic flow (OF)	13941.3	1.7 (5)	8002.3	82.46	**<0.001**
OF x AS	3929.4	3.5 (10)	1127.7	11.62	**<0.001**
OF x Angle	208.7	1.7 (5)	119.8	1.24	0.293
OF x AS x Angle	297.7	3.5 (10)	85.4	0.88	0.467
Error(OF)	9636.5	99.3 (285)	97.0		
Between subjects factor	**SS**	**df**	**MS**	**F**	***p***
Air speed (AS)	40374.4	2	20187.2	18.6	**<0.001**
Angle	188.6	1	188.6	0.17	0.678
AS x Angle	149.1	2	74.6	0.07	0.934
Error	61735.8	57	1083.1		

A.4.7 Figure 2-5 details (bees with their thorax pitched downwards)

Two factor ANOVA was conducted with one within subjects factors (optic flow) and one between subjects factors (air speed) using data for bees tethered with their thorax pitched down. The number of bees included for each level of the between subjects factor was 5 (0 $m.s^{-1}$), 7 (1.5 $m.s^{-1}$), and 7 (3 $m.s^{-1}$).

For these exploratory data analyses, we elected to include flights from bees that stopped flying briefly during the stimulation protocol. Hence the missing values for three bees (missing at most one data point), were replaced with the mean value measured for that bee at all other factor combinations. Of the 18 factor combinations for each level of the thorax pitch factor, two were found to be non-normal (3 $m.s^{-1}$ at 500 $^{o}.s^{-1}$ and 1.5 $m.s^{-1}$ at 600 $^{o}.s^{-1}$), using a Shapiro-Wilk test. Whilst the between subjects factor was heteroscedastic at half of the within subjects factors levels (Table A-24), as for bees tethered with their thorax horizontal (Section A.4.1), we suggest this will make our ANOVA slightly conservative.

Table A-24: Leven's test of equality of variances for bees with their thorax pitched down.

Factor ($^{o}.s^{-1}$)	**100**	**200**	**300**	**400**	**500**	**600**
Result	$F_{2,16}$=2.24, p=0.139	$F_{2,16}$=2.18, p=0.146	$F_{2,16}$=2.39, p=0.123	$F_{2,16}$=5.76, ***p*=0.013**	$F_{2,16}$=7.06, ***p*=0.006**	$F_{2,16}$=4.74, ***p*=0.024**

Mauchly's test of sphericity indicated that the assumption of sphericity was violated for this data, χ^2_{14}=37.08, ***p*<0.001**, and as ε=0.59, the Greenhouse-Geisser correction was used to adjust degrees of freedom for the within subjects factor (Table A-25). The main effect of air speed, including its interaction with optic flow, is significant. Surprisingly, the main effect of optic flow was not significant, in contrast to the findings for bees with their thoraxes tethered horizontally (Section A.4.1). Whilst this test has a reduced number of subjects compared relative to the previous ones (due to the insects reluctance to fly when tethered with their thorax down), which would have reduced its power, the data in Figure 2-5 shows that bees tethered with their thorax down have a qualitatively different reaction to optic flow. This suggests that tethering bees with thoraxes pitched down changed their behaviour, and indeed changed the effect optic flow has on regulating their abdomen position.

Table A-25: Repeated measures ANOVA results for bees with their thorax pitched downwards.

Within subjects	**SS**	**df**	**MS**	**F**	***p***
Optic flow (OF)	369.5	2.93 (5)	125.8	1.58	0.208
OF x AS	1310.8	5.9 (10)	223.2	2.80	**0.021**
Error(OF)	3743.4	47.0 (80)	79.7		
Between subjects	**SS**	**df**	**MS**	**F**	***p***
Air speed (AS)	13098.4	2	6549.2	8.19	**0.004**
Error	12794.3	16	799.6		

A.4.8 Figure 2-6 details (passive lifting of the abdomen)

One factor ANOVA was conducted with a single between subjects factor (air speed). Seven honeybee bodies were tested at all air speed levels. Of the 5 factor levels one was found to be slightly non-normal (4 $m.s^{-1}$) using a Shapiro-Wilk test.

Levene's test of equality of variances indicated that the assumption of homoscedasticity was not violated for this data ($F_{4,30}$=0.17, p=0.954). The main effect of the between subjects factor (air speed), is not significant (Table A-26), indicating that air speeds does not significantly affect the abdomen position of decapitated bees.

Table A-26: ANOVA results for decapitated bees.

	SS	**df**	**MS**	**F**	***p***
Air speed (AS)	206.4	4	51.6	0.83	0.517
Error	1866.3	30	62.2		

A.4.9 Figure A-1 details (air speed presentation order)

Three factor ANOVA was conducted with three within subjects factors (optic flow, air speed and order). Ten bees participated in all experiments. Bees were exposed to a triangular function of air speed levels, as described in Section A.1.1. The 5 $m.s^{-1}$ air speed point is not included in analysis as, being at the peak point of the triangular air speed ramp, bees were not exposed to this value twice in the same flight.

For these exploratory data analyses, we elected to include flights from bees that stopped briefly flying during the stimulation protocol. Hence the missing values for three bees (missing for at most two data points), were replaced with the mean value measured for that bee at all other factor combinations. Of the 24 factor combinations two were found to be non-normal (100 $^{o}.s^{-1}$ at 0 $m.s^{-1}$, first presentation; and 500 $^{o}.s^{-1}$ at 0 $m.s^{-1}$, first presentation) using a Shapiro-Wilk test.

Table A-27: Mauchly's test of sphericity for test of air speed presentation order. Order has only two factor levels and is not tested.

Effect	χ^2	**df**	***p***	ε
Optic flow (OF)	3.5	2	0.175	0.74
Air speed (AS)	19.2	9	**0.027**	0.44
Order	0	0	-	-
OF x AS	107.6	35	**<0.001**	0.30
OF x Order	0.9	2	0.957	0.99
AS x Order	33.7	9	**<0.001**	0.40
OF x AS x Order	109.5	35	**<0.001**	0.25

Mauchly's test of sphericity showed that the assumption of sphericity was violated for some main effects and interactions (Table A-27). The Greenhouse-Geisser correction was used to adjust degrees of freedom for those factors in the following ANOVA (Table A-28). The main effects of optic flow and air speed are significant for this hysteresis test, and they show a significant interaction. The effect of air speed presentation order is not significant itself, however, it did show a significant interaction with air speed, and additionally shows a significant three factor interaction with the optic flow and air speed. Optic flow does not interact significantly with the order of air speed presentation. Thus, it appears that presentation order of air speeds affects how bees respond to that stimulus and modifies how air speed interacts with optic flow, resulting in the hysteresis curves observed for triangular air speed ramps across all tested optic flow speeds (Figure A-1).

Table A-28: Results of repeated measures ANOVA for test of air speed presentation order. Un-adjusted degrees of freedom for the within subjects factors (not used in calculations) are shown in brackets.

Within subjects factors	SS	df	MS	F	*p*
Optic flow (OF)	839.6	2	419.8	5.46	**0.014**
Error(OF)	1384.3	18	76.9		
Air speed (AS)	8970.1	1.8 (4)	5122.0	64.41	**<0.001**
Error(AS)	1253.4	15.8 (36)	79.5		
Order	48.0	1	48.0	0.76	0.407
Error(Order)	572.7	9	63.6		
OF x AS	1101.7	2.4 (8)	463.5	5.81	**0.007**
Error(OFxAS)	1706.6	21.4 (72)	79.8		
OF x Order	54.6	2	27.3	0.74	0.493
Error(OFxOrder)	668.4	18	37.1		
AS x Order	1250.1	1.6 (4)	780.7	11.44	**0.002**
Error(ASxOrder)	983.8	14.4 (36)	68.3		
OF x AS x Order	685.5	2.0 (8)	348.2	5.41	**0.015**
Error(OFxASxOrder)	1140.1	17.7 (72)	64.3		

A.4.10 Figure A-2 details (optic flow presentation order)

Three factor ANOVA was conducted with two within subjects factors (optic flow and order) and one between subjects factor (air speed). The number of bees included for each level of the between subjects factor were 11 (0 $m.s^{-1}$), 12 (1.5 $m.s^{-1}$), and 12 (3 $m.s^{-1}$). Bees were exposed to a triangular function of optic flow levels, as described in Section A.1.2. The 600 $^{o}.s^{-1}$ air speed point is not included in analysis as, being at the peak point of the triangular optic flow ramp; bees were not exposed to this value twice in the same flight.

For these exploratory data analyses, we elected to include flights from bees that stopped flying briefly during the stimulation protocol. Hence the missing values for four bees (missing at most two data points), were replaced with the mean of value measured for that bee over all other factor combinations. Of the 30 factor combinations three were found to be non-normal (0 $m.s^{-1}$ at 100 $^{o}.s^{-1}$, first and second

presentations; 0 $m.s^{-1}$ at 300 $^{o}.s^{-1}$, first presentation) using a Shapiro-Wilk test. The between subjects factors were found to be slightly heteroscedastic at only one of the within subjects factors levels (Table A-29).

Table A-29: Leven's test of equality of variances for test of optic flow presentation order.

Presentation			**First**		
Factor ($^{o}.s^{-1}$)	**100**	**200**	**300**	**400**	**500**
Result	$F_{2,32}$=0.81, p=0.455	$F_{2,32}$=0.0, p=0.997	$F_{2,32}$=1.0, p=0.370	$F_{2,32}$=0.2, p=0.816	$F_{2,32}$=0.1, p=0.913
Presentation			**Second**		
Factor ($^{o}.s^{-1}$)	**100**	**200**	**300**	**400**	**500**
Result	$F_{2,32}$=9.3, **p=0.001**	$F_{2,32}$=1.2, p=0.319	$F_{2,32}$=0.2, p=0.862	$F_{2,32}$=0.4, p=0.673	$F_{2,32}$=0.4, p=0.696

Table A-30: Mauchly's test of sphericity for test of optic flow presentation order. Order has only two factor levels and is not tested.

Effect	χ^2	**df**	p	ε
Optic flow (OF)	139.1	9	**<0.001**	0.32
Order	0	0	-	-
OF x Order	113.1	9	**<0.001**	0.37

Mauchly's test of sphericity showed that the assumption of sphericity was violated for the main effect of optic flow and its interaction with presentation order (Table A-30), hence, Greenhouse-Geisser correction was used to adjust degrees of freedom for those within subject factors in the following ANOVA (Table A-31). Consistent with the results observed for normal bees (Section A.4.1), the main effects of optic flow and air speed are both significant, although the interaction between the two is not significant (this is likely to be because the reduction in air speed levels tested has reduced the power of this ANOVA test to detect this interaction relative to other tests, rather than the effect itself having changed). The order of presentation of optic flow has no significant main effect, or significant interactions associated with any other factors. This indicates that the abdomen position is relatively independent on the order of optic flow presentation, at least in the case of a simple triangular function.

Table A-31: Repeated measures ANOVA results for test of optic flow presentation order.

Within subjects factors	**SS**	**df**	**MS**	**F**	***p***
Optic flow (OF)	7312.8	1.3 (4)	5732.4	22.81	**<0.001**
OF x AS	1402.2	2.6 (8)	549.6	2.19	0.113
Error(OF)	10259.2	40.8 (128)	251.3		
Order	6.7	1	6.8	0.10	0.750
AS x Order	316.1	2	158.0	2.41	0.106
Error(Order)	2095.2	32	65.5		
OF x Order	34.1	1.5 (4)	23.0	0.19	0.759
OF x Order x AS	250.8	3.0 (8)	84.5	0.71	0.551
Error(OFxOrder)	5668.7	47.5 (128)	119.4		
Between subjects factor	**SS**	**df**	**MS**	**F**	***p***
Air speed (AS)	18473.2	2	9236.6	8.79	**0.001**
Error	33627.7	32	1050.9		

Appendix B **Supplementary material for Chapter 3**

B.1 Supplementary figures

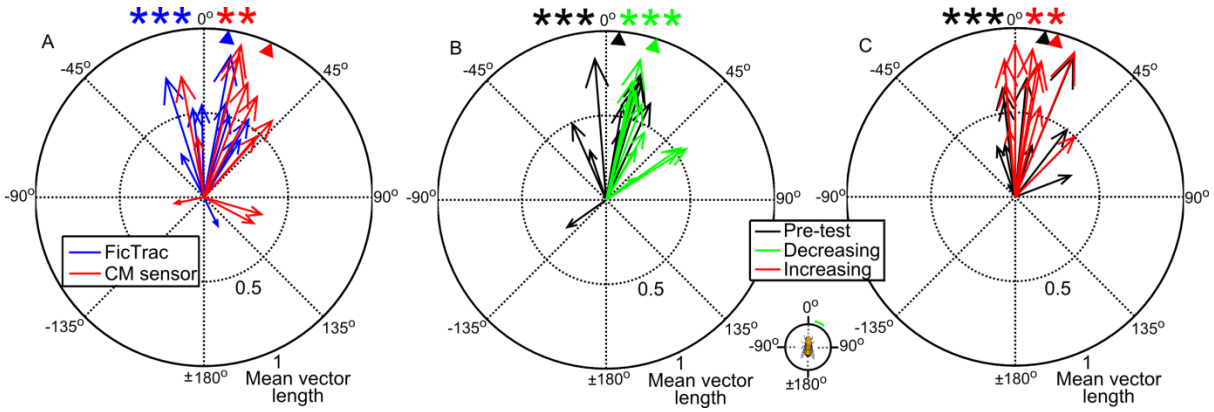

Figure B-1: Mean vector for each bee in all experimental conditions. Triangles on plot perimeter denote the average mean vector direction for each group. **A**, FicTrac and CM sensors (corresponding to distributions in Figure 3-2). **B**, Pre-test and 'decreasing' condition, and **C**, Pre-test and 'increasing' condition (corresponding to distributions in Figure 3-4). Stars (**: p<0.01, ***: p<0.001) correspond to significant findings from Rayleigh's test of uniformity for each group, and indicate that the groups distribution of mean vector angles are non-uniform.

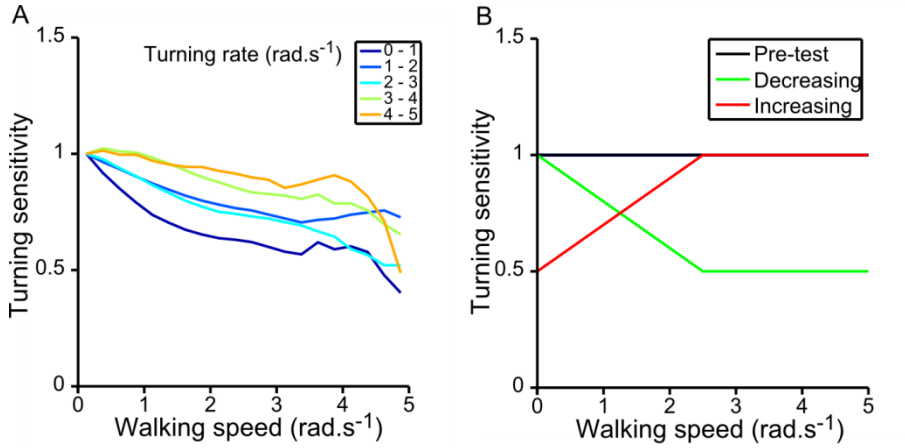

Figure B-2: Feedback sensor sensitivity to turning when affected by walking speed. **A**, The measured relationship between walking speed and turning sensitivity for CM sensors (parameterised by turning rate). Measured by comparing simultaneous measurement from FicTrac (treated as ground truth) to those made using CM sensors during open-loop stimulation with a bar rotating in alternating directions (at 6 $^{o}.s^{-1}$). **B**, Imposed coupling between walking speed and turning sensitivity, with both measured by FicTrac, as used in Figure 3-4.

Appendix C **Supplementary material for Chapter 4**

C.1 Supplementary figures

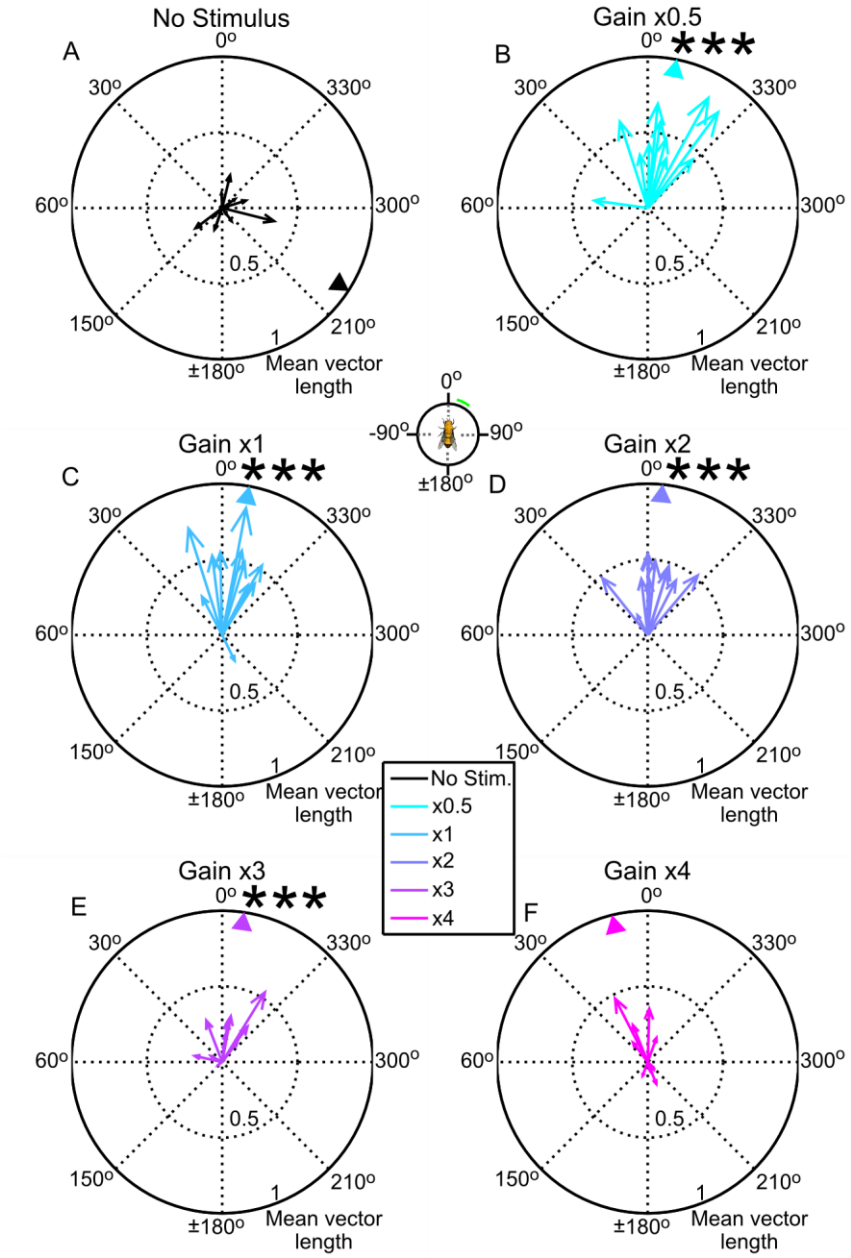

Figure C-1: Mean vectors for each bee in each stimulus condition. Mean vector lengths are plotted in Figure 4-4 for each gain condition. The average mean vector orientation of each group is shown using a triangle on the perimeter of the plot. Stars (***) denote that the orientation of the vectors in a group is significantly different from random distribution at $p<0.001$ (Section C.5). N=11 repeated all gain conditions.

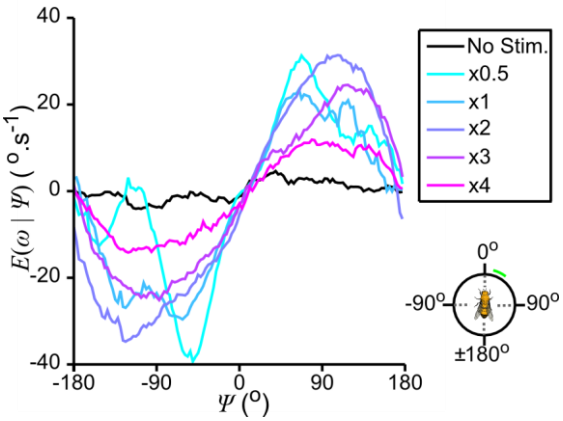

Figure C-2: The expected turning rate, ω, as function of stimulus position, ψ. This function varies depending on the gain condition. N=11 repeated all gain conditions.

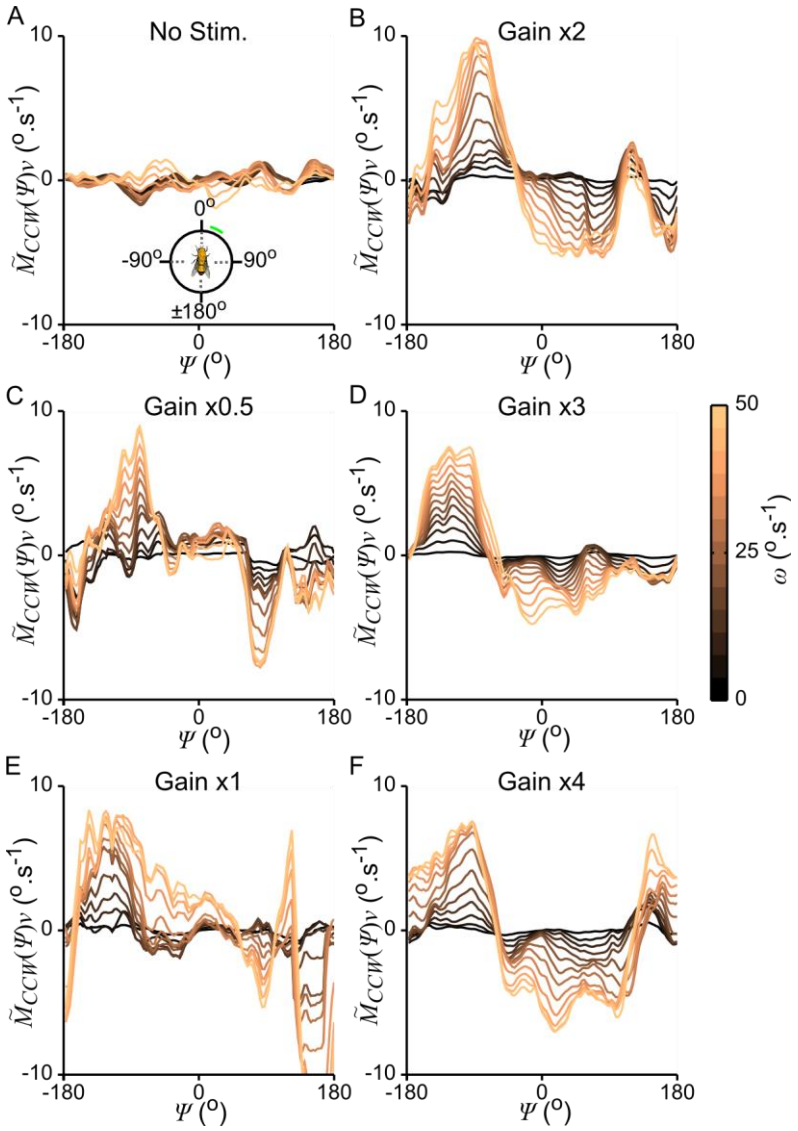

Figure C-3**:** The motion-dependent response for counter-clockwise rotation. Calculated for each gain condition using Eq. (C-11), as labelled in **A** to **F**. Curves are parameterised by turning rate, ω, in 4.2 $^{o}.s^{-1}$ increments, as for Figure 4-6. N=11 repeated all gain conditions.

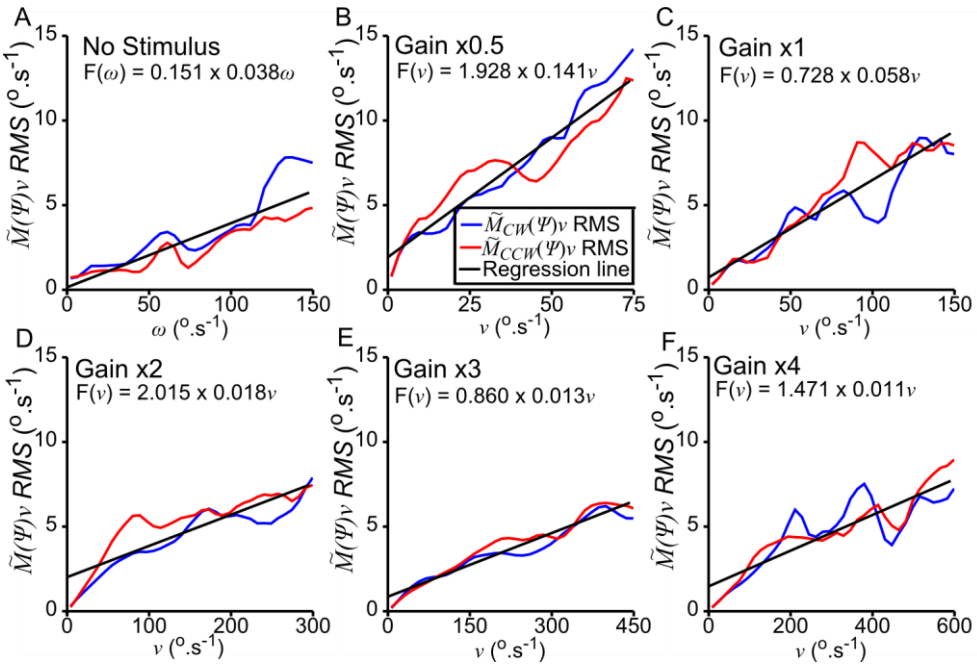

Figure C-4**:** RMS scale of the motion-dependent functions in both directions, for all gain conditions. Equations are for linear regressions (black lines) fitting the average between CW and CCW motion, and describe $a_m + b_m \times v$ (where v is the stimulus velocity) in Figure 4-7. Note that all plots span the turning rate range of 0 to 150°.s^{-1}. N=11 repeated all gain conditions.

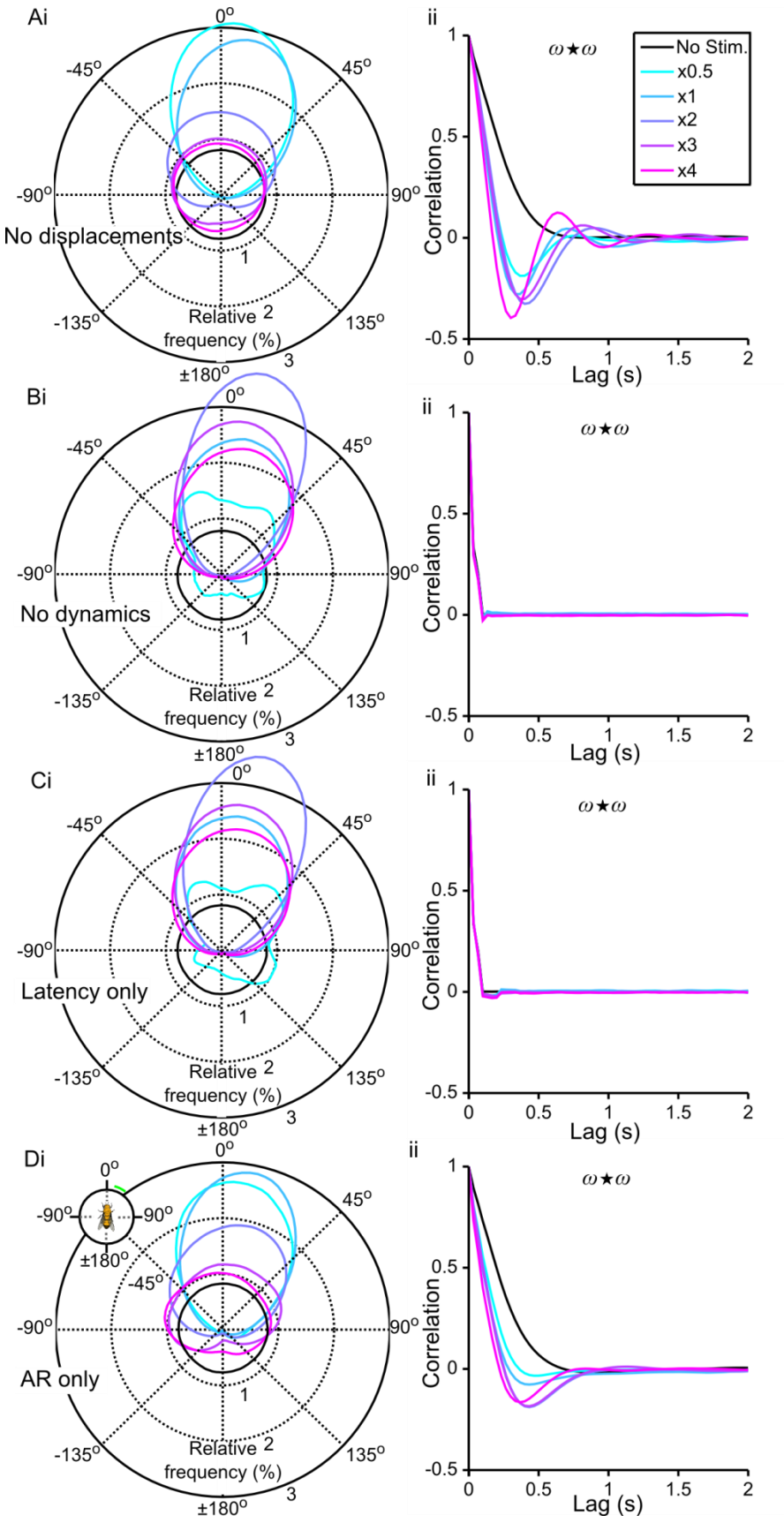

Figure C-5**:** Comparison of various model components effects on fixation. **A**, no forced displacements. **B**, neither the discrete time latency, nor the AR filter are used. **C**, the discrete time latency, but not the AR filter is used. **D**, the AR filter, but not the discrete time latency is

used. Disturbances occur in B, C and D. Except where noted specifically, all model parameters are identical to those used in Figure 4-7, and use simulation gains matched to experimental gains. For all plots, **i** shows radial histograms of stimulus position, ψ, and **ii** shows the corresponding autocorrelations of turning rate, ω.

C.2 Motion from front to back details

Using Eq. (4-17) the responses to motion in both directions, and the reflections of these responses can be expressed using the following four equations,

$$R(\psi,v)=P^A(\psi)+P^M(\psi)+\left(M^A(\psi)+M^M(\psi)+M_D^A(\psi)+M_D^M(\psi)\right)v \tag{C-1}$$

$$R(\psi,-v)=P^A(\psi)+P^M(\psi)-\left(M^A(\psi)+M^M(\psi)+M_D^A(-\psi)+M_D^M(-\psi)\right)v \tag{C-2}$$

$$R(-\psi,v)=P^A(-\psi)+P^M(-\psi)+\left(M^A(-\psi)+M^M(-\psi)+M_D^A(-\psi)+M_D^M(-\psi)\right)v \tag{C-3}$$

$$R(-\psi,-v)=P^A(-\psi)+P^M(-\psi)-\left(M^A(-\psi)+M^M(-\psi)+M_D^A(\psi)+M_D^M(\psi)\right)v \tag{C-4}$$

These equations can then be rewritten in terms of positive ψ using the identities specific to asymmetric and mirror symmetric functions, Eqs. (4-15) and (4-16), leading to,

$$R(\psi,v)=P^A(\psi)+P^M(\psi)+\left(M^A(\psi)+M^M(\psi)+M_D^A(\psi)+M_D^M(\psi)\right)v \tag{C-5}$$

$$R(\psi,-v)=P^A(\psi)+P^M(\psi)-\left(M^A(\psi)+M^M(\psi)-M_D^A(\psi)+M_D^M(\psi)\right)v \tag{C-6}$$

$$R(-\psi,v)=-P^A(\psi)+P^M(\psi)-\left(M^A(\psi)-M^M(\psi)+M_D^A(\psi)-M_D^M(\psi)\right)v \tag{C-7}$$

$$R(-\psi,-v)=-P^A(\psi)+P^M(\psi)+\left(M^A(\psi)-M^M(\psi)-M_D^A(\psi)-M_D^M(\psi)\right)v \tag{C-8}$$

Combining these equations as in Eq. (4-23) can find $M_{CW}(\psi)v$. To find $M_{CCW}(\psi)v$, firstly note that using the identities for symmetric functions (Eqs. (4-15) and (4-16)), Eqs. (4-19) and (4-20) can also be written as,

$$\left(R(\psi,v)+R(\psi,-v)-R(-\psi,v)-R(-\psi,-v)\right)/4=P^A(\psi)-M_D^A(-\psi)v \tag{C-9}$$

$$\left(R(\psi,v)-R(\psi,-v)+R(-\psi,v)-R(-\psi,-v)\right)/4=\left(M^M(\psi)+M_D^M(-\psi)\right)v \tag{C-10}$$

Then the sum of Eq. (C-10), (4-21) and $P^A(\psi)$ minus Eq. (C-9) finds $M_{CCW}(\psi)v$,

$$\begin{aligned}&\left(R(\psi,v)-3R(\psi,-v)+R(-\psi,v)+R(-\psi,-v)\right)/4+P^A(\psi)\\&=\left(M^A(\psi)+M^M(\psi)+M_D^A(-\psi)+M_D^M(-\psi)\right)v=M_{CCW}(\psi)v\end{aligned} \tag{C-11}$$

C.3 Effects of motion blur

Because of the time delays and the temporal dynamics of the responses at various levels of the visual pathway, a given neuron will not respond instantaneously to the visual stimulus that it receives. As a consequence, when an image moves rapidly across the eye the neural representation of this image will be a blurred (smoothed) version that lags behind its optical representation in the retina (Srinivasan & Bernard, 1975). Consequently, if a bar moves rapidly from left to right past the visual field of a neuron that looks in a given direction, ψ, the response of this neuron to the moving bar will be a maximum when the bar has moved past the centre of the neuron's receptive field, to the right. This will result in erroneous estimates of the sensitivities of behavioural responses to various bar positions, and the errors will depend upon the speed and direction of the movement of the bar.

Motion blurring is the suggested cause (Heisenberg & Wolf, 1984) for unusually shaped reconstructions of a position function in one study where high stimulus velocities (>200 $^{o}.s^{-1}$) were used (Bülthoff, 1982). Recent open-loop experiments have further elucidated that in *Drosophila*, the temporal dynamics of the position and motion responses persist for tens, if not hundreds of milliseconds, and may differ between the two response types (Aptekar et al., 2012; Bahl et al., 2013). Therefore, as the stimulus velocity, v, increases, motion blur would be increasingly likely to confound the results, regardless of whether an experiment is conducted in open- or closed-loop. The effects of motion blurring are likely to be most problematic in closed-loop experiments, as these typically involve a wide range of stimulus velocities, and the resulting position and motion responses cannot be accurately related to each other if they are distorted by differing extents of motion blur.

Motion blur may take two forms that affect the reconstruction of position- and motion-dependent functions. The underlying functions could be angularly translated in ψ by some angle, θ, that varied depending on v. As an example, consider position-dependent function, $\tilde{P}(\psi)$ in Figure 4-5, which is approximately equal to zero when $\psi = 0$ ($\tilde{P}(0) \approx 0$). If the stimulus is moving rapidly clockwise and passes $\psi = 0$, it will take some time for the bee to react to this (with the stimulus also rotating further), so that the bee's position-dependent response will no longer be zero at $\psi = 0$ ($\tilde{P}(\theta) = 0$), because the response lags the stimulus.

A second possibility is that if the stimulus is rotating rapidly, the response from several stimulus positions that the bee has observed in the immediate past could contribute to the responses measured at a given instant of time, and as v increases, a larger number of prior stimulus positions would contribute to any measured response. This is akin to blurring, resulting from the decay time of the response. While it is easy to gauge whether these two artefacts are likely to occur, it is unfortunately not easy to correct for them.

As an example, we will consider the effect of latency, where for any stimulus velocity, v, there is a constant, but unknown, angular translation, θ, that represents the honeybee's temporal latency in responding to the stimulus. Then Eq. (4-17) can now be rewritten:

$$R(\psi+\theta,v)=P^{A}(\psi+\theta)+P^{M}(\psi+\theta)+\begin{pmatrix}M^{A}(\psi+\theta)+M_{D}^{A}(\psi\times\mathrm{sgn}(v)+\theta)\\+M^{M}(\psi+\theta)+M_{D}^{M}(\psi\times\mathrm{sgn}(v)+\theta)\end{pmatrix}v \qquad \text{(C-12)}$$

The effect arising from θ is obvious. For rotation in the opposite direction, it is reasonable to assume that if v results in a specific θ, then motion in the opposite direction, $-v$, will probably result in a shift of $-\theta$, where the magnitude of the angular translations of the shift would be (approximately) equal, but with the polarity reversed.

This latency is then not conducive to reconstructing position- and motion-dependent functions accurately, as they are distorted by the translation. An example is shown in Figure C-6A , where the bee's zero-mean response, $\tilde{R}(\psi,v)$, based on the position- and motion- dependent functions, $P(\psi)$ and $M(\psi)$ from Figure 4-3, is progressively translated between -45° and 45°, with the opposite translation applied being to $\tilde{R}(\psi,-v)$ (Figure C-6Ai). As the functions are translated further in either direction, the reconstructions of the zero-mean functions, $\tilde{P}(\psi)$ and $\tilde{M}(\psi)v$, become inaccurate (Figure C-6Aii-iii). Whilst the specific distortion depends on the specific shape of these functions, it can particularly effect $\tilde{M}(\psi)v$, because even if this function is uniform across ψ, progressively translating the functions can give the impression that it varies (if $\tilde{P}(\psi)$ has a similarly asymmetric form to the example).

When Eq. (4-17) is used to calculate Eqs. (4-18) to (4-21), elements of $P(\psi)$ and $M(\psi)v$ would then no longer be cleanly separated (this is fully outlined in Section C.4) as θ grows larger. However, these functions can provide qualitative indications of when these functions deform either due to latency resulting in translation, or motion blurring. Eq. (4-18) ideally measures

$P^M(\psi)$, but can be influenced by $M^M(\psi)v$ if $\theta \neq 0$ (Eq. (C-17)). This function does appear to distort across all gain conditions (Figure C-6B) at turning rates greater than approximately 50 to 100 $^{o}.s^{-1}$.

Eq. (4-20) ideally measures $\left(M^M(\psi)+M_D^M(\psi)\right)v$, but can be influenced by $P^A(\psi)$ if $\theta \neq 0$ (Eq. (C-19)). Judging the distortion in this equation is more difficult because the scale of the function also changes with *v*. To facilitate comparisons, all curves were divided by their RMS value, thus equalising the scale of the curves. Interestingly, the shape of this curve appears relatively consistent for most gain conditions with $50 < \omega < 100$ $^{o}.s^{-1}$ (Figure C-6C), although it does distort as ω approaches 150 $^{o}.s^{-1}$. For some gain conditions (x1, x2 and x4), the shape of the curve is not consistent for $\omega < 25$ to 35 $^{o}.s^{-1}$. This is unlikely to be the result of motion blurring, and possibly occurs because at low stimulus velocities, the bee's motion receptors are minimally stimulated.

Surprisingly, the qualitative assessments of both of these measures of distortion indicate that it occurs at similar turning rate ranges for all gain conditions, even though the stimulus velocities are not equal. It is possible that the honeybee's turning rate also inherently distorts the reconstruction of functions in a similar way that motion blurring would be expected to do. Certainly if a bee is turning the ball rapidly in one direction or the other, then she may struggle to adjust her turning rate as dictated by the position and motion functions, which could cause latency, or even blurring, in the same manner as might be expected based on a visually guided response. Although, it is appealing to use as wide a range of measured turning rates as possible, given the distortions noted in Figure C-6, it is prudent to restrict ourselves to using a confined range for further analysis, which was arbitrarily decided to be $20 < |\omega| < 50$ $^{o}.s^{-1}$. This will reduce, and ideally prevent the effects of latency and blurring, regardless of their source, from distorting reconstructions of the position and motion functions.

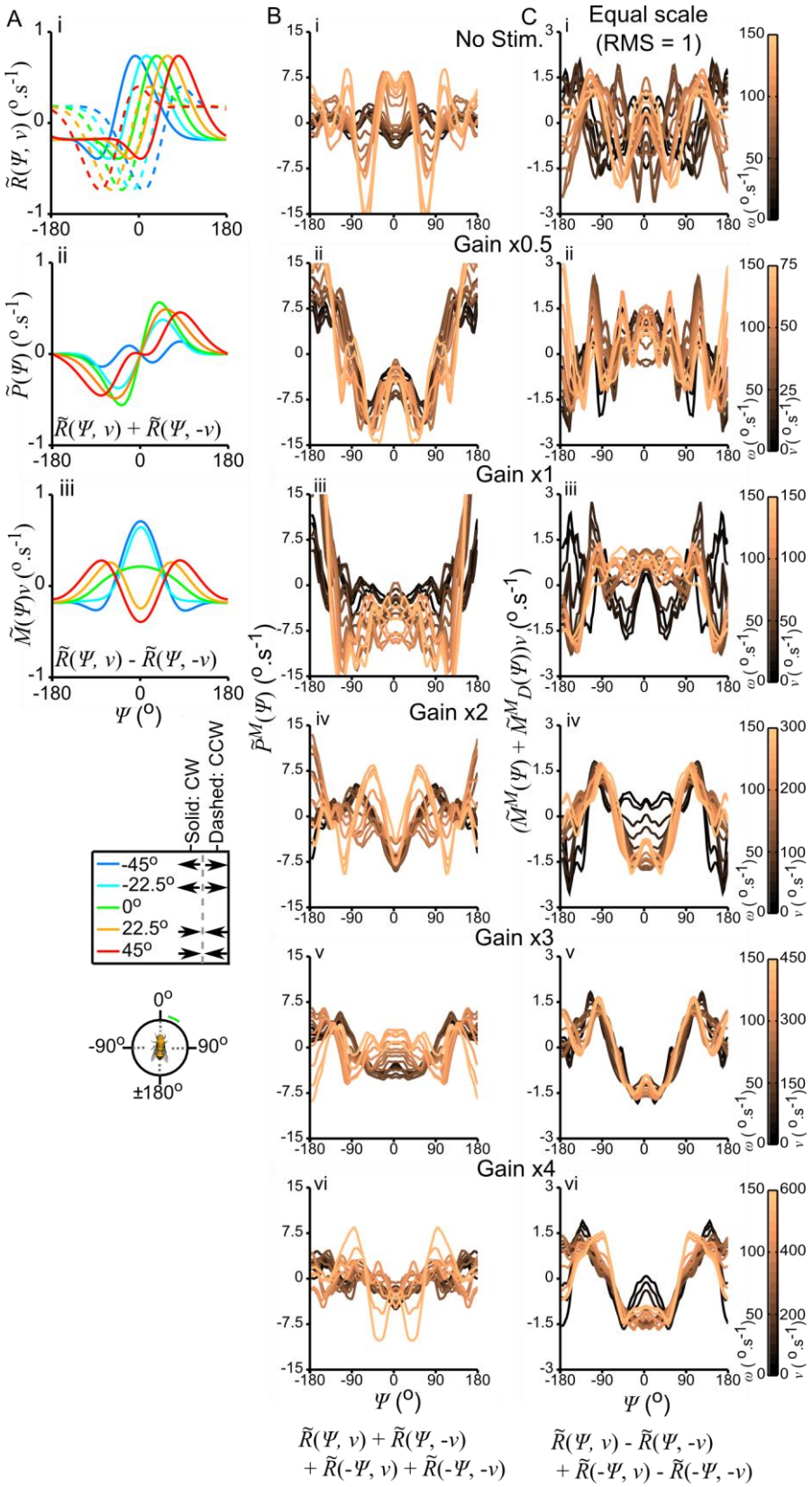

Figure C-6**:** Motion blurring could distort function reconstruction. **A**, Example of distortion caused by translating CW and CCW responses in opposite directions (Section C.3). **B**, Distortions that occur when calculating mirror-symmetric component of the position-dependent response, $\tilde{P}^{M}(\psi)$ (using Eq. (4-18)), when parameterised by turning rate, ω, for all gain conditions. **C**, Distortions that occur when calculating the sum of the mirror-symmetric

components of the motion-dependent response, $(\tilde{M}^{M}(\psi)+\tilde{M}_{D}^{M}(\psi))v$ (using Eq. (4-20)), when parameterised by ω, for all gain conditions. Lines are parameterised at 8.5 $^{o}.s^{-1}$ increments in B and **C**. Curves in C were divided by their RMS values, and have an equal (RMS = 1) scale. N=11 repeated all gain conditions.

C.4 Function translations

If an unknown angular translation, θ, is applied to Eqs. (C-5) to (C-8), such that it has positive magnitude for positive v and negative magnitude for negative v, those equations can be rewritten as,

$$\begin{aligned} R(\psi+\theta,v) &= P^{A}(\psi+\theta)+P^{M}(\psi+\theta) \\ &\quad +\left(M^{A}(\psi+\theta)+M^{M}(\psi+\theta)+M_{D}^{A}(\psi+\theta)+M_{D}^{M}(\psi+\theta)\right)v \end{aligned} \tag{C-13}$$

$$\begin{aligned} R(\psi-\theta,-v) &= P^{A}(\psi-\theta)+P^{M}(\psi-\theta) \\ &\quad -\left(M^{A}(\psi-\theta)+M^{M}(\psi-\theta)-M_{D}^{A}(\psi+\theta)+M_{D}^{M}(\psi+\theta)\right)v \end{aligned} \tag{C-14}$$

$$\begin{aligned} R(-\psi+\theta,v) &= -P^{A}(\psi+\theta)+P^{M}(\psi+\theta) \\ &\quad -\left(M^{A}(\psi+\theta)-M^{M}(\psi+\theta)+M_{D}^{A}(\psi+\theta)-M_{D}^{M}(\psi+\theta)\right)v \end{aligned} \tag{C-15}$$

$$\begin{aligned} R(-\psi-\theta,-v) &= -P^{A}(\psi-\theta)+P^{M}(\psi-\theta) \\ &\quad +\left(M^{A}(\psi-\theta)-M^{M}(\psi-\theta)-M_{D}^{A}(\psi+\theta)-M_{D}^{M}(\psi+\theta)\right)v \end{aligned} \tag{C-16}$$

If these equations are then combined to calculate Eqs. (4-18) to (4-21), the following functions would be found,

$$\begin{aligned} &\left(R(\psi+\theta,v)+R(\psi-\theta,-v)+R(-\psi+\theta,v)+R(-\psi-\theta,-v)\right)/2 = \\ &P^{M}(\psi+\theta)+P^{M}(\psi-\theta)+\left(M^{M}(\psi+\theta)-M^{M}(\psi-\theta)\right)v \end{aligned} \tag{C-17}$$

$$\begin{aligned} &\left(R(\psi+\theta,v)+R(\psi-\theta,-v)-R(-\psi+\theta,v)-R(-\psi-\theta,-v)\right)/2 = \\ &P^{A}(\psi+\theta)+P^{A}(\psi-\theta)+\left(M^{A}(\psi+\theta)-M^{A}(\psi-\theta)+2M_{D}^{A}(\psi+\theta)\right)v \end{aligned} \tag{C-18}$$

$$\begin{aligned} &\left(R(\psi+\theta,v)-R(\psi-\theta,-v)+R(-\psi+\theta,v)-R(-\psi-\theta,-v)\right)/2 = \\ &P^{M}(\psi+\theta)-P^{M}(\psi-\theta)+\left(M^{M}(\psi+\theta)+M^{M}(\psi-\theta)+2M_{D}^{M}(\psi+\theta)\right)v \end{aligned} \tag{C-19}$$

$$\begin{aligned} &\left(R(\psi+\theta,v)-R(\psi-\theta,-v)-R(-\psi+\theta,v)+R(-\psi-\theta,-v)\right)/2 \\ &= P^{A}(\psi+\theta)-P^{A}(\psi-\theta)+\left(M^{A}(\psi+\theta)+M^{A}(\psi-\theta)\right)v \end{aligned} \tag{C-20}$$

In all cases, these equations will no longer predict the same results as in Eqs. (4-18) to (4-21).

C.5 Statistical details

All tests were performed using a single factor, gain, consisting of 6 factor levels, gains x0.5, x1, x2, x3, x4, and the no-stimulus control, unless otherwise noted. All factor levels for each

data set were tested for normality (using a Shapiro-Wilk test); deviations from this are noted where they occur. Main effects were tested using either repeated measures ANOVA or Friedman's non-parametric repeated measures ANOVA equivalent, depending on the presence and severity of non-normal factors. When using ANOVA, the assumption of sphericity was also tested using Mauchly's test of sphericity, and the Greenhouse- Geisser correction was applied if this assumption was violated.

Upon finding a significant main effect, the following *post-hoc* testing procedure was used. The factor with the mean of the largest amplitude (hereafter referred to as the 'peak factor') was compared to the highest and lowest gains (x0.5 and x4), and the no stimulus condition (if it was not itself one of those factors). This comparison was made using a paired sample *t*-test for normal data, or a Wilcoxon matched-pair signed-rank test for non-normal data. Additionally, in some cases factor levels were compared to zero. For normal data, a single factor *t*-test was performed, and for non-normal data, a Wilcoxon signed rank test comparing the group median to zero was used. The two types of test, for both comparisons to zero and pairwise tests, are respectively denoted by *t* and *W* test statistics. Rayleigh's test of uniformity is denoted using a *z* test statistic.

C.5.1 Figure 4-4 details (mean vector and mean turning rate comparisons)

C.5.1.1 Mean vector length

The mean vector length for the x2 gain (W_{11}=0.82, ***p*=0.019**) and x4 gain (W_{11}=0.85, ***p*=0.042**) conditions were established to be non-uniformly distributed. Friedman's test was used to compare all factor levels, and showed the presence of a significant main effect, χ^2_5=32.20, ***p*<0.001.** *Post-hoc* comparisons were selectively made between the peak factor (x0.5 gain), the highest gain (x4), and the no stimulus condition (

Table C-1).

Table C-1: *Post-hoc* comparisons for mean vector lengths.

Factors compared	Result
x0.5 vs. No Stimulus	t_{10}=-5.99, ***p*<0.001**
x0.5 vs. x4	W_{10}=-2.93, ***p*=0.003**

C.5.1.2 Mean absolute turning rate, |ω|

All mean turning rates were found to be normally distributed. One-way repeated measures ANOVA over all factor levels found a significant main effect, $F_{5,50}$=6.08, ***p*<0.001**. Mauchly's test of sphericity indicated that this assumption was not violated in the preceding ANOVA. *Post-hoc* comparisons were selectively made between the peak factor (x3 gain), the highest and lowest gains (x0.5 and x4), and the no stimulus condition (Table C-2).

Table C-2: *Post-hoc* comparisons for absolute turning rates.

Factors compared	Result
x3 vs. No Stimulus	t_{10}=-2.58, ***p*=0.027**
x3 vs. x0.5	t_{10}=-4.01, ***p*=0.002**
x3 vs. x4	t_{10}=-1.21, p=0.255

C.5.2 Figure 4-5 details (position-dependent function comparison)

C.5.2.1 Value of $\tilde{P}^{Sc.}$

The no stimulus condition was the only factor level found to be non-uniformly distributed (W_{11}=0.81, ***p*=0.012**). One way repeated measures ANOVA over all factor levels found a significant main effect, $F_{1.71,17.06}$ = 3.78, ***p*=0.047**. Mauchly's test of sphericity indicated this assumption was violated in the preceding ANOVA, χ^2_{14}=39.75, ***p*<0.001** (ε=0.341), hence the Greenhouse-Geisser correction was applied (the original degrees of freedom were (5, 50)). *Post-hoc* comparisons were selectively made between the peak factor (x2 gain), the highest and lowest gains (x0.5 and x4), and the no stimulus condition (Table C-3).

Table C-3: *Post-hoc* comparisons for position function scales.

Factors compared	Result
x2 vs. No Stimulus	W_{10}=-2.67, ***p*=0.008**
x2 vs. x0.5	t_{10}=-2.38, ***p*=0.039**
x2 vs. x4	t_{10}=-2.28, ***p*=0.046**

Following this, all factor levels were compared to zero (Table C-4).

Table C-4: Comparison of position function scales vs. 0.

Factor vs. 0	Result
No stimulus	W_{10}=0.27, p=0.790
x0.5	t_{10}=10.54, p=0.197
x1	t_{10}=15.91, ***p*=0.019**
x2	t_{10}=21.86, ***p*=0.002**
x3	t_{10}=16.85, ***p*<0.001**
x4	t_{10}=9.22, ***p*<0.001**

C.5.3 Figure 4-6 details (motion-dependent function comparison)

C.5.3.1 Difference between left and front visual fields for clockwise motion

All differences were found to be normally distributed. One-way repeated measures ANOVA over all factor levels did not find a significant main effect, $F_{5,50}$=1.80, p=0.129. Following this, all factor levels were compared to zero (Table C-5).

Table C-5: Comparison of clockwise motion difference between left and front visual fields vs. 0.

Factor vs. 0	Result
No stimulus	t_{10}= 0.62, p=0.550
x0.5	t_{10}=-0.48, p=0.640
x1	t_{10}=0.19, p=0.853
x2	t_{10}=2.89, ***p*=0.016**
x3	t_{10}=0.97, p=0.354
x4	t_{10}=1.93, p=0.83

C.5.3.2 Differences between left and front visual fields for counter-clockwise motion

All differences were found to be normally distributed. One-way repeated measures ANOVA over all factor levels found a significant main effect, $F_{5,50}$=5.70, ***p*<0.001**. Mauchly's test of sphericity indicated that this assumption was not violated in the preceding ANOVA. *Post-hoc* comparisons were selectively made between the peak factor (x4 gain), the lowest gain (x0.5), and the no stimulus condition (Table C-6).

Table C-6: *Post-hoc* comparisons of counter-clockwise motion difference between left and front visual fields.

Factors compared	Result
x0.5 vs. No Stimulus	t_{10}=-4.27, ***p*=0.002**
x0.5 vs. x4	t_{10}=-3.65, ***p*=0.004**

Following this, all factor levels were compared to zero (Table C-7).

Table C-7: Comparisons of counter-clockwise motion difference between left and front visual fields vs. 0.

Factor vs. 0	Result
No stimulus	t_{10}=0.33, p=0.751
x0.5	t_{10}=2.38, ***p*=0.039**
x1	t_{10}=4.43, ***p*=0.001**
x2	t_{10}=6.20, ***p*<0.001**
x3	t_{10}=3.52 , ***p*=0.006**
x4	t_{10}=7.28, ***p*<0.001**

C.5.3.3 Differences between right and front visual fields for clockwise motion

All differences were found to be normally distributed. One-way repeated measures ANOVA over all factor levels found a significant main effect, $F_{5,50}$=2.64, ***p*<0.034**. Mauchly's test of sphericity indicated that this assumption was not violated in the preceding ANOVA. *Post-hoc* comparisons were selectively made between the peak factor (x4 gain), the lowest gain (x0.5), and the no stimulus condition (Table C-8).

Table C-8: *Post-hoc* comparisons of clockwise motion difference between right and front visual fields.

Factors compared	Result
x0.5 vs. No Stimulus	t_{10}=-3.09, ***p*=0.011**
x0.5 vs. x4	t_{10}=-2.83, ***p*=0.021**

Following this, all factor levels were compared to zero (Table C-9).

Table C-9: Comparisons of clockwise motion difference between right and front visual fields vs. 0.

Factor vs. 0	Result
No stimulus	t_{10}=-0.16, p=0.875
x0.5	t_{10}=0.56, p=0.586
x1	t_{10}=31.13, ***p*=0.011**
x2	t_{10}=2.72, ***p*=0.022**
x3	t_{10}=2.31, ***p*=0.044**
x4	t_{10}=3.55, ***p*=0.005**

C.5.3.4 Difference between right and front visual fields for counter-clockwise motion

Three factor levels were found to be non-normally distributed which were, no stimulus (W_{11}=0.84, ***p*=0.031**), x2 gain (W_{11}=0.75, ***p*=0.002**), and x4 gain (W_{11}=0.83, ***p*=0.021**). Because of the presence of three non-uniformly distributed factor levels, Friedman's test was used to compare all factor levels, and did not find a significant main effect, χ^2_5=3.10, p=0.684. Following this, all factor levels were compared to zero (Table C-10).

Table C-10: Comparisons of counter-clockwise motion difference between right and front visual fields vs. 0

Factor vs. 0	Result
No stimulus	W_{10}=-0.53, p=0.594
x0.5	t_{10}=-1.57, p=0.147
x1	t_{10}=-1.32, p=0.217
x2	W_{10}=0.09, p=0.929
x3	t_{10}=0.10, p=0.922
x4	W_{10}=-0.27, p=0.790

C.5.4 Figure C-6 details (mean vector comparison)

C.5.4.1 Mean vector direction

Results of Rayleigh's test of uniformity performed on the mean vector direction measured for each gain condition (Table C-11).

Table C-11: Results of Rayleigh's test of uniformity for each factor.

Factor	Result
No stimulus	z_{10}=0.80, p<0.459
x0.5	z_{10}=8.12, ***p*<0.001**
x1	z_{10}=6.75, ***p*<0.001**
x2	z_{10}=9.53, ***p*<0.001**
x3	z_{10}=5.10, p=**0.001**
x4	z_{10}=0.11, p=0.902

Appendix D **Supplementary material for Chapter 5**

D.1 Supplementary figures

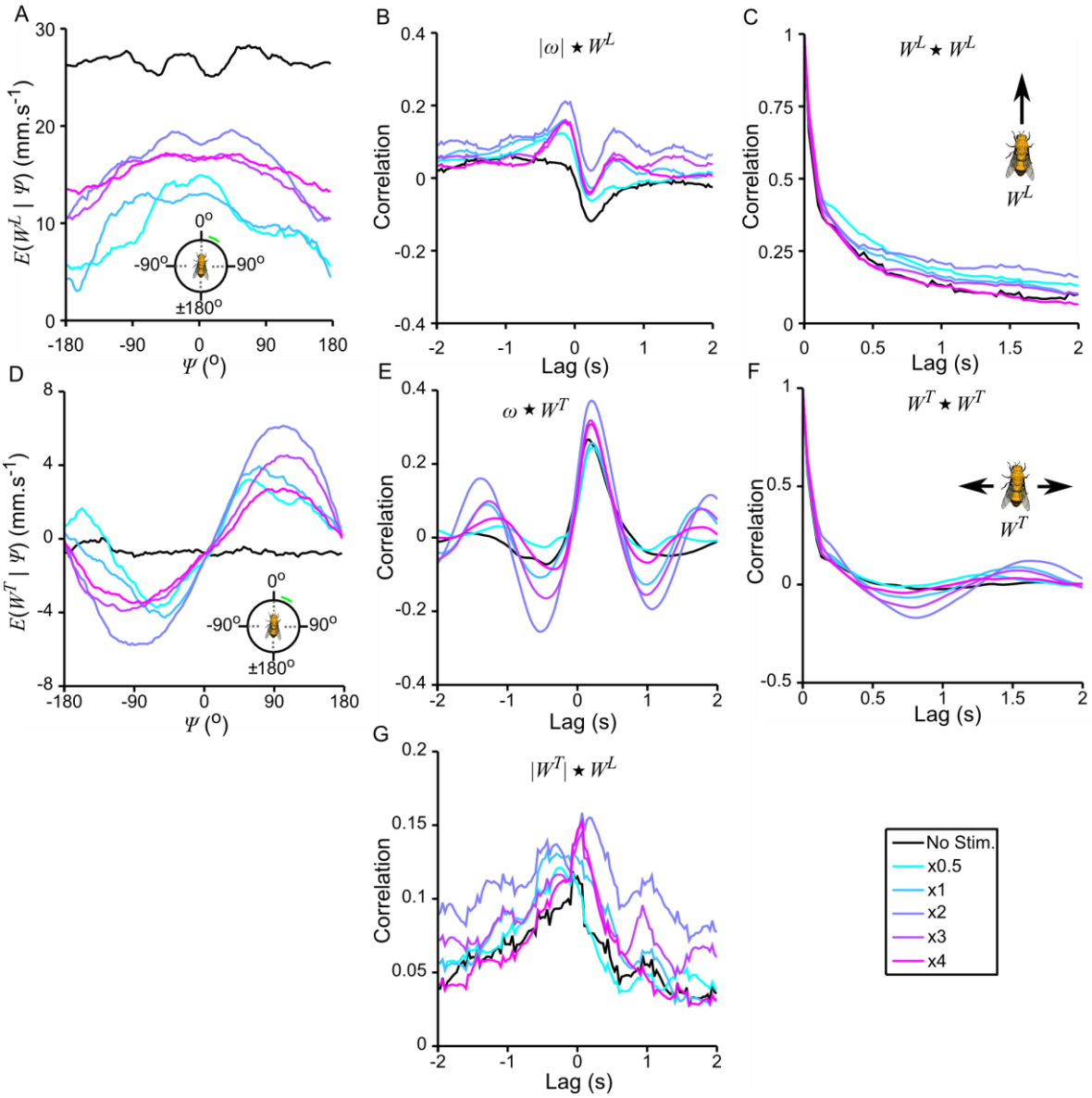

Figure D-1: Relationships between components of walking speed and other variables. **A**, the expected longitudinal speed, W^L, depending on stimulus position, ψ. **B**, the crosscorrelation between absolute turning rate, ω, and W^L. **C**, the autocorrelation of W^L. **D, E, F**, as for A, B and C, with the comparison made using transverse speed, W^T. **G**, the crosscorrelation between W^L and W^T. A and D were calculated by finding the average value of the relevant speed component at each stimulus position. Shorthand correlation notation is used to denote $x * y = \int_{-\infty}^{\infty} x(\tau)y(\tau - t)d\tau$ in plots B, C, E, F and G. All plots show each gain condition as a separate curve. N=11 bees repeated all gain conditions.

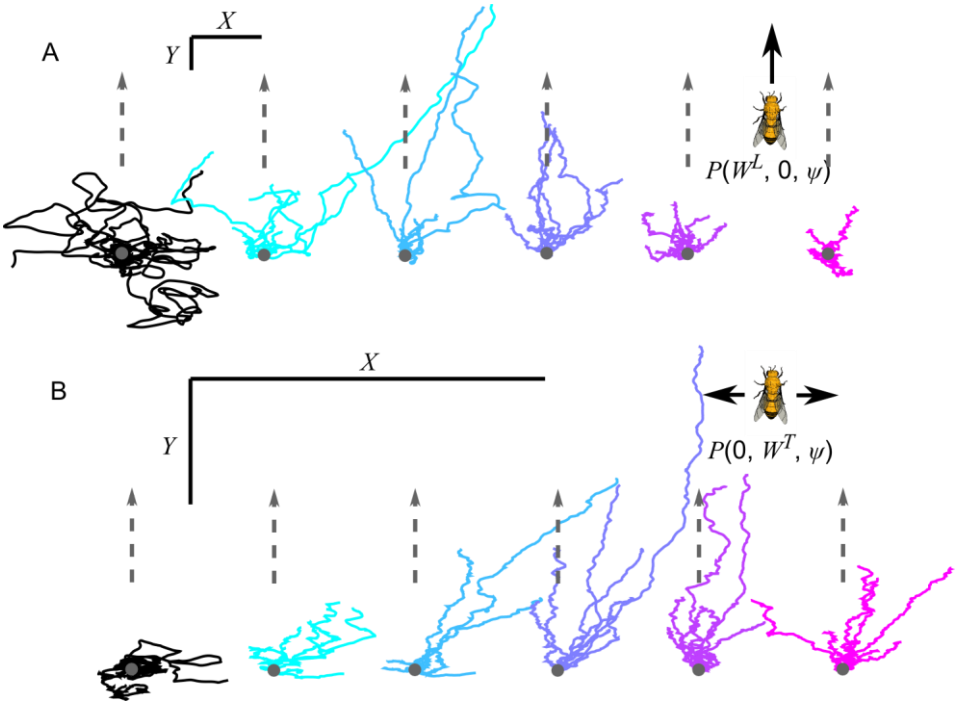

Figure D-2: Path reconstruction based on individual components of walking speed. **A**, based on modulation of longitudinal speed alone, $P(W^L,0,\psi)$. **B**, based on modulation of transverse speed alone, $P(0,W^T,\psi)$. Paths are reconstructions using Eq. (4-30). A grey dot denotes the start point of all trajectories for a given condition and the arrow represents the direction to the distant landmark represented by the fixation stimulus. All scale bars represent 500 mm. Combined paths are shown in Figure 5-4.

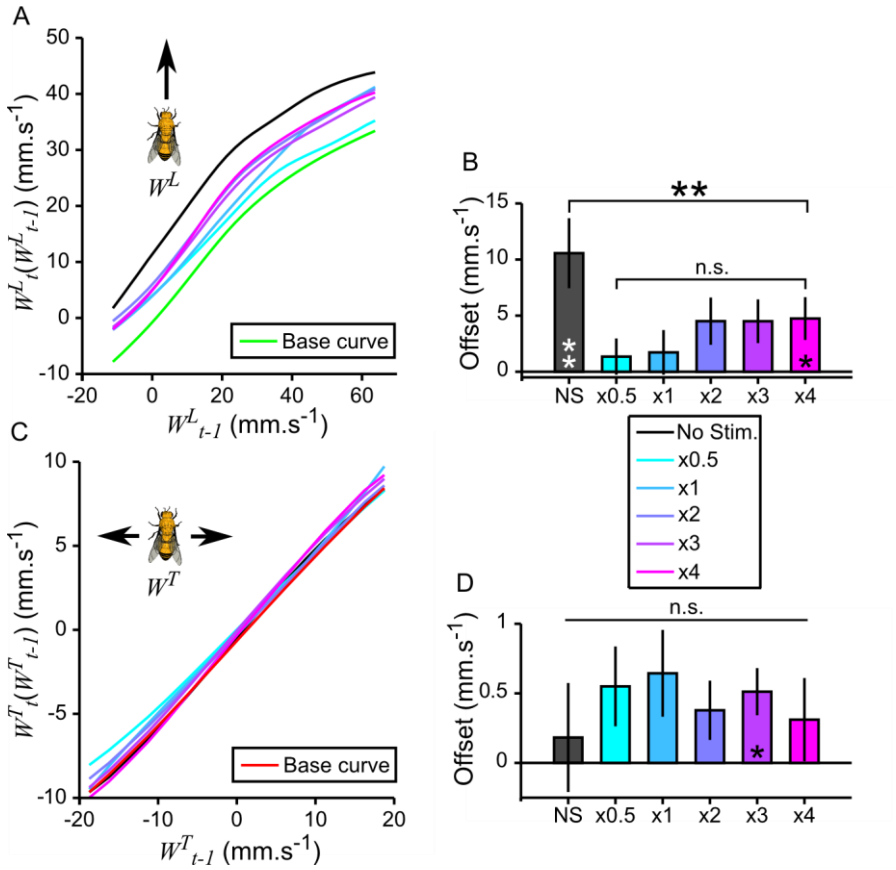

Figure D-3: Autoregressive relationship for both components of walking speed. **A**, longitudinal speed, W^L_t, as a function of turning rate, W^L_{t-1}. **B**, average offset of each curve from the base curve. **C** and **D**, as for A and B, with the comparison made using transverse speed, W^T. Both A and C are calculated using Eq. (4-36), calculation of the base curve is described in Section 5.4.3. All plots show each gain condition as a separate curve. N=11 bees repeated all gain conditions. Error bars show ± S.E.M. Bars denote statistical significance (n.s.: $p>0.05$, *: $p<0.05$, **: $p<0.01$) of the difference between the indicated groups, whereas stars in bars denote the statistical significance from zero. Full statistical details are provided in Section D.2.5.

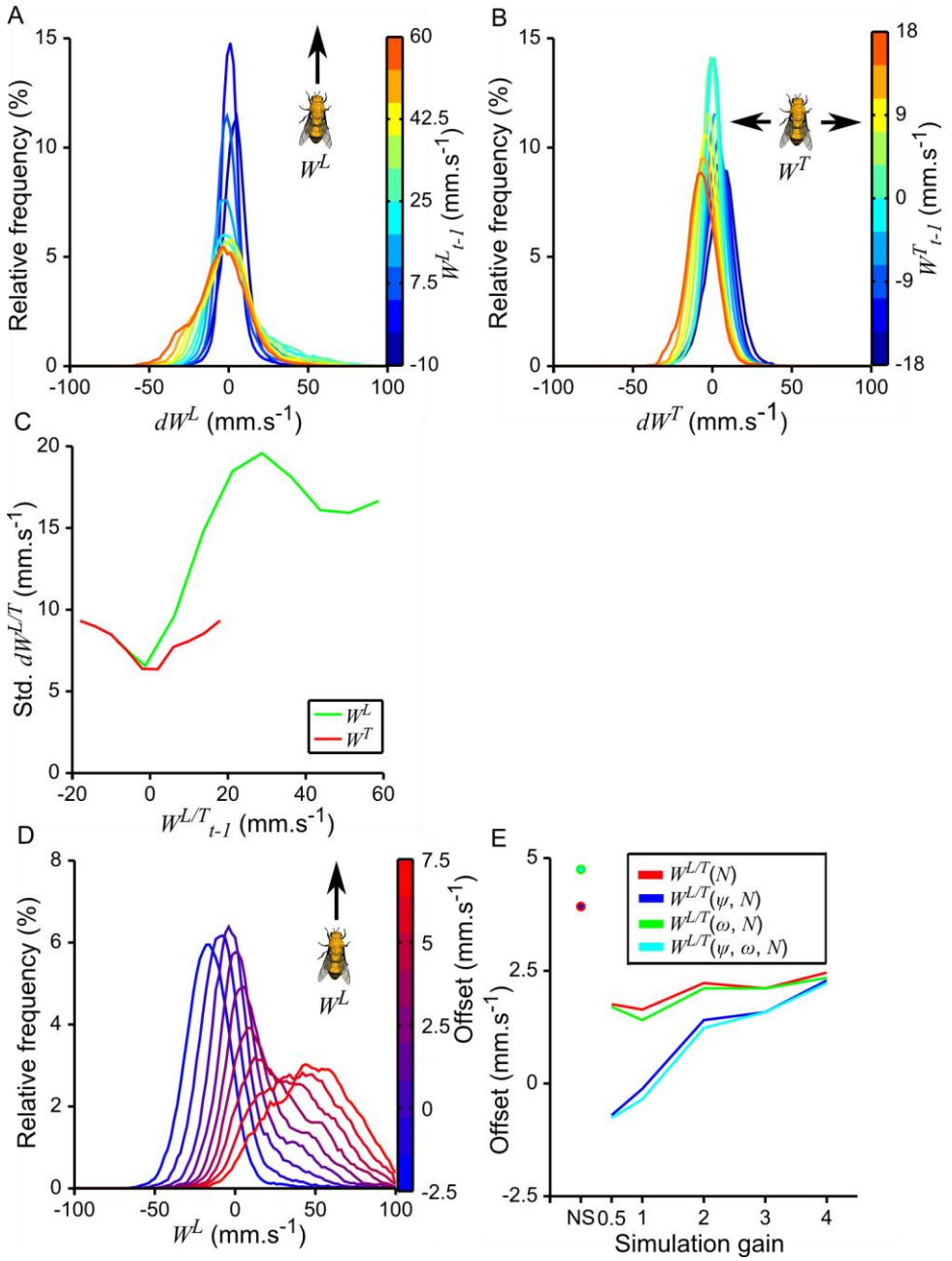

Figure D-4: Analysis of the random variation longitudinal and transverse speed in the no stimulus condition. **A**, distributions of the derivative of longitudinal speed, dW^L, parameterised by the previous longitudinal speed W^L_{t-1}. **B**, as for A, with the comparison based on transverse speed, W^T. Measured distributions for both W^L and W^T are shown in Figure 5-1. **C**, the standard deviation of the derivative of either speed component, as a function of the prior value of that speed component. The dependence of the standard deviation on the prior walking speed indicates that the walking speed does not result from low-pass filtered Gaussian noise, which would not show such dependence. **D**, distributions of W^L resulting from longitudinal speed simulations based on only low-pass filtered noise (where the standard deviation depends on W^L_{t-1}, see Section 5.4.4) and the parameterised offset value. Distributions can be similar to observed waling speed distributions (Figure 5-2) depending on the offset value. **E**, offset values used for W^L simulations in Figure 5-5 depending on gain condition and simulation specification.

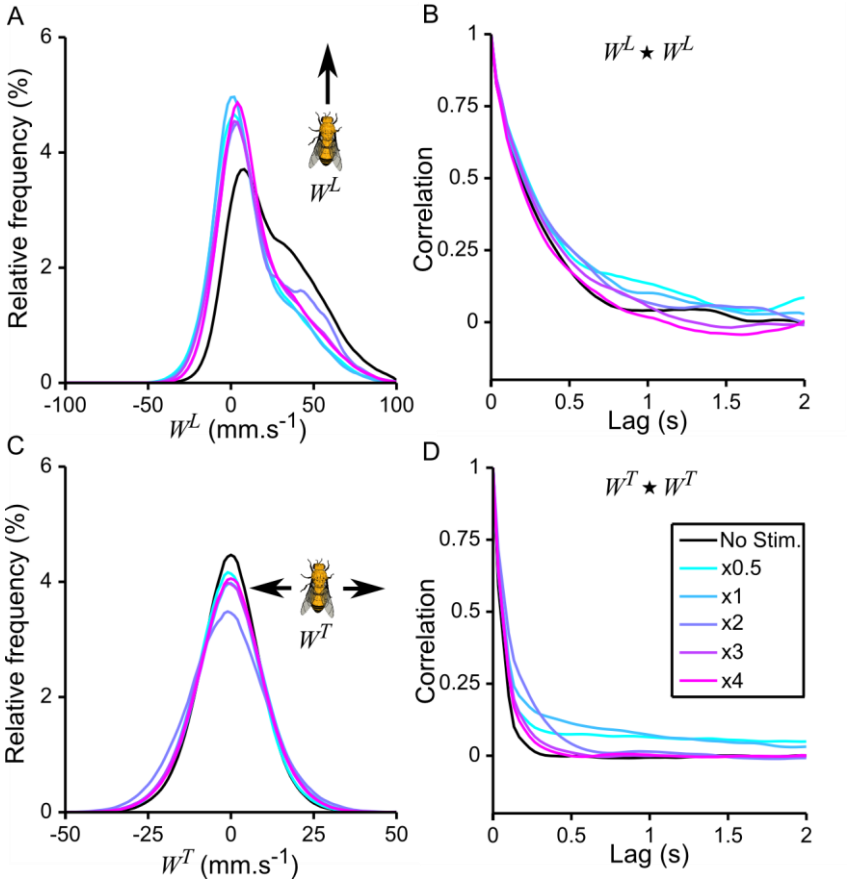

Figure D-5: Distributions and autocorrelations for simulated data in Figure 5-5. Both speed components are functions of stimulus position, turning rate, and injected noise. **A**, Frequency distributions of longitudinal speed, W^L. **B**, Autocorrelation of W^L. **C** and **D**, as for A and B, with the comparison made using transverse speed, W^T. All plots show each gain condition as a separate curve.

D.2 Statistical details

All tests of main effects are performed using a single factor, gain, consisting of 6 factor levels, corresponding to gains of x0.5, x1, x2, x3, x4, and the no-stimulus control, unless otherwise noted. All factor levels for each data set were tested for normality (using a Shapiro-Wilk test); deviations from this are noted where they occur. Main effects were tested using either repeated measures ANOVA or Friedman's non-parametric repeated measures ANOVA equivalent, depending on the presence and severity of non-normal factors. When using ANOVA, the assumption of sphericity was also tested using Mauchly's test of sphericity, and the Greenhouse-Geisser correction was applied if this assumption was violated.

Upon finding a significant main effect, the following *post-hoc* testing procedure was used. The factor with the largest magnitude mean (hereafter referred to as the 'peak factor') was compared to the highest and lowest gains, x0.5 and x4, and the no stimulus condition (if it was not itself

one of those factors). This comparison was made using a paired sample *t*-test for normal data, or a Wilcoxon matched-pair signed-rank test for non-normal data. If none of these *post-hoc* comparisons were successful, a final test between the factor levels that showed the largest difference between mean values was performed to identify the significant difference indicated by the main effects test. Additionally, in some cases factor levels were compared to zero, or between two pairs of values at each factor level. For normal data, a single factor *t*-test was performed, and for non-normal data, a Wilcoxon signed rank test comparing the group median to zero was used, which are respectively denoted by *t* and *W* test statistics.

D.2.1 Figure 5-1 (mean longitudinal and transverse speed comparison)

D.2.1.1 Mean longitudinal walking speed

Both x1 gain (W_{11}=0.79, ***p*=0.009**), and x3 gain (W_{11}=0.84, ***p*=0.030**) were found to be non-normally distributed. Friedman's test over all factor levels found a significant main effect, χ^2_5 =14.58, ***p*=0.012**. Pairwise *post-hoc* comparisons were made between the peak factor (x2 gain), the lowest and highest gains (x0.5 and x4), and the no stimulus condition. None of these *post-hoc* tests returned a significant result, prompting us to test maximum and minimum factor levels, the no stimulus and x1 gain conditions (Table D-1). A significant main effect was found between the no stimulus and x1 gain conditions, isolating the finding of the main effects test.

Table D-1: *Post-hoc* comparisons for mean longitudinal speed.

Factors compared	Result
x2 vs. x0.5	t_{10}=1.28, p=0.227
x2 vs. x4	t_{10}=0.55, p=0.593
x2 vs. No stimulus	t_{10}=-2.09, p=0.063
x1 vs. No stimulus	W_{10}=2.40, ***p*=0.016**

D.2.1.2 Mean transverse walking speed

Only data from x1 gain (W_{11}=0.81, ***p*=0.014**) was found to be non-normally distributed. One way repeated measures ANOVA performed over all factor levels did not find a significant main effect, $F_{5,50}$=1.73, p=0.145.

D.2.2 Figure 5-2 details (detailed longitudinal speed comparison)

D.2.2.1 Longitudinal speed difference between slow and fast turning rates

The difference at x2 gain was found to be non-normally distributed (W_{11}=0.86, ***p*=0.023**). One way repeated measures ANOVA performed over all factor levels found a significant main effect, $F_{2.20,21.98}$=7.05, ***p*=0.004**. Mauchly's test of sphericity indicated that this assumption was violated in the preceding ANOVA (χ^2_{14}=27.38, ***p*=0.021**, ε=0.44), hence, the Greenhouse-Geisser correction was applied (the unadjusted degrees of freedom were 5,50). Pairwise *post-hoc* comparisons were made between the peak factor (x1 gain), the lowest and highest gains (x0.5 and x4), and the no stimulus conditions (Table D-2).

Table D-2: *Post-hoc* comparisons for turning rate based longitudinal speed differences.

Factors compared	Result
x1 vs. x0.5	t_{10}=1.13, p=0.287
x1 vs. x4	t_{10}=0.88, p=0.400
x1 vs. No stimulus	t_{10}=3.80, ***p*=0.004**

Following this, all factor levels were compared to zero (Table D-3).

Table D-3: Comparisons of turning rate based longitudinal speed differences vs. 0.

Factor vs. 0	Result
No stimulus	t_{10}=-3.22, ***p*=0.009**
x0.5	t_{10}=0.94, p=0.371
x1	t_{10}=2.62, ***p*=0.026**
x2	W_{10}=2.05, ***p*=0.041**
x3	t_{10}=1.73, p=0.114
x4	t_{10}=1.83, p=0.097

D.2.2.2 Longitudinal speed difference between front and rear stimulus positions

The difference at x0.5 gain was found to be non-normally distributed (W_{11}=0.83, ***p*=0.027**). One way repeated measures ANOVA performed over all factor levels found a significant main effect, $F_{5,50}$=3.10, ***p*=0.016**. Mauchly's test of sphericity indicated that this assumption was not violated in the preceding ANOVA. Pairwise *post-hoc* comparisons were made between the peak factor (x0.5 gain), the highest gains (x4), and the no stimulus conditions (Table D-4).

Table D-4: *Post-hoc* comparisons for stimulus position based longitudinal speed differences.

Factors compared	Result
x0.5 vs. x4	W_{10}=-1.33, p=0.182
x0.5 vs. No stimulus	W_{10}=-2.58, ***p*=0.010**

Following this, all factor levels were compared to zero (Table D-5).

Table D-5: Comparison of stimulus position based longitudinal speed differences vs. 0.

Factor vs. 0	Result
No stimulus	t_{10}=-0.07, p=0.943
x0.5	W_{10}=2.80, ***p*=0.005**
x1	t_{10}=2.65, ***p*=0.024**
x2	t_{10}=5.67, ***p*<0.001**
x3	t_{10}=3.96, ***p*=0.003**
x4	t_{10}=5.20, ***p*<0.001**

D.2.3 Figure 5-3 details (detailed transverse speed comparison)

D.2.3.1 Transverse speed difference between positive and negative turning rates

The difference at x4 gain was found to be non-normally distributed (W_{11}=0.78, ***p*=0.005**). One way repeated measures ANOVA performed over all factor levels found a significant main effect, $F_{5,50}$=3.42, ***p*=0.010**. Mauchly's test of sphericity indicated that this assumption was not violated in the preceding ANOVA. Pairwise *post-hoc* comparisons were made between the peak factor (x2 gain), the lowest and highest gains (x0.5 and x4), and the no stimulus conditions (Table D-6).

Table D-6: *Post-hoc* comparisons for turning rate based transverse speed differences.

Factors compared	Result
x2 vs. x0.5	t_{10}=-2.48, ***p*=0.033**
x2 vs. x4	W_{10}=0.71, p=0.477
x2 vs. No stimulus	t_{10}=-3.69, ***p*=0.004**

Following this, all factor levels were compared to zero (Table D-7).

Table D-7: Comparisons of turning rate based transverse speed differences vs. 0.

Factor vs. 0	Result
No stimulus	t_{10}=1.37, p=0.200
x0.5	t_{10}=0.59, p=0.571
x1	t_{10}=-0.61, p=0.553
x2	t_{10}=-1.18, p=0.266
x3	t_{10}=-0.76, p=0.462
x4	W_{10}=-1.51, p=0.131

D.2.3.2 Transverse speed difference between left and right stimulus positions

The differences at both gains x0.5 (W_{11}=0.67, ***p*<0.001**) and x1 (W_{11}=0.72, ***p*=0.001**) were found to be non-normally distributed. Friedman's test over all factor levels found a significant main effect, χ^2_5 =15.41, ***p*=0.009**. Pairwise *post-hoc* comparisons were made between the peak factor (x2 gain), the lowest and highest gains (x0.5 and x4), and the no stimulus conditions (Table D-8).

Table D-8: *Post-hoc* comparisons for stimulus position based transverse speed differences.

Factors compared	Result
x2 vs. x0.5	W_{10}=-1.42, p=0.155
x2 vs. x4	t_{10}=2.17, p=0.055
x2 vs. No stimulus	t_{10}=3.33, ***p*=0.008**

Following this, all factor levels were compared to zero (Table D-9).

Table D-9: Comparisons of stimulus position based transverse speed differences vs. 0.

Factor vs. 0	Result
No stimulus	t_{10}=0.941, p=0.369
x0.5	W_{10}=2.93, ***p*=0.003**
x1	W_{10}=2.76, ***p*=0.006**
x2	t_{10}=3.54, ***p*=0.005**
x3	t_{10}=4.34, ***p*=0.001**
x4	t_{10}=4.26, ***p*=0.002**

D.2.4 Figure 5-4 details (path length comparisons)

D.2.4.1 Total path length

Path lengths for the majority of conditions were found to be non-normally distributed (NS: W_{11}=0.81, ***p*=0.011**, x0.5 gain: W_{11}=0.77, ***p*=0.004**, x1 gain: W_{11}=0.75, ***p*=0.002**, and x4 gain: W_{11}=0.83, ***p*=0.020**). Friedman's test over all factor levels found a significant main effect, χ^2_5 =19.94, ***p*=0.001**. Pairwise *post-hoc* comparisons were made between the peak factor (x2 gain), the lowest and highest gains (x0.5 and x4), and the no stimulus condition (Table D-10).

Table D-10: *Post-hoc* comparisons for final path lengths.

Factors compared	Result
x2 vs. x0.5	W_{10}=-0.89, p=0.374
x2 vs. x4	W_{10}=-2.49, ***p*=0.013**
x2 vs. No stimulus	W_{10}=-2.67, ***p*=0.008**

Following this, all factor levels were compared to zero (Table D-11).

Table D-11: Comparisons of final path lengths vs. 0.

Factor vs. 0	Result
No stimulus	W_{10}=-1.42, p=0.155
x0.5	W_{10}=2.67, ***p*=0.008**
x1	W_{10}=2.31, ***p*=0.021**
x2	t_{10}=3.81, ***p*=0.003**
x3	t_{10}=4.30, ***p*=0.002**
x4	W_{10}=1.51, p=0.131

D.2.4.2 Longitudinal and transverse based path lengths

As for the total path length comparison, the longitudinal and transverse based path lengths were also non-uniformly distributed, hence non-parametric statistical tests were used for all comparisons. The difference between both paths lengths (longitudinally and transversely based) was tested using Wilcoxon matched-pair signed-rank tests (Table D-12).

Table D-12: Comparisons between longitudinal and transverse based distances for each factor.

Factor vs. 0	Result
No stimulus	W_{10}=0.62, p=0.534
x0.5	W_{10}=-2.93, ***p*=0.003**
x1	W_{10}=-2.67, ***p*=0.008**
x2	W_{10}=-2.93, ***p*=0.003**
x3	W_{10}=-1.42**,** p=0.155
x4	W_{10}=0.89, p=0.374

D.2.5 Figure D-3 details (longitudinal and transverse speed offset comparisons)

D.2.5.1 Longitudinal speed offset

The offsets for all conditions were found to be uniformly distributed. One way repeated measures ANOVA performed over all factor levels found a significant main effect, $F_{5,50}$=4.43, ***p*=0.002**. Mauchly's test of sphericity indicated that this assumption was not violated in the preceding ANOVA. Pairwise *post-hoc* comparisons were made between the peak factor (x4 gain), the lowest gain (x0.5), and the no stimulus conditions (Table D-13).

Table D-13: *Post-hoc* comparisons for longitudinal speed offsets.

Factors compared	Result
x4 vs. x0.5	t_{10}=1.64, p=0.133
x4 vs. No stimulus	t_{10}=-3.20, ***p*=0.009**

Following this, all factor levels were compared to zero (Table D-14).

Table D-14: Comparisons of longitudinal speed offsets vs. 0.

Factor vs. 0	Result
No stimulus	t_{10}=3.23, ***p*=0.009**
x0.5	t_{10}=0.79, p=0.446
x1	t_{10}=0.83, p=0.429
x2	t_{10}=2.04, p=0.069
x3	t_{10}=2.20, p=0.052
x4	t_{10}=2.37, ***p*=0.039**

D.2.5.2 Transverse speed offset

The offsets for both gains x0.5 (W_{11}=0.81, ***p*<0.015**) and x4 (W_{11}=0.85, ***p*=0.039**) were found to be non-normally distributed. Friedman's test over all factor levels did not find a significant main effect, χ^2_5 =0.76, p=0.979. Following this, all factor levels were compared to zero (Table D-15).

Table D-15: Comparison of transverse speed offsets vs. 0.

Factor vs. 0	Result
No stimulus	t_{10}=0.44, p=0.666
x0.5	W_{10}=1.60, p=0.110
x1	t_{10}=1.97, p=0.078
x2	t_{10}=1.69, p=0.121
x3	t_{10}=2.88, ***p*=0.016**
x4	W_{10}=1.42, p=0.155